Synthesis and Characterisation of New Conjugated Polymers for Solar Cell Applications

The University Of Sheffield.

A thesis submitted in partial fulfilment of the requirements for the degree of Doctor of Philosophy

By:

Omar Mohammed Esmaeel

The University of Sheffield

Chemistry Department

September 2018

Declaration

This thesis is submitted for the degree of doctorate of philosophy (PhD) at the University of Sheffield, having been submitted for no other degree. It records the research carried out at the University of Sheffield from October 2014 to October 2018. It is entirely my original work, unless where referenced.

Signed …….

Date …….

Abstract

Significant efforts were conducted during the last few decades to find a new alternative energy resource that replaces the current conventional resources and reduce emission of greenhouse gasses and Global Warming. The traditional silicon-based inorganic solar cells are efficient but their high cost limits their use. Organic photovoltaic devices offer many features including the low production costs and flexibility of devices. In addition, these materials are commercially available and easy to process compared to inorganic materials. The development of bulk heterojunction photovoltaic devices with high power conversion efficiency is still under investigation. Moreover, enormous numbers of conjugated polymers were synthesised and studied to achieve high power conversion efficiencies by designing conjugated polymers exploiting π-electrons delocalization within the polymer backbone. The solubility of conjugated polymers is an important matter to consider, so attaching alkyl chains to the backbone of the polymer will not only enhance the solubility of these materials but also increase the charge carrier mobility through the increase of molecular weight of conjugated polymer.

In this thesis, different studies have discussed the synthesis of donor-acceptor (D-A) conjugated polymers based on benzothiadiazole (BTD) as an acceptor with donor units such as carbazole and fluorene using direct hetero arylation (DHA) polymerisation were undertaken. The synthesis of a series of conjugated polymers based on fluorinated or non-fluorinated BTD units with molecules such as naphthalene, anthracene, pyrene, carbazole, fluorene and bithiophene-based donor units is presented. The impact of fluorine substitution attached to polymer chains has clearly shown deep HOMO levels in the resulting materials, which agrees with findings in the literature. Another aspect was covered in this thesis which is the impact of extending the π-conjugated system by adding additional aromatic units to the polymers backbone. Interestingly, the results from UV-visible and cyclic voltammetry are both satisfying in obtaining low bandgap polymers regardless the type of donor units used in the conjugated polymer prepared.

Chapter 2 in this thesis concerns the synthesis and characterisation of three conjugated polymers **P1**, **P2** and **P3** based on different BTD units polymerised with a 2,6-substituted naphthalene donor monomer. The optical and the electrochemical

studies showed bandgaps for **P1** and **P2** above 2.0 eV. Interestingly, a low bandgap 1.71 eV was noticed for **P3**, which is slightly lower than the electrochemical bandgap 1.76 eV for the same polymer.

Chapter 3 covers the study of two novel conjugated polymers **P4** and **P5** synthesised by the reaction of fluorinated and non-fluorinated BTD units as acceptors with a 2,6-linked anthracene as a donor. The optical properties showed bandgaps of 1.97 and 1.99 eV for **P4** and **P5** respectively. The electrochemical bandgaps are slightly higher due to several device operating considerations.

In Chapter 4, a series of four polymers **P6**, **P7**, **P8** and **P9** based on 2,7-linked pyrene donor monomer with fluorinated and non-fluorinated BTD units were synthesised. The optical properties showed bandgaps of 2.0 eV for both **P6** and **P7**. Lower bandgaps of 1.74 and 1.79 eV were seen for **P8** and **P9** respectively; this is due to the π-conjugated system extension in **P8** and **P9** using additional thiophene units within the polymers backbone.

Chapter 5 discusses the preparation and characterisation of a new family of conjugated polymers **P10**, **P11**, **P12**, **P13**, **P14** and **P15**. These polymers are based on the same fluorinated BTD acceptor polymerised with different donor units including carbazole, fluorene and bithiophene derivatives. **P10**, **P11** and **P12** are carbazole-based conjugated polymers; these polymers have shown optical bandgaps of 1.79, 1.78 and 1.81 eV respectively. The effect of the fluorine atoms incorporation can be clearly seen in lowering the HOMO levels of **P12** using a fluorinated carbazole unit and the addition of extra thiophene units is not very effective in lowering the bandgap of **P11**.

Polymers **P13** and **P14** are fluorene-based conjugated polymers, and the optical properties of the two polymers show bandgaps of 1.86 and 1.84 eV for **P13** and **P14** respectively, those two polymers have slightly higher bandgaps compared to the carbazole-based polymers in same chapter.

The last polymer **P15** is based on a 2,2'-linked bithiophene donor monomer polymerised with fluorinated a BTD acceptor unit. This polymer surprisingly shows the lowest bandgap among all the previously synthesised polymers. The optical and the electrochemical bandgaps are 1.70 and 1.67 eV respectively.

The molecular weight determined by gel permeation chromatography analysis showed that each polymer has a different molecular weight depending on the chemical structure of the repeat unit and the solubility in organic solvents, in addition to the fraction in which the polymer was collected during the Soxhlet extraction process. The thermal gravimetric analysis TGA showed that the synthesised polymers are thermally stable at temperatures below 285 °C. The powder X-ray diffraction shows that the synthesised polymers are generally amorphous with some crystalline structure noticed in some fluorinated polymers due to the ordered π-π stacking, which is correlated to the inter/intramolecular interactions within the polymers chains.

The synthesised conjugated polymers have shown promising features for their application in organic photovoltaic (OPV) devices due to high molecular weights resulted from solubilising groups attached to these polymers and also low bandgaps. It will be worth to apply these polymers in photovoltaic devices and observe the photovoltaic characteristics such as open circuit voltage V_{oc}, short circuit current I_{sc}, fill factor FF and power conversion efficiency PCE%.

Acknowledgments

Firstly, I would like to express my sincere gratitude to my supervisor Dr Ahmed Iraqi, for his continues guidance during my PhD study. His patience, immense knowledge and motivation have helped me during the time of research and the write up of my thesis. I would also like to take this opportunity to thank all the staff in Chemistry department, especially Heather Grievson, Rob Hanson, Simon Thorpe, Sharon Spey, Sharon Curl and Nick Smith for their invaluable support.

My special thanks go to my laboratory colleagues Bunian Shareef, Bader Altayeb, and Majid Alawad. Thanks also go to my friends who supported me during study years Dr Ahmed Al-Azzawi, Dr Sulaiman Alesaie and Dr Ary Murad for their companionship that kept my spirits up during tough times.

My thanks go to my mother for her patience, emotional support when things did not go well with my research. I would not forget to give thanks to my brothers, my wife and daughters, without their existence in my life, I would not have finished my studies.

Finally, I would like to thank my sponsor, the Ministry of Higher Education and Scientific Research represented by the Iraqi Cultural Attaché – London for the financial support and guidance during my PhD study.

Table of Contents

Table of figures

Table of Tables

Table of Equations

Abbreviations

HOMO	Highest occupied molecular orbital
LUMO	Lowest unoccupied molecular orbital
fs	Femtosecond
nm	Nanometre
AM 1.5	Air Mass
D-A	Donor-Acceptor polymer
Eg^{opt}	Optical bandgap
Eg^{elec}	Electrochemical bandgap
V_{oc}	Open-circuit voltage
J_{sc}	Short-circuit current
J-V	voltage-current
FF	Fill factor
PCE	Power conversion efficiency
BHJ	Bulk heterojunction
FET	Filed-effect transistor
LED	Light-emitting diode
OPV	Organic photovoltaic
ITO	indium tin oxide
^{1}H NMR	Proton Nuclear Magnetic Resonance
^{13}C NMR	Carbon Nuclear Magnetic Resonance
^{19}F NMR	Fluorine Nuclear Magnetic Resonance
M_n	Number-average molecular weight
M_w	Weight-average molecular weight
PDI	Polydispersity index
$CDCl_3$	Deuterated chloroform
s	Singlet (NMR)

d	Doublet (NMR)
t	Triplet (NMR)
dd	Doublet of doublet (NMR)
bs	Broad singlet peak (NMR)
TGA	Thermal gravimetric analysis
UV-visible	Ultraviolet-visible spectroscopy
λ_{max}	Maximum absorption wavelength
XRD	X-ray diffraction
CV	Cyclic voltammetry
GPC	Gel permeation chromatography
EI	Electron ionization
CI	Chemical ionization
ppm	Part per million
Hz	Hertz
M	Molar
BTD	Benzothidiazole
DCM	Dichloromethane
MeOH	Methanol
AcOH	Acetic acid
$MgSO_4$	Magnesium sulphate
PE	Petroleum Ether
NBS	N-bromosuccinimide
$PC_{71}BM$	Phenyl-C_{71}-butyric acid methyl ester

Chapter 1

Introduction

Chapter 1 Introduction

1.1 Resolving Energy Demand Issues

The increase of the public awareness about Global Warming along with the increasing prices of energy have stimulated the developed countries to follow new regulations in energy production, putting into consideration renewable energy as an alternative to the conventional energy production systems represented by crude oil, coal, fossil fuel and natural gas operated energy resources.[1-3] Environmentally friendly energy systems are required to reduce the emission of the greenhouse gas by harnessing clean energy sources such as hydro, wind and solar powers, in energy production.[4-6] The main feature of the renewable energy systems is that none of these systems release materials that cause environmental pollution during their operation.[7-8] The only disadvantage related to the renewable energy systems is that their operation is dependent on climatic conditions including the weather, this in turn will affect the efficiency by reducing the power energy production causing the lack of the energy demanded.[5, 9-11] This issue can only be solved by producing hybrid systems to enhance the efficiency of the whole system and satisfy the total energy demand.[4-5, 11-12]

1.2 Solar Power

Bacquerel has first discovered the photovoltaic devices operating principle in 1839; he found that photocurrent that can be produced when illuminating a platinum electrode covered with silver bromide or silver chloride in acidic solutions.[15] Among the different energy resources available currently, solar power is the most clean energy resource with zero-carbon emissions and full dependence on the sun which produces an amount of energy of about 3.86×10^{26} Joule per second.[13] The early silicon-based p-n junction solar cell device was reported by Chapin and co-workers in 1954. The total power conversion efficiency has reached 6%.[14] In 2009, Martin has produced a silicon-based solar cell with an efficiency of 25%.[15] The advantages of silicon-based solar cells are the availability of the raw materials, high efficiency and the stability of these devices over long times. However, some drawbacks should be taken into consideration such as the thickness of the material needed to make the device in addition to other disadvantages such the loss caused by reflection and the incomplete absorption.[16-17] The most important disadvantage is the elevated cost of manufacturing the silicon-based wafers and the type of silicon used in these devices.[18] These disadvantages have induced the scientist to increase their efforts towards improving the photovoltaic devices by the modification of the solar cell models into a more complicated structure to help harvesting more solar energy directly from the sunlight.[19]

The need for a high efficient solar cell device based on organic photovoltaic materials has emerged due to many features in contrast to the inorganic carbon-neutral solar cell devices.

These features are represented by the low cost and flexibility of organic materials along with the availability of these materials and the efficiency in harvesting a wide range of solar energy operating at even low light intensity.[20]

1.3 Conjugated Polymers

Organic materials are not easily recognized as conductors of electronic charge, and it is known that polymers are often used as insulators in the electronics field. In general, organic polymers with saturated bonds are good insulators due to the tightly-bound bonding orbitals, which lead to localized covalent bonds formation. However, organic polymers which have extended π-orbital systems are behaving differently; π-electron molecular orbital formation is coming from the substantial electronic delocalization of p_z-orbitals within the repeating unit, this type of polymers called 'conjugated polymers', can be considered as semiconductors.[21] These polymers have electronic energy levels which are different from those in inorganic semiconductors. However, both organic and inorganic semiconductors have bands with organized electrons in discrete levels. Both organic and inorganic semiconductors have energy bands either completely full or completely empty.[22-24] The existence of $2p_z$-orbitals overlap with the neighbouring carbon atoms can lead to the extension of π-bonds along the polymer backbone, in addition to the delocalization of electrons in polymer chains. Most of the conjugated polymers studies were based on Shirakawa's discovery, which was the semiconducting properties in polyacetylene; this polymer was prepared through the interaction between acetylene gas and the Ziegler-Natta initiator.[25] Heeger and MacDiarmid were able to show that polymers of this type can be chemically doped with different electron acceptors such as iodine and AsF_5, which increased the conductivity values for this polymer at room temperature to reach 1000 S/cm.[26] Figure (1-1) below shows the most commonly studied conjugated polymers.

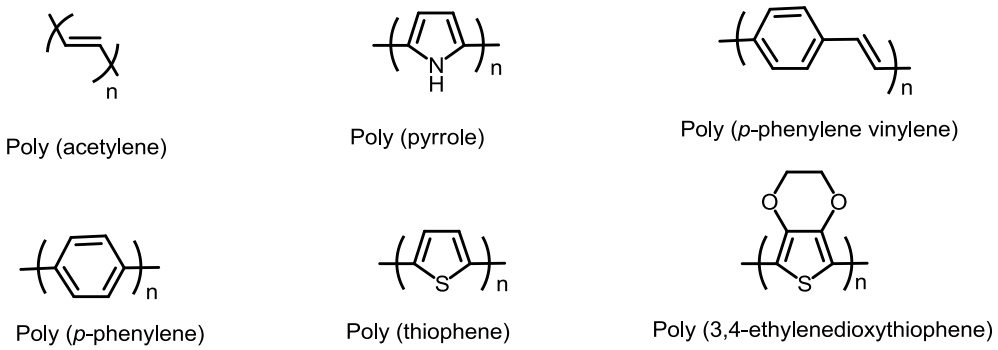

Figure 1-1: Commonly studied conjugated polymers.

The chemical structure of conjugated polymers consists of alternating single-double bonds along the polymer chains. π –bonds supporting electrons are delocalized over the molecule itself. Polyaniline can be considered as a conjugated polymer, where the p_z-orbital on the

nitrogen atom supports the delocalization of π-electrons.[27] In some conjugated polymers such as polyacetylene, the delocalization of the electrons is leading to a single (degenerate) ground state, whereas the common conjugated polymers with single-double bonds alternation give electronic structures with different energy levels. The behaviour of conjugated polymers can be changed dramatically through the chemical doping process. In general, some conjugated polymers can be oxidized partially such as polypyrrole, to produce materials called 'p-doped materials'.[27] Oxidation of poly pyrrole is shown in figure (1-2) below:

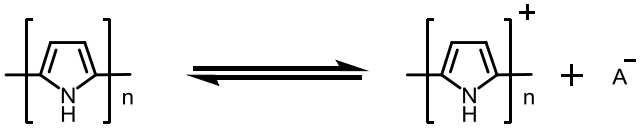

Figure 1-2: Poly pyrrole oxidation.

The molecular structure of conjugated polymers is responsible for the band gap E_g, oxidation potentials, and the position of the lowest unoccupied molecular orbital (LUMO) and the highest occupied molecular orbital (HOMO). The limited states around (LUMO) and (HOMO) levels can result in electronic and optical properties of π-conjugated polymers. The band theory illustrated that the valence band is the highest occupied band that originates from (HOMO) of each repeating unit in the polymer backbone. The conduction band is the lowest unoccupied band that originates from (LUMO) of repeating units. Figure (1-3) shows the schematic transformation of bands in conjugated polymers during the monomer addition. The bandgap (E_g) depends on (ΔE) the distance between (HOMO) and (LUMO) energy levels of the monomers and the band width W(β), which represents a hybridization function (β) of monomer levels in the polymer.[28] The bandgap of conjugated polymer can be measured by the optical absorption spectrum. Low bandgap conjugated polymers need to be designed and measured in the long wavelength infrared (IR) region.[29]

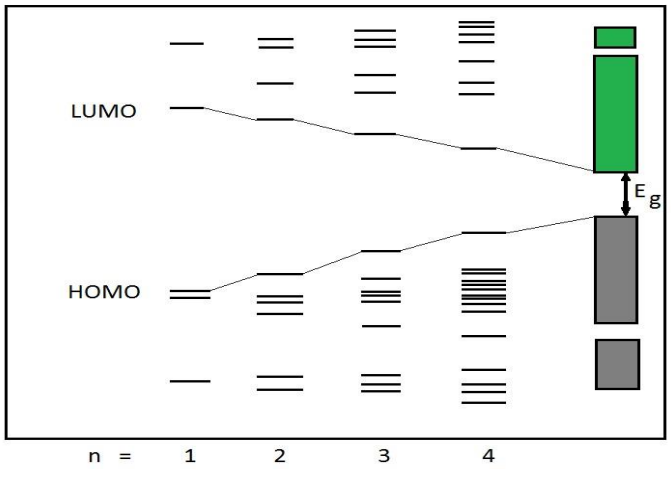

Figure 1-3: Bandgap formation during polymerisation process of π-conjugated polymers.

The enhancement of the conduction band thermal population can result in low E_g values and low bandgap; this will increase the charge carriers' number intrinsically. Moreover, the stabilization of the corresponding doped state results from the lower oxidation potential, which is associated with the low bandgaps. As a result, controlling the bandgap (E_g) in conjugated polymers is an important factor in producing materials that are technologically useful.[30]

1.4 Solubility of Conjugated Polymers

The solubility of conjugated polymers depends on six different factors. These factors are; the degree of polymerization, the number of carbons on the aliphatic group side chain, polarity of substituents, polymer backbone rigidity, the regioregularity of the polymer and the interaction forces between species in the same polymer.[31] The rigid structure of most organic conjugated polymers prevents these polymers from being soluble in common organic solvents, but this issue can be solved by adding functional side groups to the polymer structure such as alkyl or alkoxy groups[32] See figure (1-4).

Soluble conjugated polymers can be converted into thin films by one of the following techniques; roll-to-roll printing technique,[33] spin-coating technique,[34-35] ink-jet printing technique,[36-38] and screen-printing technique.[39-41] The bandgap of conjugated polymers can be modified according to the technology used by changing the molecular structure of the repeating unit.[42-43]

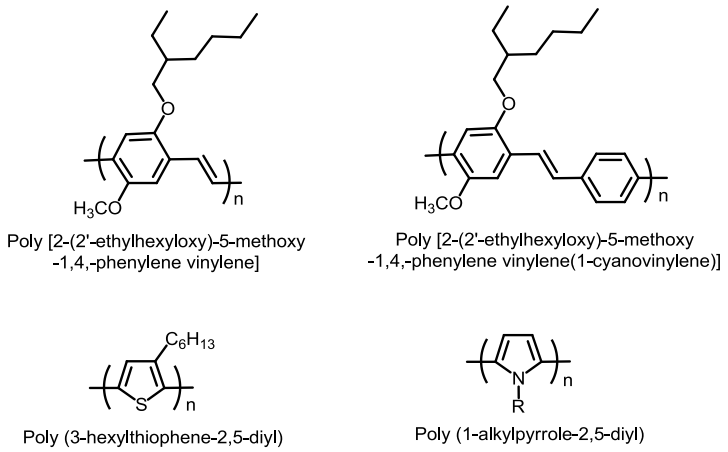

Figure 1-4: Conjugated polymers soluble in common organic solvents.

1.5 Conduction Process

Materials can be classified according to their conductivity into three main types; insulators, semiconductors and conductors. This classification is based on the energy difference between the (HOMO) and (LUMO) levels in each material. The energy difference refers to the bandgap E_g, and this is equal to the energy needed to free an electron from the outer

shell to give a 'mobile charge carrier'. Figure (1-5) shows materials bandgaps based on their conductivity. The bandgap for metals is equal to 0 eV according to the overlap between the conduction band and the valence band. Insulators have a bandgap greater than 3.0 eV. Finally, the bandgap for the semiconductors is less than 3.0 eV, which offers a good opportunity to the electrons in the valence band to be promoted through the different excitation ways.[44]

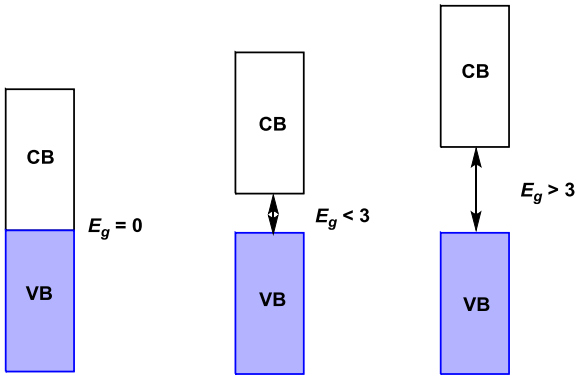

Figure 1-5: Schematic representation of the three types of materials according to their bandgap.

Conjugated polymers can be modified using one of the chemical doping methods (p doping or n doping). The band structure of polymers is modified with lower energy transitions formation and charge carrier creation (polarons and bipolarons) shown in figure (1-6) below. Charge carriers are responsible of increasing polymers conductivity.[45] π-π* transitions in conjugated polymers is characterized by λ_{max}, conjugated polymers' bandgap can be determined from the transition π-π* in neutral polymers.[46]

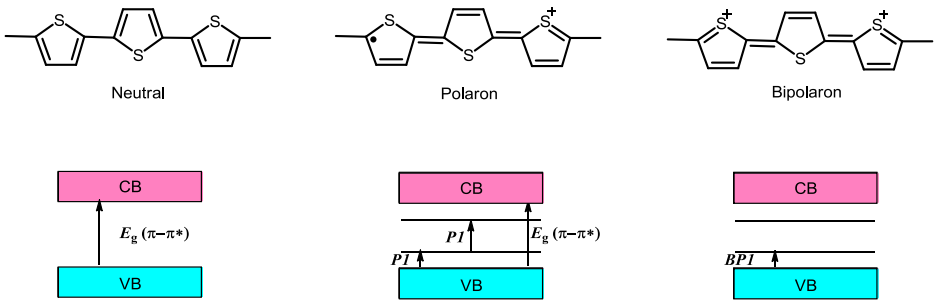

Figure 1-6: Allowed transitions of neutral, polaron and bipolaron thiophene trimers.

1.6 Conductivity in Conjugated Polymers

Full delocalization of electrons does not really take place over the whole conjugated polymer backbone. The reason behind that is that σ-bond and π-bond do not have the same length in reality. It is real that each carbon atom has an unpaired electron, which carbon atom can contributes in, to form a delocalization state, which in turn can increase the stability of the conjugated system.[47] Polymer can switch between two main states[48], see figure (1-7). In

polyacetylene as an example, these states can be degenerate and non-degenerate in conjugated aromatic systems (PPV and PPP as examples).[49-50]

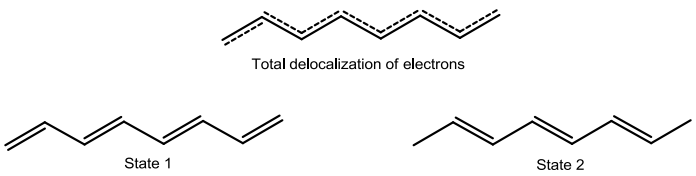

Figure 1-7: Two degenerate states of trans-polyacetylene.

There are some strategies that have been followed in order to lower the bandgap in conjugated polymers. The insertion of aromatic rings into the polymer chains to relax the bonds' length between σ-π bonds alternation. This method is also useful in increasing the electrons' delocalization due to the existence of π-electron network extension, and thus resists the Peierls effect.[51] The delocalization of π-electrons makes all conjugated polymers have semiconducting properties, and supports charge carriers as well. For better energy harvesting from solar spectrum, new conjugated polymers have been synthesized, particularly in the region between 1.4-1.9 eV.[52] The band theory explained that the increase in conductivity is either as a result of removing electrons with an oxidizing agent from the valence band (VB) with a positive charge left behind, or donating electrons to the empty conduction band (CB) by using reducing agents.[53-54] These two processes represent n-type doping and p-type doping (figure 1-8).

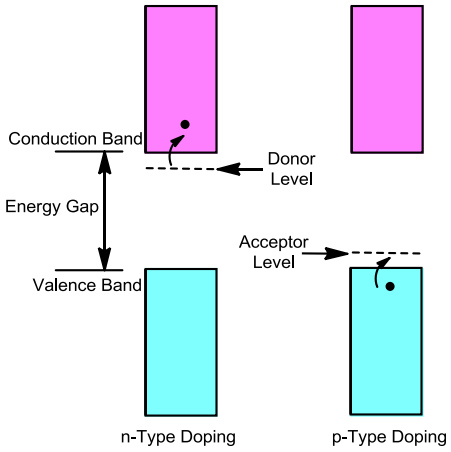

Figure 1-8: Addition of electrons to the conduction band (n-type doping) and removing electrons from valence band (p-type doping.

In these two cases, polymer conductivity is expected to occur by the free spins' movement, which is associated to the unpaired electrons, and these free spins already exist in either valence (oxidation) band or conduction (reduction) band. This seems analogous to the inorganic semiconductors doping process, in which the formation of occupied donor levels is formed below the conduction band.

The excitation of an electron can easily take place at room temperature from valence band (p-type doping) to the empty impurity level. In (n-type doping), the electron is excited from the impurity level to the conduction band.[55]

Using reduction or oxidation processes in conjugated polymers' doping generates radical cations or anions, which are known as polarons. Negative polaron is created by reduction process with one unpaired electron and one pair of electrons in the high-energy negative polaron state. In oxidation process, one electron is promoted to the new energy level between the valence and conduction bands. Another electron transfer can follow with the creation of a dianion or dication, which is called in this case (bipolaron).[55]

1.7 Conjugated Polymers' Polymerization Methods

The synthesis of conjugated polymers can be done using many different routes. There are common methods of polymerization categorized into three main types; oxidation routes, metal-catalysed routes and condensation polymerization. The description of some of these methods is shown below:

1.7.1 Metal-catalysed Polymerisation Route

To prepare conjugated polymers in metal-catalysed polymerization, nickel and palladium are often used metals. The mechanisms of the metal-catalysed reactions are similar in the three steps: the oxidative addition, the transmetalation and the reductive elimination. The subsections below are examples on this type of polymerization:

1.7.1.1 Stille Cross-coupling

This type of polymerization involves the reaction of an organic halide with an organostannane. The catalyst used in this reaction is Pd(0).[56] The general equation of this polymerization is shown in equation (1-1) below:

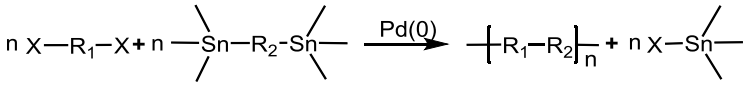

Equation 1-1: Conjugated copolymer formation via stille cross-coupling reaction.

The Stille coupling reaction has a four steps mechanism[57-58], shown in scheme (1-1) below, which consists of the oxidative addition step, the transmetalation step, the isomerisation step and the reductive elimination step.[59-60]

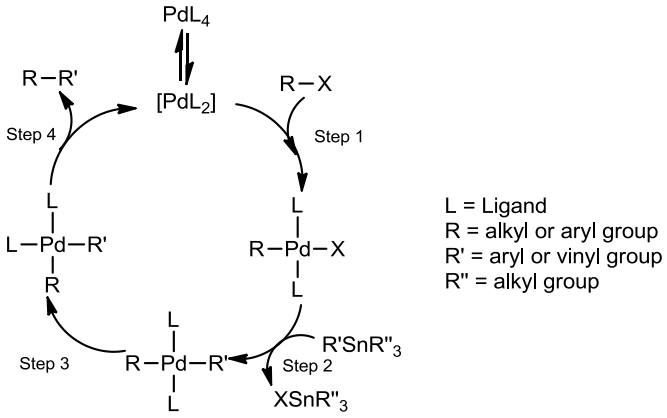

Scheme 1-1: Stille cross-coupling reaction mechanism.

1.7.1.2 Suzuki Cross-coupling

This type of polymerization uses palladium Pd(0) as a catalyst for the reaction between the acid derivatives[61] or aryl boronic esters[62-63] with aryl halides. This reaction is commonly used in copolymerization of multi-functional group's species.[64-66] Figure (1-9) shows the monomers' structures used in Suzuki cross-coupling reaction.

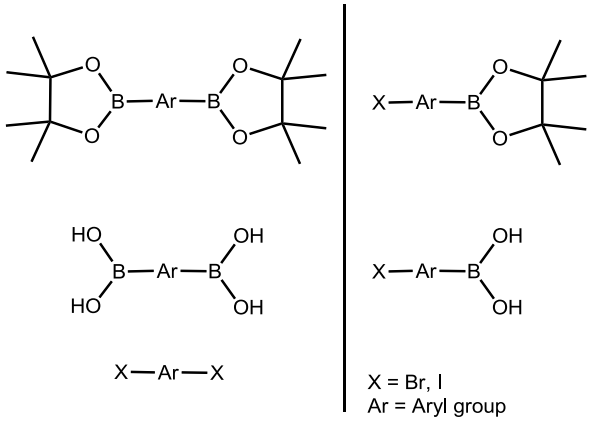

Figure 1-9: Monomers' structures used in Suzuki cross-coupling.

The four steps mechanism of Suzuki cross-coupling includes: the oxidative addition of palladium (0) to the halide forming organo-palladium (II) species (first step). This step is followed by the formation of the intermediate (second step) via the reaction between organo-palladium species and the base, trans-metalation with boronic ester which gives a complex of palladium (II) (third step). The cycleof the reaction is completed by the reductive elimination of towards product (fourth step).

1.7.1.3 Direct (Hetero) Arylation DHA

This type of polymerisation is used in many organic synthesis reactions including conjugated materials and pharmaceuticals.[67] The reaction can be conducted using a catalyst with a transition metal such as palladium to couple two aromatic rings together forming a C-C

bond.[68] One of the aromatic rings is substituted with a halogen, while the other is a simple aromatic ring C-H.[69-70] The mechanism of this reaction suggests that oxidative coupling reaction is taking place during the coupling process; a suitable base is required to neutralize the formed acid during this reaction. The direct (hetero) arylation reaction mechanism is shown in scheme (1-2) below:

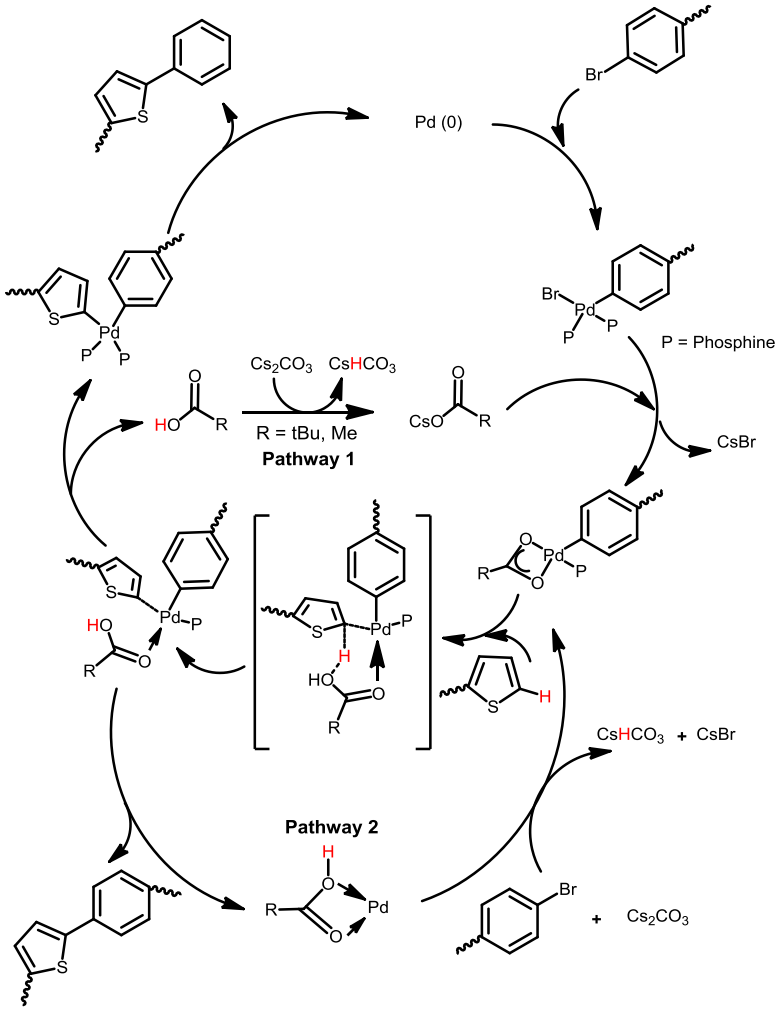

Scheme 1-2: Proposed mechanism of direct (hetero) arylation reaction.

1.8 Applications of Conjugated Polymers

Conjugated polymers in their non-doped state are intrinsic semiconductors. In fact, the bandgap of these polymers depends on two main factors; the conjugated backbone chemical constitution and the type of the substituent attached to the polymer's main chain. As a result, conjugated polymers can be good alternatives to the inorganic semiconductors due to the ease of processing.[71] The following paragraphs describe the most significant applications of conjugated polymers:

1.8.1 Field Effect Transistors

Field effect transistors were first made of organic materials in 1970. Since that time, great efforts were made to develop this device to be used in many applications in electronic devices.[72] Many features in conjugated polymers such as high charge mobility, process-ability and low-cost make conjugated polymers good candidates for field effect transistors. Conjugated polymers can play a main role in replacing the traditional amorphous silicon, which was used earlier in these devices with heating requirement of above 350 °C. The organic field effect transistor OFET consists of a thin layer of the organic semiconductor as an active layer placed between two electrodes (drain and source), these are insulated from a third electrode called (gate electrode) which changes the conductivity in both drain and source electrodes to limit the flow of the current required between these electrodes.[73] The organic active layer plays the main role in the performance of OFET devices. This explains the requirement of high charge carrier mobilities in the organic polymers in these devices. Conjugated polymers with linear chains and aromatic rings such as thiophene or benzene molecules are often used in OFET devices due to their high charge carrier or charge mobility. Stability and solubility of conjugated polymers used in OFET are very important for device processing.[74] Organic field transistor structure is shown in figure (1-10) below.

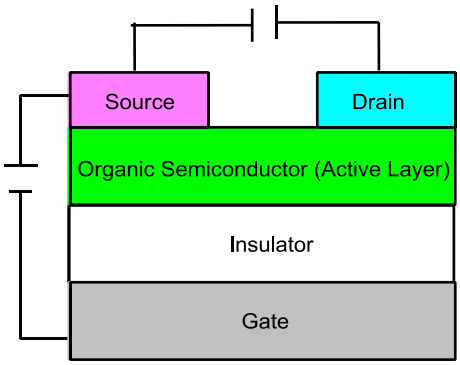

Figure 1-10: Structure of organic field effect transistor OFET.

1.8.2 Light-Emitting Diodes

Electroluminescence in organic materials such as conjugated polymers has stimulated the researchers to pay attention on developing conjugated polymer-based light emitting diodes OLEDs. Pope and co-workers have first reported the electroluminescence of anthracene crystals at voltages 400 V or above.[75] Since that time, many approaches were conducted by deploying the lifetime and quantum efficiency to develop new light emitting diodes. Two decades later, Tang and co-workers have managed to fabricate a new electroluminescence device with multi organic layers. The result of this approach shows that small voltages of 10 V or less are enough to operate a high quantum efficiency stable device.[76] Conjugated polymers were first used as active materials in LEDs by Burroughs *et al*.[77] Conjugated

polymers used in light emitting diodes must have high quantum efficiency.[78] A simple LED device structure is consisted of a thin film of conjugated polymer placed between two electrodes; anode (hole injection electrode) (generally made of ITO), which should be placed on a transparent layer such as glass or plastic, substrate should have a high work function (Φ). Cathode (electron injection electrode) is made of a metal which has a low work function (Φ) such as (Al or Ca).[79] Figure (1-11) shows a schematic structure of the single-layer polymer light-emitting diode (PLED).

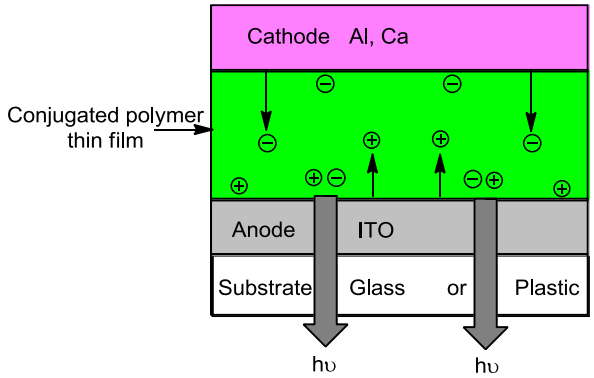

Figure 1-11: Schematic structure of a single-layer polymer light-emitting diode (PLED).

The PLED device is called an electroluminescence device because it shows non-linear *J-V* characteristics typical of diodes, which means that no current flows above and below this onset up to the given voltage and with the voltage increase, the current will increase quickly. Simply, the operation of the PLED is described as follows: charge carriers, i.e. electrons and holes are injected to the conjugated polymer from cathode and anode respectively. Electrons are introduced to the conduction band (π*) LUMO level, while holes are injected into the valence band (π) HOMO level. Figure (1-12) shows the band diagram of a single-layer PLED.[80-81]

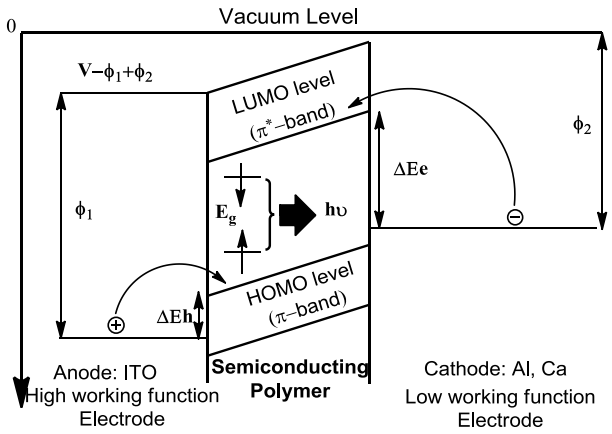

Figure 1-12: Band diagram of a single-layer PLED.

1.8 Organic Photovoltaics (OPVs)

Photocurrent in inorganic materials was first discovered by Bacquerel. Since that time, these materials were used in solar cells. Silicon as an inorganic semiconductor was used in solar cells with nearly 25% efficiency. [82] However, developing organic based solar cells is still in progress and full efficiency has not been met yet. Organic solar cells have shown short lifetimes and low efficiencies in the period between 1980 and 1990.[83] Compared to other technologies, low efficiencies obtained from organic solar cells. In the last two decades, power conversion efficiency have been clearly improved and the efficiencies recently reached above 13%.[84] In addition, many advantages are coming with organic solar cells, such as flexible substrate, high processing speed, low cost and most importantly, those organic solar cells have no emissions when operated. Synthesising polymers that absorb light with wavelength above 600 nm were studied extensively for organic solar cells use. To achieve higher values of power conversion efficiency PCE, solar cell devices need to harvest a large fraction of the solar photon flux, see figure (1-13).

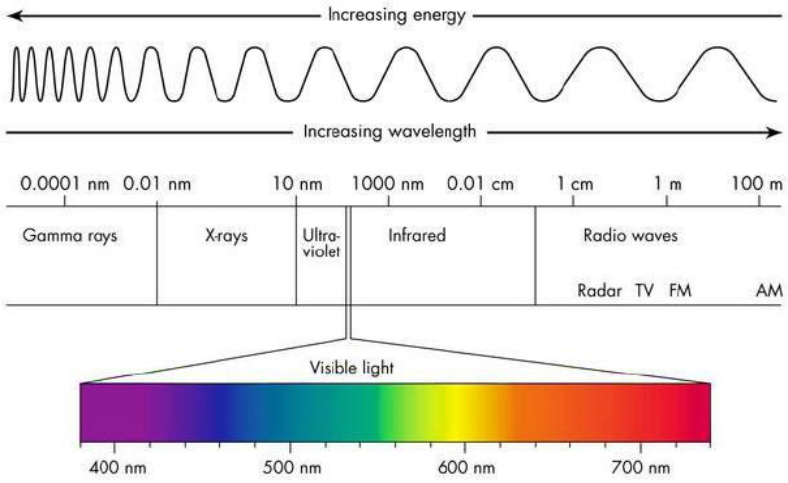

Figure 1-13: Electromagnetic spectrum diagram.

New low bandgap polymers that are able to absorb light with longer wavelength are required. Only low bandgap polymers can achieve higher PCE. Many studies have been implemented in order to extend the electronic conjugation in polymers and synthesise materials with a low bandgap that absorb light with longer wavelengths. The structural modifications of the polymer can be used to control the energy bandgap; including the modifications by polymerisation to induce quinoid structures along the polymer backbone. The planar structure of quinoid leads to more electronic conjugated systems with lower bandgaps.[85]

1.9 Conjugated Polymer- Based Organic Solar Cells

There are two points that must be considered when designing conjugated polymers for application in solar cells. First, these materials must be able to harvest energy at wavelength above 600 nm, which means to absorb sunlight and produce charges. Second, is the ability to transfer these charges.[34] These two points are correlated to the delocalized system of π-bonds, which in turn will lead to the semiconducting behaviour in conjugated polymers. Blending conjugated polymer with a fullerene derivative such as $PC_{71}BM$ will enhance the solar cell device efficiency.[86] Figure (1-14) shows some fullerene derivatives used in the fabrication of OPV devices.

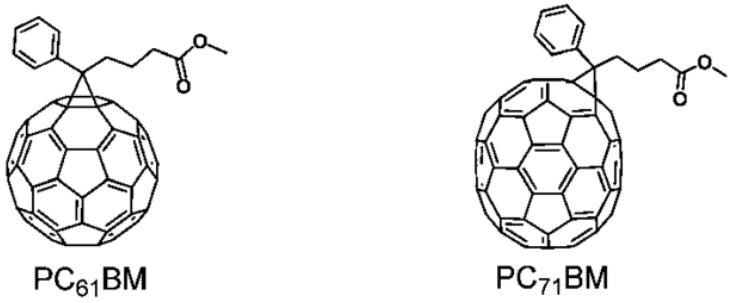

Figure 1-14: Fullerene derivatives used in OPV solar cells fabrication.

Solubilising groups are added to fullerene derivatives to solve the issue of the low solubility in these materials. It is important to observe the electron transfer from the donor (conjugated polymer) to the acceptor (fullerene derivative) which is occurring in a range of femtosecond (fs), this was determined using ultrafast spectroscopy. This speed is faster than the recombination process, which contributes in lowering the total power conversion efficiency (PCE) of the organic solar cells. The fast electron movement between the fullerene molecules and the interfacial area will slow the recombination process rate.[87]

Many approaches to developing new BHJ solar cells by mixing fullerene derivatives (electron deficient) moieties with conjugated polymers (electron rich) moieties have resulted in improving the total power conversion efficiencies.[88-90] It has been reported that combining fullerene derivatives with conjugated polymers not only will lower the conjugated polymer's bandgap through introducing new energy levels according to the molecular orbital theory (MOT), but also will significantly improve the charge carrier mobility by reducing the distance of π-π interchain stacking.[91-93]

1.9.1 Organic Photovoltaics Working Principle

The generation of photocurrent in organic photovoltaics can be illustrated in figure (1-15) below. The process consists of four stages: first, light absorption by the organic active layer

to create excitons. The second stage involves the exciton dissociation from the organic active layer forming free charges. The third stage is the charge transport under the effect of the electric field. Finally, charges will be collected by anode and cathode.[94] Electric field is required to separate the electron hole pair, which is supplied by the difference of the work functions of anode and cathode (high work function material as the anode and low work function as the cathode).[95] It is important to refer that designing D-A conjugated polymers for solar cell application should consider the morphology of the interfacial area in which the electron-hole charge separation is taking place and to avoid the barrier of the interfacial potential.[96]

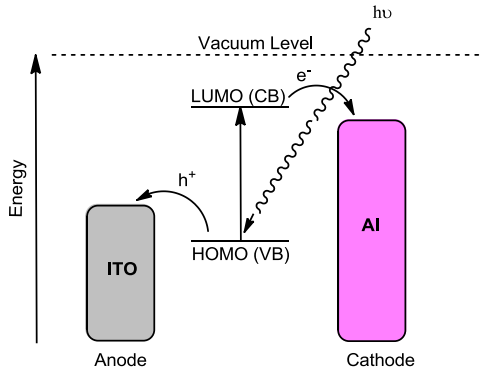

Figure 1-15: Light conversion into electricity current in a single-layer solar cell.

Blending the organic conjugated polymer as a donor with suitable fullerene derivative as an acceptor in a bilayer device has many advantages in designing D-A polymers with different bandgaps, which in turn controls the sensitivity to solar energy represented by photons in the visible range of spectrum.[95] When the organic active layer in a bilayer device absorbs sunlight, an exciton will form. The split of the formed exciton results in an electron-hole formation, leading to the electron transfer from the donor's LUMO to the acceptor's LUMO as depicted in figure (1-16) below:

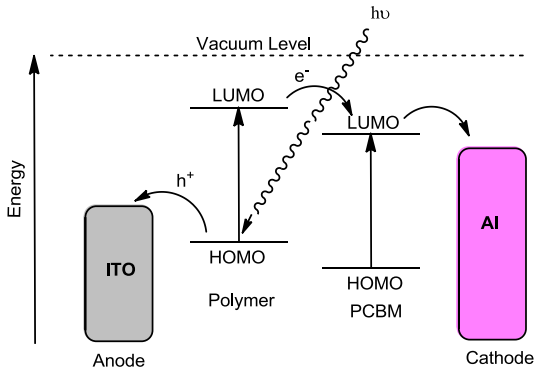

Figure 1-16: Light conversion into electricity current in BHJ solar cell.

1.9.2 Organic Photovoltaic device architectures

Making organic solar cells requires two main important criteria; first, the ability of the organic semiconductor in absorbing light and producing charge carrier mobility. Second, the organic semiconductor should be able to transfer the formed charges to produce electrical current. These requirements are connected to the delocalized system of the π-bonds within the organic semiconductor, which results in the semiconducting properties in the organic material. There are different architectures based on the active layer placement within the solar cell device as shown in the next paragraphs:

1.9.2.1 Single layer device

The single layer device is the simplest structure of organic solar cells, in which the organic semiconductor is placed between two electrodes. The first electrode is the anode which is a glass or quartz substrate coated with indium tin oxide (ITO), and the second electrode is the cathode which is made of calcium or aluminium as shown in figure (1-17) below.[97-98] The first organic single layer solar cell device was reported in the 1980's uses polyacetylene and polythiophenes as the active layer placed between two different electrodes. This device showed a PCE value of nearly 1%. The main issue with this model is that the light is not completely absorbed by the active layer, which makes the photocurrent generated very low.[97-99]

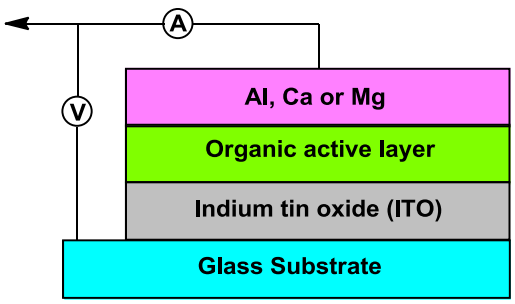

Figure 1-17: Schematic structure of the single layer device solar cell.

1.9.2.2 Bilayer devices

Figure (1-18) shows a schematic structure of the bilayer solar cell device. In this device, the organic active layer and the acceptor layer are stacked together and placed between the anode and cathode. The interfacial area between acceptor and donor can help the dissociation of electron from donor's excited state[100-102]. Because of the 10-20 nm distances between the active layer and the interface, only few excitons can reach the interfacial area and a small portion of the absorbed photons will be able to lead the exciton charge separation. Due to this, lower quantum efficiencies will result from the bilayer device.[103] To

obtain high conversion of absorbed light into photovoltage, electron-hole pairs have to be created at the normal diffusion distance from the interfacial area which is 10 nm.[104-105]

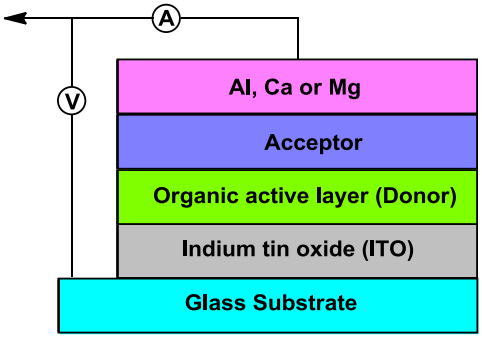

Figure 1-18: Structure of the bilayer device solar cell.

1.9.2.3 Bulk Heterojunction devices

A bulk heterojunction is defined as blending the acceptor and the donor together in the solar cell device active layer forming an interpenetrating network structure.[106-109] The idea of blending the donor and the acceptor is to increase the interfacial area which leads to increase of the charge generation and charge carrier mobility.[108] The formed excitons will travel for short distances to reach the interfacial area; this is considered as a solution to the recombination of the charges in the bilayer devices.[107]

The active layer in this type of solar cell devices is fabricated by casting films from a solution of the fullerene derivative (as electron acceptor) and the conjugated polymer (as electron donor). [31] To obtain high power conversion efficiencies, there are some important requirements to consider. First, the morphology of the active layer, and the process of active layer casting including spin-coating or solvent-casting.[110] Second, using thermally stable conjugated polymers is essential to avoid the aggregation that could happen during the annealing process.[111-112] Third, controlling the blending ratio of both conjugated polymer and the acceptor in the active layer to yield a high efficiency.[113] Figure (1-19) shows a schematic structure of the bulk heterojunction solar cell device.

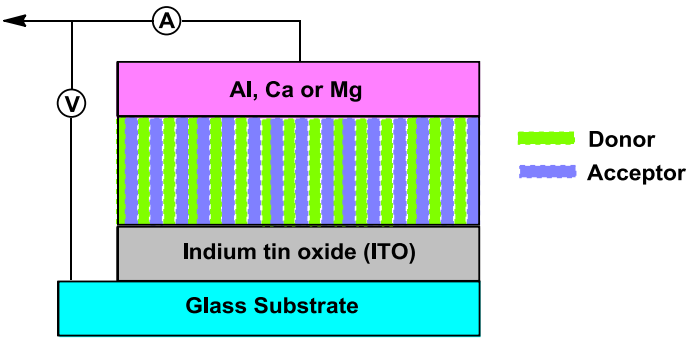

Figure 1-19: Structure of BHJ solar cell device.

1.9.3 Bandgap Engineering in Conjugated Polymers

Numerous studies have intensively focused on designing new low bandgap polymers for better results in organic photovoltaics. There are some important factors that can play the main role in affecting the bandgap of the synthesized polymer, these include; the alternation of the donor and acceptor, the effect of resonance, the effect of the substituents and the alternation bond length.[31, 114]

Introducing different electron-withdrawing and electron-donating substituents into the polymer's backbone, such as fluorine atoms, can play a main role in tuning the bandgap of the polymer not only by stabilising the HOMO and LUMO of the conjugated polymer, but also in improving the hole mobility. Fluorine atoms can affect the intra and/or inter-molecular interactions through the non-covalent interactions, which in turn will give more planar structure leading to enhanced π-π stacking of the polymer chains as shown in figure (1-20) below.[115-117]

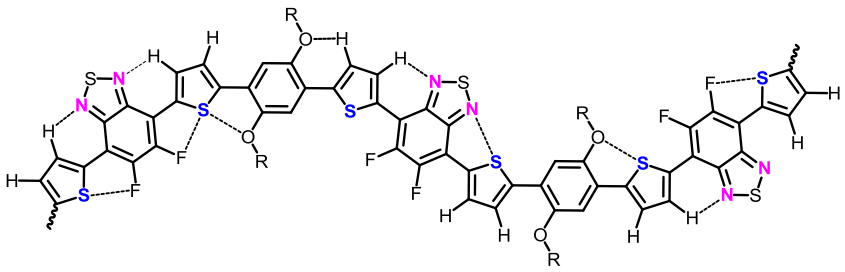

Figure 1-20: Non-covalent interaction within the conjugated polymer chain.

The use of π-conjugated polymers is closely linked to their low bandgap energy. The main structure of the conjugated polymers' backbone is made of aromatic rings; these rings show two different resonance states: the aromatic resonance state and the quinoid resonance state. The latter state is known to have less stability than the aromatic state, so it has a lower bandgap. However, more electronic delocalisation results from the quinoid structure as it is destroying the aromatic configuration of the polymer's backbone. [31, 118-119] An example on the aromatic, quinoid resonance structures and the bandgap are depicted in figure (1-21)[118, 120] below.

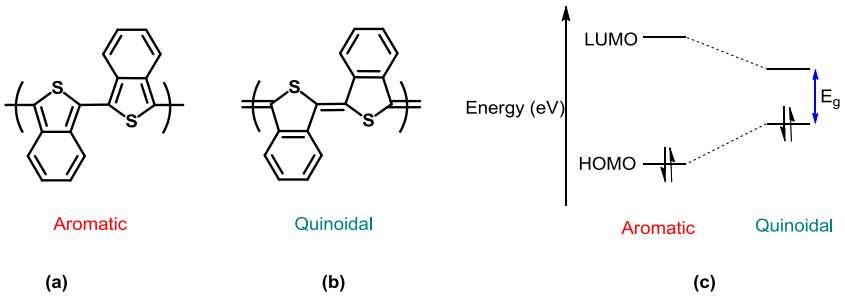

Figure 1-21: (a) Aromatic resonance structure. **(b)** Quinoidal resonance structure. **(c)** Energy bandgap difference between the two states.

Copolymerising donor and acceptor moieties together, known as D-A polymers, is to extend the π-system within the polymer chains.[121] This alternation between the donor and the acceptor will increase the delocalization of the π electrons through forming the quinoid structure along the polymer chain leading to a lower bandgap.[31] Moreover, the intermolecular charge transfer (ICT) between the LUMO of the acceptor and the HOMO of the donor is responsible of lowering the overall polymer's bandgap. The molecular orbital theory (MOT) gives a clear explanation of how the bandgap in D-A polymer is lowered through the formation of new HOMO and LUMO levels in the resulted D-A polymer as shown in figure (1-22) below.[31] The valence band will be broadened due to the interaction of the levels with low energy. In the same way, the LUMO levels for both acceptor and the donor will overlap to increase the conduction band magnitude after the electrons distribution on the new molecular energy levels.[114, 122] The difference between LUMO levels of both donor and acceptor is represented by ΔE, and the ideal ΔE in BHJ devices is 0.3 eV to enable the charge separation process.[123] Polymers with low bandgaps are required in BHJ devices, lowering the bandgap will result in higher power conversion efficiency values obtained.

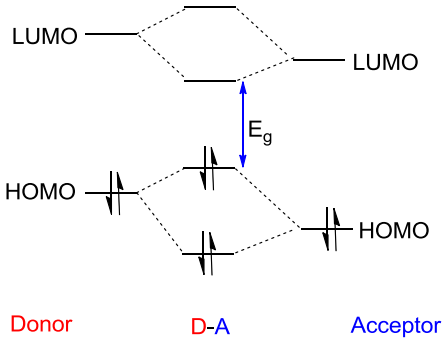

Figure 1-22: New energy levels formed after the copolymerisation of donor and acceptor monomers.

There are basic rules in designing conjugated polymers for solar cell applications including the energy gap difference between the LUMO levels of the donor and the fullerene derivative which must be around 0.3 eV, and higher energy gap will cause energy loss within the active layer of the BHJ solar cell (Figure 1-23).[123]

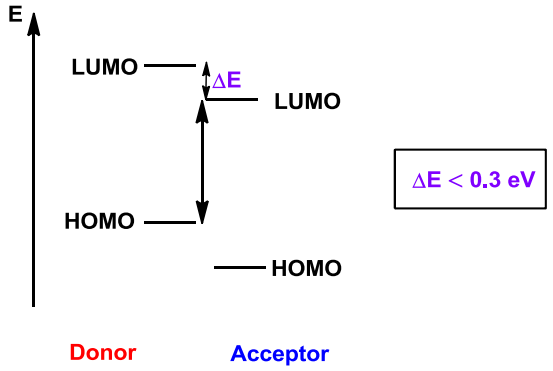

Figure 1-23: Energy levels of donor and acceptor showing the required offset energy.

Most importantly, the design of new conjugated polymers should follow the calculation principle of the Konarka efficiency map to check the possible power conversion efficiency obtained from the LUMO level of the donor and the bandgap of the polymer calculated by the cyclic voltammetry as shown in figure (1-24) below.[124] the anticipation from this map illustrates that obtaining a PCE of 10% is possible in BHJ devices using a blend of a donor and fullerene acceptor with energy difference of 0.3 eV between their LUMO levels.[124]

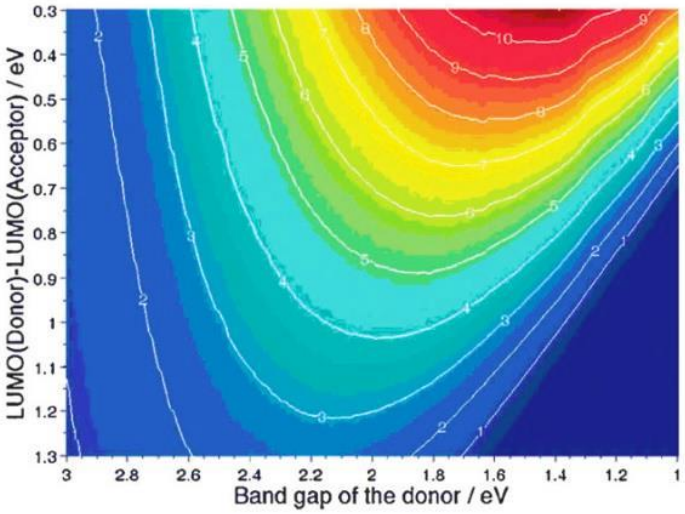

Figure 1-24: Konarka efficiency map for conjugated polymers.

1.9.4 Organic Solar Cell Characteristics

The performance of organic solar cells is determined by power conversion efficiency PCE%, which is dependent on several important parameters; these include, open circuit voltage V_{oc}, short current circuit density J_{sc} and fill factor FF.[83, 121] The relationship between these parameters can be explained via the *J-V* characteristic shown in figure (1-25) where the device is tested under both illuminated and dark conditions. The standard device operating

conditions also include air mass (AM1.5) and an intensity of solar light 100 W/cm^2 at room temperature 25°C. These conditions are the standard laboratory testing conditions.[125-126]

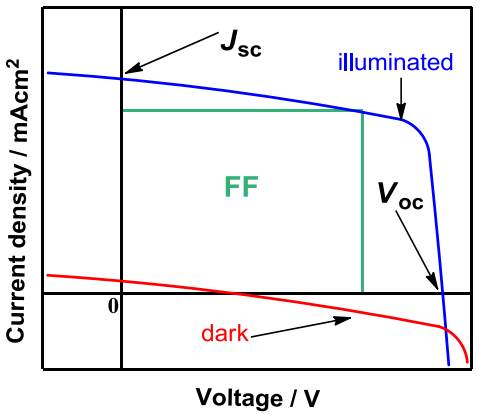

Figure 1-25: Current-voltage *J-V* characteristics curve under dark and illuminated conditions.

The overall efficiency of the organic BHJ device is calculated based on the given equation:

$$PCE = V_{oc} \times J_{sc} \times FF / I_{light}$$

Where I_{light} represents the incident solar radiation. V_{oc} is measured in V, I_{light} and FF are measured in W/m^2. Under the standard AM1.5, PCE of the solar cell device is calculated using the following equation:

$$PCE_{AM1.5} = (P_{out} / P_{in})\, M = (V_{oc} \times J_{sc} / P_{in})\, M$$

Where P_{out} is the output current of the BHJ device under illumination, P_{in} is the incident light intensity calculated by the reference-calibrated cell. *M* is the mismatch factor of the spectral deviations.[83]

Short circuit current density J_{sc} is the maximum electrical current flow out of the BHJ device when no voltage is applied between the anode and cathode.[127] This is due to the built-in electric field resulting from the work-function differences of both anode and cathode materials. The J_{sc} is highly dependent on the charge mobility of the blend used in BHJ device fabrication, and the active layer morphology plays the main role affecting the latter. Solvent selection is also important in improving the morphology of the active layer. Casting an active layer of MDMO-PPV: PCBM from chlorobenzene solution showed an improved morphology with horizontal dimensions of 0.1 µm compared to the toluene-cast active layer with horizontal dimensions of 0.5 µm.[83]

Open circuit voltage V_{oc} can be defined as the maximum device voltage at which no current flows within the photovoltaic device. This characteristic is correlated to the material distinction between the n-type LUMO and the p-type HOMO.[121, 127] The exciton dissociation

to form free charge carriers requires an energy difference of about 0.3 eV between the LUMO of the donor and the LUMO of the acceptor. High Value of V_{oc} can be seen in polymers with lower HOMO levels, but low-lying HOMO levels would also increase the J_{sc} value through increasing the bandgap of the polymer. According to the literature, active layer morphology can affect the value of V_{oc}.[83, 128] Noteworthy, V_{oc} will decrease with the temperature increase due to the high mobility of the free charges and the recombination processes.[129-130]

Fill Factor FF is identified as the maximum output power collected from the photovoltaic device. This characteristic explains the ability of extracting the charge carriers from the solar cell device. It can also be defined as the rectangular area in the current-voltage *J-V* plot, which is perpendicular on the two other characteristics V_{oc} and J_{sc} in the plot.[131-134] Fill factor is affected by different factors including the active layer thickness, the electrode efficiency in collecting free charges and the area of the solar cell device.[135-136]

Fill factor FF is important to understand the mechanism of the solar cells for different materials. Both *J-V* plot and FF provide information about the material used in solar cell fabrication.

1.10 Features of Aromatic Compounds Used as Donors or Acceptors in Conjugated Polymers

Fused rings were extensively used as donor units in D-A conjugated polymers for use in electronic devices. The use of aromatic fused rings is important to control the HOMO level and the energy bandgap of the targeted conjugated polymers.[128] Molecules such as **naphthtalene**, **anthracene** and **pyrene** offer a planar structure; they also enrich the π-conjugated system in conjugated polymer with electrons. The existence of these moieties in the polymer will play a main role in the morphology of this polymer by enhancing the crystalline structure through the van-der-Waals interactions.[137] Examples of naphthalene, anthracene and pyrene-based conjugated polymers are depicted in figure (1-26) below. Kwon and co-workers[138] have synthesized **PENTBT** which is a D-A conjugated polymer of 1,5-dialkoxy-2,6-napthalene-diyl with BTD-based acceptor, this polymer has shown both optical and electrochemical bandgaps of 1.75 eV. HOMO level of this naphthalene-based polymer is -5.42 eV. An example on the using 9,10-disubstituted anthracene unit as a donor unit is the polymer **PPATBT** synthesized by Almeataq *et al*.[139] This polymer has a HOMO level of -5.44 eV, the optical and the electrochemical bandgaps were 1.84 and 2.23 eV respectively. Yang and co-workers have synthesized a pyrene-based conjugated polymer **P(DTPP-alt-1,6-PY)**.[140] The optical properties of this polymer have shown a bandgap of 1.65 eV, while the electrochemical bandgap was 1.84 eV.

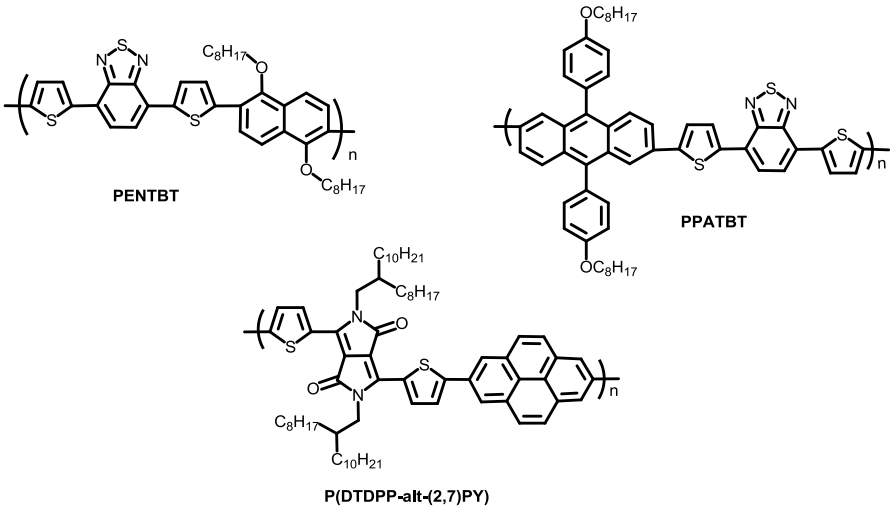

Figure 1-26: Examples on naphthalene, anthracene and pyrene-based conjugated polymers.

Carbazole and **fluorene** as electron-rich units were also widely used in conjugated polymers, carbazole as a fluorene like structural counterpart is only different by the nitrogen atom in its central pyrrole ring.[141] These aromatic units are of high importance due to their chemical and physical properties when used in conjugated polymers. Using fluorene or carbazole in a conjugated polymer will result in improving the hole-mobility due to the high-ordered chemical structure and their chemical and thermal stability.[128, 142-143] The planar structure of these units will help in reducing the steric hindrance between the polymer chains. Furthermore, the solubility of the conjugated polymers containing carbazole or fluorene units can be enhanced by attaching alkyl chains to the 9-position of these units.[144]

Goker and co-workers have synthesized four conjugated polymers **PSBSC, PSBSFL, PFBFC** and **PFBFFL**.[145] These polymers contain carbazole and fluorene donor units polymerized with different benzooxadiazole derivatives as shown in figure (1-27) below.

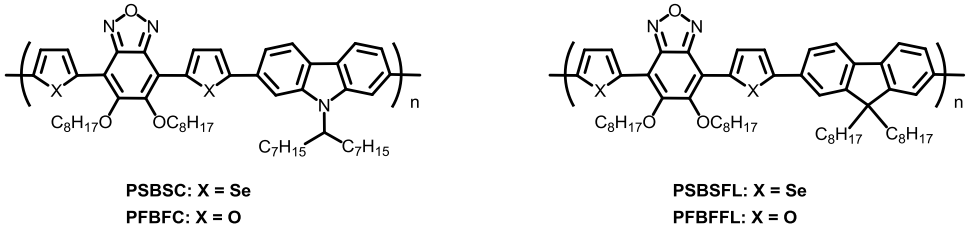

Figure 1-27: Carbazole and fluorene conjugated polymers synthesized by Goker *et al*.

The optical properties of the synthesized polymer have shown optical bandgaps for **PSBSC, PSBSFL, PFBFC** and **PFBFFL** of about 1.98, 1.95, 1.88 and 2.07 eV respectively. Deep HOMO levels were noticed when measured by cyclic voltammetry due to the incorporation of the carbazole and fluorene electron-rich units. The electrochemical bandgaps were 2.04,

2.15, 2.18 and 2.02 eV respectively. The highest PCE% was noticed in polymer **PFBFC** with power conversion efficiency of about 1.89%.

Benzothiadiazole: BTD is one of the most attractive electron acceptor units used in conjugated polymers synthesis for the application in electronic devices.[146-149] The BTD molecule has a high electron affinity and functionalisation features.[150] BTD is considered as a building block towards narrow bandgap D-A conjugated polymers, especially when this molecule flanked by two thiophene side units to form a D-A-D monomer which in turn results in low bandgap when used in π-conjugated polymers synthesis.[151-152] The electron-accepting ability of BTD is weaker than other electron-acceptor molecules. Due to the rigid structure of BTD, branched alkyl chain is attached to the backbone to increase the solubility and obtaining high molecular weights in the resulting conjugated polymers. It is important to note that modification of the molecular structure is crucial to enhance the accepting properties of conjugated polymers for solar cell applications. Many studies on conjugated polymers were conducted using BTD as an acceptor. The synthesis of **PCDTBT** by Blouin *et al*. by the reaction of a BTD derivative with a 9-substituted carbazole as a donor moiety gave a polymer that is thermally stable showing an optical bandgap of 1.88 eV and a PCE of 3.6%. Figure (1-28) below shows the chemical structure of **PCDTBT**.[153]

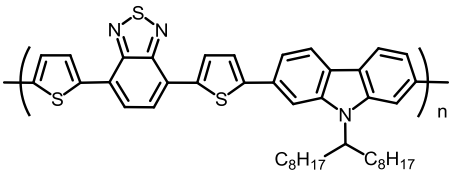

PCDTBT

Figure 1-28: Chemical Structure of **PCDTBT**.

Other approaches in using fluorinated BTD as an electron acceptor were reported.[154-156] Luke *et al*. has studied the effect of the fluorination on the conjugated polymers **PCDTffBT**, **PCffDTBT** and **PCffDTffBT**.[157] These polymers possess high thermal stability (above 350 °C) and optical bandgaps of 1.86, 1.82 and 1.88 respectively. The effect of the fluorine atoms incorporation on the polymers morphology is clear, especially on **PCffDTffBT** as more fluorine atoms are attached to the polymer's backbone. This resulted in ordered structure and π-π stacking due to the Coulomb interactions caused by the intermolecular interactions between polymer chains.[157] Figure (1-29) below shows the chemical structure of **PCDTffBT**, **PCffDTBT** and **PCffDTffBT.**

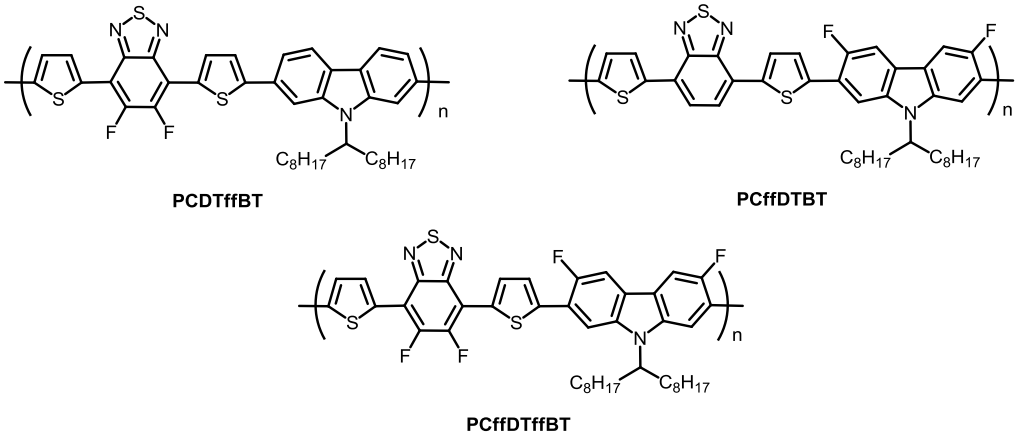

Figure 1-29: Chemical structure of some fluorinated polymers.

1.11 Aims and Objectives

The increased demand of energy along with the Global Warming caused by greenhouse gases prompted researchers to search for new renewable energy systems including wind-powered turbines, hydro-power systems and solar cells. These systems will significantly lower the emissions of the harmful gases and satisfy the energy demand. Inorganic solar cells, which are the conventional devices have good efficiencies but are still produced at high costs due to the high temperature used in their processing. Organic solar cells as alternatives offer many advantages, including cost-effective materials, flexibility when processed and light weight. Moreover, it is possible to improve the chemical structure of the active materials to obtain higher PCE values. Organic BHJ devices based on blends of electron donor and acceptor were extensively studied during the last decades, and efficiencies with a PCE of above 13% have been achieved. The BHJ devices are not commercially available yet, and still under investigation. Researchers are exploring different chemical structure to obtain better results; obstacles such as low solar absorption of BHJ devices are common where only 70% of the solar flux is been absorbed, which means that they are not very efficient in sunlight harvesting. Another issue is the electron-hole recombination, which reduces the total output energy of the organic solar cells. Improvements within BHJ devices are required to make the organic solar cells more effective. First, the optical bandgap should be in the range of (1.2-1.9 eV). Second, the LUMO energy levels of the conjugated polymer and the fullerene acceptor have to be controlled to enhance the charge separation and reduce the energy loss. Third, when mixed with each other, the active layer of conjugated polymer and fullerene should have a high V_{oc} based on a low HOMO level of the conjugated polymer. Fourth, solubility of the materials is very important for both processing and solution casting. Finally, good hole-mobility is required to increase the charge transport along the active layer. The morphology of the D-A configuration in BHJ devices can also affect the charge mobility in devices if there is an enhanced π-π stacking between polymer chains.

In this thesis, we are motivated to enhance the optical and electrochemical properties of conjugated polymers for the application in photovoltaic devices; this can be done by designing and synthesising novel series of D-A copolymers based on benzothiadiazole BTD as an acceptor with different donor monomer units and compare the physical and chemical properties of the resulting copolymers. Although polymers based on BTD were widely covered in the literature,[158-160] fluorine atoms substitution of the BTD moiety was targeted in this work to study the effects of the incorporation of these atoms on the physical and the electrochemical behaviour of the targeted conjugated polymers. Polymers with non-fluorinated BTD acceptor units were also prepared in order to compare with fluorinated

polymers. To improve the solubility of the targeted D-A copolymers, branched alkyl chains are attached to the backbone of each polymer as solubilising groups. These groups are also useful to obtain high molecular weight of the conjugated polymers. As a result, the morphology of these polymers will be investigated from two main aspects; the incorporation of fluorine atoms and attaching branched solubilising groups. Fluorine can play a main role in ordering the chemical structure of polymer to be more planar through the interaction between atoms with different electronegativity values. It has been hypothesized that fluorine can improve the crystalline morphology in conjugated polymers through the non-covalent Coulomb interactions with hydrogen, oxygen and sulfur.[155]

The concept of conjugated polymers is based on the electron density distribution of π-bond electrons along the backbone of the polymer due to the alternation of π bonds. It could be also useful to extend the π-delocalized system either on the donor or the acceptor moieties through adding additional thiophene units to these molecules and compare the optical and the electrochemical properties of the extended system polymers to the polymers with less conjugation. The more aromatic units attached the more electron density within the polymer chain. As a result, lower bandgap conjugated polymer, more charge carriers and high PCE values, with respect to the extent in which the conjugation is broken due to the twist of the aromatic units within polymer chains.

The aims of this work are to prepare and investigate the properties of a series of D-A copolymers using donor units incorporating planar aromatic rings of different sizes such as: naphthalene, anthracene, pyrene, carbazole, fluorene and bithiophene respectively, these units are flanked by thiophene units to extend the π-conjugated system. These donor units will be copolymerised with fluorinated or non-fluorinated BTD units to investigate the optical and the electrochemical properties and will also be compared with their analogous copolymers. Donor units were mainly functionalised with solubilising groups to increase the solubility and in turn the molecular weight of the resulting polymers.

Chapter 1 References

1. Erdinc, O.; Uzunoglu, M., Optimum design of hybrid renewable energy systems: Overview of different approaches. *Renewable and Sustainable Energy Reviews* **2012,** *16* (3), 1412-1425.
2. Goedecke, M.; Therdthianwong, S.; Gheewala, S. H., Life cycle cost analysis of alternative vehicles and fuels in Thailand. *Energy Policy* **2007,** *35* (6), 3236-3246.
3. Straatman, P. J.; Van Sark, W. G., A new hybrid ocean thermal energy conversion–Offshore solar pond (OTEC–OSP) design: A cost optimization approach. *Solar Energy* **2008,** *82* (6), 520-527.
4. Shaahid, S.; Elhadidy, M., Technical and economic assessment of grid-independent hybrid photovoltaic–diesel–battery power systems for commercial loads in desert environments. *Renewable and sustainable energy reviews* **2007,** *11* (8), 1794-1810.
5. Zhou, W.; Lou, C.; Li, Z.; Lu, L.; Yang, H., Current status of research on optimum sizing of stand-alone hybrid solar–wind power generation systems. *Applied Energy* **2010,** *87* (2), 380-389.
6. Kornelakis, A., Multiobjective particle swarm optimization for the optimal design of photovoltaic grid-connected systems. *Solar Energy* **2010,** *84* (12), 2022-2033.
7. Nayar, C.; Islam, S.; Dehbonei, H.; Tan, K.; Sharma, H., Power electronics for renewable energy sources. In *Power Electronics Handbook (Third Edition)*, Elsevier: 2011; pp 723-766.
8. Hepbasli, A., A key review on exergetic analysis and assessment of renewable energy resources for a sustainable future. *Renewable and sustainable energy reviews* **2008,** *12* (3), 593-661.
9. Al-Alawi, A.; Al-Alawi, S. M.; Islam, S. M., Predictive control of an integrated PV-diesel water and power supply system using an artificial neural network. *Renewable energy* **2007,** *32* (8), 1426-1439.
10. Yang, H.; Lu, L.; Zhou, W., A novel optimization sizing model for hybrid solar-wind power generation system. *Solar energy* **2007,** *81* (1), 76-84.
11. Chen, F.; Duic, N.; Alves, L. M.; da Graça Carvalho, M., Renewislands—Renewable energy solutions for islands. *Renewable and Sustainable Energy Reviews* **2007,** *11* (8), 1888-1902.
12. Ekren, O.; Ekren, B. Y., Size optimization of a PV/wind hybrid energy conversion system with battery storage using simulated annealing. *Applied Energy* **2010,** *87* (2), 592-598.
13. Facchetti, A., π-Conjugated polymers for organic electronics and photovoltaic cell applications. *Chemistry of Materials* **2010,** *23* (3), 733-758.
14. Chapin, D. M.; Fuller, C.; Pearson, G., A new silicon p-n junction photocell for converting solar radiation into electrical power. *Journal of Applied Physics* **1954,** *25* (5), 676-677.
15. Becquerel, M. E., Memoire sur les Effets Electriques Produits sous l'Influence des Rayons Solaires. *Comptes Rendus Hebdomadaires des Seances de L'Academie des Sciences* **1839,** *9*, 561-567.
16. Prince, M.; Wolf, M., New developments in silicon photovoltaic devices. *Journal of the British Institution of Radio Engineers* **1958,** *18* (10), 583-594.
17. Moon, P., Proposed standard solar-radiation curves for engineering use. *Journal of the Franklin Institute* **1940,** *230* (5), 583-617.
18. Goetzberger, A.; Knobloch, J.; Voss, B., Crystalline silicon solar cells. *editorial John Wiley & Sons Ltd* **1998,** *1*.

19. Wolf, M., Limitations and possibilities for improvement of photovoltaic solar energy converters: Part I: Considerations for earth's surface operation. *Proceedings of the IRE* **1960,** *48* (7), 1246-1263.
20. Liang, Y.; Xu, Z.; Xia, J.; Tsai, S. T.; Wu, Y.; Li, G.; Ray, C.; Yu, L., For the bright future—bulk heterojunction polymer solar cells with power conversion efficiency of 7.4%. *Advanced materials* **2010,** *22* (20), E135-E138.
21. Lennard-Jones, J. E., The electronic structure of some polyenes and aromatic molecules I–The nature of the links by the method of molecular orbitals. *Proc. R. Soc. Lond. A* **1937,** *158* (894), 280-296.
22. Stenger-Smith, J. D., Intrinsically electrically conducting polymers. Synthesis, characterization, and their applications. *Progress in Polymer Science* **1998,** *23* (1), 57-79.
23. Nalwa, H. S., *Handbook of organic conductive molecules and polymers*. Wiley: 1997.
24. Salzner, U.; Lagowski, J.; Pickup, P.; Poirier, R., Comparison of geometries and electronic structures of polyacetylene, polyborole, polycyclopentadiene, polypyrrole, polyfuran, polysilole, polyphosphole, polythiophene, polyselenophene and polytellurophene. *Synthetic Metals* **1998,** *96* (3), 177-189.
25. Ito, T.; Shirakawa, H.; Ikeda, S., Simultaneous polymerization and formation of polyacetylene film on the surface of concentrated soluble Ziegler-type catalyst solution. *Journal of polymer science: polymer chemistry edition* **1974,** *12* (1), 11-20.
26. Chiang, C. K.; Fincher Jr, C.; Park, Y. W.; Heeger, A. J.; Shirakawa, H.; Louis, E. J.; Gau, S. C.; MacDiarmid, A. G., Electrical conductivity in doped polyacetylene. *Physical review letters* **1977,** *39* (17), 1098.
27. Wallace, G. G., Conjugated polymers: New materials for photovoltaics. *Chemical Innovation* **2000,** *30*, 14.
28. Roncali, J., Synthetic principles for bandgap control in linear π-conjugated systems. *Chemical reviews* **1997,** *97* (1), 173-206.
29. Ajayaghosh, A., Donor–acceptor type low band gap polymers: polysquaraines and related systems. *Chemical Society Reviews* **2003,** *32* (4), 181-191.
30. Tolbert, L. M., Solitons in a box: the organic chemistry of electrically conducting polyenes. *Accounts of chemical research* **1992,** *25* (12), 561-568.
31. Cheng, Y.-J.; Yang, S.-H.; Hsu, C.-S., Synthesis of conjugated polymers for organic solar cell applications. *Chemical reviews* **2009,** *109* (11), 5868-5923.
32. Katz, E.; Gevorgyan, S.; Orynbayev, M.; Krebs, F. C., Out-door testing and long-term stability of plastic solar cells. *The European Physical Journal-Applied Physics* **2006,** *36* (3), 307-311.
33. Knobloch, A.; Manuelli, A.; Bernds, A.; Clemens, W., Fully printed integrated circuits from solution processable polymers. *Journal of applied physics* **2004,** *96* (4), 2286-2291.
34. Wang, G.; Moses, D.; Heeger, A. J.; Zhang, H.-M.; Narasimhan, M.; Demaray, R., Poly (3-hexylthiophene) field-effect transistors with high dielectric constant gate insulator. *Journal of Applied Physics* **2004,** *95* (1), 316-322.
35. Friend, R.; Gymer, R.; Holmes, A.; Burroughes, J.; Marks, R.; Taliani, C.; Bradley, D.; Dos Santos, D.; Bredas, J.; Lögdlund, M., Electroluminescence in conjugated polymers. *Nature* **1999,** *397* (6715), 121.
36. Chang, S.-C.; Bharathan, J.; Yang, Y.; Helgeson, R.; Wudl, F.; Ramey, M. B.; Reynolds, J. R., Dual-color polymer light-emitting pixels processed by hybrid inkjet printing. *Applied physics letters* **1998,** *73* (18), 2561-2563.

37. Hebner, T.; Wu, C.; Marcy, D.; Lu, M.; Sturm, J., Ink-jet printing of doped polymers for organic light emitting devices. *Applied Physics Letters* **1998,** *72* (5), 519-521.
38. Chang, S. C.; Liu, J.; Bharathan, J.; Yang, Y.; Onohara, J.; Kido, J., Multicolor organic light-emitting diodes processed by hybrid inkjet printing. *Advanced Materials* **1999,** *11* (9), 734-737.
39. Pschenitzka, F.; Sturm, J., Three-color organic light-emitting diodes patterned by masked dye diffusion. *Applied physics letters* **1999,** *74* (13), 1913-1915.
40. Rogers, J. A.; Bao, Z.; Raju, V., Nonphotolithographic fabrication of organic transistors with micron feature sizes. *Applied physics letters* **1998,** *72* (21), 2716-2718.
41. Shaheen, S. E.; Radspinner, R.; Peyghambarian, N.; Jabbour, G. E., Fabrication of bulk heterojunction plastic solar cells by screen printing. *Applied Physics Letters* **2001,** *79* (18), 2996-2998.
42. Reyes-Reyes, M.; Kim, K.; Dewald, J.; López-Sandoval, R.; Avadhanula, A.; Curran, S.; Carroll, D. L., Meso-structure formation for enhanced organic photovoltaic cells. *Organic letters* **2005,** *7* (26), 5749-5752.
43. Lu, H.-H.; Liu, C.-Y.; Jen, T.-H.; Liao, J.-L.; Tseng, H.-E.; Huang, C.-W.; Hung, M.-C.; Chen, S.-A., Excimer Formation by Electric Field Induction and Side Chain Motion Assistance in Polyfluorenes. *Macromolecules* **2005,** *38* (26), 10829-10835.
44. Thomas, C. A. Donor-Acceptor methods for band gap reduction in conjugated polymers: the role of electron rich donor heterocycles. University of Florida, 2002.
45. Argun, A. A.; Aubert, P.-H.; Thompson, B. C.; Schwendeman, I.; Gaupp, C. L.; Hwang, J.; Pinto, N. J.; Tanner, D. B.; MacDiarmid, A. G.; Reynolds, J. R., Multicolored electrochromism in polymers: structures and devices. *Chemistry of Materials* **2004,** *16* (23), 4401-4412.
46. Dyer, A. L.; Reynolds, J. R., Electrochromism of conjugated conducting polymers. *Handbook of Conducting Polymers* **2007,** *1*, 1-63.
47. Singh, A. K.; Prakash, R. In *Conduction mechanism in electronic polymers: Effect of morphology*, Advanced Optoelectronic Materials and Devices, 2008. AOMD 2008. 2nd National Workshop on, IEEE: 2008; pp 65-74.
48. Gustafsson, G.; Inganäs, O.; Nilsson, J.; Liedberg, B., Thermal undoping in poly (3-alkylthiophenes). *Synthetic metals* **1988,** *26* (3), 297-309.
49. Naarmann, H.; Theophilou, N., New process for the production of metal-like, stable polyacetylene. *Synthetic Metals* **1987,** *22* (1), 1-8.
50. Druy, M.; Rubner, M.; Walsh, S., An experimental approach towards the synthesis and characterization of environmentally stable conducting polymers. *Synthetic metals* **1986,** *13* (1-3), 207-217.
51. Admassie, S.; Inganäs, O.; Mammo, W.; Perzon, E.; Andersson, M. R., Electrochemical and optical studies of the band gaps of alternating polyfluorene copolymers. *Synthetic metals* **2006,** *156* (7-8), 614-623.
52. Grigore, L.; Petty, M., Polyaniline films deposited by anodic polymerization: Properties and applications to chemical sensing. *Journal of Materials Science: Materials in Electronics* **2003,** *14* (5-7), 389-392.
53. Fukuda, M.; Sawada, K.; Yoshino, K., Synthesis of fusible and soluble conducting polyfluorene derivatives and their characteristics. *Journal of Polymer Science Part A: Polymer Chemistry* **1993,** *31* (10), 2465-2471.
54. Longo, C.; De Paoli, M.-A., Dye-sensitized solar cells: a successful combination of materials. *Journal of the Brazilian Chemical Society* **2003,** *14* (6), 898-901.

55. Chance, R. R.; Bredas, J.; Silbey, R., Bipolaron transport in doped conjugated polymers. *Physical Review B* **1984,** *29* (8), 4491.
56. Stille, J. K., The palladium-catalyzed cross-coupling reactions of organotin reagents with organic electrophiles [new synthetic methods (58)]. *Angewandte Chemie International Edition in English* **1986,** *25* (6), 508-524.
57. Casado, A. L.; Espinet, P., Mechanism of the Stille reaction. 1. The transmetalation step. Coupling of R1I and R2SnBu3 catalyzed by trans-[PdR1IL2](R1= C6Cl2F3; R2= vinyl, 4-methoxyphenyl; L= AsPh3). *Journal of the American Chemical Society* **1998,** *120* (35), 8978-8985.
58. Adam, S.-Y. L.; Dai, W.-C., A facile and highly efficient sonochemical synthesis of organostannane via Barbier reaction. *Tetrahedron* **1997,** *53* (3), 859-868.
59. Casado, A. L.; Espinet, P., On the configuration resulting from oxidative addition of RX to Pd (PPh3) 4 and the mechanism of the cis-to-trans isomerization of [PdRX (PPh3) 2] complexes (R= aryl, X= halide). *Organometallics* **1998,** *17* (5), 954-959.
60. Littke, A. F.; Fu, G. C., The First General Method for Stille Cross-Couplings of Aryl Chlorides. *Angewandte Chemie International Edition* **1999,** *38* (16), 2411-2413.
61. Morin, J.-F.; Leclerc, M., 2, 7-Carbazole-based conjugated polymers for blue, green, and red light emission. *Macromolecules* **2002,** *35* (22), 8413-8417.
62. Yu, W.-L.; Cao, Y.; Pei, J.; Huang, W.; Heeger, A. J., Blue polymer light-emitting diodes from poly (9, 9-dihexylfluorene-alt-co-2, 5-didecyloxy-para-phenylene). *Applied physics letters* **1999,** *75* (21), 3270-3272.
63. Liu, B.; Yu, W.-L.; Lai, Y.-H.; Huang, W., Blue-light-emitting fluorene-based polymers with tunable electronic properties. *Chemistry of materials* **2001,** *13* (6), 1984-1991.
64. Miyaura, N.; Suzuki, A., Palladium-catalyzed cross-coupling reactions of organoboron compounds. *Chemical reviews* **1995,** *95* (7), 2457-2483.
65. Miura, Y.; Oka, H.; Morita, M., Syntheses and Characterization of Poly (1, 3-phenylene-2-amino-1, 3-phenylene) s and Dimer and Tetramer Model Compounds. *Macromolecules* **1998,** *31* (7), 2041-2046.
66. Ding, J.; Tao, Y.; Day, M.; Roovers, J.; D'Iorio, M., Electrochemical and fluorescent properties of alternating copolymers of 9, 9-dioctylfluorene and oxadiazole as blue electroluminescent and electron transport materials. *Journal of Optics A: Pure and Applied Optics* **2002,** *4* (6), S267.
67. Mercier, L. G.; Leclerc, M., Direct (hetero) arylation: a new tool for polymer chemists. *Accounts of chemical research* **2013,** *46* (7), 1597-1605.
68. Ackermann, L., Carboxylate-assisted transition-metal-catalyzed C− H bond functionalizations: mechanism and scope. *Chemical reviews* **2011,** *111* (3), 1315-1345.
69. Alberico, D.; Scott, M. E.; Lautens, M., Aryl− aryl bond formation by transition-metal-catalyzed direct arylation. *Chemical reviews* **2007,** *107* (1), 174-238.
70. Lyons, T. W.; Sanford, M. S., Palladium-catalyzed ligand-directed C− H functionalization reactions. *Chemical reviews* **2010,** *110* (2), 1147-1169.
71. Yamamoto, T.; Zhou, Z.-h.; Kanbara, T.; Shimura, M.; Kizu, K.; Maruyama, T.; Nakamura, Y.; Fukuda, T.; Lee, B.-L.; Ooba, N., π-conjugated donor− acceptor copolymers constituted of π-excessive and π-deficient arylene units. Optical and electrochemical properties in relation to CT structure of the polymer. *Journal of the American Chemical Society* **1996,** *118* (43), 10389-10399.
72. Horowitz, G., Organic field-effect transistors. *Advanced materials* **1998,** *10* (5), 365-377.
73. Di, C.-a.; Yu, G.; Liu, Y.; Zhu, D., High-performance organic field-effect transistors: Molecular design, device fabrication, and physical properties. ACS Publications: 2007.

74. Allard, S.; Forster, M.; Souharce, B.; Thiem, H.; Scherf, U., Organic semiconductors for solution-processable field-effect transistors (OFETs). *Angewandte Chemie International Edition* **2008,** *47* (22), 4070-4098.
75. Pope, M.; Kallmann, H.; Magnante, P., Electroluminescence in organic crystals. *The Journal of Chemical Physics* **1963,** *38* (8), 2042-2043.
76. Tang, C. W.; VanSlyke, S. A.; Chen, C., Electroluminescence of doped organic thin films. *Journal of Applied Physics* **1989,** *65* (9), 3610-3616.
77. Burroughes, J.; Bradley, D.; Brown, A.; Marks, R.; Mackay, K.; Friend, R.; Burns, P.; Holmes, A., Light-emitting diodes based on conjugated polymers. *nature* **1990,** *347* (6293), 539.
78. Gustafsson, G.; Cao, Y.; Treacy, G.; Klavetter, F.; Colaneri, N.; Heeger, A., Flexible light-emitting diodes made from soluble conducting polymers. *Nature* **1992,** *357* (6378), 477.
79. Bernius, M. T.; Inbasekaran, M.; O'Brien, J.; Wu, W., Progress with light-emitting polymers. *Advanced Materials* **2000,** *12* (23), 1737-1750.
80. Kido, J.; Hongawa, K.; Okuyama, K.; Nagai, K., White light-emitting organic electroluminescent devices using the poly (N-vinylcarbazole) emitter layer doped with three fluorescent dyes. *Applied Physics Letters* **1994,** *64* (7), 815-817.
81. Yang, Y.; Pei, Q., Electron injection polymer for polymer light-emitting diodes. *Journal of applied physics* **1995,** *77* (9), 4807-4809.
82. Green, M. A.; Emery, K.; King, D. L.; Igari, S.; Warta, W., Solar cell efficiency tables (version 19). *Progress in Photovoltaics: Research and Applications* **2002,** *10* (1), 55-61.
83. Brabec, C. J., Organic photovoltaics: technology and market. *Solar energy materials and solar cells* **2004,** *83* (2), 273-292.
84. Zhao, W.; Li, S.; Yao, H.; Zhang, S.; Zhang, Y.; Yang, B.; Hou, J., Molecular optimization enables over 13% efficiency in organic solar cells. *Journal of the American Chemical Society* **2017,** *139* (21), 7148-7151.
85. Firouzi, R.; Zahedi, M., Polyacenes electronic properties and their dependence on molecular size. *Journal of Molecular Structure: THEOCHEM* **2008,** *862* (1-3), 7-15.
86. Chen, S.; Du, X.; Ye, G.; Cao, J.; Sun, H.; Xiao, Z.; Ding, L., Thermo-cleavable fullerene materials as buffer layers for efficient polymer solar cells. *Journal of Materials Chemistry A* **2013,** *1* (37), 11170-11176.
87. Wang, G.; Swensen, J.; Moses, D.; Heeger, A. J., Increased mobility from regioregular poly (3-hexylthiophene) field-effect transistors. *Journal of applied physics* **2003,** *93* (10), 6137-6141.
88. He, Z.; Zhong, C.; Su, S.; Xu, M.; Wu, H.; Cao, Y., Enhanced power-conversion efficiency in polymer solar cells using an inverted device structure. *Nature photonics* **2012,** *6* (9), 591.
89. You, J.; Dou, L.; Yoshimura, K.; Kato, T.; Ohya, K.; Moriarty, T.; Emery, K.; Chen, C.-C.; Gao, J.; Li, G., A polymer tandem solar cell with 10.6% power conversion efficiency. *Nature communications* **2013,** *4*, 1446.
90. Lin, Y.; Wang, J.; Zhang, Z. G.; Bai, H.; Li, Y.; Zhu, D.; Zhan, X., An electron acceptor challenging fullerenes for efficient polymer solar cells. *Advanced materials* **2015,** *27* (7), 1170-1174.
91. Bürgi, L.; Turbiez, M.; Pfeiffer, R.; Bienewald, F.; Kirner, H. J.; Winnewisser, C., High-mobility ambipolar near-infrared light-emitting polymer field-effect transistors. *Advanced Materials* **2008,** *20* (11), 2217-2224.

92. Tsao, H. N.; Cho, D. M.; Park, I.; Hansen, M. R.; Mavrinskiy, A.; Yoon, D. Y.; Graf, R.; Pisula, W.; Spiess, H. W.; Müllen, K., Ultrahigh mobility in polymer field-effect transistors by design. *Journal of the American Chemical Society* **2011,** *133* (8), 2605-2612.
93. Li, Y.; Singh, S. P.; Sonar, P., A High Mobility P-Type DPP-Thieno [3, 2-b] thiophene Copolymer for Organic Thin-Film Transistors. *Advanced Materials* **2010,** *22* (43), 4862-4866.
94. Wang, X.; Perzon, E.; Delgado, J. L.; de la Cruz, P.; Zhang, F.; Langa, F.; Andersson, M.; Inganäs, O., Infrared photocurrent spectral response from plastic solar cell with low-band-gap polyfluorene and fullerene derivative. *Applied physics letters* **2004,** *85* (21), 5081-5083.
95. Yu, G.; Heeger, A. J., Charge separation and photovoltaic conversion in polymer composites with internal donor/acceptor heterojunctions. *Journal of Applied Physics* **1995,** *78* (7), 4510-4515.
96. Sariciftci, N.; Braun, D.; Zhang, C.; Srdanov, V.; Heeger, A.; Stucky, G.; Wudl, F., Semiconducting polymer-buckminsterfullerene heterojunctions: Diodes, photodiodes, and photovoltaic cells. *Applied physics letters* **1993,** *62* (6), 585-587.
97. Petritsch, K., *Organic solar cell architectures*. na: 2000.
98. Brabec, C. J.; Shaheen, S. E.; Winder, C.; Sariciftci, N. S.; Denk, P., Effect of LiF/metal electrodes on the performance of plastic solar cells. *Applied physics letters* **2002,** *80* (7), 1288-1290.
99. Glenis, S.; Tourillon, G.; Garnier, F., Influence of the doping on the photovoltaic properties of thin films of poly-3-methylthiophene. *Thin Solid Films* **1986,** *139* (3), 221-231.
100. Peumans, P.; Yakimov, A.; Forrest, S. R., Small molecular weight organic thin-film photodetectors and solar cells. *Journal of Applied Physics* **2003,** *93* (7), 3693-3723.
101. Spanggaard, H.; Krebs, F. C., A brief history of the development of organic and polymeric photovoltaics. *Solar Energy Materials and Solar Cells* **2004,** *83* (2-3), 125-146.
102. Tang, C. W., Two-layer organic photovoltaic cell. *Applied Physics Letters* **1986,** *48* (2), 183-185.
103. Winder, C.; Sariciftci, N. S., Low bandgap polymers for photon harvesting in bulk heterojunction solar cells. *Journal of Materials Chemistry* **2004,** *14* (7), 1077-1086.
104. Rand, B. P.; Peumans, P.; Forrest, S. R., Long-range absorption enhancement in organic tandem thin-film solar cells containing silver nanoclusters. *Journal of Applied Physics* **2004,** *96* (12), 7519-7526.
105. Peumans, P.; Forrest, S., Very-high-efficiency double-heterostructure copper phthalocyanine/C 60 photovoltaic cells. *Applied Physics Letters* **2001,** *79* (1), 126-128.
106. Schilinsky, P.; Waldauf, C.; Brabec, C. J., Recombination and loss analysis in polythiophene based bulk heterojunction photodetectors. *Applied Physics Letters* **2002,** *81* (20), 3885-3887.
107. Tessler, N.; Denton, G.; Friend, R., Lasing from conjugated-polymer microcavities. *Nature* **1996,** *382* (6593), 695.
108. Graupner, W.; Leising, G.; Lanzani, G.; Nisoli, M.; De Silvestri, S.; Scherf, U., Femtosecond relaxation of photoexcitations in a poly (para-phenylene)-type ladder polymer. *Physical review letters* **1996,** *76* (5), 847.
109. Hide, F.; Diaz-Garcia, M. A.; Schwartz, B. J.; Andersson, M. R.; Pei, Q.; Heeger, A. J., Semiconducting polymers: a new class of solid-state laser materials. *Science* **1996,** *273* (5283), 1833-1836.

110. Ma, W.; Yang, C.; Gong, X.; Lee, K.; Heeger, A. J., Thermally stable, efficient polymer solar cells with nanoscale control of the interpenetrating network morphology. *Advanced Functional Materials* **2005,** *15* (10), 1617-1622.
111. Bartelt, J. A.; Beiley, Z. M.; Hoke, E. T.; Mateker, W. R.; Douglas, J. D.; Collins, B. A.; Tumbleston, J. R.; Graham, K. R.; Amassian, A.; Ade, H., The importance of fullerene percolation in the mixed regions of polymer–fullerene bulk heterojunction solar cells. *Advanced Energy Materials* **2013,** *3* (3), 364-374.
112. Liu, Y.; Zhao, J.; Li, Z.; Mu, C.; Ma, W.; Hu, H.; Jiang, K.; Lin, H.; Ade, H.; Yan, H., Aggregation and morphology control enables multiple cases of high-efficiency polymer solar cells. *Nature communications* **2014,** *5*, 5293.
113. Gebeyehu, D.; Maennig, B.; Drechsel, J.; Leo, K.; Pfeiffer, M., Bulk-heterojunction photovoltaic devices based on donor–acceptor organic small molecule blends. *Solar Energy Materials and Solar Cells* **2003,** *79* (1), 81-92.
114. Bakhshi, A.; Kaur, A.; Arora, V., Molecular engineering of novel low band gap conducting polymers. **2012**.
115. Nguyen, T. L.; Choi, H.; Ko, S.-J.; Uddin, M. A.; Walker, B.; Yum, S.; Jeong, J.-E.; Yun, M.; Shin, T.; Hwang, S., Semi-crystalline photovoltaic polymers with efficiency exceeding 9% in a~ 300 nm thick conventional single-cell device. *Energy & Environmental Science* **2014,** *7* (9), 3040-3051.
116. Lee, W.; Choi, H.; Hwang, S.; Kim, J. Y.; Woo, H. Y., Efficient Conventional-and Inverted-Type Photovoltaic Cells Using a Planar Alternating Polythiophene Copolymer. *Chemistry–A European Journal* **2012,** *18* (9), 2551-2558.
117. Guo, X.; Kim, F. S.; Jenekhe, S. A.; Watson, M. D., Phthalimide-based polymers for high performance organic thin-film transistors. *Journal of the American Chemical Society* **2009,** *131* (21), 7206-7207.
118. Roncali, J., Molecular engineering of the band gap of π-conjugated systems: Facing technological applications. *Macromolecular Rapid Communications* **2007,** *28* (17), 1761-1775.
119. Tadesse, T., Introduction to the Application of Organic Polymers for Photovoltaic Devices Organic Electronics Approach: Critical Review. *Review of Knowledge Economy* **2015,** *2* (2), 65-79.
120. Wudl, F.; Kobayashi, M.; Heeger, A., Poly (isothianaphthene). *The Journal of Organic Chemistry* **1984,** *49* (18), 3382-3384.
121. Bian, L.; Zhu, E.; Tang, J.; Tang, W.; Zhang, F., Recent progress in the design of narrow bandgap conjugated polymers for high-efficiency organic solar cells. *Progress in Polymer Science* **2012,** *37* (9), 1292-1331.
122. Chao, C.-Y.; Chao, C.-H.; Chen, L.-P.; Hung, Y.-C.; Lin, S.-T.; Su, W.-F.; Lin, C.-F., Band structure engineering for low band gap polymers containing thienopyrazine. *Journal of Materials Chemistry* **2012,** *22* (15), 7331-7341.
123. Scharber, M. C.; Mühlbacher, D.; Koppe, M.; Denk, P.; Waldauf, C.; Heeger, A. J.; Brabec, C. J., Design rules for donors in bulk-heterojunction solar cells—Towards 10% energy-conversion efficiency. *Advanced materials* **2006,** *18* (6), 789-794.
124. Li, J.; Grimsdale, A. C., Carbazole-based polymers for organic photovoltaic devices. *Chemical Society Reviews* **2010,** *39* (7), 2399-2410.
125. Günes, S.; Neugebauer, H.; Sariciftci, N. S., Conjugated polymer-based organic solar cells. *Chemical reviews* **2007,** *107* (4), 1324-1338.

126. Benanti, T. L.; Venkataraman, D., Organic solar cells: An overview focusing on active layer morphology. *Photosynthesis research* **2006,** *87* (1), 73-81.
127. Haruk, A. M.; Mativetsky, J. M., Supramolecular approaches to nanoscale morphological control in organic solar cells. *International journal of molecular sciences* **2015,** *16* (6), 13381-13406.
128. Zhou, H.; Yang, L.; You, W., Rational design of high performance conjugated polymers for organic solar cells. *Macromolecules* **2012,** *45* (2), 607-632.
129. Al-Khazzar, A. A. A., Behavior of Four Solar PV Modules with Temperature Variation. *International Journal of Renewable Energy Research (IJRER)* **2016,** *6* (3), 1091-1099.
130. Dubey, S.; Sarvaiya, J. N.; Seshadri, B., Temperature dependent photovoltaic (PV) efficiency and its effect on PV production in the world–a review. *Energy Procedia* **2013,** *33*, 311-321.
131. Qi, B.; Wang, J., Fill factor in organic solar cells. *Physical Chemistry Chemical Physics* **2013,** *15* (23), 8972-8982.
132. Mihailetchi, V.; Wildeman, J.; Blom, P., Space-charge limited photocurrent. *Physical review letters* **2005,** *94* (12), 126602.
133. Goodman, A. M.; Rose, A., Double Extraction of Uniformly Generated Electron-Hole Pairs from Insulators with Noninjecting Contacts. *Journal of Applied Physics* **1971,** *42* (7), 2823-2830.
134. Dongaonkar, S.; Servaites, J. D.; Ford, G. M.; Loser, S.; Moore, J.; Gelfand, R. M.; Mohseni, H.; Hillhouse, H. W.; Agrawal, R.; Ratner, M. A., Universality of non-Ohmic shunt leakage in thin-film solar cells. *Journal of Applied Physics* **2010,** *108* (12), 124509.
135. Jeong, W. I.; Lee, J.; Park, S. Y.; Kang, J. W.; Kim, J. J., Reduction of collection efficiency of charge carriers with increasing cell size in polymer bulk heterojunction solar cells. *Advanced Functional Materials* **2011,** *21* (2), 343-347.
136. Gupta, D.; Bag, M.; Narayan, K., Area dependent efficiency of organic solar cells. *Applied Physics Letters* **2008,** *93* (16), 384.
137. Köhler, A.; Bässler, H., *Electronic processes in organic semiconductors: An introduction*. John Wiley & Sons: 2015.
138. Kwon, S. G.; Kim, Y. H.; Kim, S. O. Development of organic solar cell material with alkoxyl as side chain. KR1042530B1, 2011.
139. Almeataq, M. S.; Yi, H.; Al-Faifi, S.; Alghamdi, A. A.; Iraqi, A.; Scarratt, N. W.; Wang, T.; Lidzey, D. G., Anthracene-based donor–acceptor low band gap polymers for application in solar cells. *Chemical Communications* **2013,** *49* (22), 2252-2254.
140. Yang, D. S.; Kim, K. H.; Cho, M. J.; Jin, J. I.; Choi, D. H., Donor–acceptor alternating π-conjugated polymers containing Di (thiophen-2-yl) pyrene and 2, 5-Bis (2-octyldodecyl) pyrrolo [3, 4-c] pyrrole-1, 4 (2H, 5H)-dione for organic thin-film transistors. *Journal of Polymer Science Part A: Polymer Chemistry* **2013,** *51* (6), 1457-1467.
141. Zhu, E.; Bian, L.; Hai, J.; Tang, W.; Zhang, F., Towards High-Efficiency Organic Solar Cells: Polymers and Devices Development. In *Solar Cells-New Aspects and Solutions*, InTech: 2011.
142. Muthukumar, M.; Ober, C.; Thomas, E., Competing interactions and levels of ordering in self-organizing polymeric materials. *Science* **1997,** *277* (5330), 1225-1232.
143. Wallace, J.; Chen, S., Fluorene-based conjugated oligomers for organic photonics and electronics. In *Polyfluorenes*, Springer: 2008; pp 145-186.
144. Brabec, C.; Scherf, U.; Dyakonov, V., *Organic photovoltaics: materials, device physics, and manufacturing technologies*. John Wiley & Sons: 2011.

145. Goker, S.; Hizalan, G.; Kutkan, S.; Arslan Udum, Y.; Cirpan, A.; Toppare, L., Incorporation of different conjugated linkers into low band gap polymers based on 5, 6-Bis (octyloxy)-2, 1, 3 benzooxadiazole for tuning optoelectronic properties. *Journal of Polymer Science Part A: Polymer Chemistry* **2016,** *54* (16), 2459-2467.
146. Haeussler, M.; King, S.; Eng, M.; Haque, S.; Bilic, A.; Watkins, S.; Wilson, G.; Chen, M.; Scully, A., Photo-spectroscopic properties of benzothiadiazole-containing pendant polymers for photovoltaic applications. *Journal of Photochemistry and Photobiology A: Chemistry* **2011,** *220* (2-3), 102-112.
147. Melucci, M.; Favaretto, L.; Bettini, C.; Gazzano, M.; Camaioni, N.; Maccagnani, P.; Ostoja, P.; Monari, M.; Barbarella, G., Liquid-Crystalline Rigid-Core Semiconductor Oligothiophenes: Influence of Molecular Structure on Phase Behaviour and Thin-Film Properties. *Chemistry–A European Journal* **2007,** *13* (36), 10046-10054.
148. Sonar, P.; Singh, S. P.; Sudhakar, S.; Dodabalapur, A.; Sellinger, A., High-mobility organic thin film transistors based on benzothiadiazole-sandwiched dihexylquaterthiophenes. *Chemistry of Materials* **2008,** *20* (9), 3184-3190.
149. Beaujuge, P. M.; Subbiah, J.; Choudhury, K. R.; Ellinger, S.; McCarley, T. D.; So, F.; Reynolds, J. R., Green Dioxythiophene-Benzothiadiazole Donor− Acceptor Copolymers for Photovoltaic Device Applications. *Chemistry of Materials* **2010,** *22* (6), 2093-2106.
150. Akhtaruzzaman, M.; Tomura, M.; Nishida, J.-i.; Yamashita, Y., Synthesis and characterization of novel dipyridylbenzothiadiazole and bisbenzothiadiazole derivatives. *The Journal of organic chemistry* **2004,** *69* (9), 2953-2958.
151. Jayakannan, M.; Van Hal, P. A.; Janssen, R. A., Synthesis and structure-property relationship of new donor–acceptor-type conjugated monomers and polymers on the basis of thiophene and benzothiadiazole. *Journal of Polymer Science Part A: Polymer Chemistry* **2002,** *40* (2), 251-261.
152. Park, Y. S.; Kim, D.; Lee, H.; Moon, B., Donor− Acceptor− Donor-Type Liquid Crystal with a Pyridazine Core. *Organic letters* **2006,** *8* (21), 4699-4702.
153. Blouin, N.; Michaud, A.; Leclerc, M., A low-bandgap poly (2, 7-carbazole) derivative for use in high-performance solar cells. *Advanced Materials* **2007,** *19* (17), 2295-2300.
154. Lai, Y.-Y.; Chang, H.-H.; Lai, Y.-Y.; Liang, W.-W.; Tsai, C.-E.; Cheng, Y.-J., Angular-shaped 4, 10-dialkylanthradiselenophene and its donor–acceptor conjugated polymers: synthesis, physical, transistor, and photovoltaic properties. *Macromolecules* **2015,** *48* (19), 6994-7006.
155. Uddin, M. A.; Lee, T. H.; Xu, S.; Park, S. Y.; Kim, T.; Song, S.; Nguyen, T. L.; Ko, S.-j.; Hwang, S.; Kim, J. Y., Interplay of intramolecular noncovalent coulomb interactions for semicrystalline photovoltaic polymers. *Chemistry of Materials* **2015,** *27* (17), 5997-6007.
156. Zhong, W.; Liang, J.; Hu, S.; Jiang, X.-F.; Ying, L.; Huang, F.; Yang, W.; Cao, Y., Effect of monofluoro substitution on the optoelectronic properties of Benzo [c][1, 2, 5] thiadiazole based organic semiconductors. *Macromolecules* **2016,** *49* (16), 5806-5816.
157. Cartwright, L.; Yi, H.; Iraqi, A., Effect of fluorination pattern and extent on the properties of PCDTBT derivatives. *New Journal of Chemistry* **2016,** *40* (2), 1655-1662.
158. Efrem, A.; Lim, C.-J.; Lu, Y.; Ng, S.-C., Synthesis and characterization of dithienobenzothiadiazole-based donor–acceptor conjugated polymers for organic solar cell applications. *Tetrahedron Letters* **2014,** *55* (35), 4849-4852.
159. Livi, F.; Zawacka, N. K.; Angmo, D.; Jørgensen, M.; Krebs, F. C.; Bundgaard, E., Influence of side chain position on the electrical properties of organic solar cells based

on dithienylbenzothiadiazole-alt-phenylene conjugated polymers. *Macromolecules* **2015,** *48* (11), 3481-3492.

160. Khlyabich, P. P.; Rudenko, A. E.; Street, R. A.; Thompson, B. C., Influence of polymer compatibility on the open-circuit voltage in ternary blend bulk heterojunction solar cells. *ACS applied materials & interfaces* **2014,** *6* (13), 9913-9919.

Chapter 2

Synthesis and Characterisation of Naphthalene-based D-A Low Bandgap Polymers

2.1 Introduction

Polymer photovoltaics that have an active layer of conjugated polymer have attracted great interest from researchers in the last decades due to the many advantages in the various applications of these polymers including solar cells. This includes flexibility, lightweight, and their low cost compared to the traditional inorganic materials used for these purposes. With the enhancement made in the processing of organic solar cells and bandgap engineering, power conversion efficiency of over 11% was achieved by scientists.[1] Researchers have focused on designing low band gap polymers to increase the sunlight proportion harvested by the polymer, which in turn increase the power conversion efficiency (PCE%).[2-5] The targeted polymers should have optimal electronic and physical properties; this includes the HOMO and LUMO energy levels and sunlight absorption extent. In addition, to achieve a good charge mobility and efficient exciton dissociation, it is important to address the morphology of the polymer as a donor against the fullerene derivative as an acceptor in solar cell devices. [6-8]

The tuning the polymer's band gap is possible over the visible range; this depends on the polymer structure, especially the one based on alternating donor-acceptor D-A copolymers,[9] or through changing the side-chains of polymers.[10] Controlling the intramolecular charge transfer (ICT) can enable the fine-tuning of the polymer's bandgap through the use of conjugated polymers with alternating donor-acceptor monomers.[11-13] To obtain good PCE%, the frontier orbitals of energy levels of the polymer and the band gap should be optimised.[14, 15]

Benzothiadiazole (BTD) is a very common moiety which has been used in a large number of conjugated polymers due to its thiadiazole unit, which represents the electron withdrawing part of the conjugated polymer backbone.[16] Combining the BTD unit as a strong electron acceptor with a suitable electron donor alternatively can lead to polymers with low band gaps and good charge transfer.[17-20] The BTD unit was further modified and used in synthesis of polymers for bulk hetero-junction (BHJ) solar cells, these modifications were made by replacing the sulphur atom with oxygen[21], selenium[22] or nitrogen[23], also by replacing the benzene ring with more electron-withdrawing rings such as pyridine[24] or pyridazine.[25] Furthermore, introducing fluorine atoms can lead to interesting enhancements on the power conversion efficiency of BHJ solar cells.[26] It is important to retain the LUMO level in conjugated polymers above -3.9eV because this could lead to an inefficient dissociation of the exciton.[27, 28] There are many attempts to synthesize low band gap conjugated polymers capable of absorbing a wide range of the spectrum which are meant to harvest a wide area of

sunlight. One approach has used fluorinated benzothiadiazole as an acceptor with four thiophene units as donors, **FBT-Th4(1,4)** has low a band gap of 1.62 eV with a HOMO level of -5.36 eV and a LUMO level of -3.74 eV.[29] It has been noticed that this polymer has a λ_{max} of 692 nm compared to λ_{max} 560 nm of the conjugated polymer **P-TBTT-P** which has no fluorine atoms and fewer thiophenes in its structure.[30] The latter has a band gap of 2.19 eV and HOMO, LUMO levels were -5.89 and -3.70 eV respectively. The effects of introducing extra thiophene units and also fluorine atoms on the BTD have resulted in considerable red-shift in λ_{max} of about 132 nm. Furthermore, the **FBT-Th4(1,4)** is a very good example of BHJ polymers that are based on the donor-acceptor concept, as it showed a PCE of 9.2% when applied in solar cell fabrication.[29] **PENTBT** was also compared to our synthesised polymers **P1**, **P2**, **P3**, this polymer was synthesized according to the Suzuki cross coupling polymerisation[31], using 1,5-dioctyloxynaphthalene as a donor part. To compare the effect of the donor moiety, the synthesized polymers were compared to **PPDTBT** which has a benzene ring instead of naphthalene two fused rings.

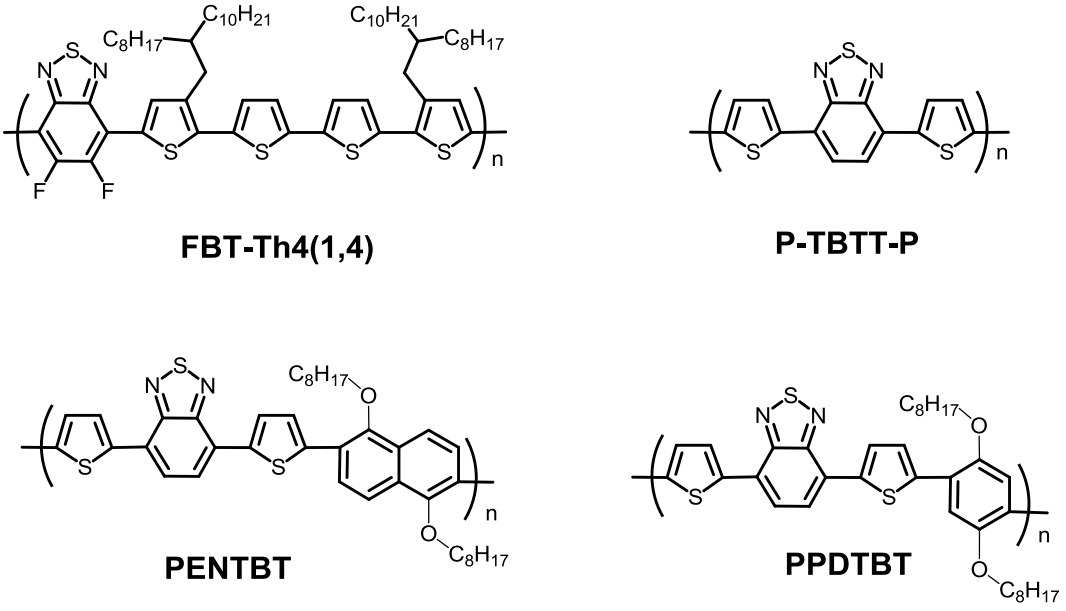

Figure 0-1: Chemical structure of studied polymers. [29, 31, 46, 50]

Naphthalene is a molecule which can form a molecular crystalline structure through the interactions via van der Waals forces. It has a high charge mobility compared to the organic, non-crystalline materials. The naphthalene molecule has many features, these include; flatness, aromatic and large, in addition to being a neutral molecule and its outer orbitals are filled.[32] Naphthalene flanked with two thiophene was used as a donor moiety with benzothiadiazole as an acceptor to synthesize the donor molecule which was used as a small molecule in organic solar cell fabrication,[33] and the material was

used as donor-acceptor-donor organic material in solar cell fabrication showing PCE of 4.13%. Noteworthy, no studies were conducted on using an unsubstituted naphthalene unit in conjugated polymers for the use in BHJ solar cells.

In this chapter, we present the synthesis and characterization of narrow bandgap polymers, consisting of alternating benzothiadiazole BTD moiety as an acceptor unit and 2,6-linked naphthalene flanked by two bithiophene units as a donor unit. Branched alkyl chains were attached to the thiophene in the synthesised donor monomer to increase the solubility in the resulting polymers. The effects of fluorine atom incorporation on the BTD moiety have also been investigated. The photophysical and electrochemical properties were studied and compared to other naphthalene-based analogous polymers.

2.2 Results and discussion

2.2.1 Synthesis of Monomers

The synthetic route to the acceptor and donor synthesized in this chapter is presented in scheme (2-1) below. The BTD acceptor was synthesized according to the literature.[34] The first step of the synthetic route involved the benzothiadiazole ring closure reaction between 1,2-diamine-4,5-difluorobenzene- **(SM1)** and thionyl chloride catalysed by triethylamine and the reaction mixture was refluxed overnight. The purification process was done by a silica gel plug column to yield the product **(1)** as ivory crystals.

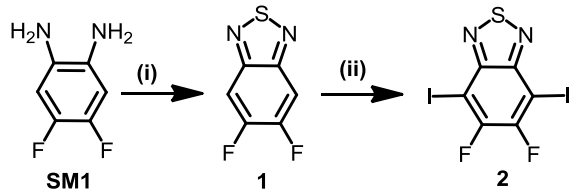

(i) $SOCl_2$, $CHCl_3$, Et_3N, r.t. **(ii)** Fuming H_2SO_4, I_2.

Scheme 0-1: Synthesis of BTD acceptor.

The proposed mechanism of the BTD ring closure reaction is depicted in scheme (2-2) below:

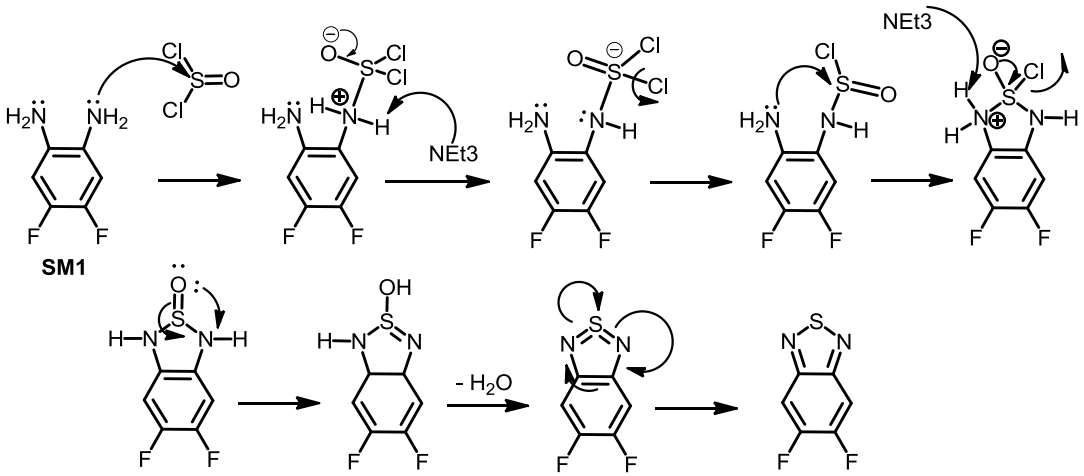

Scheme 0-2: Suggested mechanism of BTD ring closure.

This step was followed by the iodination of the fluorinated BTD using iodine and fuming sulphuric acid to yield 5,6-difluoro-4,7-diiodobenzo[*c*][1,2,5]thiadiazole **(2)**. Unsuccessful attempts to synthesise 5,6-difluoro-4,7-dibromobenzo[*c*][1,2,5] thiadiazole were made by Iraqi group, but only iodination worked due to the active iodine electrophile I_2^+ as a result of the oxidation reaction of I_2 by SO_3 group in fuming sulphuric acid. The oxidation reaction of I_2 is shown in equation (2-1) below shows.

$$2I_2 + H_2SO_4 + 2SO_3 \longrightarrow 2I^+_2 + 2HSO_4^- + SO_2$$

Equation 0-1: Oxidation reaction of I_2.

The purity of product **(2)** was confirmed using ^{19}F NMR showing a single peak at -105.00 ppm as a proton-free compound as shown in figure (2-2) below:

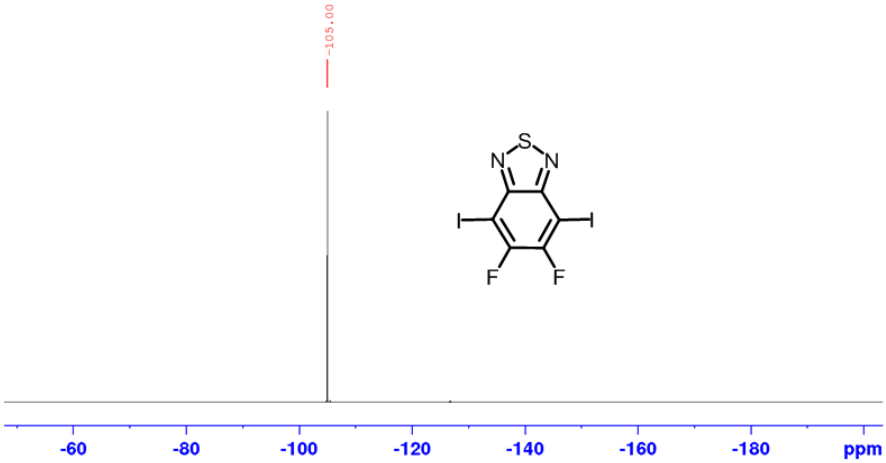

Figure 0-2: ^{19}F NMR spectra of 5,6-difluoro-4,7-diiodobenzo[c][1,2,5]thiadiazole **(2).**

The donor moiety **M1** was synthesized according to modified procedures in the literatures.[35-40] A schematic synthetic route is shown in scheme (2-3) below:

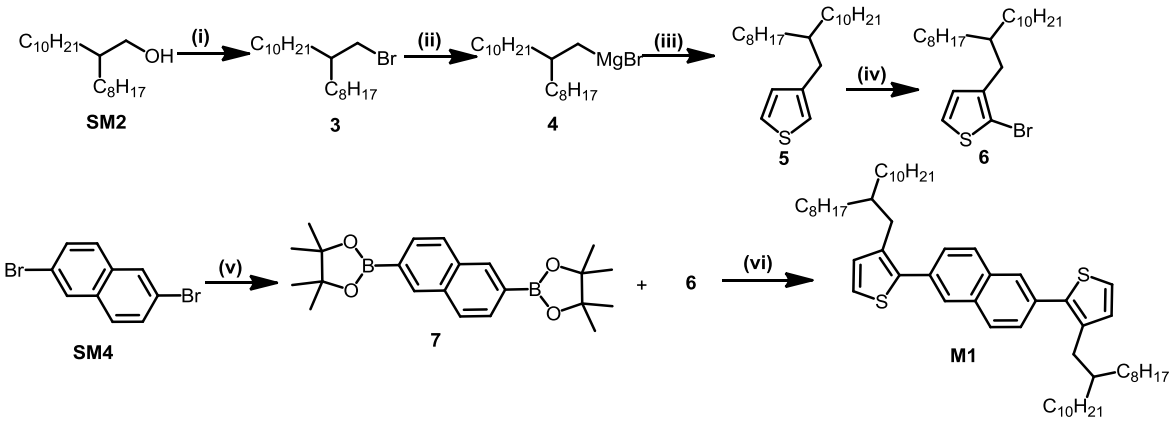

(i) NBS, PPh_3, DCM. **(ii)** Mg, dry THF. **(iii)** 3-bromothiophene (**SM3**), $Ni(dppp)Cl_2$, dry THF, drop-wise. **(iv)** NBS, $CHCl_3$, AcOH. **(v)** bis(pinacolato)diboron, KOAc, $Pd(dppf)Cl_2$. **(vi)** compound **(6),** $Pd(OAc)_2$, tri(*o*-tolyl)phosphine, dry THF, aq. sol. of $NaHCO_3$.

Scheme 0-3: Synthetic routes to **M1** donor monomer.

The formation of donor moiety **M1** includes eight steps, these can be illustrated by the following; the first step is the bromination of 2-octyldodecan-1-ol **(SM2)** using N-bromosuccinimide and triphenyl phosphine according to the proposed mechanism shown in scheme (2-4) below:

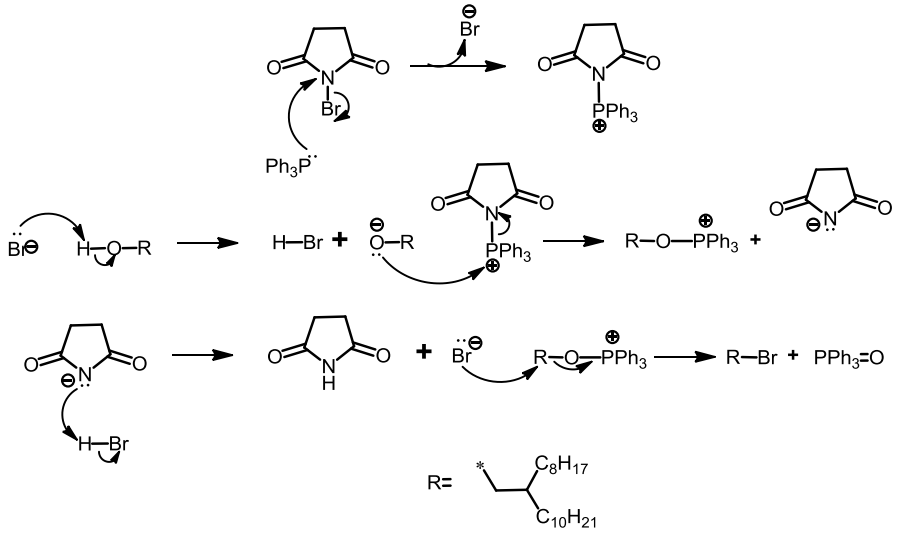

Scheme 0-4: Bromination process of 2-octyldodecan-1-ol.

This exothermic reaction yielded 1-bromo-2-octyldodecane **(3)** as a colourless liquid after a purification. Compound **(4)** was prepared by adding a suspension of **(3)** to stirred magnesium turnings in maintaining the reflux process resulting compound **(4)** which was used in the next step with no further purification. The next the Kumada cross-coupling of **(4)** with 3-bromothiophene **(SM3)** and $Ni(dppp)Cl_2$ that has been dissolved earlier in dry THF and the reaction mixture stirred overnight. Work-up and

purification via silica gel column chromatography is followed to afford 3-(2-octyldodecyl)thiophene **(5)** as a colourless oil. The suggested mechanism of Kumada cross-coupling is shown in scheme (2-5) below:

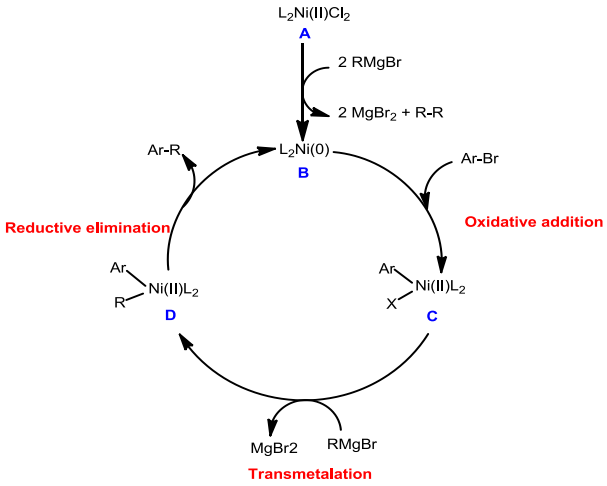

Scheme 0-5: General mechanism of Kumada cross-coupling.

The bromination of **(5)** with N-bromosuccinimide in the presence of acetic acid yielded **(6)** as a colourless oil, column chromatography has also been used to purify this compound. Next is the reaction between 2,6-dibromonaphthalene **(SM2)** with bis(pinacolato)diboron catalysing with Pd(dppf)Cl_2 and potassium acetate to obtain 2,6-bis(4,4,5,5-tetramethyl-1,3,2-dioxaborolan-2-yl)naphthalene **(7)** as a grey solid. The purification of **(7)** is done by washing the resulting precipitate with methanol, which was earlier passed through basic alumina to remove the acidic species. The final step is the Suzuki-coupling between **(6)** and **(7)** catalysed with Pd$(OAc)_2$ to yield **(M1)** as a green sticky liquid. ^{1}H NMR of the donor monomer **(M1)** is depicted in figure (2-3) below:

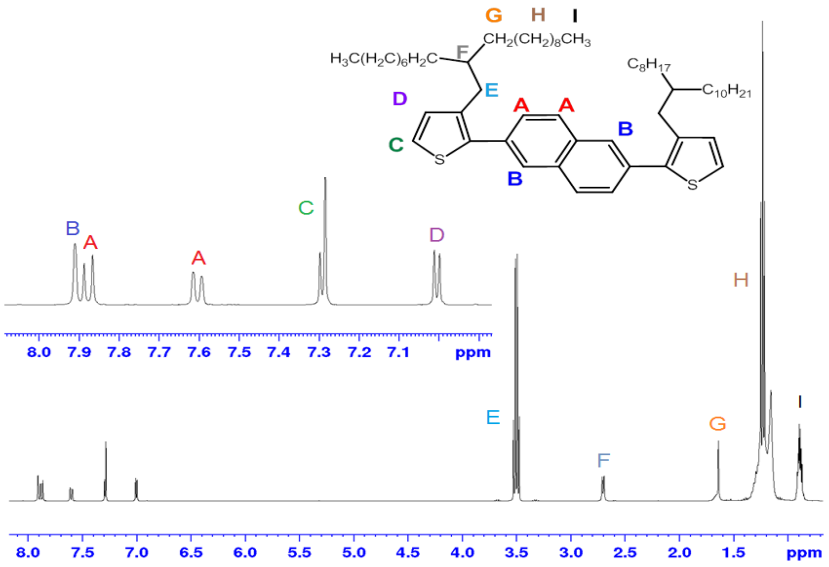

Figure 0-3: ^{1}H NMR spectra of **(M1).**

2.2.2 Synthesis of Polymers

The final donor monomer **M1** was reacted with three different BTD monomers, these are; 4,7-dibromobenzo[c][1,2,5]thiadiazole **(SM11)**, 5,6-difluoro-4,7-diiodobenzo[*c*][1,2,5]thiadiazole **(2),** and 4,7-bis(5-bromothiophen-2-yl)benzo[*c*][1,2,5]thiadiazole **(SM12)** respectively *via* direct hetero arylation (DHA)[41] polymerisation in the presence of $Pd_2(dba)_3$, P(*o*-MeOPh)$_3$, Cs_2CO_3, and pivalic acid obtain afford **P1**, **P2** and **P3** respectively. The procedure used $Pd_2(dba)_3$ as a catalyst and (*o*-OMePh)$_3$P as a ligand in a sealed tube under an inert atmosphere according to the procedure in the literature[41]. The amount of solvent used in these polymerizations is 1cm^3 and the polymerization reaction time is variable for each polymer synthesis from 24 hours to 3 days depending on the precipitate formation of polymer observed at the bottom of the polymerization tube. The polymers were then washed with NH_4OH solution to remove any catalyst residue and then extracted using Soxhlet extraction with different solvents (methanol, acetone, hexane, toluene, and chloroform) collecting toluene and sometimes hexane portions for the following steps. The next step was the precipitation of the polymers by the drop-wise addition of polymer solution fraction into methanol to afford the polymers as solid materials. However, these polymers were soluble in chloroform at room temperature for further characterization studies. To confirm the chemical structure and the molecular weight of the synthesized polymers, ^{1}H NMR spectroscopy, GPC and elemental analysis studies were conducted. Elemental analysis showed a little deviation in elemental analysis due to technical reasons; this might be attributed to the combustion process of polymers. This could be

associated with some homopolymerisation routes during the polymerisation process. Synthetic routes to polymers **P1**, **P2**, and **P3** are shown in scheme (2-6 below).

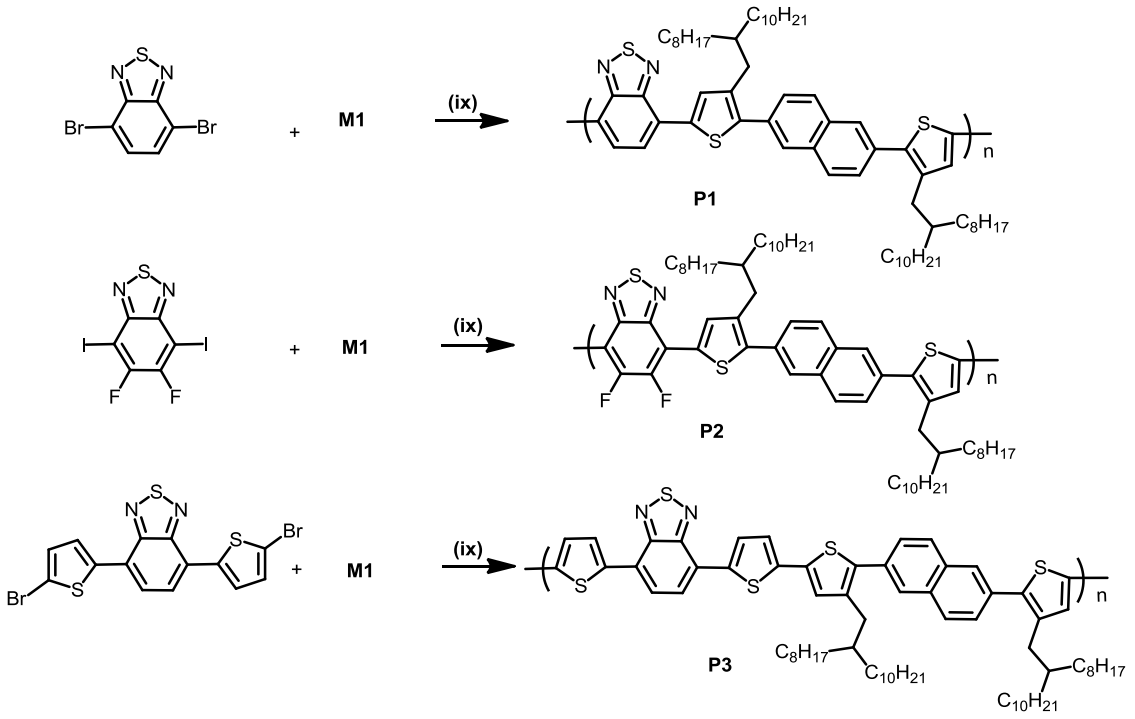

(ix) $Pd_2(dba)_3$, P(*o*-MeOPh)$_3$, Cs_2CO_3, pivalic acid, 1cm^3 dry THF, 120 °C.

Scheme 0-6: Synthetic routes to the naphthalene-BTD based conjugated polymers.

2.2.3 GPC Analysis

Gel permeation chromatography analysis GPC was conducted in toluene as the eluent at 100 °C. Polymer **P3** has showed the highest molecular weight value among the other polymers of its family, the toluene fraction of **P3** showed number-average molecular weight (M_n = 33,400), which is higher than **P1** by about four times (M_n = 8,500 Da), the low molecular weight for **P1** is expected as this polymer was collected from hexane fraction. This means that this polymer might have shorter polymeric chains. **P2** has displayed a value of (M_n = 26,000 Da), which also has been collected from toluene fraction. It is hypothesised that the existence of fluorine atoms will reduce both M_n and M_w of conjugated polymers due to the aggregation and the strong π-π stacking of polymer's backbone.[42, 43] However, it can be clearly seen from the GPC results that incorporation of fluorine atoms within the BTD unit has an influence of increasing the M_n and M_w in **P2**. This influence has increased even more when additional thiophene units were inserted into the polymer's backbone of **P3**, GPC analysis data are shown in table (2-1) below:

Table 0-1: GPC data for **P1**, **P2** and **P3**.

Polymer	Fraction	Yield %	M_n (Da)[a]	M_w (Da)[a]	PDI[b]
P1	hexane	34%	8,500	15,100	1.77
P2	toluene	39%	26,000	44,500	1.71
P3	toluene	52%	33,400	38,600	1.15

[a] Detected by differential refractive index (DRI) of the hexane and toluene fractions of the polymer have been measured. [b] is the Polydispersity index.

2.2.4 Optical Properties of Polymers

Absorption behaviour of polymers was investigated in both solution and thin film using chloroform as a solvent. Table (2-2) shows the absorption maximum values of solution, film and absorption maxima onset for the synthesized polymers, band gaps were also calculated from the absorption maxima onset of polymers' thin films.

Table 0-2: UV-visible data for **P1, P2** and **P3.**

Polymer	λ_{max} Solution (nm)	λ_{max} Film (nm)	ε ($M^{-1}cm^{-1}$)		λ_{max} onset Solution (nm)	λ_{max} onset Film (nm)	Eg(opt)[c] (eV)
			π-π* [d]	ICT [e]			
P1[a]	499	521	15,300	14,900	561	589	2.10
P2[b]	508	537	24,700	27,600	587	612	2.00
P3[b]	550	577	43,800	31,000	681	725	1.71

[a] Hexane fraction. [b] Toluene fraction. [c] Optical band gap ($E_{g\ opt}$), determined from the absorption maxima onset of UV-vis in polymers thin films. [d] Absorption coefficient for (π-π*) at λ_{max}=355 nm for **P1** and **P2**, λmax=390 nm for **P3**, [e] Absorption coefficient for (ICT) at λ_{max}=499 nm for **P1** and λ_{max}=508 nm for **P2**, λmax=550 nm for **P3.**

Table (2-2) and figures (2-4a), (2-4b) illustrates that solutions of **P1** and **P2** have slightly different absorption maxima peaks at 499 and 508nm respectively, it can be clearly seen that **P2** absorption peaks are red-shifted compared to **P1.** These two polymers were compared to the analogue polymer **PENTBT**[46] which has shown absorption maxima of 532 nm. However, relative to **P1** and **P2**, **P3** has shown a red-shifted absorption peak by 42 nm. This could be attributed to the extended conjugation

related to the addition of two thiophene segments into the backbone of **P3** that could make the structure of the polymer more planar and more rigid compared to **P1** and **P2**. The three synthesized polymers showed two absorption bands in solutions and as thin films. Compared to their solution absorption spectra, the UV-visible spectra have displayed red-shifts absorption band. This is attributed to the polymer chains aggregation in solid states of these polymers.[44-46]

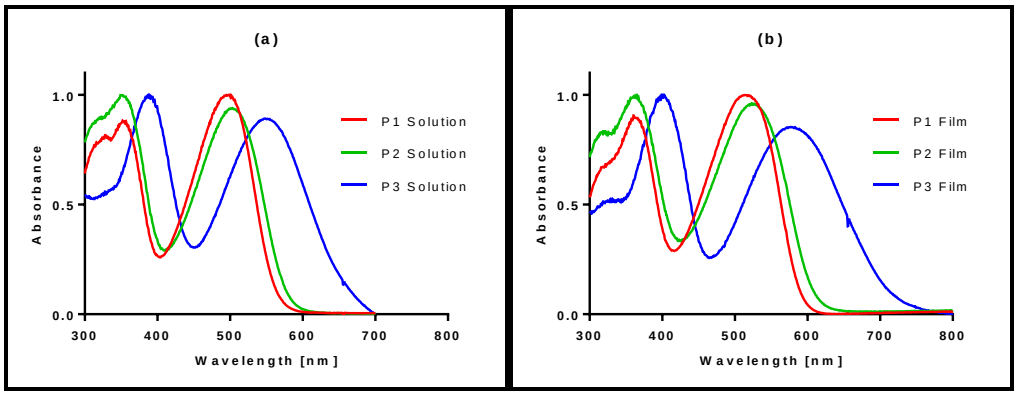

Figure 0-4: UV-visible for **P1, P2** and **P3 (a)** in solutions **(b)** as thin films

Low energy absorption bands correspond to the intramolecular charge transfer (ICT) state, whereas the higher energy absorption bands are due to the π-π* electronic transitions. The synthesized polymers **P1** and **P2** have shown optical band gaps of 2.10 eV and 2.0 eV respectively, while the analogous polymer **PENTBT**[31] that has alkoxy chains attached to the naphthalene segment has shown a band gap of 1.75eV. It is clearly seen that the band gap of **P2** is lower than that of **P1** by 0.1 eV, this is due to introducing two fluorine atoms at the 5,6-positions of the BTD.[47, 48] Interestingly, the optical band gap of **P3** was 1.71 eV, which means that extending the conjugation for the polymer backbone has improved and lowered the band gap by about 0.3 eV compared to **P1** and **P2**. Nguyen *et al*.[49] have synthesized a BTD based conjugated polymer **PPDTBT** that consists of a BTD acceptor moiety and benzene ring flanked with two thiophene segments, which has an optical band gap of 1.72 eV, this polymer **PPDTBT** was compared to **P3** which has shown a lower bandgap of 1.71 eV due to the use of naphthalene unit instead of benzene in **P3**.

2.2.5 Electrochemical Properties of Polymers

Studies on cyclic voltammetry (CV) were done by drop-casting polymeric films from chloroform solutions, using tetrabutylammonium perchlorate as electrolyte and acetonitrile as a medium. The HOMO levels of the synthesized polymers were calculated from the oxidation potential onsets while the LUMO levels were calculated from the onsets of the reduction potential in each polymer. The results shown in table

(2-3) were compared to those of analogous synthesized polymers with naphthalene units showing that the HOMO level for **P1** was equal to -5.41, which is almost similar to that of the corresponding polymer **PENTBT** with HOMO level of -5.42 eV. The HOMO level for **P2** was equal to -5.60 eV which is deeper compared to **P1** and this could be attributed to the incorporation of two fluorine atoms attached to the BTD moiety. **P3** has shown a shallower HOMO level of about 5.31 eV which is due to absence of fluorine atoms compared to **P2**. This was even shallower than its counterpart **PTDNTBT** that has shown a HOMO level of about -5.38 eV. The results obtained from cyclic voltammetry for the synthesised polymers **P1, P2** and **P3** are in good agreement with the UV results.

Table 0-3: Cyclic voltammetry results for **P1, P2** and **P3.**

Polymer	HOMO (eV)[a]	LUMO (eV)[b]	E_g (eV)[c]
P1	-5.41	-3.31	2.10
P2	-5.60	-3.57	2.03
P3	-5.31	-3.55	1.76
PENTBT	-5.42	-3.67	1.75

[a] HOMO level of the polymer calculated from the oxidation potential onset, [b] LUMO level of the polymer calculated from the reduction potential onset, [c] electrochemical band gap.

The LUMO levels were also compared to the analogous polymers; **P1, P2** and **PENTBT** have LUMO levels of (-3.31, -3.57 and -3.67 eV) respectively. It can be seen that the synthesized polymers **P1** and **P2** have shallower LUMO levels compared to the deeper LUMO level of **PENTBT**, the different structure in **P1, P2** and **PENTBT** may play the main role in varying the LUMO levels. It can be clearly seen that both HOMO and LUMO levels of **P2** are deeper than that of **P1**, especially with the two fluorine atoms in **P2** chemical structure. The electrochemical band gaps for **P1**, **P2** and **P3** are (2.10, 2.03 and 1.76 eV) respectively, these band gaps are higher than the corresponding polymers **PENTBT, PTDNTBT** that have shown band gaps of 1.75, 1.69 eV respectively. This again could be attributed to the chemical structure and the order in which the donor and the acceptor have been arranged. Electrochemical band gaps and optical band gaps are slightly different due to the interfacial energy barrier between the electrode used in this technique and the polymeric thin film during the reduction/oxidation reactions.

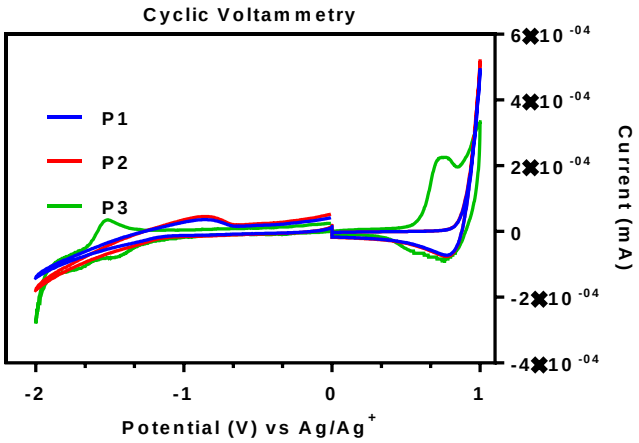

Figure 0-5: Cyclic voltammetry plots for **P1, P2** and **P3.**

2.2.6 Polymers' XRD Studies

The powder X-ray diffraction for **P1, P2** and **P3** were investigated to study the morphology of the synthesized polymers. As shown in figure (2-6) below, it can be seen that **P1** has a wide angle broad peak at 2Θ value of 20.27^{o}, this value corresponds a π-π stacking of 4.37 Å distance. While **P2** displays a sharp peak at 2Θ value of 20.64^{o} which corresponds to 4.29 Å, This is due to attaching fluorine atoms to the BTD moiety that improves the molecular ordering with promoting interchain interactions with the adjacent aromatic rings which in turn promotes the π-π stacking of the polymer backbone in its solid state. Interestingly, **P3** has also shown a sharper peak at 2Θ value of 21.06° which corresponds to a distance of 4.21 Å. This is attributed to the π-π stacking ordering resulted from the aromatic rings and the thiophene segments added to the backbone of the polymer. The general trend of the prepared polymers shows amorphous structure for the polymers powder in solid state due to the steric hindrance caused by the long alkyl chains attached to the polymers backbone, which plays the main role in disrupting the π-π stacking formation in solid state, or the twisting of the polymer chains out of plane between the BTD and the nearest thiophene unit. XRD of **P1** has almost a similar trend to the corresponding counterpart **PENTBT.**[31]

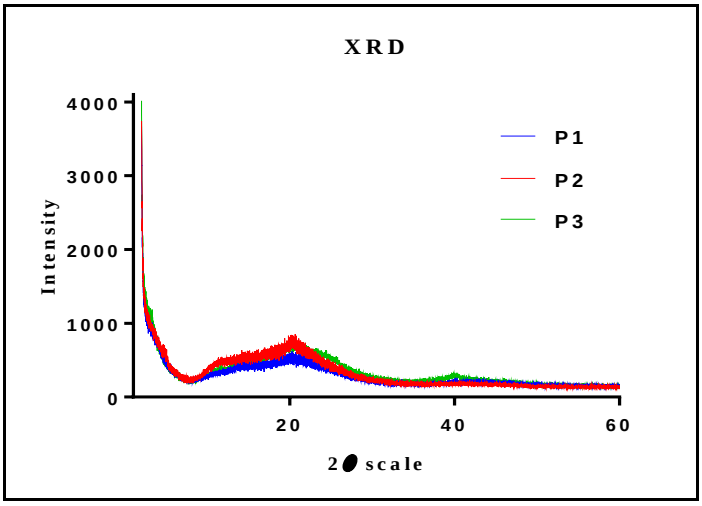

Figure 0-6: Powder X-Ray diffraction plots for **P1, P2** and **P3.**

2.2.7 Thermal Gravimetric Analysis Studies

The thermal properties of the synthesized polymers were confirmed by thermogravimetric analysis (TGA) at a rate of 10^{o}C/min under nitrogen atmosphere. TGA plot in figure (2-7) shows high thermal stabilities over 400 ^{o}C for **P1**, **P2**, and **P3** based on the temperature of the primary decomposition (T_d) which represents 5% weight loss. However, **P1**, **P2**, and **P3** have different decomposition behaviors, this could be attributed to the different chemical structure of these polymers and also to the difference in the M_w of each polymer. TGA data are illustrated in table (2-4) below.

Table 0-4: TGA data for **P1, P2** and **P3.**

Polymer	D/ $^{\circ}$C[a]	TPWL (%)[b]	EPWL(%)[c]	R_m/wt %[d]
P1	457-509	60	71	26
P2	451-497	57	53	42
P3	429-478	51	36	56

[a] D is the degradation onset. [b] TPWL is the percentage of theoretical weight loss. [c] EPWL is the percentage of experimental weight loss. [d] R_m is the remaining weight after heating to 800 °C.

The thermal degradation for all the synthesized polymers is similar regardless the chemical structure of each polymer. Each polymer showed one curve within the thermal degradation plot, which means that one degradation step is taking place within the increase of temperature. The step degradation starts from 457 to 509 °C for **P1** and from 451 to 497 °C for **P2** and from 429 to 478 for **P3**. This degradation is probably due to the loss of the alkyl chains attached to the thiophene units within the backbone of the

polymers. The residual mass of the polymers for **P1** and **P2** after the heating event is recorded to be 26 and 42 respectively. **P3** shows the most remaining mass among the other polymers with 56% sample weight residual due to the rigid structure of this polymer related to the aromatic units within the repeat unit.

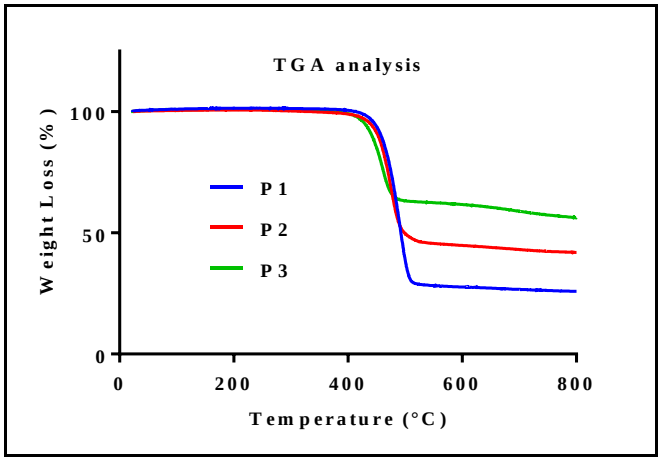

Figure 0-7: TGA plots for **P1, P2** and **P3.**

2.3 Conclusion

The chemical structure of conjugated polymers based on D-A configuration is an important aspect that researchers should focus on. However, designing a D-A conjugated polymer requires a suitable donor molecule which gives high charge carrier mobility. Naphthalene is considered as one of the molecules that gives the base of crystalline structure, this in turn will improve the morphology of the resulted polymer leading to enhanced charge carrier mobility.

In this chapter, a series of naphthalene and BTD conjugated polymers have been synthesized with an expectation of lowering the bandgap in these polymers. The molecular weight calculated by GPC showed that **P1** has a molecular weight of (M_n=33,400 Da) which is the lowest compared to **P2** and **P3** that showed (M_n=26,000 Da) and (M_n=8,500 Da) respectively. **P1** is based on BTD and naphthalene with no fluorine atoms in its structure showing a bandgap of 2.10 eV in both UV-visible and cyclic voltammetry, while **P2** has shown slightly narrower bandgap 2.00 eV and this was attributed to the incorporation of the fluorine atoms. It was hypothesised that the incorporation of fluorine atoms will enhance the ordering of π-π stacking through inter/intramolecular interactions within the polymer chains. Introducing fluorine atoms resulted in lowering both HOMO and LUMO levels of **P2** at the same time. **P3** shows even narrower bandgap compared to the first two polymers 1.71 eV, which means that the addition of thiophene segment led to the extension of the conjugated system of the polymer, this in turn has made the HOMO level shallower (-5.31eV) compared to **P1** and **P2** (-5.41, -5.60 eV).

The chemical structure of the synthesized polymers **P1**, **P2**, and **P3** were confirmed by ^{1}H NMR and elemental analysis and also other techniques such as powder X-ray diffraction, TGA, UV-visible and cyclic voltammetry.

The thermal gravimetric analysis revealed that **P1**, **P2**, and **P3** have shown a very good thermal stability (above 300 °C) when exposed to high temperature up to 800 °C, with retaining polymers weights above this temperature of about (26, 42 and 56%) for **P1**, **P2**, and **P3** respectively.

Powder X-ray diffraction studies have proven that the synthesized polymers are generally amorphous with showing some crystallinity behaviour in **P2** at 2Θ value of 20.64^o that corresponds to 4.29 Å; this was attributed to the fluorine atoms and the formation of hydrogen bond interactions between the polymer chains. Polymer **P3** has less crystallinity trends than **P2** with a sharp peak at 2Θ value of 21.06°, which

corresponds to a distance of 4.21 Å; this was due to the extended π-conjugated system and the π-π stacking of the aromatic rings within the polymer.

The increased molecular weight of **P2** and **P3** could result in high charge carrier mobility and high V_{oc} values if they are applied in photovoltaic devices. Noteworthy, the low bandgap of **P3** makes it a suitable polymer for solar cell applications due to the difference between the LUMO levels of **P3** and fullerene derivative $PC_{71}BM$, which is 0.25 eV. Figure (2-8) below shows HOMO and LUMO levels of the synthesized polymers **P1**, **P2** and **P3** compared to the fullerene derivative $PC_{71}BM$.

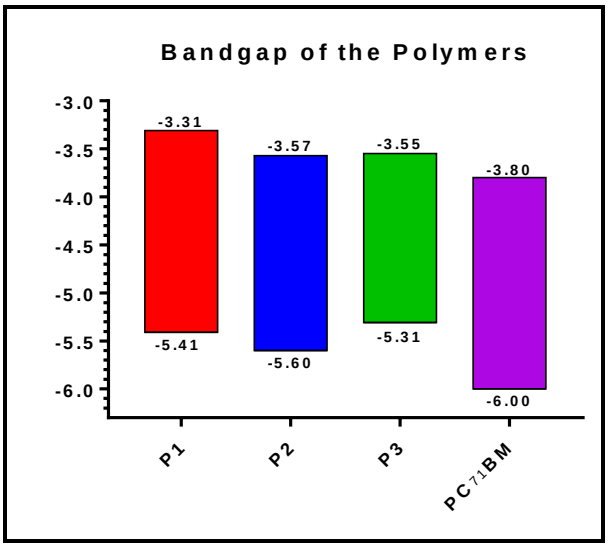

Figure 0-8: HOMO and LUMO levels of **P1**, **P2** and **P3** compared to $PC_{71}BM$.

Chapter 2 References

1. Z. Wu, C. Sun, S. Dong, X.-F. Jiang, S. Wu, H. Wu, H.-L. Yip, F. Huang and Y. Cao, *J. Am. Chem. Soc*, 2016, **138**, 2004-2013.
2. C. J. Brabec, C. Winder, N. S. Sariciftci, J. C. Hummelen, A. Dhanabalan, P. A. van Hal and R. A. Janssen, *Advanced Functional Materials*, 2002, **12**, 709-712.
3. A. Dhanabalan, J. Van Duren, P. Van Hal, J. Van Dongen and R. Janssen, *Advanced Functional Materials*, 2001, **11**, 255-262.
4. J. Van Duren, A. Dhanabalan, P. Van Hal and R. Janssen, *Synthetic metals*, 2001, **121**, 1587-1588.
5. C. Winder and N. S. Sariciftci, *Journal of Materials Chemistry*, 2004, **14**, 1077-1086.
6. C. J. Brabec, *Solar energy materials and solar cells*, 2004, **83**, 273-292.
7. A. Banerji, M. W. Tausch and U. Scherf, *Educación Química*, 2013, **24**, 17-22.
8. R. Tipnis, D. Laird and M. Mathai, *Material Matters*, 2008, **3**, 92.
9. F. Meyers, A. Heeger and J. Brédas, *The Journal of chemical physics*, 1992, **97**, 2750-2758.
10. H. Van Mullekom, J. Vekemans, E. Havinga and E. Meijer, *Materials Science and Engineering: R: Reports*, 2001, **32**, 1-40.
11. P. M. Beaujuge and J. R. Reynolds, *Chemical reviews*, 2010, **110**, 268-320.
12. R. S. Ashraf, I. Meager, M. Nikolka, M. Kirkus, M. Planells, B. C. Schroeder, S. Holliday, M. Hurhangee, C. B. Nielsen and H. Sirringhaus, *Journal of the American Chemical Society*, 2015, **137**, 1314-1321.
13. J. Kim, M. H. Yun, G.-H. Kim, J. Lee, S. M. Lee, S.-J. Ko, Y. Kim, G. K. Dutta, M. Moon and S. Y. Park, *ACS applied materials & interfaces*, 2014, **6**, 7523-7534.
14. M. K. Siddiki, J. Li, D. Galipeau and Q. Qiao, *Energy & Environmental Science*, 2010, **3**, 867-883.
15. A. Yassar, F. Garnier, H. Jaafari, N. Rebiere-Galy, M. Frigoli, C. Moustrou, A. Samat and R. Guglielmetti, *Applied physics letters*, 2002, **80**, 4297-4299.
16. A. Efrem, C.-J. Lim, Y. Lu and S.-C. Ng, *Tetrahedron Letters*, 2014, **55**, 4849-4852.
17. P.-L. T. Boudreault, A. Najari and M. Leclerc, *Chemistry of Materials*, 2010, **23**, 456-469.
18. J. Chen and Y. Cao, *Accounts of chemical research*, 2009, **42**, 1709-1718.
19. O. InganÄs, F. Zhang and M. R. Andersson, *Accounts of Chemical Research*, 2009, **42**, 1731-1739.
20. J. Peet, A. J. Heeger and G. C. Bazan, *Accounts of Chemical Research*, 2009, **42**, 1700-1708.
21. W. Nie, C. M. MacNeill, Y. Li, R. E. Noftle, D. L. Carroll and R. Coffin, *Macromolecular rapid communications*, 2011, **32**, 1163-1168.
22. W. Zhao, W. Cai, R. Xu, W. Yang, X. Gong, H. Wu and Y. Cao, *Polymer*, 2010, **51**, 3196-3202.
23. L. Zhang, C. He, J. Chen, P. Yuan, L. Huang, C. Zhang, W. Cai, Z. Liu and Y. Cao, *Macromolecules*, 2010, **43**, 9771-9778.
24. N. Blouin, A. Michaud, D. Gendron, S. Wakim, E. Blair, R. Neagu-Plesu, M. Belletête, G. Durocher, Y. Tao and M. Leclerc, *Journal of the American Chemical Society*, 2008, **130**, 732-742.
25. D. Gendron, P. O. Morin, A. Najari and M. Leclerc, *Macromolecular rapid communications*, 2010, **31**, 1090-1094.

26. H. Zhou, L. Yang, A. C. Stuart, S. C. Price, S. Liu and W. You, *Angewandte Chemie*, 2011, **123**, 3051-3054.
27. S. H. Park, A. Roy, S. Beaupré, S. Cho, N. Coates, J. S. Moon, D. Moses, M. Leclerc, K. Lee and A. J. Heeger, *Nature photonics*, 2009, **3**, 297-302.
28. S. Zhang, H. Fan, Y. Liu, G. Zhao, Q. Li, Y. Li and X. Zhan, *Journal of Polymer Science Part A: Polymer Chemistry*, 2009, **47**, 2843-2852.
29. Z. Chen, P. Cai, J. Chen, X. Liu, L. Zhang, L. Lan, J. Peng, Y. Ma and Y. Cao, *Advanced Materials*, 2014, **26**, 2586-2591.
30. G. S. Collier, L. A. Brown, E. S. Boone, M. Kaushal, M. N. Ericson, M. G. Walter, B. K. Long and S. M. Kilbey, *Journal of Materials Chemistry C*, 2017, **5**, 6891-6898.
31. KR1042530B1, 2011.
32. H. Bässler and A. Köhler, *Journal*, 2015.
33. Y. Jeon, T.-M. Kim, J.-J. Kim and J.-I. Hong, *New Journal of Chemistry*, 2015, **39**, 9591-9595.
34. N. Wang, Z. Chen, W. Wei and Z. Jiang, *Journal of the American Chemical Society*, 2013, **135**, 17060-17068.
35. M. Scheuble, Y. Gross, D. Trefz, M. Brinkmann, J. López Navarrete, M. Ruiz Delgado and S. Ludwigs, *Macromolecules*, 2015, **48**, 7049-7059.
36. Y. Takamura, K. Takenaka, T. Toda, H. Takeshita, M. Miya and T. Shiomi, *Macromolecular Chemistry and Physics*, 2018, **219**.
37. L. Du, W. Xiong, S.-C. Cheng, H. Shi, W. K. Chan and D. L. Phillips, *The Journal of Physical Chemistry Letters*, 2017, **8**, 2475-2479.
38. L. Verheyen, B. Timmermans and G. Koeckelberghs, *Polymer Chemistry*, 2017, **8**, 2327-2333.
39. P. Sonar, S. P. Singh, Y. Li, Z.-E. Ooi, T.-j. Ha, I. Wong, M. S. Soh and A. Dodabalapur, *Energy & Environmental Science*, 2011, **4**, 2288-2296.
40. H. Zhao, C. Xu, B. Wang, J. Zhao, C. Cui and X. Zhang, *Int. J. Electrochem. Sci*, 2012, **7**, 10685-10697.
41. P.-O. Morin, T. Bura, B. Sun, S. I. Gorelsky, Y. Li and M. Leclerc, *ACS Macro Letters*, 2014, **4**, 21-24.
42. L. Cartwright, A. Iraqi, Y. Zhang, T. Wang and D. G. Lidzey, *RSC Advances*, 2015, **5**, 46386-46394.
43. T. Umeyama, Y. Watanabe, E. Douvogianni and H. Imahori, *The Journal of Physical Chemistry C*, 2013, **117**, 21148-21157.
44. R. Noriega, J. Rivnay, K. Vandewal, F. P. Koch, N. Stingelin, P. Smith, M. F. Toney and A. Salleo, *Nature materials*, 2013, **12**, 1038-1044.
45. T. Huser and M. Yan, *Journal of Photochemistry and Photobiology A: Chemistry*, 2001, **144**, 43-51.
46. T.-Q. Nguyen, I. B. Martini, J. Liu and B. J. Schwartz, *The Journal of Physical Chemistry B*, 2000, **104**, 237-255.
47. C. Du, W. Li, Y. Duan, C. Li, H. Dong, J. Zhu, W. Hu and Z. Bo, *Polymer Chemistry*, 2013, **4**, 2773-2782.
48. L. Cartwright, H. Yi and A. Iraqi, *New Journal of Chemistry*, 2016, **40**, 1655-1662.
49. T. L. Nguyen, H. Choi, S.-J. Ko, M. A. Uddin, B. Walker, S. Yum, J.-E. Jeong, M. Yun, T. Shin and S. Hwang, *Energy & Environmental Science*, 2014, **7**, 3040-3051.

Chapter 3

Synthesis and Characterisation of Anthracene-based D-A Narrow Bandgap Polymers

3.1 Introduction

The development of conjugated polymers has seen major advances during the last decade; this is attributed to the importance of these polymers in the various electronics applications of PSCs, LEDs and FETs. However, these polymers can offer flexibility in processing, are lightweight and also have a low-cost compared to their inorganic materials.[1] Different building blocks were used by scientists such as diketopyrrole-pyrrole, benzobisthiadiazole and naphthalene diimide; these building blocks were used as acceptors.[2-4] As it was mentioned in chapter two, the use of fused rings such as naphthalene, anthracene and pyrene helps to form the base of a crystalline structure and increase the charge mobility through the available π bonds in their chemical structure.[5] There are two general processes for the charge to be transported; interchain and intrachain transports. Interchain transport can be classified into two main classes; the first one in which the charges are transported by hopping in the ordered chain, while the second hypothesises that the charge transport is taking place at the loose ends of the polymeric chain, and this is the similar to transport in small molecules with small structures, in this case, charge transport within the inter/intrachain (figure 3-1) is a common known type in which the charge transport comes from the delocalization of π-electrons travel along the polymer chain or to the adjacent polymer chain.[6]

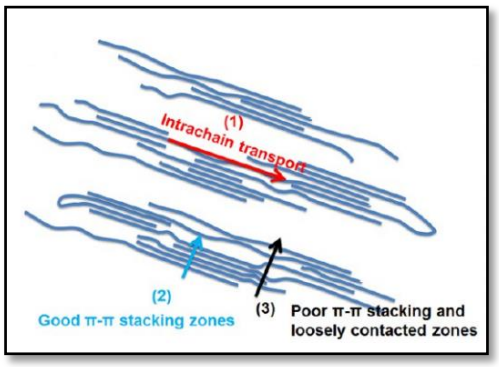

Figure 0-1: Charge transportation along the conjugated polymer.

The use of branched alkyl chains is the main key to improve both solubility and increase carrier mobility of the synthesized polymers. However, this will also affect the π-π stacking by reducing the distance between the polymeric chains.[1] Donor-acceptor conjugated polymers based on anthracene have been synthesized by Ai and coworkers,[7] polymers **P-A-** and **P-B-** (shown in scheme 3-1 below) are different in the alkyl chain attached to the polymer's backbone. The optical bandgap of **P-A-** and **P-B-** are 1.95 and 1.93 eV respectively. In this study, the author showed the differences in

polymer properties when attaching a branched alkyl chain to **P-A-** and a linear alkyl chain to **P-B-**.

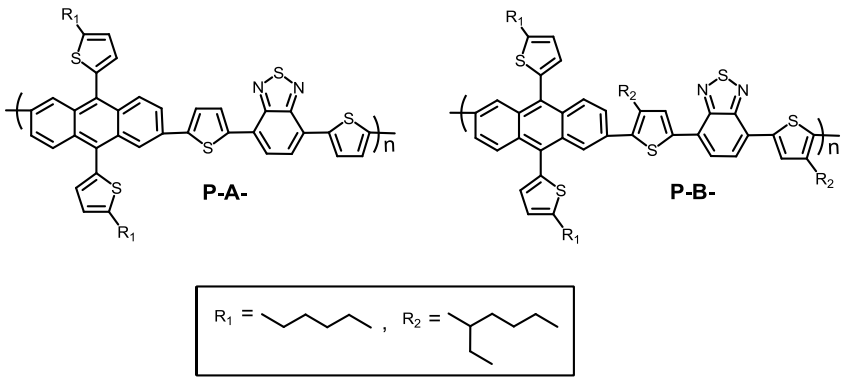

Scheme 0-1: Anthracene and BTD based conjugated polymers synthesized by Ai *et al*[7].

Another study was done by Almeataq *et al*.[8] using anthracene based conjugated polymers, alkoxy benzene was attached to the anthracene unit before proceeding to the final polymers. In this study, the BTD itself has two octyloxy groups attached to increase the solubility of the prepared polymers, as it is shown in scheme (3-2) below.

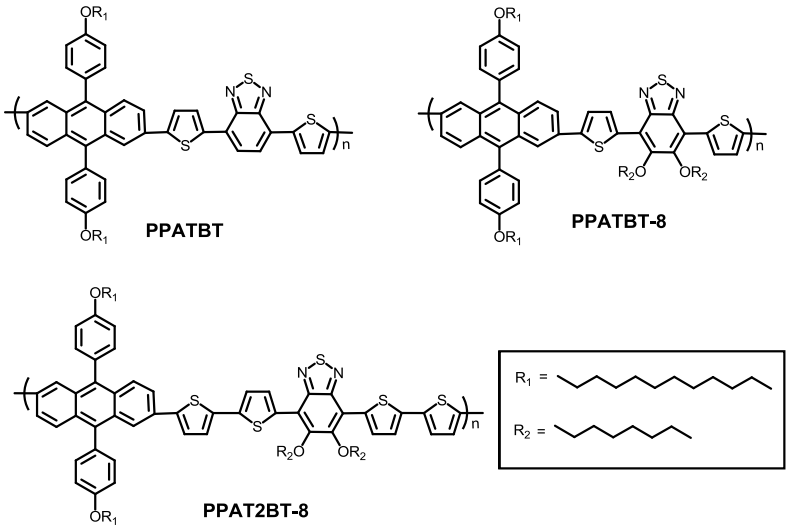

Scheme 0-2: Anthracene and BTD based conjugated polymers synthesized by Almoetaq *et al*[8].

In this chapter, we present the preparation and characterisation of two novel conjugated polymers based on 2,6-linked anthracene consisting of alternating thiophene moieties as the donor and fluorinated or non-fluorinated BTD as an acceptor. The difference between the synthesised polymers and the above mentioned polymers is the fluorine atoms attached, and the anthracene moiety used as a donor has no aromatic rings attached to its structure on positions 9 and 10. The electrochemical,

optical and thermal properties were studied and compared to the counterpart polymers with an anthracene-based configuration.

3.2 Results and Discussion

3.2.1 Synthesis of Monomer

The synthetic steps to the donor monomer **(M2)** are similar to the synthetic steps of compounds in chapter 2, except for the naphthalene unit, which is replaced in this chapter with an anthracene moiety instead of the naphthalene moiety in chapter 2. Scheme (3-3) below is showing the synthetic routes towards **(M2)** donor unit.

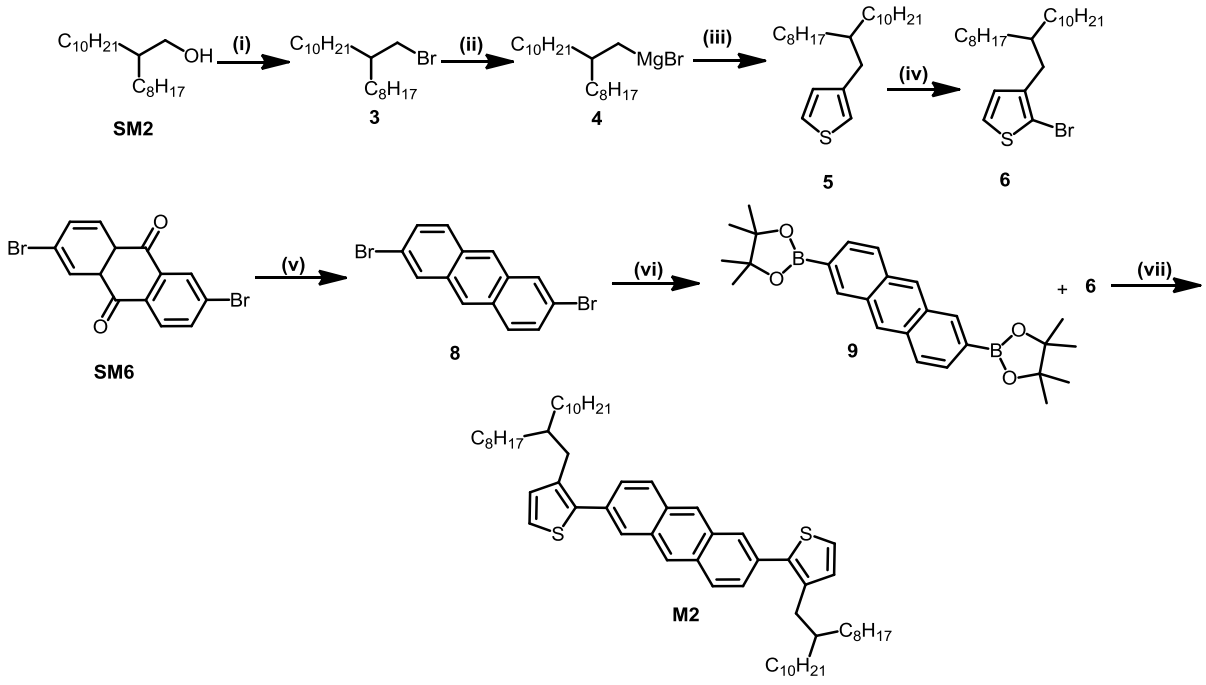

(i) NBS, PPh_3, DCM. **(ii)** Mg, dry THF. **(iii)** 3-Bromothiophene (SM3), $Ni(dppp)Cl_2$, dry THF, drop-wise. **(iv)** NBS, $CHCl_3$, AcOH. **(v)** AcOH, HI, H_3PO_2. **(vi)** Bis(pinacolato)diboron, KOAc, $Pd(dppf)Cl_2$. **(vii)** Compound **(6)**, $Pd(OAc)_2$, tri(*o*-tolyl)phosphine, dry THF, Aq. Sol. of $NaHCO_3$.

Scheme 0-3: Synthetic routes to **(M2)** donor monomer.

The synthesis of compounds **(3**, **4**, **5**, and **6)** was previously mentioned in (chapter 2) of this thesis. Compound **(8)** was synthesized according to a modified procedure by Škalamera *et al*.[9] by the reduction of 2,6-dibromoanthracene-9,10-dione **(SM5)** using a combination of three acids; acetic acid, hydroiodic acid, and hydrophosphorous acid and heating the mixture to reflux for 72 hours. Work-up followed to afford 2,6-dibromoanthracene **(8)** as yellow solid. The mechanism to the reduction process of 2,6-dibromoanthracene-9,10-dione is still unknown , scheme (3-4) below shows the reduction reaction of 2,6-dibromoanthracene-9,10-dione:

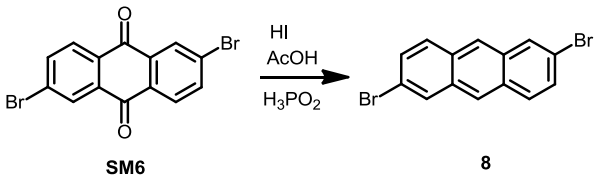

SM6 **8**

Scheme 0-4: Reduction reaction of 2,6-dibromoanthracene-9,10-dione.

This reaction was followed by the synthesis of 2,2'-(2,6-anthracenediyl)bis[4,4,5,5-tetramethyl]-1,3,2-dioxaborolane **(9)** by dissolving 2,6-dibromoanthracene **(8)** in dry DMF, adding bis(pinacolato)diboron, a solution of potassium acetate, and the catalyst Pd(dppf)Cl_2. The reaction mixture was stirred for 48 hours at 100 °C. Upon completion, the reaction mixture was extracted with $CHCl_3$, washed with distilled water and dried over $MgSO_4$, the resulting precipitate after removing the solvent *in vacuo* was washed with basic MeOH to remove any unreacted materials to yield 2,2'-(2,6-anthracenediyl)bis[4,4,5,5-tetramethyl]-1,3,2-dioxaborolane **(9)** as a black solid. The final step is the Suzuki coupling of 2,2'-(2,6-anthracenediyl)bis[4,4,5,5-tetramethyl]-1,3,2-dioxaborolane **(9)** and 2-bromo-(3-octyldodecyl)thiophene **(6)** using $Pd(OAc)_2$ as a catalyst to yield **(M2)** as a yellow sticky liquid. ^{1}H NMR of donor monomer **(M2)** is depicted in figure (3-2) below:

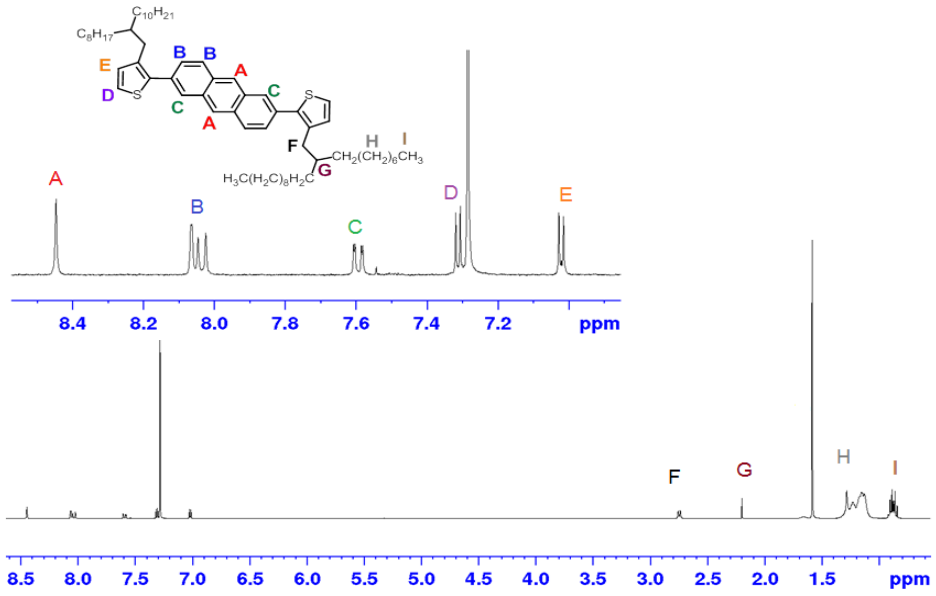

Figure 0-2: ^{1}H NMR spectra of **(M2).**

The purity of all other synthesized compounds was confirmed by ^{1}H NMR, ^{13}C NMR, elemental analysis and mass spectroscopy.

3.2.2 Synthesis of Polymers

M2 was reacted with two different BTD acceptor monomers 4,7-dibromobenzo[c][1,2,5]thiadiazole **(SM11)** and 5,6-difluoro-4,7-diiodo-benzo[*c*][1,2,5]thiadiazole **(2)**. A direct hetero arylation polymerization process was followed to synthesize the two targeted polymers by using both donor and acceptor moieties in a ratio of 1:1 equivalents in a sealed tube, this polymerization was catalysed with $Pd_2(dba)_3$, (*o*-OMePh)$_3$P as a ligand and dry THF as the solvent at 120 °C. The reaction time is different for each polymer depending on the precipitation of the polymer out of the reaction solution. These polymers **P5** and **P6** were washed with NH_4OH solution to remove any remaining catalyst. The fractionation of the polymers was done by Soxhlet extraction with different solvent starting from methanol, acetone, hexane and ending with toluene. This process was followed by the precipitation of the polymers in methanol to afford **P5** and **P6** as dark red solids. The chemical structures of **P4** and **P5** were confirmed by ^{1}H NMR, GPC and elemental analysis. (3-5) below shows the synthetic routes to the targeted polymers:

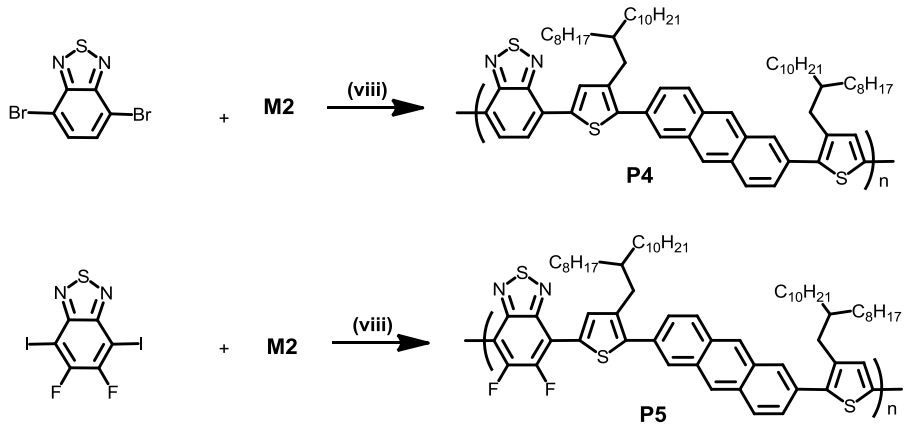

(viii) $Pd_2(dba)_3$, P(*o*-MeOPh)$_3$, $CsCO_3$, pivalic acid, 1cm^3 Dry THF, 120 °C.

Scheme 0-5: Synthetic routes to **P4** and **P5**.

3.2.3 GPC analysis

GPC measurements were conducted using chloroform as an eluent at 40 °C. Polymer **P4** has shown a slightly high number average molecular weight (M_n = 16,000 Da), compared to **P5** which has a (M_n of 15,900 Da), these polymers were both collected in the toluene fraction. A comparison between **P4** and **PPATBT** prepared by Al-moetaq *et al*.[8] illustrates that the number average molecular weight of **P4** is almost five times the molecular weight of **PPATBT**. This might be due to the steric effects of the thienyl segments attached to positions 9 and 10 on the anthracene moiety. It could also be attributed to the decreased solubility of the polymer when more aromatic structures are

present within the polymer chain which makes the overall structure more rigid. Polymers **P4** and **P5** can be compared to the first family of polymers that have been synthesized (results and discussion, Chapter 2), the anthracene based polymers have shown higher molecular weight compared to the naphthalene counterpart such as **P1** that has shown a M_n of 8,500 Da. This is attributed to the solubility of the polymer which was collected in hexane fraction, also the structure of the polymer **P4** with the anthracene unit that has an additional fused ring compared to the naphthalene based polymer **P1**. The GPC results of **P2** and **P3** are clearly showing higher molecular weights than those of **P4** and **P5** due to the decreased solubility and aggregation of these polymers due to the anthracene incorporation although they were collected in similar toluene fraction. Table (3-1) below illustrates the GPC results of **P4** and **P5**.

Table 0-1: GPC data of **P4** and **P5.**

Polymer	Fraction	Yield %	M_n (Da)[a]	M_w (Da)[a]	PDI[b]
P4	toluene	93%	16,000	38,900	2.43
P5	toluene	91%	15,900	28,000	1.76

[a] Detected by differential refractive index (DRI), toluene fractions of the polymer has been measured. [b] is the Polydispersity index.

3.2.4 Optical properties of the polymers

The optical properties of the synthesized polymers were studied as both solutions and thin films. Table (3-2) shows the UV-visible data that includes the absorption maxima values in both solutions and films, absorption maxima onsets for the synthesized polymers and optical band gaps calculated from λ_{max} onset of the plot.

Table 0-2: UV-visible data for **P4** and **P5.**

Polymer	λ_{max} Solution (nm)	λ_{max} Film (nm)	ε ($M^{-1}cm^{-1}$)		λ_{max} onset Solution (nm)	λ_{max} onset Film (nm)	Eg(opt)[b] (eV)
			π-π* [c]	ICT [d]			
P4[a]	512	522	18,100	13,000	597	628	1.97
P5[a]	512	533	24,700	27,600	602	623	1.99

[a] Toluene fraction. [b] Optical band gap ($E_{g\ opt}$), determined from the absorption maxima onset of UV-vis in polymers thin films. [c] Absorption coefficient for (π-π*) at λ_{max}=348 nm for both **P4** and **P5**, [d] Absorption coefficient for (ICT) at λ_{max}=512 nm for **P4** and **P5.**

Table (3-2) and figures (3-3a, b) show that the absorption behaviour of **P4** and **P5** have a similar trend in both solution and thin films with differences at some points. Both polymers have similar λ_{max} value at 512 nm, peaks at this value correspond to π-π* transition. The absorption maximum of **P5** in thin film is slightly red shifted compared to **P4** by about 11 nm. This might be attributed to the effect of the fluorine atoms on the chemical structure of **P5**. However, the absorption maxima of **PPATBT** for both solution and thin film are red shifted with λ_{max} values of 532 and 563 respectively. The optical band gap of polymers **P4** and **P5** are 1.97 and 1.99 respectively, these are similar to **P1** and **P2** (chapter 2 results and discussion) although they have different building blocks based on naphthalene donor unit. Compared to **PPATBT** which was synthesized by Al-meataq *et al*.,[8] the synthesized polymers showed higher band gap due to the existence of the attached alkoxy benzene ring on the anthracene unit which means that **PPATBT** has an extended conjugated system on the donor unit with a band gap of 1.86 eV compared to **P4** and **P5**. It can be clearly seen that the extent to which the extension of the conjugated system is effective and can shift the absorption maxima for both solution and thin film onto a red shifted peaks, it can also lower the band gap of the polymers significantly through the intramolecular charge transfer and the electronic delocalization of π orbitals.

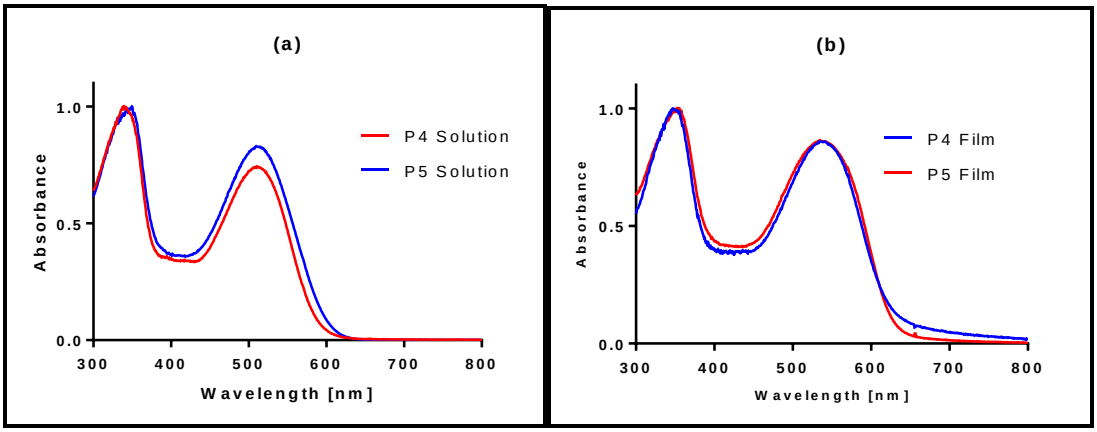

Figure 0-3: UV-visible for **P4** and **P5** (a) in solutions (b) as thin films

3.2.5 Electrochemical Properties

The cyclic voltammetry (CV) studies were conducted by casting polymeric films from chloroform solutions. Table (3-3) and figure (3-4) illustrate the HOMO and LUMO levels, as well as the electrochemical band gap of **P4** and **P5**. The HOMO level is calculated from the onset of the oxidation state, while the LUMO level is determined from the reduction onset. Each polymer has shown different oxidation and reduction states based on the differences its chemical structure. The HOMO levels of **P4** and **P5** are -5.45 and -5.55 eV respectively, with slightly deep HOMO level for **P5** due to the fluorine effect that lowers the HOMO level of this polymer. LUMO levels were calculated for **P4** and **P5** to be -3.40 and -3.32 eV respectively, no fluorine effect has been noticed on the LUMO level of the fluorinated polymer **P5**.

Table 0-3: Cyclic voltammetry results for **P4** and **P5**.

Polymer	HOMO (eV)[a]	LUMO (eV)[b]	E_g (eV)[c]	Eg(opt)[b] (eV)
P4	-5.45	-3.40	2.09	1.97
P5	-5.55	-3.32	2.23	1.99

[a] HOMO level of the polymer calculated from the oxidation potential onset, [b] LUMO level of the polymer calculated from the reduction potential onset, [c] electrochemical band gap.

The electrochemical properties of the synthesized polymers were compared to the previously synthesized polymers (chapter 2 results and discussion) which are based on naphthalene donor unit, the HOMO levels of **P1** and **P2** were -5.41 and -5.60 eV, these levels are close to the HOMO levels of **P4** and **P5**. This means that when switching from naphthalene to an anthracene donor unit, the HOMO levels would not be

significantly affected by this change. The LUMO levels for **P1** and **P2** are -3.31 and -3.57 eV respectively; this will give an idea that the fluorine atoms effect on **P2** is higher than the effect on **P5**. The electrochemical properties of the synthesized polymers in this chapter were also compared to **PPATBT** which is based on anthracene-BTD donor-acceptor polymer. The calculated HOMO level for **PPATBT** is -5.44, which is very similar to this of **P4**. The calculated LUMO level is -3.21 which is shallower compared to these of **P4** and **P5**, showing a band gap of 2.23 eV which is in the end is wider than those of **P4** and **P5**.

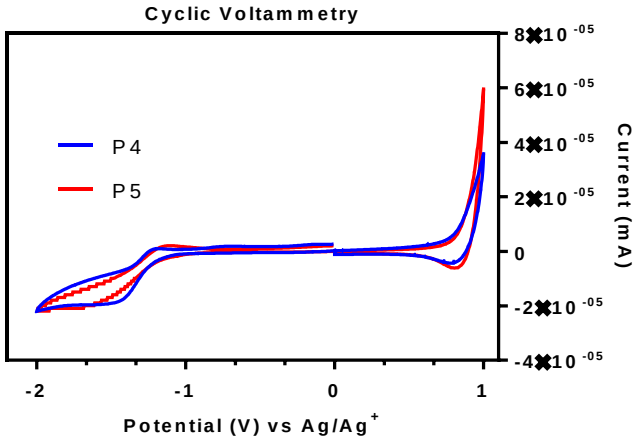

Figure 0-4: Cyclic voltammetry plots for **P4** and **P5.**

3.2.6 Polymers' XRD studies

The morphology of the prepared polymers **P4** and **P5** were studied via powder X-ray diffraction. Figure (3-5) shows that **P4** has a completely different behaviour than that of **P5**. It can be seen that **P4** displays a very broad peak in the π-π stacking area of the polymer with the highest peak of 2Θ value of 21.3°, which corresponds a distance value of 4.14 Å between the polymer chains, which means that **P4** shows amorphus structure. This is due to the steric hindrance of the side alkyl chains which prevent the polymeric chains from stacking together. However, **P5** has shown very sharp peaks of 2Θ at 21.5 and 23.8°, these peaks correspond a distance 4.12 and 3.73 Å respectively. These peaks can be attributed to the strong π-π stacking of the polymer chains together due to the intermolecular forces between the neighboring chains, which in turn results from the contribution of the fluorine atoms on the BTD moiety. It is important to refer to the fact that introducing florine atoms to the polymer backbone can increase the intermolecular and the intramolecular interaction between the polymer chains and between the polymer units, which may lead to more crystalline structures resulted from

the non-covalent bonding of S···H and also F···H.[10] It was also proven that the fluorine atoms will not cause any steric hindrance when attached to the polymer's backbone.

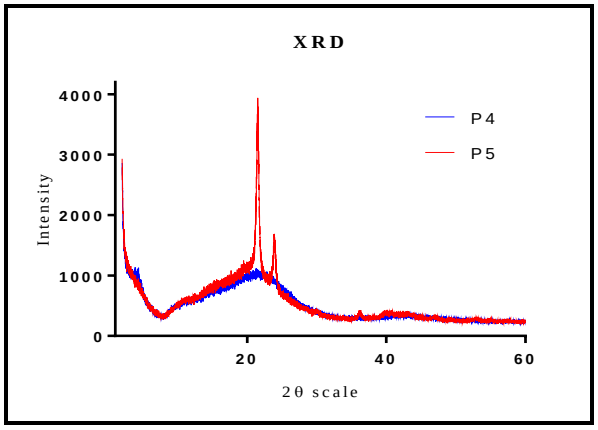

Figure 0-5: Powder X-Ray diffraction plots for **P4** and **P5**.

3.2.7 Thermal Gravimetric Analysis Studies

The synthesized polymers were investigated by thermal gravimetric analysis TGA as shown in figure (3-6). By observing the TGA data in table (3-4) below, it can be seen that both polymers have shown very good thermal stability against the temperature raise within the time. Although **P4** has started to decompose at 279 °C, the first weight loss of the alkyl chains started at 433 °C and ended at 513 °C. The thermal degradation for **P5** started at higher temperature of 307 °C compared to **P4**, as the first weight loss has begun at 443 °C and ended at 482 °C. By moving to the second weight loss which is related to the degradation of the aromatic rings, it is clear that **P5** has much more thermal stability than **P4** by showing a weight loss range between 603-648 °C compared to **P4** which has shown a weight loss between 561-618 °C. Comparing these polymers to the previously prepared series of polymers (Chapter 2 – results and discussion) has clearly shown that **P4** and **P5** have less thermal stability than the first family of synthesized polymers **P1**, **P2** and **P3**. This might be associated to the lower molecular weight of M_n for **P4** and **P5** compared to **P2** and **P3**.

Table 0-4: TGA data for **P4** and **P5.**

Polymer	D_1/ °C[a]	D_2/ °C[a]	TPWL (%)[c]	EPWL(%)[d]	R_m/wt %[e]
P4	433-513	561-618	45	35	6.25
P5	443-482	603-648	49	57	5.65

[a] D_1 is the first degradation onset. [b] D_2 is the second degradation onset. [c] TPWL is the percentage of theoretical weight loss. [d] EPWL is the percentage of experimental weight loss. [e] R_m is the remaining weight after heating to 800 °C.

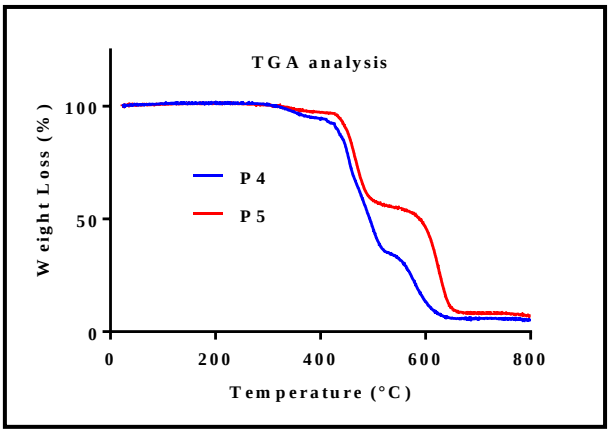

Figure 0-6: TGA plots for **P4** and **P5.**

3.3 Conclusion

Two polymers have been synthesized in this chapter based on BTD as an acceptor and anthracene bithiophene as a donor moiety. Alkyl chains were attached to the thiophene units in order to increase the solubility of the synthesized polymers. Anthracene can be considered as a very good donor molecule due to its ability to form crystalline structure as well as the increased charge mobility which can be offered by this molecule. Two different BTD molecules were used in the polymers synthesises to compare the differences between fluorinated and the non-fluorinated polymers. Direct (hetero) arylation polymerization method was used to synthesize the two polymers by using Pd (0) as a catalyst. The resulted polymers were checked by different analytical techniques such as ^{1}H NMR, elemental analysis, GPC, UV-vis, CV and XRD. The results from the GPC have shown the number average molecular weight for both polymers are around 16,000 Da, which is higher than the non-fluorinated polymer **PPABTB** prepared by Al-meataq *et al*.[8] that showed *Mn* of 3,500 Da. A red shift was noticed within the UV-visible plots for the solution of the fluorinated polymer **P5** compared to the non-fluorinated polymer **P4**; this shows the effect of the fluorine atoms on the polymer structure. The optical band gaps for **P4** and **P5** were calculated from the absorption maxima onset in the thin film state of the two polymers, showing bandgaps of 1.97 and 1.99 eV for **P4** and **P5** respectively. Cyclic voltammetry studies revealed that the electrochemical bandgaps of the polymers are higher than those calculated from the UV-vis, and that the electrochemical bandgap of **P5** is slightly higher than the bandgap of **P4** due to the fluorine effect by lowering the HOMO and the LUMO of the synthesized polymer at the same time. The thermal stability of the prepared polymers was investigated by TGA, and the thermal behaviour of **P4** and **P5** were stable at temperatures above 270 °C reaching high temperature up to 800 °C. Interestingly, the XRD plot for **P5** has shown sharp peaks at region of π-π stacking showing that this polymer has some crystalline structures compared to the **P4** that has a broad peak with an amorphous structure.

It can be clearly seen that attaching fluorine atoms to anthracene-alt-BTD conjugated polymers has an influence on both bandgap and morphology of **P5**. It has been hypothesised that low-lying HOMO level of conjugated polymer is accompanied by high V_{oc} value which in turn leads to a high PCE% values.[11] XRD plot showed improved crystalline structure of **P5** compared to that of **P4** due to ordered π-π stacking. This polymer might enhance the morphology of the active layer of photovoltaic devices when blended with fullerene derivative leading to high charge carrier mobility and high power conversion efficiency.

Chapter 3 References

1. T. Lei, J.-Y. Wang and J. Pei, *Accounts of chemical research*, 2014, **47**, 1117-1126.
2. J. D. Yuen and F. Wudl, *Energy & Environmental Science*, 2013, **6**, 392-406.
3. C. B. Nielsen, M. Turbiez and I. McCulloch, *Advanced Materials*, 2013, **25**, 1859-1880.
4. X. Zhan, A. Facchetti, S. Barlow, T. J. Marks, M. A. Ratner, M. R. Wasielewski and S. R. Marder, *Advanced Materials*, 2011, **23**, 268-284.
5. A. Köhler and H. Bässler, *Electronic processes in organic semiconductors: An introduction*, John Wiley & Sons, 2015.
6. V. Coropceanu, J. Cornil, D. A. da Silva Filho, Y. Olivier, R. Silbey and J.-L. Brédas, *Chemical reviews*, 2007, **107**, 926-952.
7. L. Ai, X. Ouyang, Q. Liu, S. Wang, R. Peng, A. Islam and Z. Ge, *Dyes and Pigments*, 2015, **115**, 73-80.
8. M. S. Almeataq, H. Yi, S. Al-Faifi, A. A. Alghamdi, A. Iraqi, N. W. Scarratt, T. Wang and D. G. Lidzey, *Chemical Communications*, 2013, **49**, 2252-2254.
9. Đ. Škalamera, J. Veljković, L. Ptiček, M. Sambol, K. Mlinarić-Majerski and N. Basarić, *Tetrahedron*, 2017, **73**, 5892-5899.
10. K. Reichenbächer, H. I. Süss and J. Hulliger, *Chemical Society Reviews*, 2005, **34**, 22-30.
11. L. Huo, J. Hou, S. Zhang, H. Y. Chen and Y. Yang, *Angewandte Chemie*, 2010, **122**, 1542-1545.

Chapter 4

Synthesis and Characterisation of Pyrene-based D-A Conjugated Polymers

4.1 Introduction

The increased attention given to conjugated polymers is due to their importance in electronic devices fabrication as well as the various advantages over organic small molecules and inorganic semiconductors.[1] These polymers can be designed and synthesized with different properties, structures and functional groups to fit the need of the organic based electrical devices.[1]These materials can be used in various optoelectronic devices such as light emitting diodes LED, field-effect transistors and solar cells,[2] as they offer great solution for the issues of energy as well as technology development.[3] Compared to small organic molecules and inorganic materials, conjugated polymers have many advantages such as their light weight, low cost and good flexibility. The most important advantage is that conjugated polymers have good solubility meaning they can be easily processed from solutions.[3]

Pyrene is a molecule that has unique and attractive photophysical and electronic properties. This has encouraged researchers to focus their research on their application in electronic devices, especially in the last decade.[4-6] This has made it possible to put pyrene organic compounds as alternative candidates to inorganic-based semiconductors compounds.[7] Recently, researchers are emphasizing the modification of new conjugated systems through several methods such as designing the molecular structure, morphology optimization and the choice of donor and acceptor repeat units for high performance materials used in electronic devices. Pyrene based conjugated polymers were invested as active layers in OFETs, OLEDs and solar cells.[7]

Conjugated polymers based on 1,6- substituted pyrene and phenyleneethylene units (figure 4-1) were synthesized by Gang *et al*.[8] These polymers were studied from different aspects including the cyclic voltammetry CV, and the main purpose of these polymers is their use as sensors to detect other materials. The electrochemical properties of the two synthesized polymers **PyPE-1** and **PyPE-2** have shown a band gap of 2.07 eV.

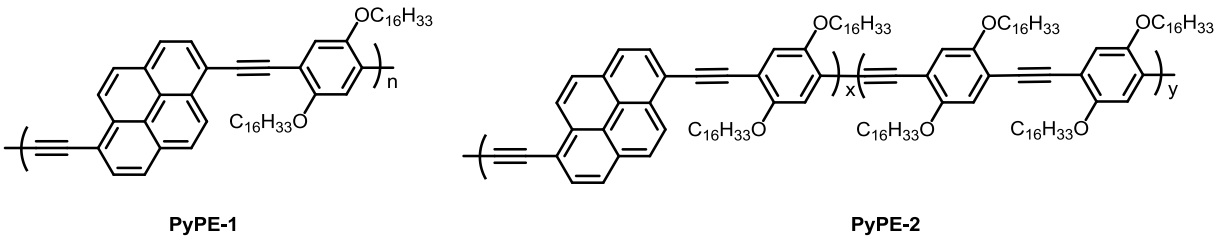

Figure 0-1: Chemical structure of pyrene-based conjugated polymers **PyPE-1** and **PyPE-2** synthesized by Gang *et al.*[8]

Another research study by Yang *et al.*[9] revealed the difference in the optical and the electrochemical properties of the 1,6- and the 2,7-substituted pyrene systems in the synthesized D-A polymers **P(DTDPP-alt-(1,6)PY) P(DTDPP-alt-(2,7)PY)** shown in figure (4-2) below. The optical properties of **P(DTDPP-alt-(2,7)PY)** have shown a narrower band gap of 1.65 eV compared to **P(DTDPP-alt-(1,6)PY)** which showed a band gap of 1.71 eV. The electrochemical band gaps calculated by the cyclic voltammetry were 1.85 and 1.84 eV for **P(DTDPP-alt-(1,6)PY)** and **P(DTDPP-alt-(2,7)PY)** respectively**.** The thermal gravimetric analysis of the 2,7-pyrene substituted polymer has a higher thermal stability than that of the 1,6-substituted polymer due to the distortions between the pyrene moiety and the acceptor unit.[9]

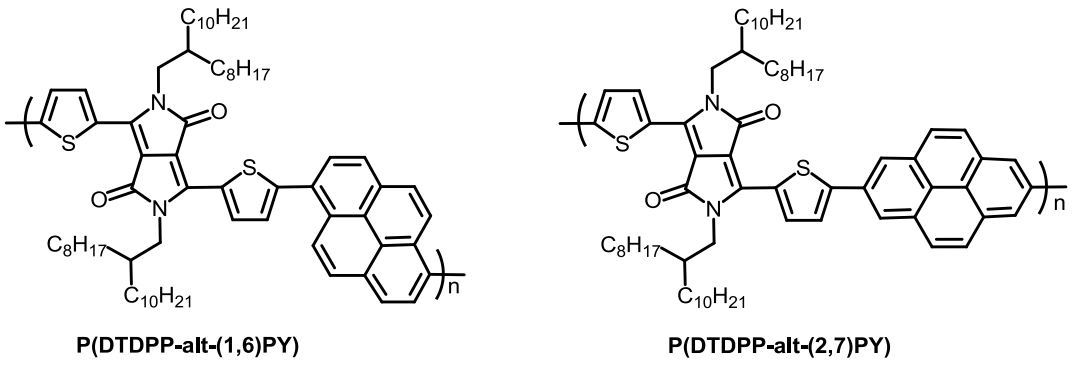

Figure 0-2: Chemical structure of pyrene-based conjugated polymers **P(DTDPP-alt-(1,6)PY)** and **P(DTDPP-alt-(2,7)PY)** synthesized by Yang *et al*.[9]

In this chapter, four polymers have been synthesized based on 2,7-linked pyrene moiety flanked by two thiophene units as a donor to synthesize the target polymers along with different fluorinated and non-fluorinated BTD units as acceptors. Alkyl chains were attached to the thiophene units to increase the solubility of the targeted polymers and to ease the characterization of the synthesized polymers. The synthesised polymers are compared to the pyrene-based polymers **P(DTDPP-alt-(1,6)PY)** and **P(DTDPP-alt-(2,7)PY)**prepared by Yang *et al*.[9]

4.2 Results and Discussion

4.2.1 Synthesis of Monomer

Similar reactions were followed to prepare 2-bromo-3-(2-octyldodecyl)thiophene **(6)** (see Chapters 2 and 3). Compound **(10)** was synthesized according to the procedure by Ji *et al*[10] by reacting pyrene with bis(pinacolato)diboron catalysing with $[Ir(OMe)COD]_2$ and 4,4'-di-*tert*-butyl-2,2'bipyridine, and the mixture was stirred at 80 ˚C for 16 hours. Upon completion, distilled water was added and the reaction mixture was extracted with chloroform. The solvent was reduced *in vacuo* and the product was precipitated from basic MeOH, and the product 2,7-bis(4,4,5,5,-tetramethyl-1,3,2,-dioxaborolan-2-yl)pyrene **(10)** was collected as a grey powder. This product was then reacted with 2-bromo-(3-octyldodecyl)thiophene **(6)** *via* Suzuki coupling reaction using $Pd(OAc)_2$, tri(*o*-tolyl)phosphine, and a saturated aqueous solution of $NaHCO_3$ to afford 2,7-bis(3-(2-octyldodecyl)thiophen-2-yl)pyrene **(M3)** after purification with silica gel column chromatography eluting with PE only. **(M3)** was collected as a green liquid. Synthetic routes to **(M3)** are pictured in scheme (4-1) below:

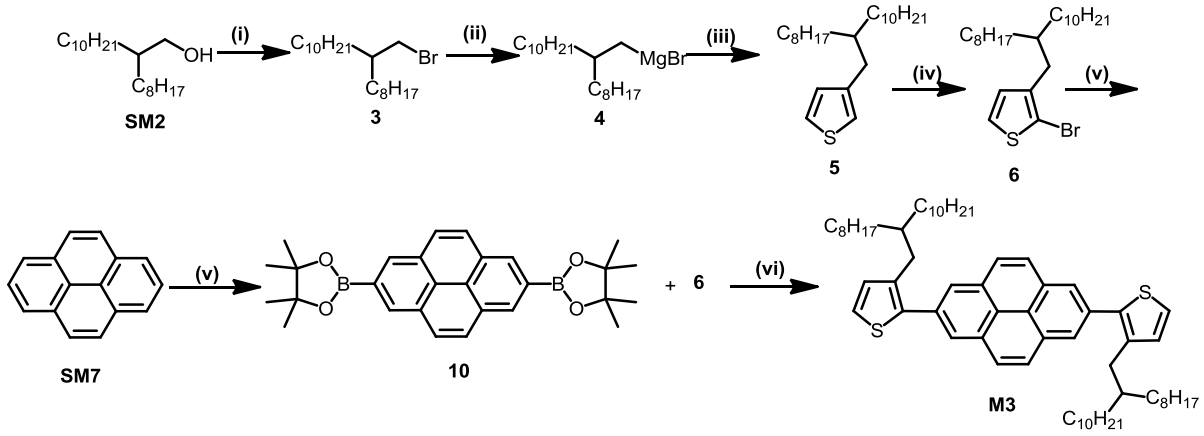

(i) NBS, PPh_3, DCM. **(ii)** Mg, dry THF. **(iii)** 3-Bromothiophene (SM3), $Ni(dppp)Cl_2$, dry THF, drop-wise. **(iv)** NBS, $CHCl_3$, AcOH. **(v)** Bis(pinacolato)diboron, $[Ir(OMe)COD]_2$, 4,4'-di-*tert*-butyl-2,2'-bypyridine. **(vi)** Compound **(6)**, $Pd(OAc)_2$, tri(*o*-tolyl)phosphine, dry THF, Aq. Sol. of $NaHCO_3$.

Scheme 0-1: Synthetic routes to 2,7-bis(3-(2-octyldodecyl)thiophen-2-yl)pyrene **(M3)**.

The ^1H NMR spectra for **(M3)** is depicted in figure (4-3) showing four peaks in the aromatic region of the plot at 8.26, 8.12, 7.37 and 7.08 ppm as doublet peaks due to the coupling to the nearest proton or due to the long range coupling in pyrene unit, these peaks correspond the four aromatic proton environments in **(M3)**. The chemical structure of 2,7-bis(3-(2-octyldodecyl)thiophen-2-yl)pyrene **(M3)** was confirmed by other techniques including mass spectroscopy, and elemental analysis.

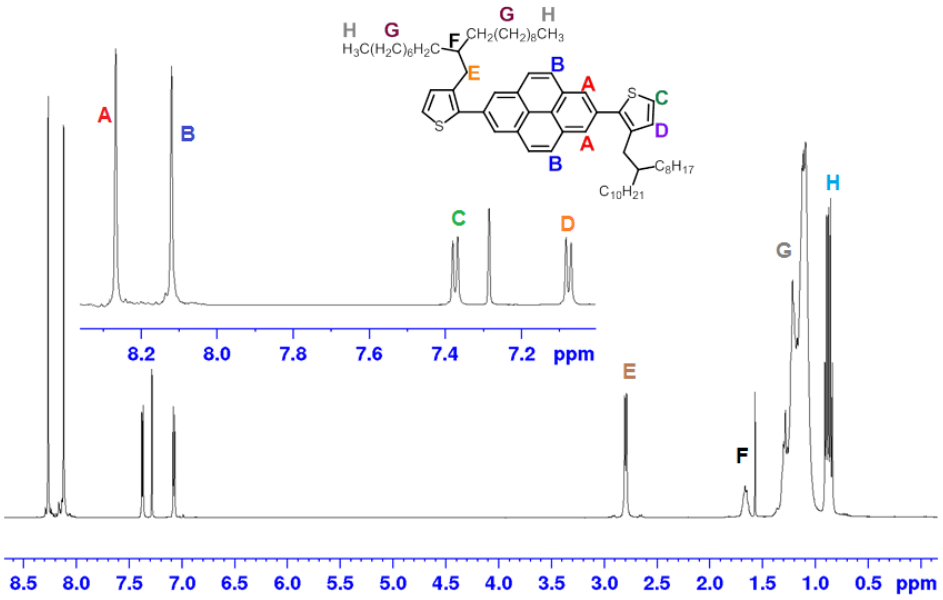

Figure 0-3: ^{1}H NMR spectrum of 2,7-bis(3-(2-octyldodecyl)thiophen-2-yl)pyrene **(M3)**.

4.2.2 Synthesis of Polymers

The donor monomer 2,7-bis(3-(2-octyldodecyl)thiophen-2-yl)pyrene **(M3)** was reacted with different acceptor monomers, these include; 4,7-dibromobenzo[c][1,2,5] thiadiazole **(SM11)**, 4,7-diiodo-5,6-difluorobenzo[*c*][1,2,5]thiadiazole **(2)**, 4,7-bis(5-bromothiophen-2-yl)benzo[*c*][1,2,5]thiadiazole **(SM12)** and 4,7-bis(5-bromothiophen-2-yl)5,6-difluorobenzo[*c*][1,2,5]thiadiazole **(SM13)** respectively *via* a direct hetero arylation polymerization (DHA)[11] procedure to synthesize the two targeted polymers by using both donor and acceptor moieties in a ratio of 1:1 equivalents in a sealed tube specially made for this kind of polymerisation. The polymerization reaction was catalysed with $Pd_2(dba)_3$, , pivalic acid and (*o*-OMePh)$_3$P as a ligand using dry THF as the solvent at 120 °C. The reaction time is different for each polymer depending on the polymer precipitation out of the reaction solution. The resulting polymers were washed with NH_4OH solution to remove any remaining catalyst. This step was followed by fractionation of polymers by extracting using a Soxhlet apparatus with different solvent starting from methanol, acetone, hexane and ending with toluene. This process was followed by the precipitation of the polymers in methanol to afford **P6** and **P7** as dark red solids, **P8** and **P9** as dark purple solids. The chemical structures of polymers were confirmed by ^{1}H NMR and elemental analysis. Scheme (4-2) below shows the synthetic routes of the targeted polymers:

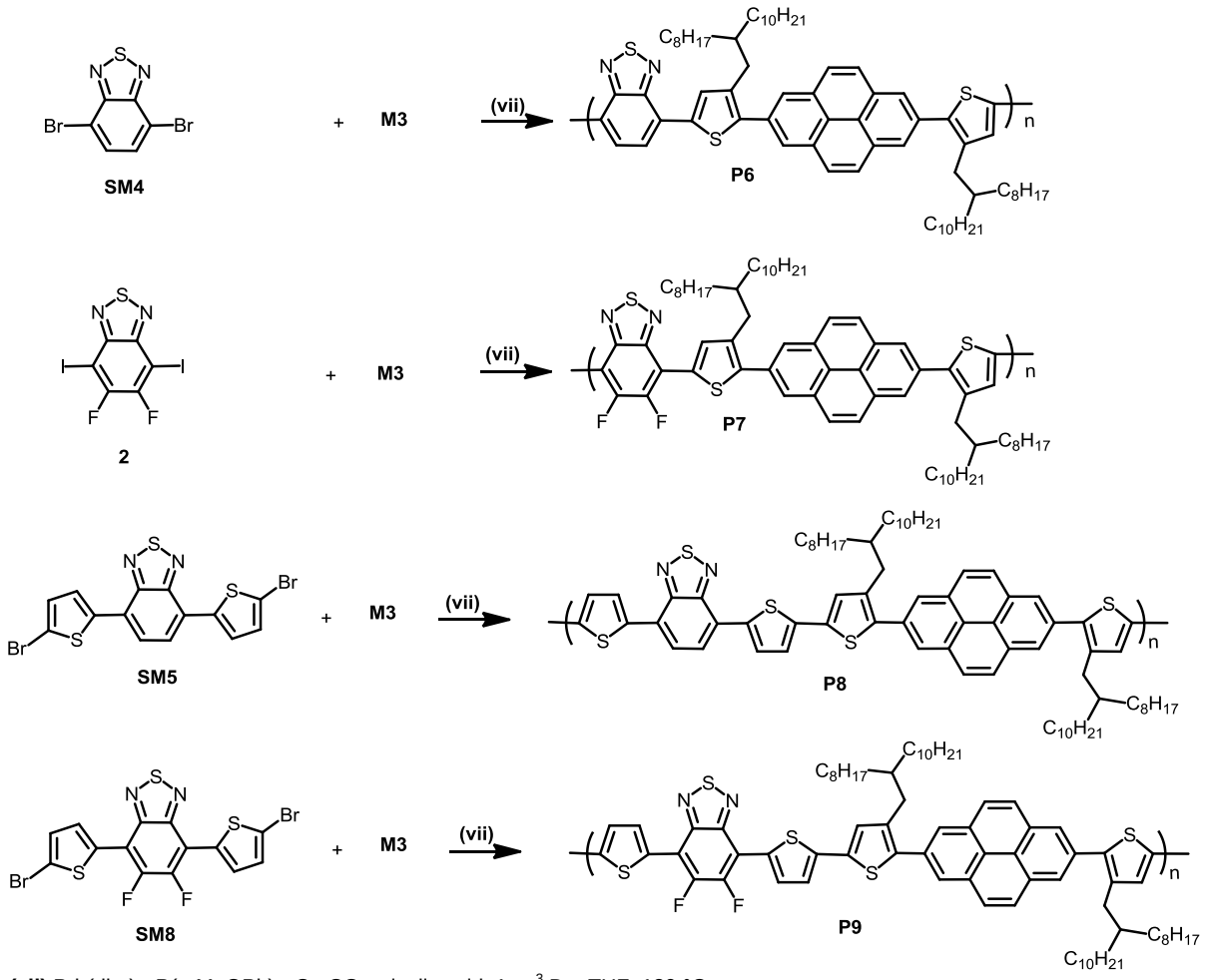

(vii) $Pd_2(dba)_3$, P(*o*-MeOPh)$_3$, Cs_2CO_3, pivalic acid, 1cm^3 Dry THF, 120 °C.

Scheme 0-2: Synthetic routes to the pyrene-BTD based conjugated polymers.

Polymers **P6**, **P7**, **P8** and **P9** were also characterized using GPC, TGA, powder XRD. The optical and the electrochemical properties were studied by using UV-visible and cyclic voltammetry CV techniques.

4.2.3 GPC analysis

GPC studies were conducted using toluene as a flow rate mark at room temperature. It can be seen from table (4-1) that **P6** shows the highest number average molecular weight of 17.2 KDa with the highest yield collected in toluene fraction, followed by **P7** which has a M_n of about 10.3 KDa. Although it was anticipated that **P6** and **P7** would show lower molecular weight according to the current chemical structures that show a steric effect between the substituted thiophene rings and the adjacent BTD moiety. Lower M_n has been noticed for **P8** and **P9** in toluene fractions with a M_n of 5.3 KDa and 8.6 KDa and yields of 35 and 43% respectively. This is due to the precipitation of the polymer around the reaction tube showing the maximum molecular weight obtained. This could be ascribed to the aggregation of the polymer caused by the rigid structure

of pyrene unit. Pyrene polymers prepared by Yang *et al*. **P(DTDPP-alt-(1,6)PY)** and **P(DTDPP-alt-(2,7)PY)** have shown a number average molecular weights *Mn* of 22.9 and 30.4 KDa respectively. These polymers **P(DTDPP-alt-(1,6)PY)** and **P(DTDPP-alt-(2,7)PY)** have high poly dispersity indexes of 2.94 and 15.85 respectively.[9]

Table 0-1: GPC data of **P6, P7, P8** and **P9.**

Polymer	Fraction	Yield %	M_n(Da)[a]	M_w(Da)[a]	PDI[b]
P6	toluene	68%	17,200	27,000	1.57
P7	toluene	39%	10,300	25,700	2.49
P8	toluene	35%	5,300	8,700	1.64
P9	toluene	43%	8,600	17,100	1.98

[a] Detected by differential refractive index (DRI), toluene fractions of the polymer has been measured. [b] is the Polydispersity index.

4.2.4 Optical properties of the polymers

Optical properties of the synthesized polymers were studied in both solution and thin film states.

Table 0-2: UV-visible data for **P4** and **P5.**

Polymer	λ_{max} Solution (nm)	λ_{max} Film (nm)	ε ($M^{-1}cm^{-1}$)		λ_{max} onset Solution (nm)	λ_{max} onset Film (nm)	Eg(opt)[b] (eV)
			π-π* [c]	ICT [d]			
P6[a]	505	530	35,200	24,800	586	610	2.00
P7[a]	503	523	76,100	36,500	590	608	2.00
P8[a]	550	561	51,600	33,100	703	712	1.74
P9[a]	540	563	59,200	44,200	679	690	1.79

[a] Toluene fraction. [b] Optical band gap ($E_{g\ opt}$), determined from the absorption maxima onset of UV-vis in polymers thin films. [c] Absorption coefficient for (π-π*) at λ_{max}=345 nm, [d] Absorption coefficient for (ICT) at λ_{max}=530 nm**.**

Table (4-2) above shows the absorption maxima and the band gap as calculated from the absorption maxima onset for each polymer. The low energy absorption bands are

related to the intramolecular charge transfer (ICT) whereas the bands at high energy absorption correspond to π-π* transitions as shown in figure (4-3). The optical properties revealed that **P6** and **P7** have shown almost the same λ_{max} values in solutions of around 505 nm, while λ_{max} in thin films were shown at 530 and 523nm for **P6** and **P7** respectively, although **P7** has two fluorine atoms attached to the BTD unit. It is clear that the peak for **P7** is slightly blue shifted compared to **P6** in both solution and thin film states, the same effect has been noticed with the fluorinated BTD polymer **P9**.Polymers **P8** and **P9** have shown much higher λ_{max} values compared to the first two polymers as the conjugated system has extended by adding additional thiophene units into the polymer backbone. The value of λ_{max} were shown at 550 and 540 nm in solution, 560 and 563 nm in thin film state for **P8** and **P9** respectively. The band gaps for **P6** and **P7** were calculated to be 2.00 eV, while **P8** and **P9** have band gaps of 1.74 and 1.79 respectively. It has been reported that inserting thiophene units into the polymer's backbone next to the BTD moiety will improve not only the interchain interactions but also the charge mobility along the polymer's chains,[12, 13] this could be the main reason for the red shifted peaks and narrow band gaps in **P8** and **P9**. The synthesized polymers were compared to their pyrene based counterparts **P(DTDPP-alt-(1,6)PY)** and **P(DTDPP-alt-(2,7)PY),** these polymers have shown lower band gaps at 1.71 and 1.65 eV respectively. Figure (4-4) below shows the UV-visible spectrum for **P6**, **P7**, **P8** and **P9** in both solution and solid state.

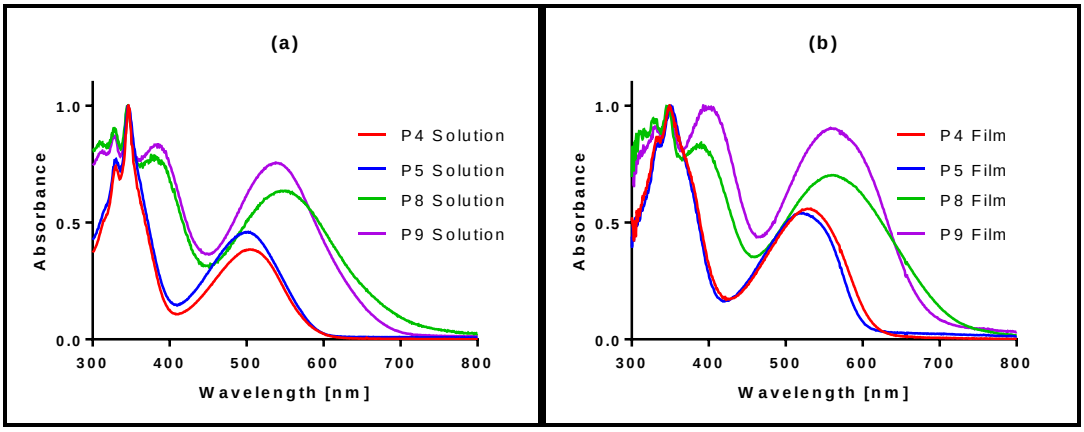

Figure 0-4: UV-visible for **P6, P7, P8** and **P9** (a) in solutions (b) as thin films

A comparison of optical results obtained for **P6**, **P7**, **P8** and **P9** to the previously synthesised conjugated polymers has shown that **P6** and **P7** have optical bandgaps almost similar to those of **P1**, **P2**, **P4** and **P5**, which means that the optical properties shall remain the same when switching the donor unit from naphthalene to anthracene then pyrene regardless to the number of fused rings exist in the donor unit. The low optical bandgap of **P8** and **P9** can be compared to this of **P3** as the conjugated system

in these polymers is extended by flanking additional thiophene units leading to more electron density along the polymers backbone.

4.2.5 Electrochemical Properties

The electrochemical properties for **P6**, **P7**, **P8** and **P9** were determined by casting polymeric films of the synthesized polymers on platinum electrode before running cyclic voltammetry studies. Table (4-3) below shows the HOMO, LUMO and the electrochemical band gap of each polymer. The HOMO level was calculated from the onset of the oxidation potential (E_{ox}) (figure 4-5), whereas the LUMO level was calculated from the onset of the reduction potential (E_{red}) according to the following equations:[14]

$$\text{HOMO} = - e\ (E_{ox} - 4.80)\ \text{eV}$$

$$\text{LUMO} = - e\ (E_{red} - 4.80)\ \text{eV}$$

The band gap of the polymer was calculated by subtracting the LUMO level from the HOMO level according to the following equation:[14]

$$E_g^{elec} = - (\text{HOMO} - \text{LUMO})\ \text{eV}$$

The information collected from the HOMO and LUMO levels calculations revealed that **P6** shows deeper HOMO level of -5.24 eV followed by **P8** which shows a HOMO level of -5.11 eV. Shallower HOMO levels were noticed for **P7** at -5.55 eV and **P9** at -5.47eV. Many studies hypothesised that the introduction of fluorine atoms will lower both HOMO and LUMO levels at the same time,[15-17] polymers **P7** and **P9** have shown almost similar band gaps according to their band gaps calculated from cyclic voltammetry (figure 3-4). The electrochemical band gaps for **P6** and **P8** are close to 2.00 eV. While polymers **P7** and **P9** have shown slightly lower electrochemical band gaps of 1.93 and 1.97 eV respectively, this is attributed to the extended conjugated system resulting from the insertion of the two thiophene rings into the **P7** and **P9** polymers' backbone. Previously synthesised polymers in chapters (2 and 3) have shown almost similar bandgaps for **P1**, **P2, P4** and **P5**. Polymer **P3** showed lower bandgap of 2.23 eV, this is due to the extended π-conjugated system in this polymer. It could be suggested that switching between different fused rings (naphthalene, anthracene and pyrene) used as donor units will sustain the bandgap of the polymer regardless to the number of fused rings in each unit, unless adding other aromatic units along the polymers backbone.

Table 0-3: Cyclic voltammetry results for **P6, P7, P8** and **P9.**

Polymer	HOMO (eV)[a]	LUMO (eV)[b]	E_g (eV)[c]
P6	-5.24	-3.22	2.02
P7	-5.55	-3.55	2.00
P8	-5.11	-3.17	1.93
P9	-5.47	-3.50	1.97

[a]HOMO level of the polymer calculated from the oxidation potential onset, [b] LUMO level of the polymer calculated from the reduction potential onset, [c] electrochemical band gap.

Comparing the electrochemical properties of the synthesized polymers **P6**, **P7**, **P8** and **P9** to **P(DTDPP-alt-(1,6)PY)** and **P(DTDPP-alt-(2,7)PY)** prepared by Yang *et al.*,[9] these polymers have shown higher band gaps due to the differences in the acceptor units. The electrochemical band gaps for **P(DTDPP-alt-(1,6)PY)** and **P(DTDPP-alt-(2,7)PY)** are 1.85 and 1.84eV respectively.

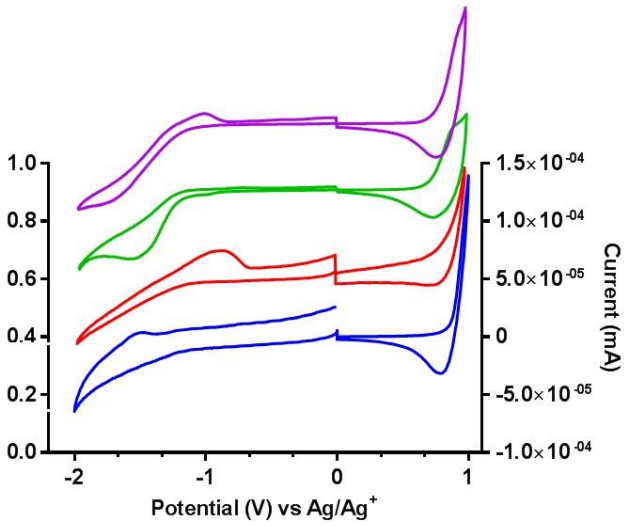

Figure 0-5: Cyclic voltammetry plots for **P6, P7, P8** and **P9.**

4.2.6 Polymers' XRD studies

The morphology of synthesized polymers **P6**, **P7**, **P8** and **P9** were studied using powder X-ray diffraction. Figure (4-6) revealed that polymers **P6**, **P8** and **P9** have very broad peaks at 2Θ of 21.6, 21.9 and 21.5° which correspond a distance between the polymer chains of about 4.11, 4.05 and 4.12 Å respectively.**P7** showed a sharp peak at 2Θ values of 24.3° which corresponds a distance between the polymer chains of 3.6 Å

that belongs to the ordered π-π stacking, this might be related to the crystalline structure and the arrangement of the polymeric chains due to the fluorine atoms attached to the BTD units. These fluorine atoms will enhance the order of the molecules via the interchain interaction between the polymer chains, the effect of attaching fluorine atoms can also improve the planarity of the polymer structure. In general, the synthesized polymers **P6**, **P7**, **P8** and **P9** have shown amorphous structure due to the existance of the branched alkyl chains that could cause steric hindrance for the neighbouring molecules.

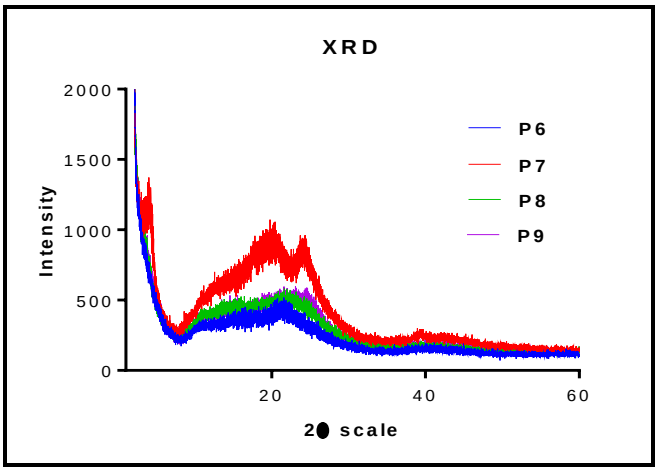

Figure 0-6: Powder X-Ray diffraction plots for **P6, P7, P8** and **P9**.

4.2.7 Thermal Gravimetric Analysis Studies

The thermal gravimetric analysis for the synthesized polymers **P6**, **P7**, **P8** and **P9** were investigated to check the thermal stability of these polymers at a temperature up to 800 °C as shown in figure (4-7) below. It is clear that polymers **P6**, **P7**, **P8** and **P9** have different thermal behaviour compared to the previously synthesized polymers by showing one degradation plot for each polymer.

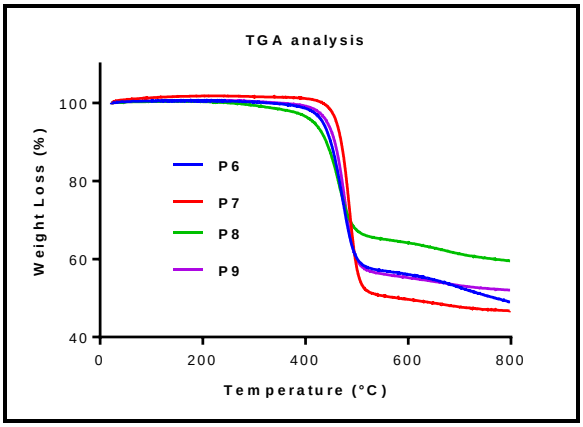

Figure 0-7: TGA plots for **P6, P7, P8** and **P9.**

Table (4-4) below illustrates the data collected from the TGA plots for each polymer; It can be seen from the data below that all of the synthesized polymers have high thermal degradation temperatures except for **P8**, this exception is due to the low molecular weight obtained for this polymer according to the GPC studies. Other polymers **P6**, **P7** and **P9** have shown thermal degradation temperatures above 300 °C. In general, all synthesized polymers have good thermal stability and the remaining percentages for **P6**, **P7**, **P8** and **P9** were in the range of 49-52%, which indicates the high temperatures >800° C that can be applied to check the thermal stability of the synthesized polymers.

Table 0-4: TGA data for **P6, P7, P8** and **P9.**

Polymer	D/°C[a]	TPWL (%)[b]	EPWL(%)[c]	R_m/wt %[d]
P6	440-501	48	58	49.0
P7	467-501	50	52	46.8
P8	433-490	46	66	59.5
P9	445-506	44	51	52.0

[a] D is the degradation onset. [b]TPWL is the percentage of theoretical weight loss. [c] EPWL is the percentage of experimental weight loss. [d] R_m is the remaining weight after heating to 800 °C.

4.3 Conclusion

A novel family of polymers **P6**, **P7**, **P8** and **P9** were synthesized in this chapter, these polymers are based on BTD or fluorinated BTD as acceptors, and 2,7-bithiophenepyrene as a donor. Alkyl chains were attached to the thiophene segments to increase the solubility of the resulting polymers. The polymerization method which has been followed is the direct hetero arylation (DHA) catalysed by tris(dibenzylideneacetone) dipalladium(0) $Pd_2(dba)_3$, tris(4-methoxyphenyl)phosphine, pivalic acid and cesium carbonate. The solvent used in all polymerization procedures is dry THF in a sealed reaction tube with a gas regulator fitted and under an inert atmosphere. All the prepared polymers were collected as dark coloured powders after washing with ammonium hydroxide and extracting with Soxhlet using a series of solvents. These polymers were characterized using different analysis techniques including ^{1}H NMR and elemental analysis. Other techniques were used to study the thermal, optical and electrochemical properties of these polymers using TGA, UV-visible and cyclic voltammetry respectively. Gel permeation chromatography GPC was used to check the molecular weight of the resulted polymers, as well as powder X-ray diffraction to study the morphology of these polymers. It can be seen from the GPC results that **P6** has shown the highest number average molecular weight about 17,200 Da compared to **P7**, **P8** and **P9**, while **P8** has shown the lowest M_n of about 5,300 Da compared to the other prepared polymers. The optical properties revealed that **P8** and **P9** have shown red shifts compared to **P6** and **P7**. The optical band gaps calculated from the absorption maxima onset of polymers **P6**, **P7**, **P8** and **P9** were 2.00, 2.00, 1.74 and 1.79 eV respectively. The main reason that **P8** and **P9** have smaller band gaps is the extended conjugation due to the insertion of thiophene segments into the polymers' backbone. The electrochemical properties of the polymers **P6**, **P7**, **P8** and **P9** have shown bandgaps around 2.00 eV which seem to be higher than these calculated from the UV-visible absorption maxima onset, especially for **P8** and **P9**. The results of the powder XRD have shown some sharp peaks for **P7** in Lamellar distance and the π-π stacking which have not been noticed for **P6**, **P8** and **P9**, and the latter group of polymers seem to be amorphous with no sharp peaks appeared in their XRD plots. All polymers have shown very good thermal stability according to the TGA results with degradation curves starting from above 300° C, except for **P8** that has shown a degradation curve starting from 210° C due to its low molecular weight determined by GPC analysis. The remaining percentages of **P6**, **P7**, **P8** and **P9** were in the range between 49-52%, which means that these polymers are highly stable at temperatures up to 800° C.

Fluorinated conjugated polymers **P7** and **P9** in this chapter have promising optical and electrochemical along with good thermal stability. Figure (4-8) shows the LUMO and LUMO levels of synthesised conjugated polymers **P6**, **P7**, **P8** and **P9** compared to the HOMO and LUMO levels of $PC_{71}BM$. It can be seen that **P7** and **P9** are compatible to be applied in solar cell devices due to the perfect distance (0.3 eV or less) between the LUMO levels of both polymer and $PC_{71}BM$. Moreover, fabrication of a photovoltaic device is possible by using active layer of conjugated polymer and fullerene derivative in different blending ratios.

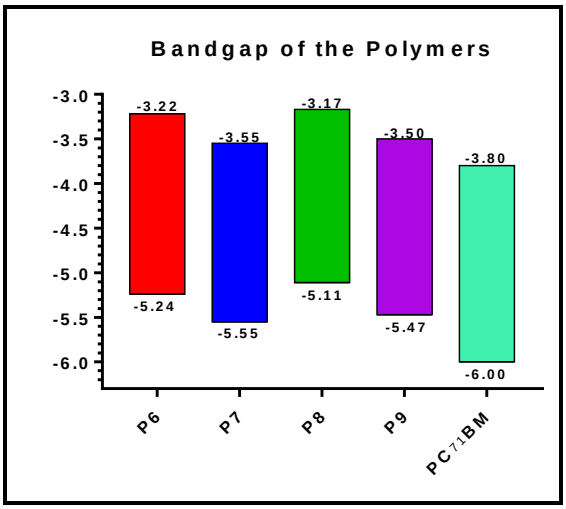

Figure 0-8: Bandgap and HOMO/LUMO levels of polymers **P6, P7, P8** and **P9**.

Chapter 4 References

1. X. Guo, M. Baumgarten and K. Müllen, *Progress in Polymer Science*, 2013, **38**, 1832-1908.
2. L. Bian, E. Zhu, J. Tang, W. Tang and F. Zhang, *Progress in Polymer Science*, 2012, **37**, 1292-1331.
3. S. Kola, J. Sinha and H. E. Katz, *Journal of Polymer Science Part B: Polymer Physics*, 2012, **50**, 1090-1120.
4. J. E. Anthony, *Angewandte Chemie International Edition*, 2008, **47**, 452-483.
5. Y. Shirota and H. Kageyama, *Chemical reviews*, 2007, **107**, 953-1010.
6. J. Wu, W. Pisula and K. Müllen, *Chemical reviews*, 2007, **107**, 718-747.
7. T. M. Figueira-Duarte and K. Müllen, *Chemical reviews*, 2011, **111**, 7260-7314.
8. G. He, N. Yan, J. Yang, H. Wang, L. Ding, S. Yin and Y. Fang, *Macromolecules*, 2011, **44**, 4759-4766.
9. D. S. Yang, K. H. Kim, M. J. Cho, J. I. Jin and D. H. Choi, *Journal of Polymer Science Part A: Polymer Chemistry*, 2013, **51**, 1457-1467.
10. L. Ji, K. Fucke, S. K. Bose and T. B. Marder, *The Journal of organic chemistry*, 2014, **80**, 661-665.
11. P.-O. Morin, T. Bura, B. Sun, S. I. Gorelsky, Y. Li and M. Leclerc, *ACS Macro Letters*, 2014, **4**, 21-24.
12. J. A. Letizia, M. R. Salata, C. M. Tribout, A. Facchetti, M. A. Ratner and T. J. Marks, *Journal of the American Chemical Society*, 2008, **130**, 9679-9694.
13. D. E. Janzen, M. W. Burand, P. C. Ewbank, T. M. Pappenfus, H. Higuchi, D. A. da Silva Filho, V. G. Young, J.-L. Brédas and K. R. Mann, *Journal of the American Chemical Society*, 2004, **126**, 15295-15308.
14. J. Hou, Z. a. Tan, Y. Yan, Y. He, C. Yang and Y. Li, *Journal of the American Chemical Society*, 2006, **128**, 4911-4916.
15. Y. Zhang, S.-C. Chien, K.-S. Chen, H.-L. Yip, Y. Sun, J. A. Davies, F.-C. Chen and A. K.-Y. Jen, *Chemical Communications*, 2011, **47**, 11026-11028.
16. S. Albrecht, S. Janietz, W. Schindler, J. Frisch, J. Kurpiers, J. Kniepert, S. Inal, P. Pingel, K. Fostiropoulos and N. Koch, *Journal of the American Chemical Society*, 2012, **134**, 14932-14944.
17. A. Iyer, J. Bjorgaard, T. Anderson and M. E. Köse, *Macromolecules*, 2012, **45**, 6380-6389.

Chapter 5

Synthesis and Characterisation of Carbazole, Fluorene and Bithiophene-Based Conjugated Polymers.

5.1 Introduction

Meeting the world's energy needs could be a real challenge to minimize the current damages to the environment. For this reason, researchers both in academia and industry have shown interest into the enhancement of solar cells based on polymeric materials.[1-3] Using BHJ techniques to design conjugated polymers as active materials in solar cells fabrication has many advantages such as processing ease, providing large interfacial area as well as lowering the total cost of the final product compared to the inorganic solar cells.[4]

Polymers that contain carbazole in their structure have been studied and used in many different applications such as light-emitting diodes, photorefractive materials and solar cell devices.[5] There are several reasons behind using the carbazole-based polymers including; first, the carbazole moiety can form holes or radical cations. Second, it is possible to attach different groups to the carbazole moiety. Third, charge motilities are relatively high in some carbazole-based polymers. Finally, the low cost of the carbazole as a starting material is resulting from simply distilling coal tar.[6] Many attempts were carried out to figure the ideal polymeric characteristics using carbazole moiety as a donor part and benzothiadiazole BTD or fluorinated benzothiadiazole as an acceptor. Blouin *et al*.[7] have used 9,9-dioctyl-2,7-dibromocarbazole as a donor and the BTD acceptor to get the polymer **PCDTBT** through the Suzuki cross-coupling reaction, which was then used to fabricate a BHJ solar cell device. The structure of the prepared polymer is depicted in figure (5-1) below:

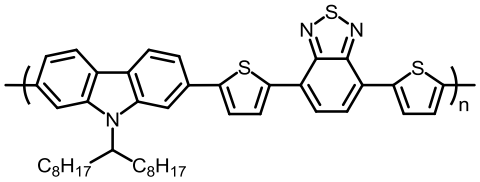

PCDTBT

Figure 0-1: Chemical structure of **PCDTBT** synthesized by Blouin *et al*[7].

Another family of 2,7-carbazole-based polymers was synthesized by Morin *et al*.,[8] these polymers have shown very good thermal stability, see figure (5-2) below. The optical and the luminescence properties were studied in terms of using these polymers in light-emitting diodes LEDs, due to their red, blue and green light emission.

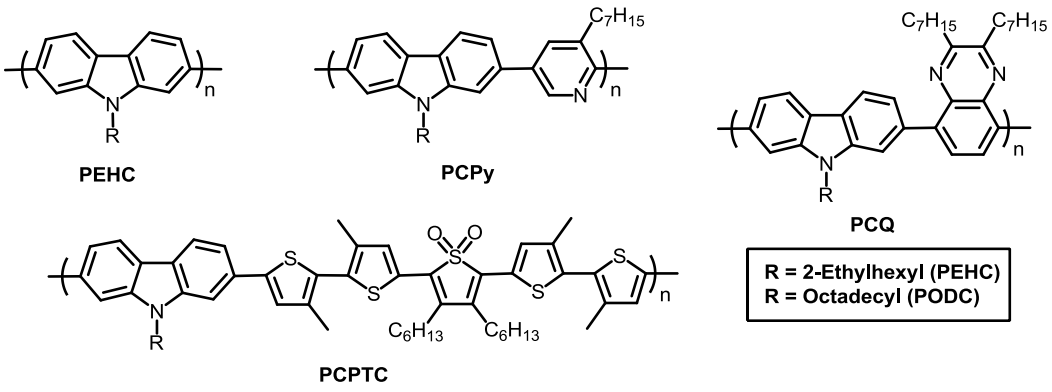

Figure 0-2: Conjugated polymers synthesized by Morin *et al*.[8]

Fluorene moiety was used to synthesize a number of polymers in this chapter. According to the literature, the characteristics of the fluorene unit make it a good example to be used as a photoactive material. Especially after the discovery of exposing the fluorene compound to ultraviolet light and noticing the photochemical effect caused which was preceded by a phosphorescence phenomenon.[9] In addition, there are many properties of the fluorene unit which depends on the chemical configuration;[10, 11] this makes this molecule suitable for use in the π-conjugated polymer systems and applicable in many optoelectronic devices.[12] The use of fluorene-based conjugated polymers mainly includes the organic solar cells, LEDs and as imaging and sensing agents.[13] A study published by Hou *et al*.[14] included the polymerization of 9,9-dioctylfluorene as a donor with bithiophene-BTD as an acceptor through the Suzuki coupling reaction, polymer **PFO-DBT** is shown in figure (5-3) below. The resulting polymer can emit red light in a saturated level with a quantum efficiency of 1.4%.

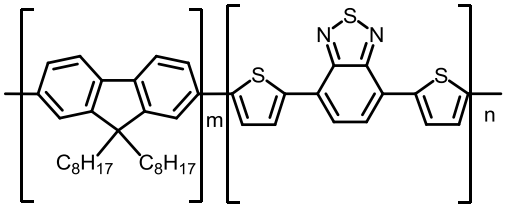

Figure 0-3: Fluorene-based copolymer **PFO-DBT** synthesized by Hou *et al*.[14]

Another non-fluorinated version bithiophene-based polymer **POD2T-DTBT** was synthesized by Ong *et al*[15] and used to fabricate a high-mobility FET device as well as a solar cell device, see figure (5-4).

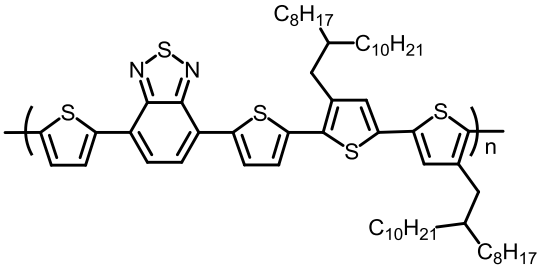

Figure 0-4: The chemical structure of **POD2T-DTBT** synthesized by Ong *et al*.[15]

This chapter will discuss the synthesis and characterization of a series of carbazole-BTD based and fluorene-BTD based conjugated polymers, in addition to a bithiophene-BTD based polymer. The acceptor molecule used in the polymers prepared is fluorinated benzothiadiazole. Alkyl chains were attached to the thiophene segments to increase solubility of the polymer and to ease their processing.

Polymer characterization includes all the techniques used to analyse the targeted polymers obtained during this study including ^{1}H NMR, elemental analysis, GPC, UV-visible, cyclic voltammetry and powder XRD. We will also compare the synthesized polymers to their counterpart polymers synthesized by other researchers based on the different segments used in these polymers to study the differences when attaching fluorine atoms to the BTD moiety as well as the effects on extending the conjugated system within the polymers backbones.

5.2 Results and Discussion

5.2.1 Synthesis of Monomers

Similar synthesis reactions from previous chapters were followed to obtain compound **(5)**. The synthetic routes to **(M4)** are shown in scheme (5-1) below:

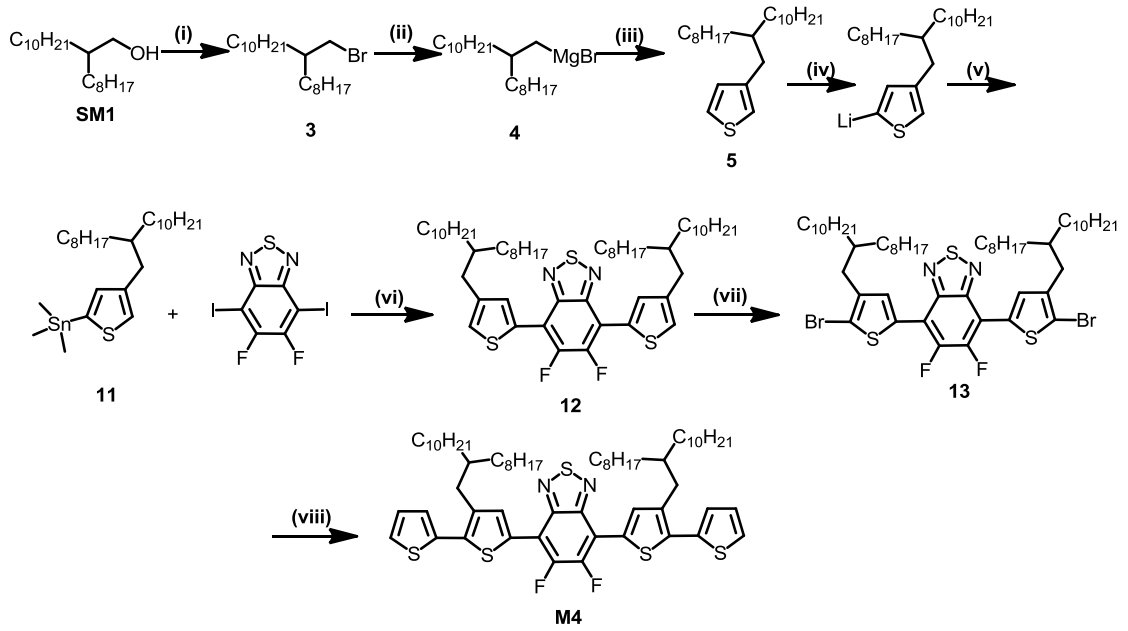

(i) NBS, PPh_3, DCM. **(ii)** Mg, dry THF. **(iii)** 3-Bromothiophene (SM3), $Ni(dppp)Cl_2$, dry THF, drop-wise. **(iv)** n-BuLi, $CHCl_3$, 0°C. **(v)** $Sn(Me)_2Cl$. $CHCl_3$, 0°C. **(vi)** $Pd(PPh)_3Cl_2$. Compound **(2)**, dry THF, reflux **(vii)** NBS, AcOH, $CHCl_3$. **(viii)** Tri(butylstannyl)thiophene, $Pd(PPh)_3Cl_2$, dry THF, reflux.

Scheme 0-1: Synthetic routes to 5,6-difluoro-4,7-bis(3-(2-octyldodecyl)-[2,2'-bithiophen]-5-yl)benzo[*c*][1,2,5] thiadiazole **(M4)**.

Compound **(5)** was then reacted with n-BuLi which abstracts a proton from the 5-position of thiophene to obtain a 5-lithium substituted thiophene segment, and this in turn was reacted with trimethyltin chloride to obtain (4-(2-octyldodecyl)thiophene-2-yl)trimethylstannane **(11)** as a yellow liquid. This compound was used for the next reaction without further purification due to its sensitivity, and the chemical structure was confirmed by ^1H NMR and mass spectroscopy techniques. The resulting compound (4-(2-octyldodecyl)thiophene-2-yl)trimethylstannane **(11)** was coupled with 4,7-diiodo-5,6-difluorobenzo[*c*][1,2,5]thiadiazole **(2)** in a Stille coupling reaction (2:1 equivalents), catalysed with $Pd(PPh_3)Cl_2$ to obtain 5,6-difluoro-4,7-bis(4-(2-octyldodecyl)thiophen-2-yl)benzo[*c*][1,2,5]thiadiazole **(12)**. This compound was used in direct arylation polymerization reactions with different monomers but no reaction has taken place. This might be due to the steric hindrance caused by the branched alkyl chains substituted in position 3 of the thiophene units. Further reactions were conducted to overcome the steric hindrance problem starting with bromination of 5,6-difluoro-4,7-bis(4-(2-octyldodecyl)thiophen-2-yl)benzo[*c*][1,2,5]thiadiazole **(12)** with NBS in a medium of $CHCl_3$ and acetic acid (1:1, v/v) to yield 5,6-difluoro-4,7-bis(3-(2-octyldodecyl)-[2,2'-bithiophen]-5-yl)benzo[*c*][1,2,5] thiadiazole **(13)** as an orange powder. The next reaction is the addition of two thiophene segments to compound **(13)** by the reaction of the mentioned compound with 2-(tributylstannane)thiophene **(SM7)** *via* Stille coupling

reaction catalysed with $Pd(PPh_3)Cl_2$ to obtain the final acceptor monomer 5,6-difluoro-4,7-bis(3-(2-octyldodecyl)-[2,2'-bithiophen]-5-yl)benzo[*c*][1,2,5] thiadiazole **(M4)** as a dark red powder. The chemical structure of **(M4)** was confirmed using ^{1}H NMR, ^{13}C NMR, mass spectroscopy, and elemental analysis. The ^{1}H NMR spectra of the final acceptor monomer 5,6-difluoro-4,7-bis(3-(2-octyldodecyl)-[2,2'-bithiophen]-5-yl)benzo[*c*][1,2,5] thiadiazole **(M4)** is shown in figure (5-5) below:

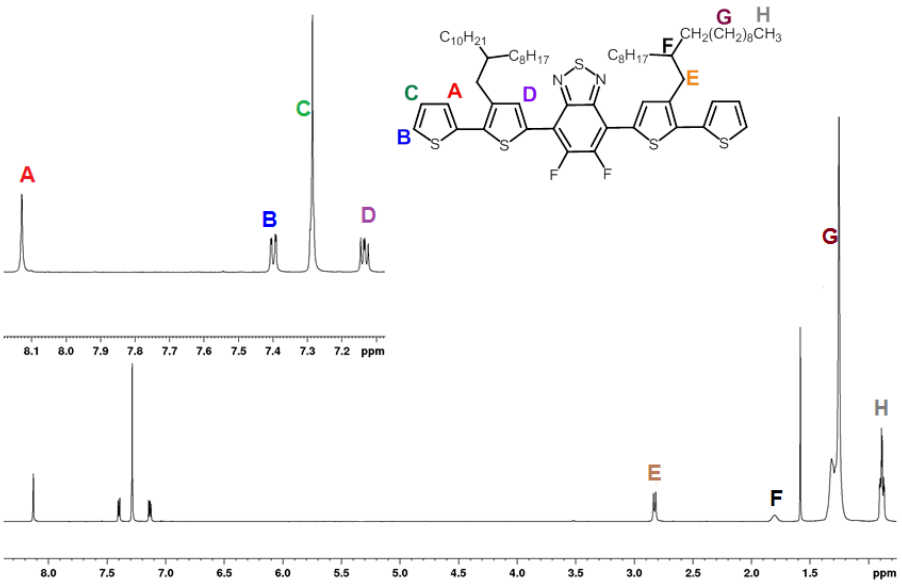

Figure 0-5: ^{1}H NMR spectrum of 5,6-difluoro-4,7-bis(3-(2-octyldodecyl)-[2,2'-bithiophen]-5-yl)benzo[*c*][1,2,5] thiadiazole **(M4)**.

Two carbazole donor monomers have been synthesized according to the procedures in the literatures.[16-19] Scheme (5-2) shows the synthetic routes to **(M5)** and **(M6)**.

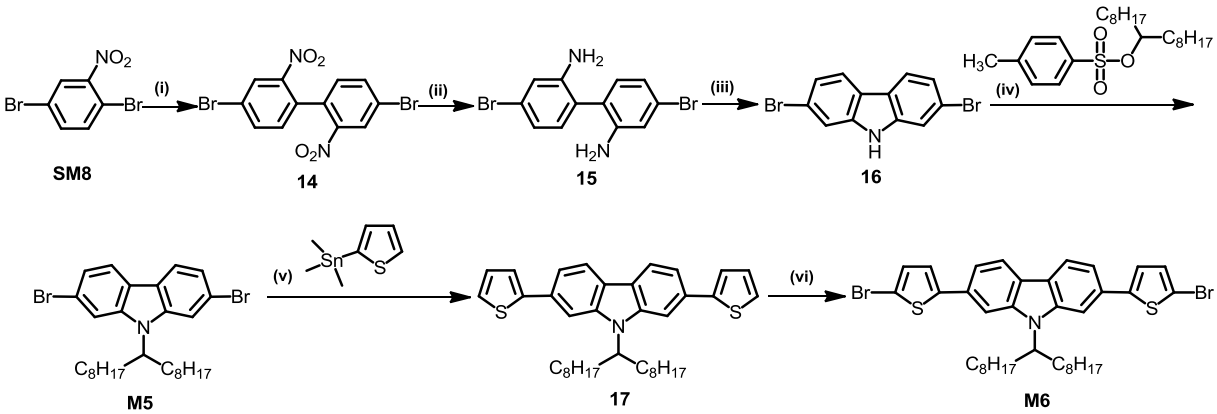

(i) Cu powder, DMF. **(ii)** Sn powder, 32% HCl. **(iii)** H_3PO_4. **(iv)** KOH, DMSO. **(v)** $Pd(PPh3)_2Cl_2$. dry THF **(vi)** NBS, AcOH, $CHCl_3$, r.t.

Scheme 0-2: Synthetic routes to carbazole donor monomers **(M5)** and **(M6)**.

The synthesis reactions have started with an Ullmann coupling reaction of 1,4-dibromo-2-nitrobenzene **(SM8)**, this reaction was catalysed with Cu powder to yield 4,4'-dibromo-2,2'-dinitro-1,1'-biphenyl **(14)** as pale yellow crystals. The suggested mechanism of this reaction can be seen in scheme (5-3) below:

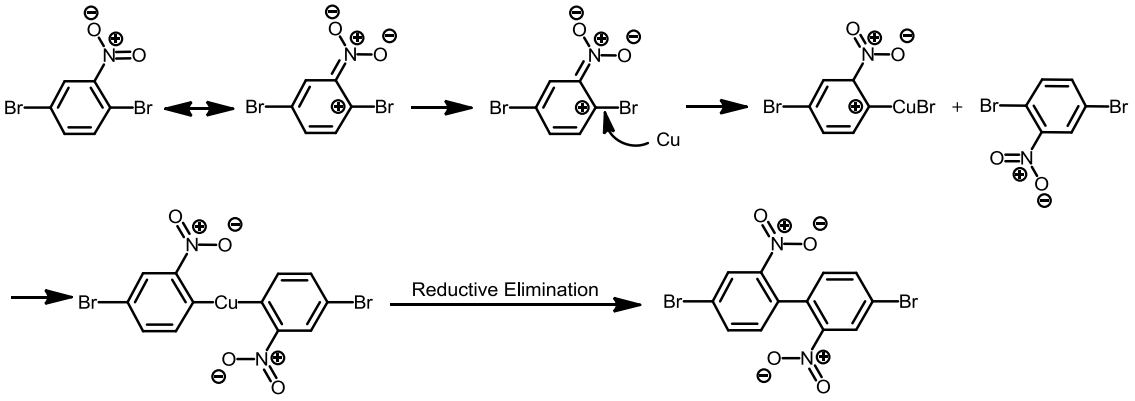

Scheme 0-3: Suggested mechanism to 4,4'-dibromo-2,2'-dinitro-1,1'-biphenyl **(14)**.

Compound **(14)** was then reduced over tin powder using HCl and ethanol; this reaction will generate tin chloride which in turn will be the active material of the reduction reaction to give 2,2'-diamino-4,4'-dibromo-1,1'-biphenyl **(15)** as brown crystals. The reduction reaction can be illustrated in the following general equation (5-1) below:

$$2ArNO_2 + 12H^+ + 3Sn \longrightarrow 2\,ArNH_2 + 4H_2O + 3Sn_4{}^+$$

Equation 0-1: Reduction equation of 4,4'-dibromo-2,2'-dinitro-1,1'-biphenyl **(14)** to 2,2'-diamine-4,4'-dibromo-1,1'-biphenyl **(15)**.

2,7-Dibromo-*9H*-carbazole **(16)** was prepared by reacting 2,2'-diamino-4,4'-dibromo-1,1'-biphenyl **(15)** with concentrated phosphoric acid at 185 °C. The reaction mixture was then poured onto distilled water, filtered and washed again with distilled water. The resulting crude product was recrystallized using a combination of toluene and hexane to afford 2,7-dibromo-*9H*-carbazole **(16)** as an off-white powder. The ^{1}H NMR spectrum identifies the product with 4 signals in the spectra. The broad signal at δ 8.10 ppm is linked to the proton 9H on the carbazole ring system. It is the single proton from the amine with an integral half that of the other aromatic protons of the carbazole. The next signal is that arising at δ 7.90 ppm which is a doublet in relation to protons. The next signal is at δ 7.59 ppm as a doublet due to coupling with near protons. The protons signal also gives rise to the signal at δ 7.39 ppm as a doublet of doublet.

It can be assumed that the reaction mechanism is achieved through a two-step process, the first of which would be the protonation of the amino group to $–NH_3^+$ which would develop a leaving group and the secondary amino group $–NH_2$ acts as a nucleophile. The second step would likely be an intermolecular cyclisation reaction to yield the product. The key step of the reaction mechanism involves a cationic 4π-electrocyclic ring closure as shown in scheme (5-4).

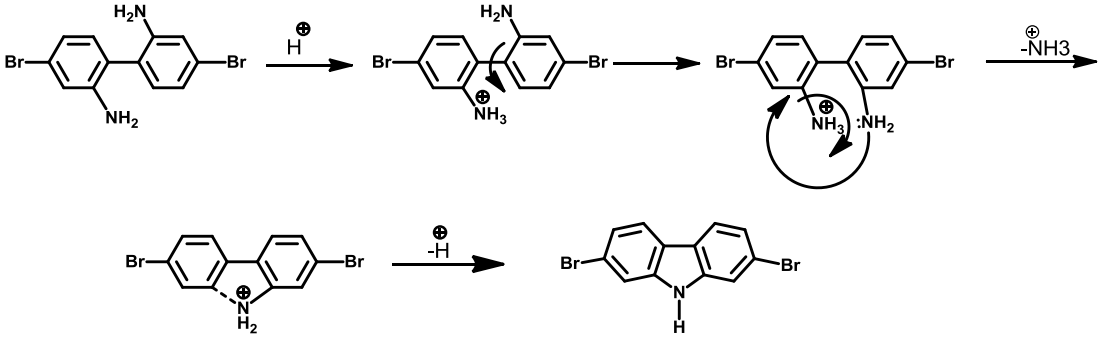

Scheme 0-4: Proposed mechanism to 2,7-dibromo-9H-carbazole **(16)**.

The alkylation reaction of nitrogen atom in compound 2,7-dibromo-9*H*-carbazole **(16)** was carried out at room temperature overnight in DMSO as solvent as seen in scheme (5-5). The KOH was ground and used in excess (4.6 equivalent) to push the reaction towards the product. Then the reaction mixture was poured onto water and extracted with hexane to yield the first carbazole monomer 2,7-dibromo-9-(heptadecan-9-yl)-9*H*-carbazole **(M5)**.

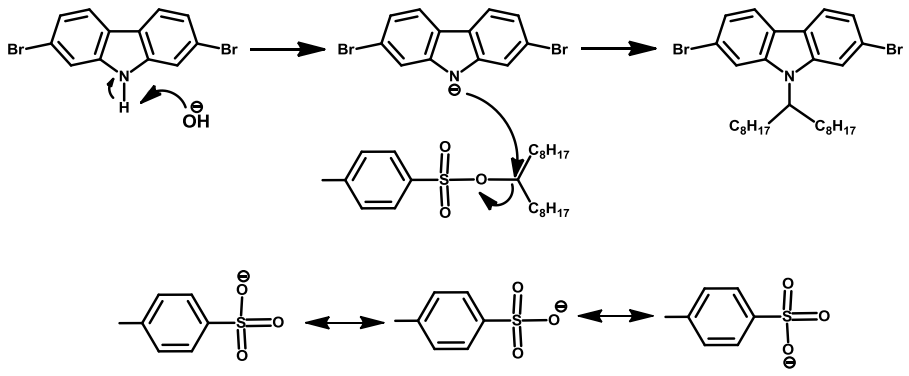

Scheme 0-5: Alkylation reaction of 2,7-dibromo-9*H*-cabazole **(16)**.

The ^{1}H NMR spectra of 2,7-dibromo-9-(heptadecan-9-yl)-9*H*-carbazole **(M5)**.is shown in figure (5-6) below:

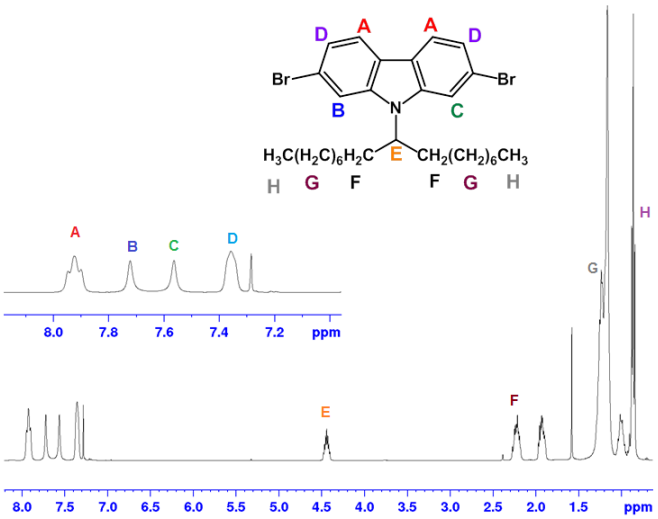

Figure 0-6: ^{1}H NMR spectrum of 2,7-dibromo-9-(heptadecan-9-yl)-9H-carbazole **(M5)**.

Further reactions were conducted on 2,7-dibromo-9-(heptadecan-9-yl)-9H-carbazole **(M5)** to extend the conjugation of the system by adding thiophene segments. **(M5)** was reacted with 2-(tributylstannyl)thiophene catalysed with $PdCl_2(PPh_3)_2$ in a Stille coupling reaction to afford 9-(heptadecan-9-yl)-2,7-di(thiophen-2-yl)-9H-carbazole **(17)** as a pale yellow solid. This product was then brominated using N-bromosuccinimide in a mixture of $CHCl_3$ and acetic acid to afford the second carbazole monomer 2,7-bis(5-bromothiophen-2-yl)-9-(heptadecan-9-yl)-9*H*-carbazole **(M6)** as a green oil. The structure of **(M6)** was confirmed using different techniques including ^{1}H NMR and mass spectroscopy. Figure (5-7) below shows the ^{1}H NMR spectrum of **(M6)**.

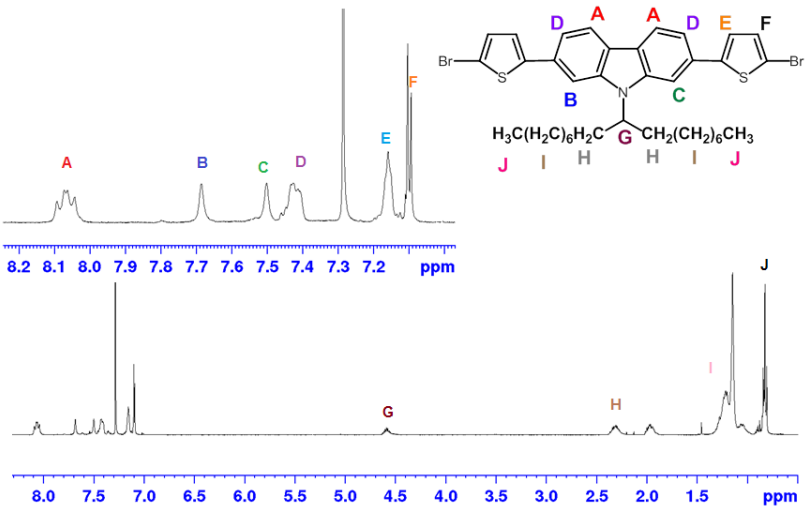

Figure 0-7: ^{1}H NMR spectrum of 2,7-bis(5-bromothiophen-2-yl)-9-(heptadecan-9-yl)-9H-carbazole **(M6)**.

Similar to carbazole monomers **(M5)** and **(M6)**, two fluorene monomers were synthesized scheme (5-6) below:

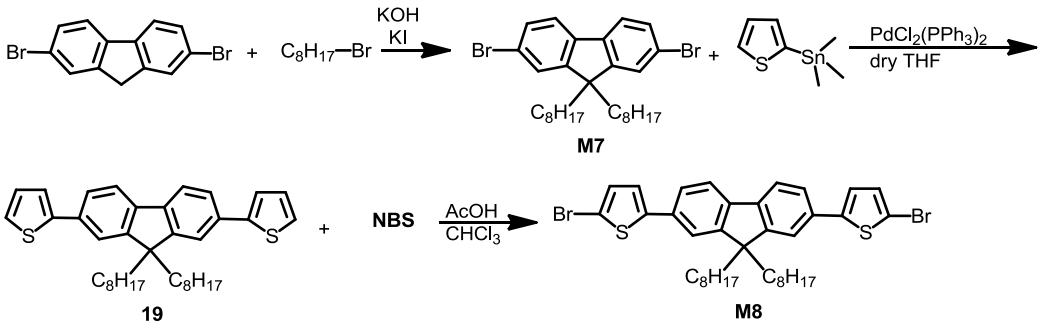

Scheme 0-6: Synthetic routes to fluorene donor monomers **(M7)** and **(M8)**.

The first fluorene monomer was prepared by attaching two octyl groups to 2,7-dibromo-9*H*-fluorene **(SM9)** using 1-bromooctane, KOH, and KI to obtain 2,7-dibromo-9,9-dioctyl-9*H*-fluorene **(M7)**. This monomer has been analysed using different analytical techniques. ^{1}H NMR spectra is depicted in figure (5-8) which shows the disappearance of the peak that corresponds the 9- position proton of the starting material and the rise of the multiplet peak at 1.26-1.03 that correspond the –CH_2 protons of the attached octyl groups.

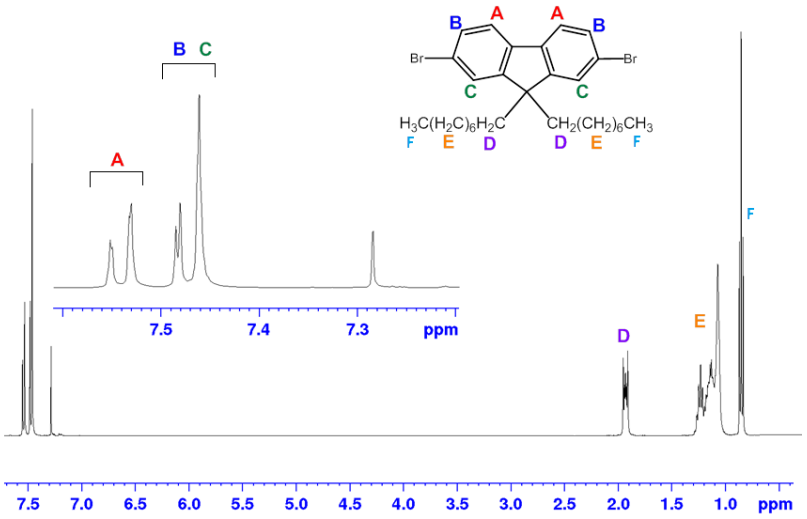

Figure 0-8: ^{1}H NMR spectrum of 2,7-dibromo-9,9-dioctyl-9*H*-fluorene **(M7)**.

Compound **(18)** was synthesized by the reaction of 2,7-dibromo-9,9-dioctyl-9*H*-fluorene **(M7)** with 2-(tributylstannyl)thiophene *via* Stille coupling reaction catalysed with $Pd(OAc)_2$ and tri(o-tolyl)phosphine. The reaction mixture was stirred at 125 °C. After 18 hours, the reaction mixture was washed with brine solution and extracted with diethyl ether. The crude product was purified using silica gel column chromatography to afford

2,2'-bithiophene-9,9-dioctyl-9*H*-fluorene-2,7-diyl **(18)** as a light green oil. The synthesis of a fluorene moiety flanked with two thiophene segments is meant to increase the conjugation of the donor monomer. The bromination of this compound **(18)** was done by the reaction with N-bromosuccinimide in a mixture of $CHCl_3$ and acetic acid to obtain the donor monomer **(M8)** as dark green oil. The structure of the **(M8)** was confirmed by different analytical techniques. ^{1}H NMR spectrum of 5,5'-bis(2-bromothiophene)-9,9-dioctyl-9*H*-fluorene-2,7-diyl **(M8)** is shown in figure (5-9) below:

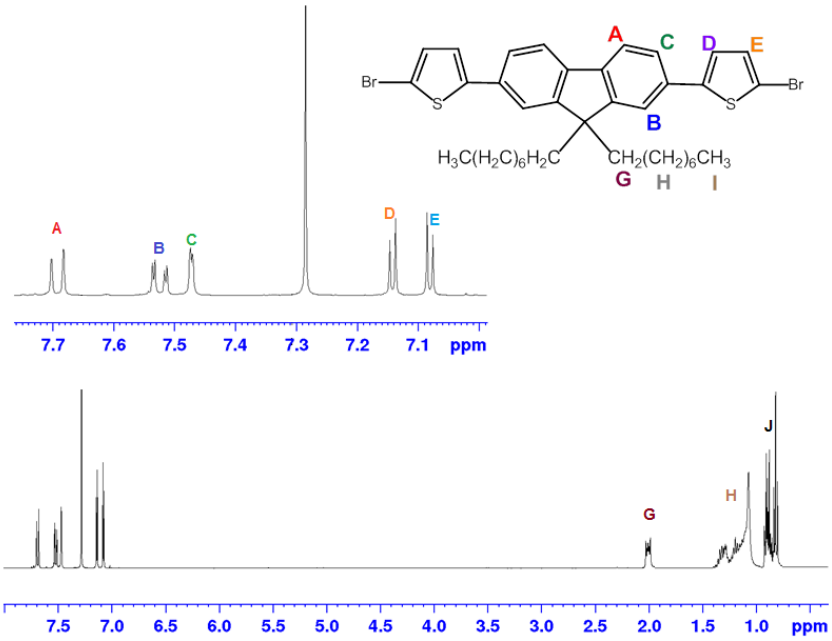

Figure 0-9: ^{1}H NMR spectra of 5,5'-bis(2-bromothiophene)-9,9-dioctyl-9*H*-fluorene-2,7-diyl **(M8)**.

To study the difference between the effects of different structures of donor moieties attached to the BTD acceptor monomer, **(M9)** was prepared by the reaction of 2,2'-bithiophene **(SM15)** with N-bromosuccinimide in a mixture of $CHCl_3$ and acetic acid to obtain monomer 5,5'-dibromo-2,2'-bithiophene **(M9)**. It is expected that using small molecules structures will result in a flat configuration of the resulting polymer which in turn will enhance the polymer's band gap. Equation (5-2) below shows the bromination reaction of 2,2'-bithiophene.

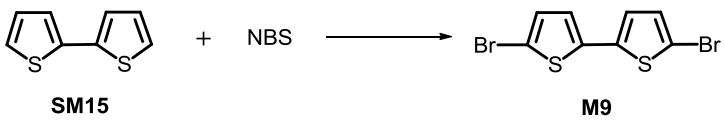

Equation 0-2: Bromination of 2,2'-bithiophene **(M9)**.

Figure (5-10) below shows the ^{1}H NMR spectrum of 5,5'-dibromo-2,2'-bithiophene **(M9)**.

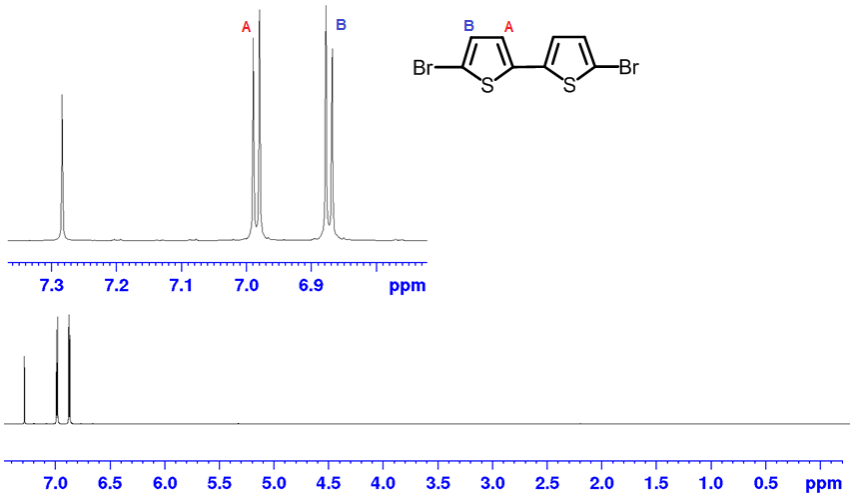

Figure 0-10: ^{1}H NMR spectrum of 5,5'-dibromo-2,2'-bithiophene **(M9)**.

5.2.2 Synthesis of polymers

The BTD acceptor monomer **(M4)** was reacted with **(M5)**, **(M6)**, **(SM14)**, **(M7)**, **(M8)** and **(M9)** respectively *via* a unique direct hetero arylation polymerization (DHA)[20] to afford **P10**, **P11**, **P12**, **P13**, **P14** and **P15** respectively. using $Pd_2(dba)_3$ as a catalyst and (*o*-OMePh)$_3$P as a ligand in a sealed tube under an inert atmosphere according to the procedure in the literature[20]. The solvent used in these polymerizations is dry THF and the polymerization reaction time is variable for each polymer synthesis from 24 hours to 3 days depending on the precipitate of the polymer observed at the bottom of the polymerization tube. The polymers were then washed with NH_4OH solution to remove any catalyst residue and then extracted using Soxhlet from different solvents (methanol, acetone, hexane, toluene, and chloroform) collecting toluene and chloroform and sometimes hexane portions for the following steps. The next step was the precipitation of the polymers by the drop-wise addition of polymer solution fraction into methanol to afford the polymers as solid materials. These polymers were soluble in chloroform at room temperature for further characterization studies. To confirm the chemical structure and the molecular weight of the synthesized polymers, ^{1}H NMR spectroscopy, GPC and elemental analysis studies were conducted. Elemental analysis has shown a little deviation in elemental analysis can be noticed due to technical reasons that might be attributed to the combustion process of polymers. Synthetic routes to polymers **P10**, **P11**, **P12**, **P13**, **P14** and **P15** are shown in schemes (5-7), (5-8) and (5-9) below

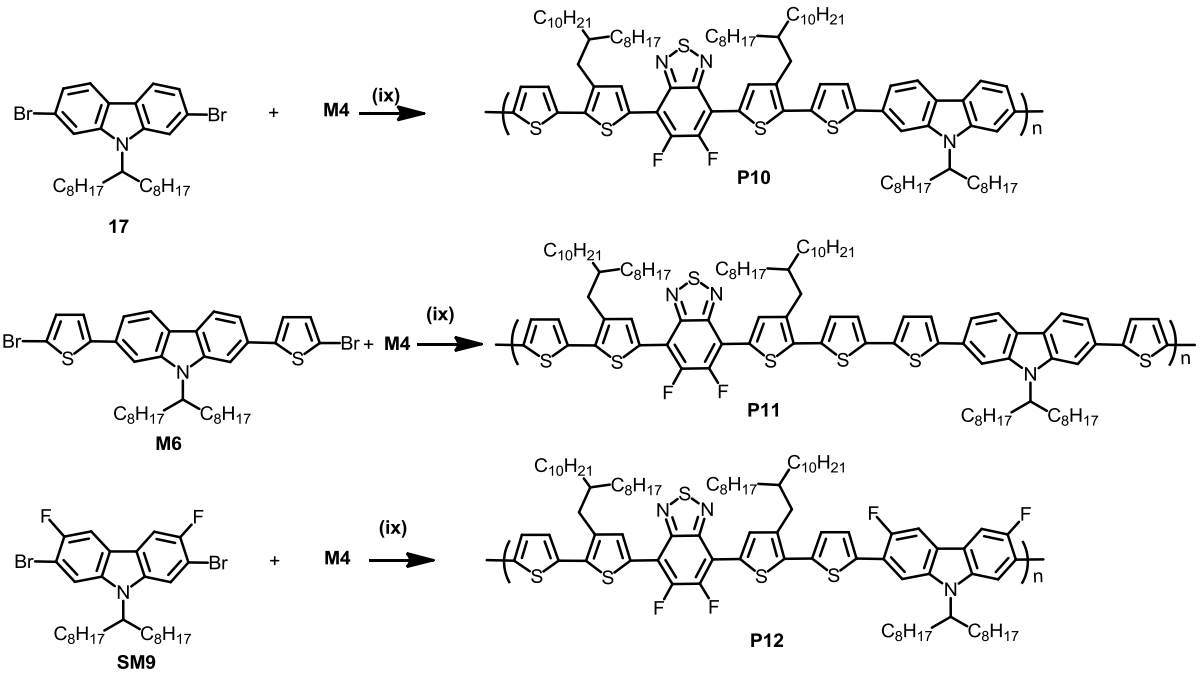

(ix) $Pd_2(dba)_3$, P(*o*-MeOPh)$_3$, Cs_2CO_3, pivalic acid, 1cm^3 dry THF, 120 °C.

Scheme 0-7: Synthetic routes to the carbazole-BTD based conjugated polymers.

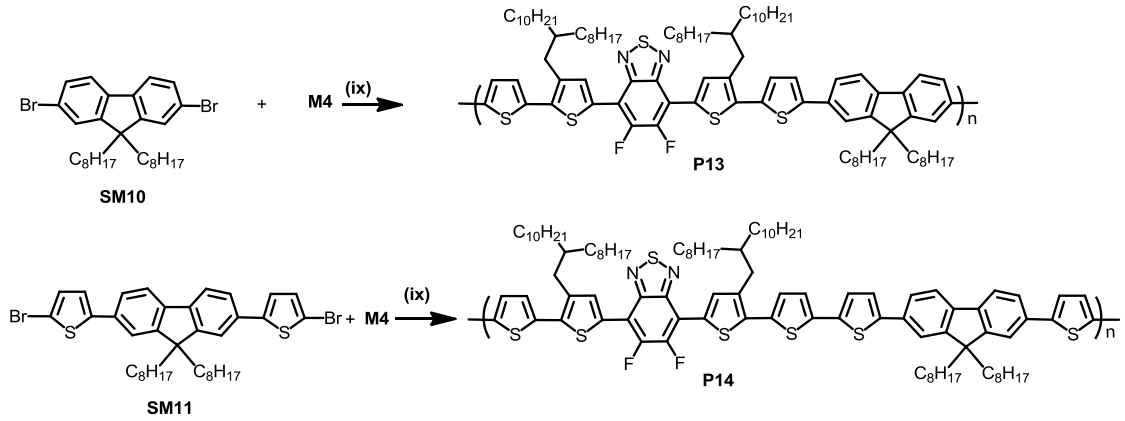

(ix) $Pd_2(dba)_3$, P(*o*-MeOPh)$_3$, Cs_2CO_3, pivalic acid, 1cm^3 dry THF, 120 °C.

Scheme 0-8: Synthetic routes to the fluorene-BTD based conjugated polymers.

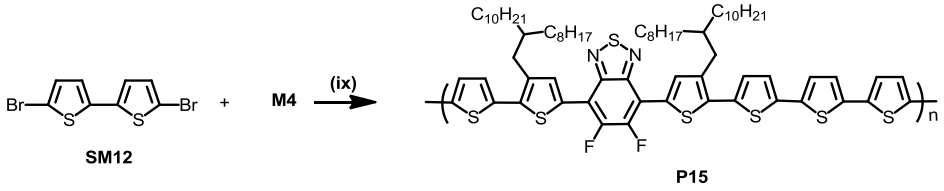

(ix) $Pd_2(dba)_3$, P(*o*-MeOPh)$_3$, Cs_2CO_3, pivalic acid, 1cm^3 dry THF, 120 °C.

Scheme 0-9: Synthetic route to the bithiophene-BTD based conjugated polymer.

5.2.3 GPC analysis

GPC analysis was conducted for the synthesized polymers **P10, P11, P12, P13, P14** and **P15**. Table (5-1) below shows the polymer fraction collected after the Soxhlet extraction, number average molecular weight M_n, weight average molecular weight and the polydispersity index for each polymer.

Table 0-1: GPC data of **P10, P11, P12, P13, P14** and **P15.**

Polymer	Fraction	Yield %	M_n (Da)[a]	M_w (Da)[a]	PDI[b]
P10	toluene	80%	20,700	51,500	2.46
P11	toluene	65%	15,800	39,300	2.48
P12	hexane	58%	16,900	66,500	3.93
P13	toluene	55%	13,200	36,000	2.72
P14	toluene	50%	7,900	17,400	2.20
P15	toluene	59%	13,200	19,200	1.45

[a] Detected by differential refractive index (DRI), toluene fractions of the polymer has been measured. [b] is the polydispersity index.

It can be noticed from the data collected in the table above that all polymers have been collected in toluene fraction except for **P12** which was collected in hexane due to the high solubility of this polymer in wide range of organic solvents and this in turn might be attributed to the extra fluorine atoms attached to the carbazole moiety. The number average molecular weight M_n for this family of polymers is between 7,900 Da and 20,700 Da. **P10** shows the highest *Mn* among other polymers of about 20,700 Da, while **P14** showed the lowest *Mn* of about 7,900 Da. The weight average molecular weight M_w is much higher than M_n, which is clearly seen in the polydispersity index; this might be due to the bulky structure of these polymers and the existence of the branched alkyl chains in these polymers. In general, the carbazole-based polymers have higher M_n than fluorene-based polymers although they have the same number of branched alkyl chains attached to both carbazole and fluorene moieties. The yield of the collected polymers in toluene and hexane fractions is between 50-80%. **P15** has different GPC characteristics as it has fewer alkyl chains in its chemical structure. This polymer has shown an M_n of about 13,200 Da and M_w of about 19,200 Da with polydispersity index of 1.45.

By comparison with carbazole-based polymers **P10**, **P11** and **P12** with the non-fluorinated carbazole-based counterpart, **PCDTBT**[7] shows higher M_n and M_w of about 37,000 and 73,000 Da respectively. Other fluorene-based polymers **P13** and **P14** were compared to the non-fluorinated polymer **PFO-DBT** synthesized by Hou *et al*.[14], this polymer has been prepared several times with different D-A monomer ratios showing different M_n values between 11,000-35,000 Da which is compatible with or above the M_n of **P13** and **P14**. These results are much higher than the molecular weights of **P10**, **P11** and **P12** due to the different polymerization method used to synthesize **PCDTBT** and **PFO-DBT**, which is the Suzuki polymerization process which, in general, reported to give polymers with high molecular weights[21]. The molecular weight of **P15** was compared to the non-fluorinated counterpart polymer **POD2T-DTBT** which showed an M_n of about 35,000 Da and PDI of 1.63.

5.2.4 Optical properties of the polymers

UV-visible data for the synthesized polymers **P10, P11, P12, P13, P14** and **P15** were studied as solutions in chloroform and as thin films cast from chloroform solutions. Data collected in table (5-2) below shows the absorption maxima, the onset of absorption maxima in both solution states and as thin films, and the optical bandgap for each polymer.

Table 0-2: UV-visible data for **P10, P11, P12, P13, P14** and **P15.**

Polymer	λ_{max} Solution (nm)	λ_{max} Film (nm)	ε ($M^{-1}cm^{-1}$)		λ_{max} onset Solution (nm)	λ_{max} onset Film (nm)	Eg(opt)[c] (eV)
			π-π* [d]	ICT [e]			
P10[a]	529	566	47,000	41,000	625	692	1.79
P11[a]	523	553	28,300	25,600	632	693	1.78
P12[b]	522	552	52,600	45,400	654	683	1.81
P13[a]	527	557	52,600	48,700	621	667	1.86
P14[a]	519	553	27,800	19,300	619	672	1.84
P15[a]	559	603	12,200	31,600	721	728	1.70

[a] Toluene fraction. [b] Hexane fraction. [c] Optical band gap ($E_{g\ opt}$), determined from the absorption maxima onset of UV-vis in polymers thin films. [d] Absorption coefficient for (π-π*), [e] Absorption coefficient for (ICT).

It can be clearly seen from figure (5-11) below that in all polymers, the absorption maxima in thin films is red-shifted compared to these of the solution states by around 30 nm or more. **P15** has shown an even more red-shifted peak in thin film by around 43 nm, this might be due to the aggregation occurring during the film casting from the chloroform solution. The bandgap calculations revealed that carbazole-based polymers **P10** and **P11** have shown same optical bandgaps of 1.79 and 1.78 eV respectively, although **P11** has additional thiophene units added to the polymer's backbone. The hypothesis that explains this phenomenon is that the lower molecular weight of **P11** compared to that of **P10**, which is the origin of this difference. The bandgap of **P12** is 1.81 eV, which is slightly bigger than these of **P10** and **P11** due to the existence of additional fluorine atoms on the carbazole segment due to the effects of additional fluorine units attached to the carbazole segment. **P13** and **P14** which are fluorene-based polymers have shown bandgaps of, 1.86, 1.84 eV respectively. This could be attributed to the difference in chemical structure of carbazole and fluorene units as carbazole has a nitrogen atom holding two unpaired electrons, and these electrons can contribute in conjugated system of the polymer. **P15** has shown the most interesting bandgap value of 1.70 eV. This could be ascribed to the planar structure in solid state leading to an ordered π-π stacking and then low bandgap. The polymer **P15** has the best optical properties among this family of polymers in terms of the low bandgap required for solar cell applications.

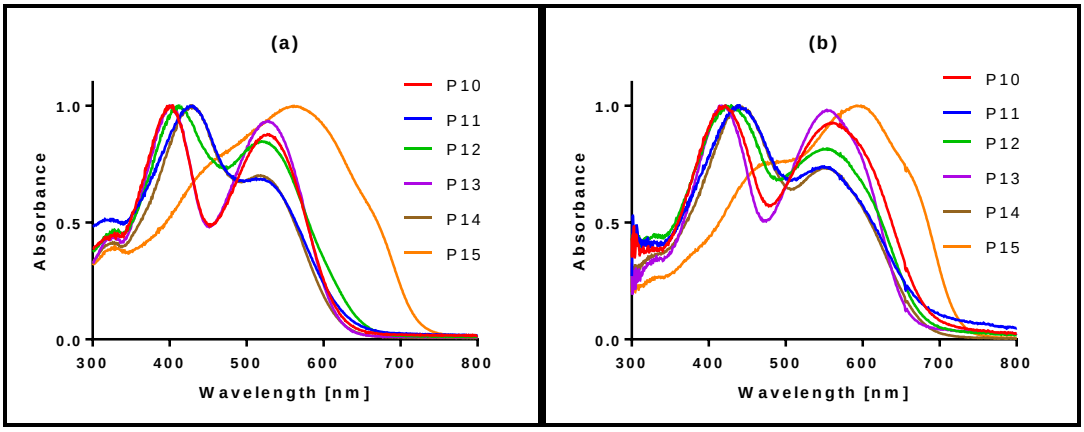

Figure 0-11: UV-visible for **P10, P11, P12, P13, P14** and **P15 (a)** in solutions **(b)** as thin films

The optical properties carbazole-based polymers **P10, P11** and **P12** were compared to the previously synthesized polymer **PCDTBT**[7]. Those polymers showed bandgaps of 1.79, 1.79 and 1.81 eV for **P10**, **P11** and **P12** respectively, compared to **PCDTBT** which has absorption maxima at 545 nm and a bandgap of 1.88 eV. This could be attributed to the extended π-bond system in **P10, P11** and **P12** leading to more electron density and then lower bandgaps. Fluorene-based polymers **P13** and **P14**

were compared to **PFO-DBT**[14]. **P13** and **P14** have shown optical bandgaps of 1.86 and 1.84 eV respectively, these bandgaps are lower than that of **PFO-DBT** which has a bandgap of 2.01 eV. This could be ascribed to the difference in the chemical structure of **P13** and **P14** with additional thiophene units attached to the polymers backbone and more extended π-conjugation compared to **PFO-DBT**. Polymer **P15** has an optical bandgap of 1.70 eV, this polymer was compared to **POD2T-DTBT**[15] with an absorption maxima 780 nm and a bandgap of 1.59 eV. It could be suggested that **P15** showed lower optical bandgap than its counterpart due to the high molecular weight of (M_n = 35,000 Da) for **POD2T-DTBT** compared to the molecular weight of (M_n = 12,200 Da) for **P15**. In general, it can be seen that the synthesized polymers **P10, P11, P12, P13** and **P14** have lower optical bandgaps than their counterparts except for **P15** where its counterpart has showed lower bandgap, which ascribed to the low molecular weight of **P15**.

The optical properties of synthesised polymers were also compared to the previously synthesised polymers in chapters (2, 3, and 4 in this thesis) which are based on naphthalene (**P1**, **P2** and **P3**), anthracene (**P3** and **P4**) and pyrene (**P6**, **P7**, **P8** and **P9**); the UV-visible results revealed that the optical bandgap for the bandgap for polymers **P1**, **P2**, **P4**, **P5**, **P6** and **P7** is between 1.97 and 2.10 eV regardless the chemical structure of these polymers. The other part of the previously prepared polymers **P3**, **P8** and **P9** have shown narrower bandgap between 1.71 and 1.79 eV, this is attributed to the extension of π-conjugated system in these polymers using additional thiophene units within the polymers backbone.

5.2.5 Electrochemical Properties

The electrochemical properties for polymers **P10, P11, P12, P13, P14** and **P15** have been studied; properties such as HOMO, LUMO and the electrochemical bandgap were determined using cyclic voltammetry on polymer films and are given in table (5-3) below.

Table 0-3: Cyclic voltammetry results for polymers **P10, P11, P12, P13, P14** and **P15.**

Polymer	HOMO (eV)[a]	LUMO (eV)[b]	Eg (eV)[c]
P10	-5.40	-3.69	1.71
P11	-5.36	-3.56	1.80
P12	-5.50	-3.62	1.88
P13	-5.22	-3.42	1.80
P14	-5.40	-3.46	1.94
P15	-5.14	-3.47	1.67

[a] HOMO level of the polymer calculated from the oxidation potential onset, [b] LUMO level of the polymer calculated from the reduction potential onset, [c] electrochemical band gap.

From table (5-3) above and figure (5-12) below, it can be seen that the HOMO of the polymers is dependent on the chemical configuration of these polymers, and deeper HOMO level has been noticed for **P12** as more fluorine atoms have been attached to the donor along with these which already exist on the acceptor. This confirms the hypothesis that the fluorine atoms on the conjugated polymer will lower both HOMO and LUMO levels of the conjugated polymer compared to the non-fluorinated versions of conjugated polymers. HOMO levels for the carbazole-based polymers **P10**, **P11** and **P12** were -5.40, -5.36 and -5.22 eV respectively; Whereas **P13** and **P14** have displayed HOMO levels of -5.22 and -5.40 eV respectively. The HOMO level of **P15** is shallower relative to the other synthesized polymers with a value of -5.14 eV. Deep LUMO levels were seen in **P10** and **P12** with values of -3.69 and -3.69 eV respectively, although **P10** has only two fluorine atoms on its acceptor moiety. Whereas **P11, P13, P14, P15** have shown shallower LUMO levels of -3.56, -3.42, -3.46 and -3.47 eV respectively.

A comparison to other carbazole-based conjugated polymers described in the literature, carbazole-based polymers such as **PCDTBT**[7] that has shown a HOMO level of -5.5eV, LUMO level of 3.6 eV and a bandgap of about 1.90 eV. This bandgap is higher than the bandgap of **P10**, **P11** and **P12**, which might be due to the effect of the fluorine atoms attached to these polymers. Fluorene-based conjugated polymers **P13**, **P14** were compared to the polymer **PFO-DBT,**[14] which has different HOMO and LUMO levels due to the different donor/acceptor quantities used in polymer synthesis, the best electrochemical results for **PFO-DBT** were noticed at HOMO level of -5.47 eV and

LUMO level of -3.46 eV and the calculated bandgap was 2.01eV, which is higher than the bandgap of **P13** and **P14**. This can be simply explained as the use of more aromatic units within polymers **P13** and **P14** backbone which will lead to the more conjugation and more electron density along the polymer chains. **P15** was also compared to its counterpart **POD2T-DTBT**[15] with HOMO level -5.18 eV, with no further information about the LUMO level and the electrical bandgap to compare.

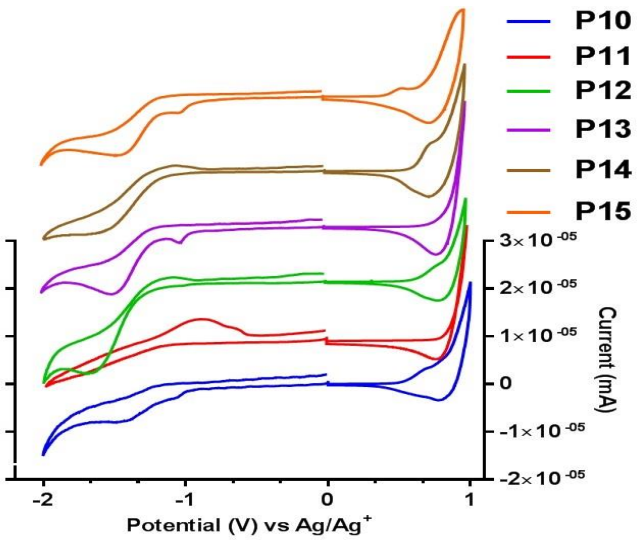

Figure 0-12: Cyclic voltammetry plots for **P4** and **P5.**

5.2.6 Polymers' XRD studies

XRD studies on polymers **P10, P11, P12, P13, P14** and **P15** were undertaken on powders to study the morphology of the synthesized polymers. Figure (5-13) below shows the XRD for the synthesized polymers.

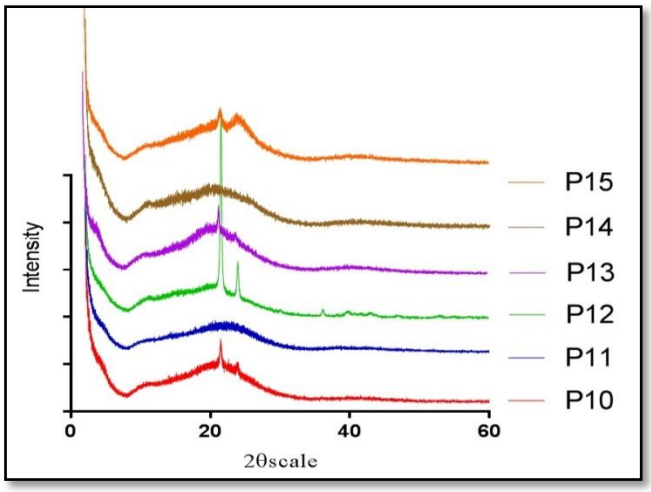

Figure 0-13: Powder X-Ray diffraction plots for **P10, P11, P12, P13, P14** and **P15.**

The XRD results for the polymers revealed that **P10, P12, P13** and **P15** have sharp peaks at *2Θ* of 21.5°, which means that these polymers, and especially **P12**, have a good π-π stacking which corresponds a distance of 4.12 Å between the polymer chains. Another small sharp peak at *2Θ* of 23.8° has been noticed for polymers **P10, P12** and **P15** which correspond a distance of 3.73 Å in the same π-π stacking area on the XRD plots. It has been proven through the X-ray diffraction for the polymer powders that the existence of the fluorine atoms within the polymer can form hydrogen bonding which in turn will enhance the polymer aggregation and improve the π-π stacking[22]. The remaining polymers **P11** and **P14** have not shown any sharp peaks within the plots, which means that these polymers are amorphous and do not show any crystalline structures according to XRD studies. Moreover, polymers with less conjugation such as **P10, P12, P13** and **P15** have shown sharp peaks within their XRD plots which might indicate that the less conjugation the more crystalline structure due to the arranged π-π stacking. Compared to the previously synthesized polymers in chapters (2, 3 and 4), **P5** and **P7** have shown similar sharp peaks at the same area of the XRD plots, which means that they have some crystalline structure compared to **P10, P12, P13** and **P15.** Other synthesized polymers **P1, P2, P3** and **P4** seem to be amorphous and these are similar to **P11** and **P14** in this chapter.

5.2.7 Thermal Gravimetric Analysis Studies

Polymers thermal stability has been studied through thermal gravimetric analysis TGA technique. Figure (5-14) and table (5-4) show the weight loss against the temperature raise and the data collected from these curves.

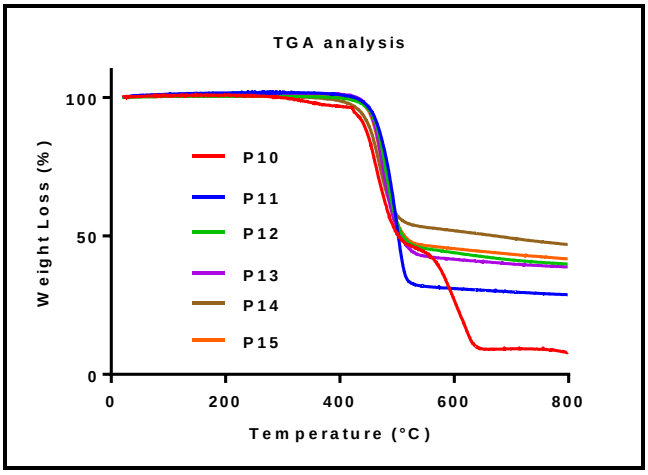

Figure 0-14: TGA plots for **P10, P11, P12, P13, P14** and **P15.**

From figure (5-12) above, it can be clearly seen that all the polymers have one degradation step except for **P10** which shows two degradation steps, where the

degradation step starts from 245 °C, all other polymers **P11**, **P12**, **P13**, **P14** and **P15** degradations start from 385 °C and above. It is hypothesized that different factors may affect the degradation process including the possession of high concentration of polymeric chain ends[22]. The degradation onsets (5% weight loss) calculated from the TGA curve for **P10**, **P11**, **P12**, **P13**, **P14** and **P15** were approximately 424, 455, 453, 452, 435 and 450 C respectively. Other thermal properties collected from the thermal degradation curves are shown in table (5-4) have been discussed. The percentage of remaining mass for **P10** after raising the temperature up to 800 °C is 8.45%, whereas polymers **P11, P12, P13, P14** and **P15** have retained 28.5, 39.8, 38.4, 47.2 and 41.7% of their original sample mass respectively. This can be considered as a confirmation on the good thermal stability of these polymers.

Table 0-4: TGA data for **P10, P11, P12, P13, P14** and **P15.**

Polymer	D/ °C[a]	TPWL (%)[b]	EPWL(%)[c]	R_m/wt %[d]
P10	1st 435-494, 2nd 561-632	57	49	8.45
P11	464-516	52	34	28.5
P12	458-509	56	50	39.8
P13	449-507	58	46	38.4
P14	441-499	52	53	47.2
P15	448-510	69	47	41.7

[a] D is the degradation onsets. [b] TPWL is the percentage of theoretical weight loss. [c] EPWL is the percentage of experimental weight loss. [d] R_m is the remaining weight after heating to 800 °C.

5.3 Conclusion

A series of conjugated polymers have been synthesized in this chapter, polymers **P10, P11, P12** are based on BTD and carbazole donor moieties. Polymers **P13** and **P14** consist of a BTD and fluorene moieties, whereas **P15** is based on BTD and bithiophene. The conjugated systems of **P11** and **P14** have been extended with two thiophene segments to compare the properties of these polymers with the rest of the family of polymers. The procedure used to synthesize the polymers **P10, P11, P12, P13, P14** and **P15** is through direct hetero-arylation (DHA) polymerisation catalysed using Pd (0), P(*o*-OMePh)$_3$ pivalic acid and cesium carbonate in THF in dry sealed tube under an inert atmosphere. The synthesized polymers were characterized with ^{1}H NMR and elemental analysis, and the optical properties such as λ_{max} and the optical bandgap were determined using UV-visible spectroscopy. The number average molecular weight *Mn*, weight average molecular weight *Mw* and the polydispersity index PDI were studied using GPC techniques. The electrochemical properties including HOMO, LUMO and the electrochemical bandgap were determined using cyclic voltammetry. The thermal and the morphological properties of these polymers were investigated with TGA and powder XRD respectively. The number average molecular weight M_n for the polymers is between 7,900 and 20,700 Da, with a lower molecular weight observed for **P14**. The UV-visible spectroscopy revealed that the polymers with extended conjugated systems have shown red-shifted absorption peaks compared to the non-extended conjugated system polymers; this could be attributed to the electron density along the conjugated system of the polymer chains. **P15** has the most red-shifted absorption peak among all polymers. The optical bandgaps for **P10, P11, P12, P13, P14** and **P15** were 1.79, 1.79, 1.81, 1.86, 1.84, 1.70 eV respectively. The bandgap in these polymers are lower than those observed for synthesised polymers in chapter (2, 3 and 4), except for polymers **P3**, **P8** and **P9** where the π-conjugated system is extended leading to more electron densities along the polymers backbone. The data collected from the cyclic voltammetry have shown lower HOMO levels of **P10**, **P12** and **P14**. **P12** have shown the lowest HOMO level at 5.50 eV due to the incorporation of the extra fluorine atoms attached to the carbazole unit. The electrochemical bandgaps for **P10, P12, P13, P14** and **P15** were 1.71, 1.80, 1.88, 1.80, 1.94, 1.67 eV, these bandgaps are calculated from the reduction onsets and the oxidation onsets. The prepared polymers are amorphous in general but **P10, P12, P13** and **P15** have shown some sharp peaks at their π-π stacking area of the XRD plots. The synthesized polymers have shown good thermal stabilities with degradation curves starting from 385 °C and above, except for polymer **P10** where the degradation step is starting from

245 °C. From the results above, it can be hypothesized that fluorination of the acceptor or the donor moieties can be useful to obtain polymers with lower HOMO and LUMO levels and these polymers can be used in different device applications. The extension of the π-conjugated systems can produce polymers with good optical and electrochemical properties to the extent that the more aromatic segments added the less conjugation obtained due to the perpendicular configuration of the aromatic rings on each other which in turn will cause the breakage of the conjugation.

The synthesised polymers are in good compatibility with the electrochemical properties of the fullerene derivatives, especially $PC_{71}BM$ that possesses a HOMO level of about -6.0 eV and a LUMO level of about -3.8 eV. This makes it possible to apply the synthesised polymers in photovoltaic devices where the energy gap between the LUMO levels (V_{oc}) of donor (conjugated polymer) and acceptor ($PC_{71}BM$) is close to the required optimal difference of 0.3 eV. Moreover, the low bandgaps obtained from both optical and electrochemical properties along with the good thermal stability of synthesised polymers make them good candidates for the application in solar cell devices using blending ratios of (1:1, 1:2 and 1:3) polymer:$PC_{71}BM$ and to determine the solar cell characteristics such as PCE%, *FF*, I_{sc} and V_{oc}. Figure (5-15) below shows the electrochemical bandgaps and the HOMO/LUMO level for **P10**, **P11**, **P12**, **P13**, **P14**, **P15** and $PC_{71}BM$.

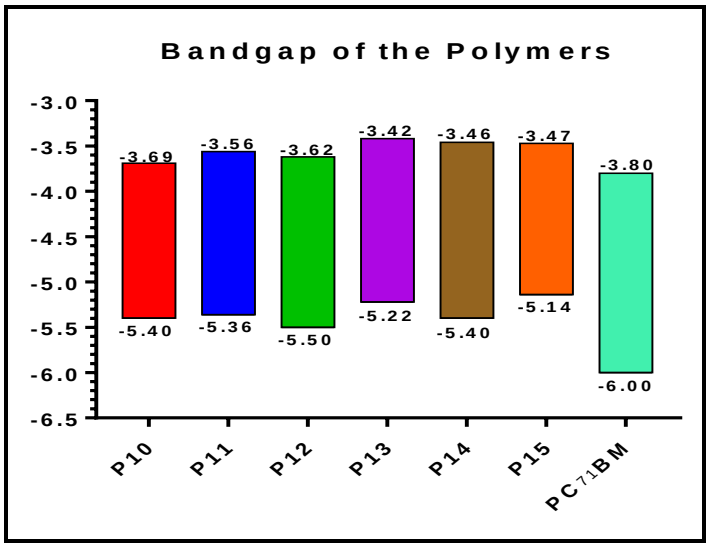

Figure 0-15: Bandgap and HOMO/LUMO levels of polymers **P10, P11, P12, P13, P14** and **P15**.

Chapter 5 References

1. C. J. Brabec, N. S. Sariciftci and J. C. Hummelen, *Advanced functional materials*, 2001, **11**, 15-26.
2. C. Winder and N. S. Sariciftci, *Journal of Materials Chemistry*, 2004, **14**, 1077-1086.
3. H. Hoppe and N. S. Sariciftci, *Journal of materials research*, 2004, **19**, 1924-1945.
4. M. M. Wienk, J. M. Kroon, W. J. Verhees, J. Knol, J. C. Hummelen, P. A. van Hal and R. A. Janssen, *Angewandte Chemie*, 2003, **115**, 3493-3497.
5. G. Wang, S. Qian, J. Xu, W. Wang, X. Liu, X. Lu and F. Li, *Physica B: Condensed Matter*, 2000, **279**, 116-119.
6. J. Pearson and M. Stolka, *Poly (N-vinylcarbazole)*, Gordon & Breach Publishing Group, 1981.
7. N. Blouin, A. Michaud and M. Leclerc, *Advanced Materials*, 2007, **19**, 2295-2300.
8. J.-F. Morin and M. Leclerc, *Macromolecules*, 2002, **35**, 8413-8417.
9. G. Rieveschl and F. E. Ray, *Chemical Reviews*, 1938, **23**, 287-389.
10. U. Scherf and E. J. List, *Advanced Materials*, 2002, **14**, 477-487.
11. P. Chen, G. Yang, T. Liu, T. Li, M. Wang and W. Huang, *Polymer international*, 2006, **55**, 473-490.
12. R. Abbel, A. P. Schenning and E. Meijer, *Journal of Polymer Science Part A: Polymer Chemistry*, 2009, **47**, 4215-4233.
13. S. W. Thomas, G. D. Joly and T. M. Swager, *Chemical reviews*, 2007, **107**, 1339-1386.
14. Q. Hou, Y. Xu, W. Yang, M. Yuan, J. Peng and Y. Cao, *Journal of Materials Chemistry*, 2002, **12**, 2887-2892.
15. K. H. Ong, S. L. Lim, H. S. Tan, H. K. Wong, J. Li, Z. Ma, L. C. Moh, S. H. Lim, J. C. De Mello and Z. K. Chen, *Advanced Materials*, 2011, **23**, 1409-1413.
16. E. Bundgaard and F. C. Krebs, *Polymer Bulletin*, 2005, **55**, 157-164.
17. M. Takahashi, K. Masui, H. Sekiguchi, N. Kobayashi, A. Mori, M. Funahashi and N. Tamaoki, *Journal of the American Chemical Society*, 2006, **128**, 10930-10933.
18. V. H. Fell, A. Mikosch, A.-K. Steppert, W. Ogieglo, E. Senol, D. Canneson, M. Bayer, F. Schoenebeck, A. Greilich and A. J. Kuehne, *Macromolecules*, 2017, **50**, 2338-2343.
19. G. Garbay, L. Muccioli, E. Pavlopoulou, A. Hanifa, G. Hadziioannou, C. Brochon and E. Cloutet, *Polymer*, 2017, **119**, 274-284.
20. P.-O. Morin, T. Bura, B. Sun, S. I. Gorelsky, Y. Li and M. Leclerc, *ACS Macro Letters*, 2014, **4**, 21-24.
21. B. Hohl, L. Bertschi, X. Zhang, A. D. Schlüter and J. Sakamoto, *Macromolecules*, 2012, **45**, 5418-5426.
22. L. Cartwright, H. Yi and A. Iraqi, *New Journal of Chemistry*, 2016, **40**, 1655-1662.

Chapter 6

Conclusions and Future Work

Conclusions and Future Work

6.1 Conclusions

In this work, new families of D-A conjugated polymers were designed, synthesised and characterised successfully. The series of polymers synthesised are based on the copolymerisation reaction of BTD or fluorinated BTD as acceptor units with naphthalene, anthracene, pyrene, carbazole, fluorene and bithiophene respectively as donor units. Thiophene units were added to either BTD monomers or donor monomers to extend the π-delocalised electronic structure. Two main effects were studied in details in this thesis; first is the incorporation of fluorine atoms, second is the effect of adding and extending the conjugated system via flanking additional thiophene segments next to the acceptor or the donor units. Due to the anticipated rigidity of the polymers, branched alkyl chains were attached to the backbone of the polymers to increase both molecular weights and the solubility of the resulting polymers. The synthesised organic compounds and monomers were characterised using different techniques to check their structure including ^{1}H NMR, ^{13}C NMR, mass spectroscopy and elemental analysis.

In chapter 2 of this thesis, three conjugated polymers **P1**, **P2** and **P3** based on fluorinated and non-fluorinated BTD as acceptors were polymerised *via* direct hetero arylation (DHA) with 2,6-linked naphthalene flanked by two 3-alkyl substituted thiophene units. These polymers were synthesised and characterized using different analytical techniques. Polymer **P3** has additional thiophene segments attached to the BTD acceptor. The GPC results showed the number average molecular weight M_n values of (8,500, 26,000 and 33,400 Da) for **P1**, **P2** and **P3** respectively. According to these results, **P1** showed the lowest M_n among this family of polymers. However, the highest M_n value was observed for **P3**. The optical properties of **P1**, **P2** and **P3** were investigated in two states; as solutions and thin films. These results revealed that the onset of absorbance maxima for **P3** is the highest at 725 nm, which is higher than that of **P1** and **P2** with absorbance maxima onsets at 589 and 612 nm respectively, the red shifted peak of **P3** can be ascribed to the extended conjugated system and the ordered π-π stacking in this polymer. **P1**, **P2** and **P3** showed optical bandgaps of 2.10, 2.00 and 1.71 eV respectively. The cyclic voltammetry has shown slightly higher bandgaps of about 2.10, 2.03 and 1.76 eV for **P1**, **P2** and **P3** respectively. Interestingly, the lowest bandgap polymer was noticed in **P3** among this family of polymers with excellent optical and electrochemical properties. The red shifted peak and the low optical and electrochemical bandgaps of **P3** can be ascribed to the extended π-

conjugated system and the ordered π-π stacking of this polymer. These polymers were studied in terms of thermal stability using TGA. All the polymers possess high thermal stability against the raise of the temperature with time, the thermal degradation started above 400 °C for **P1**, **P2**, and **P3**. The powder XRD plots revealed that **P1**, **P2**, and **P3** are amorphous and no crystalline structure has been observed, this could be related to the steric hindrance effect of the alkyl chains attached to the backbone of the polymer.

Chapter 3 describes the design, synthesis and characterization of two novel conjugated polymer **P4** and **P5** based on 2,6-linked anthracene unit flanked by two thiophene units and polymerised *via* direct arylation with different BTD monomers. The resulting polymers have number average molecular weights M_n of 16,000 and 15,900 Da for **P4** and **P5** respectively. The optical properties of these polymers have shown bandgaps of 1.97 eV for **P4** and 1.99 eV for **P5**. It can be suggested that the incorporation of fluorine atoms has lowered the HOMO level and lead to a slightly smaller bandgap in **P5**, which was confirmed by the cyclic voltammetry. Different and higher bandgaps were obtained from the cyclic voltammetry measurements for **P4** and **P5** of 2.09 and 2.23 eV respectively; this is attributed to the steric hindrance caused by the branched alkyl chain, which might distort the planar structure of **P4** and **P5**. The morphology of **P4** and **P5** was studied by powder XRD. This study revealed that **P4** has shown amorphous structure compared to **P5** which has a crystalline structure, this is due to the Coulomb interaction between the different atoms within the same polymeric chain which lead to an ordered π-π stacking with a distance of 3.75 Å between polymer chains. The thermal gravimetric analysis revealed that **P4** and **P5** are thermally stable at temperatures up to 400 °C.

In chapter 4, four polymers **P6**, **P7**, **P8** and **P9** were synthesised by the reaction of fluorinated and non-fluorinated BTD monomers with 2,7-linked pyrene monomer flanked by two thiophene segments through the direct arylation reaction polymerisation. Results from GPC showed average number molecular weights of 17,200, 10,300, 5300 and 8600 Da for **P6**, **P7**, **P8** and **P9** respectively. Low M_n was noticed for **P8** ascribed to the additional thiophene units added to the backbone of the polymer. **P9** has slightly higher M_n than **P8** attributed to the effect of fluorine atoms attached which is more soluble than **P8**. The UV-visible studied showed optical bandgaps of 2.00 eV for both polymers **P6** and **P7**. The extension of the conjugated system in **P8** and **P9** resulted in lowering the bandgaps to be 1.74 and 1.79 respectively, with a clear effect of the fluorine atoms in lowering the HOMO level of **P9** resulting in a slightly wider bandgap compared to **P8**. According to the results from cyclic voltammetry, polymers **P7** and **P9** have shown deep HOMO levels of -5.55 and -5.47 eV respectively. This confirms the

effect of attaching fluorine atoms to the backbone of these polymers. The structures of the synthesized polymers are amorphous in general with some crystalline peaks noticed for **P7** at 2Θ value of 24.3° which corresponds to a distance of 3.6 Å due to ordered π-π stacking as a result of the Coulomb interactions. **P6**, **P7**, **P8** and **P9** showed thermal stability at temperatures under 300 °C, with single degradation step that is different than the previously synthesised polymers. This might be correlated to the rigid structure of the repeat unit leading to a thermally stable behaviour of these polymers.

Chapter 5 discussed the design, synthesis and characterisation of six polymers **P10**, **P11**, **P12**, **P13**, **P14** and **P15**. All these polymers have been synthesised using fluorinated BTD monomer **M4** flanked with four thiophene units, alkyl chains were also attached to this monomer to increase the solubility and the molecular weight of the resulting polymers. The first three polymers **P10**, **P11** and **P12** have been synthesized by the polymerisation of BTD monomer **M4** with different carbazole monomers. GPC results showed Mn of 20,700, 15,800 and 16,900 Da for **P10**, **P11** and **P12** respectively. Unlike other carbazole-based polymers, **P12** was very soluble in common organic solvents; this is attributed to the impact of fluorine atoms attached to the carbazole monomer. The optical bandgaps for **P10**, **P11** and **P12** are 1.79, 1.78 and 1.81 eV. The bandgap for **P12** is clearly wider than that of **P10** and **P11** due to the fluorine atoms impact lowering the HOMO level of the **P12**. It can be clearly seen from the cyclic voltammetry data that **P12** has the deepest HOMO level among other carbazole-based polymers due to the fluorine atoms effect. The XRD plots of **P10** and **P12** have shown some sharp peaks in the π-π stacking region of the plot, which is attributed to the Coulomb interactions caused by fluorine atoms. However, **P11** has an amorphous structure according to its XRD plot. The TGA studies showed that **P11** and **P12** are thermally stable at temperatures under 380 °C. The thermal behaviour of **P10** is slightly different than the other polymers as the thermal degradation of this polymer started at 245 °C, which makes it less stable than **P11** and **P12**. This could be related to the chemical structure of **P10** which has less number of aromatic rings than **P11** and less fluorine substitution than **P12**.

Two fluorine-based polymers **P13** and **P14** were also studied in chapter 5, these polymers are basically different from the others in the number of thiophene units attached to the polymers backbone. They were both obtained from the direct arylation polymerisation reaction of the fluorinated BTD monomer **M4** with two different fluorene monomers. The number average molecular weights are 13,200 and 7,900 Da for **P13** and **P14** respectively. The low molecular weight for **P14** is expected as the number of

thiophene units without substituents has increased leading to more rigid structure of the polymer chains and lower solubility. The optical bandgaps obtained from the UV-visible for **P13** and **P14** are 1.86 and 1.84 eV respectively, the latter showed a slightly lower bandgap due to the extended π-conjugation system in this polymer. The electrochemical bandgaps for **P13** and **P14** are 1.80 and 1.94 eV respectively; this could be related to the aggregation of **P14** when casting polymer films over the platinum electrode in the cyclic voltammetry study. Both polymers showed amorphous structures according to the XRD plots with a small sharp peak which appeared at 2Θ value of 21.5° for **P13** which corresponded to a distance of 4.12 Å between the polymer chains. The thermal behaviour of **P13** and **P14** was also studied, showing that both polymers are highly stable at temperatures up to 400 °C.

The last polymer in this chapter **P15** was also synthesized *via* direct arylation polymerisation. This polymer consists of fluorinated BTD acceptor monomer with bithiophene donor monomer polymerised via direct arylation polymerisation reaction. The molecular weight obtained from GPC analysis showed an M_n value of about 13,200 Da. The optical bandgap of **P15** is 1.70 eV, which is the lowest among other polymers discussed in this chapter, with a red-shifted UV-visible plot due to the more electron density caused by the thiophene units along the polymer chains. The results from cyclic voltammetry confirmed the low bandgap of **P15** by showing an electrochemical bandgap of 1.67 eV, with HOMO and LUMO levels of -5.14 and -3.47 eV respectively. The morphology of **P15** was studied by powder XRD, these results showed an amorphous structure in general with some sharp peaks at 21.5 and 23.8° that correspond to distances of 4.12 and 3.73 Å respectively between polymer chains. The thermal properties revealed that **P15** is thermally stable at temperatures up to 400 °C.

To conclude, polymers based on naphthalene, anthracene and pyrene have almost similar optical and electrochemical properties when polymerised with BTD monomers. All the synthesised polymers have good thermal stability and showed amorphous structures due to the existence of the alkyl chains with some sharp peaks in XRD plots attributed to the ordered π-π stacking which might be resulted from the incorporation of fluorine atoms attached to the backbone of the polymers.

6.2 Future work

A number of polymers prepared in this thesis have shown promising optical and physical properties for their application as electron donors in bulk heterojunction solar

cells. Future work should include studies on their use in active layers of BHJ solar cells as electron donors to either $PC_{71}BM$ acceptor or other small molecule acceptors.

In this thesis, a full description of the preparation and properties of BTD-based D-A conjugated polymers was provided. Low bandgap polymers are possible to be made by extending the π-conjugation on insertion of extra thiophene units on the polymer backbone. The molecular weight obtained for some polymers was not high enough for optimal charge transport. New conjugated polymers can be made with attaching additional branched alkyl or alkoxy chains to the polymer backbone. This will solve the solubility issue and also will enhance the optical and the chemical properties of the resulting polymers by increasing the molecular weight for the polymer and also lowering the bandgap of these polymers due to the improved charge carrier mobility. Figure (6-1) below shows the chemical structure for some suggested polymers with different alkyl chain.

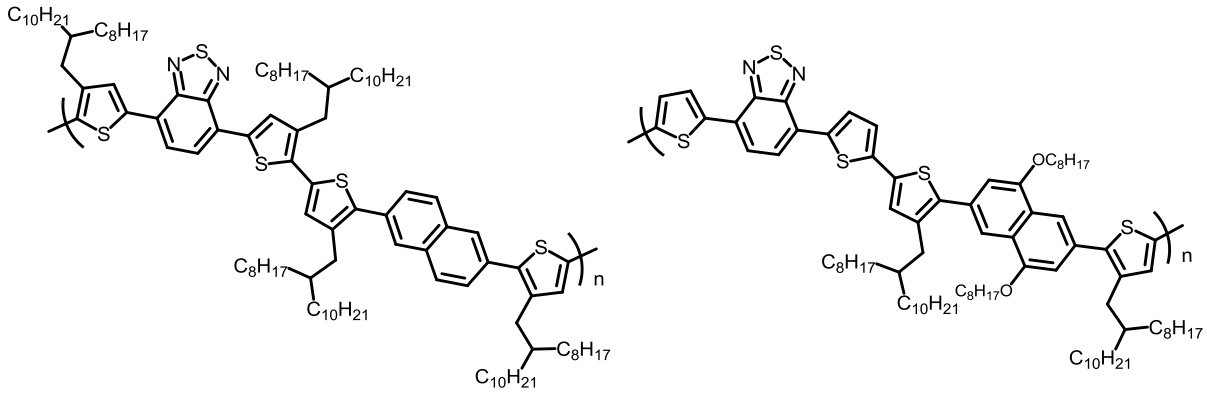

Figure 0-1: Chemical structure of suggested conjugated polymers with different alkyl chains.

This work has also included a discussion on the effects of attaching fluorine atoms and their impact on lowering HOMO and LUMO energy levels of D-A conjugated polymers. Fluorine atoms have a direct impact on ordering the π-π stacking of polymer chains via the Coulomb interactions. It is recommended to attach more fluorine atoms to the aromatic units on polymer chains, as this could be an effective way in ordering the morphology of the resulting conjugated polymers.

All polymers described in this thesis are based on BTD unit as an acceptor. It could be useful to replace BTD with other acceptor units in the hope of obtaining conjugated polymers with improved optical and electrochemical properties. Alternative acceptors such as thieno[3,4-*c*]pyrrole-4,6-dione TPD and 2,1,3-naphthodiazole can be used and compared with the recently prepared polymers in terms of electrochemical and optical

properties. Figure (6-2) below shows the chemical structure of some suggested conjugated polymers with different acceptor units.

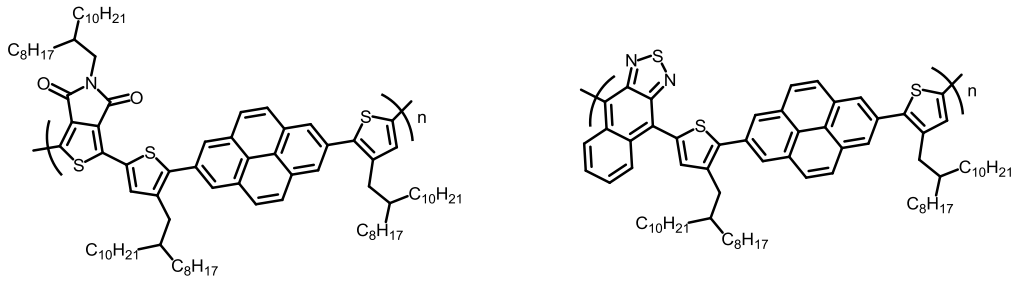

Figure 0-2: Chemical structure of suggested conjugated polymers with different acceptor units.

In chapter 5 of this thesis, polymer **P15** which is based on BTD and 2,2'-bithiohene showed the lowest bandgap (1.70 eV) among other synthesised polymers. However, the chemical structure of conjugated polymer could be further enhanced by using donor units such as thiophene, thieno[3,2-b]thiophene or 2,2'-bithiophene in conjugated polymers, see figure (6-3) below. These molecules are proven to minimise the steric hindrance caused by the bulky alkyl chains attached to the polymers backbone.

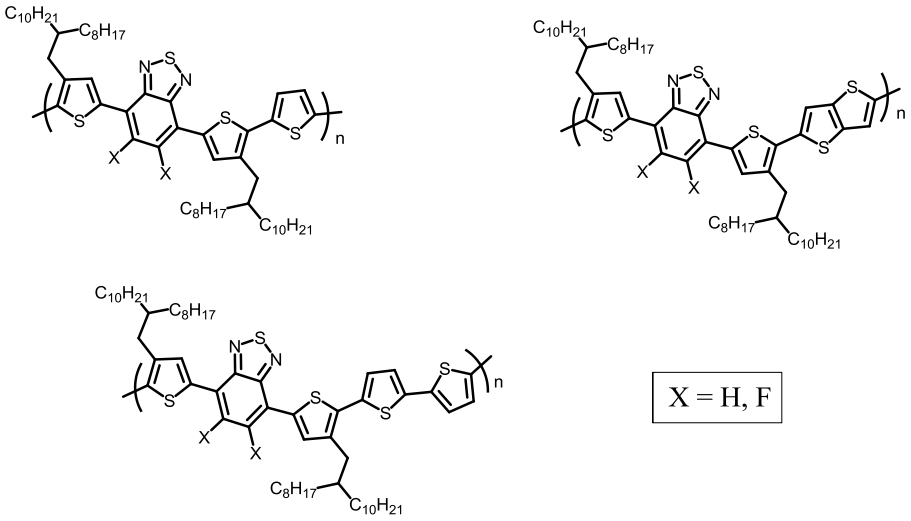

Figure 0-3: Chemical structure of suggested conjugated polymers with halogen atoms attached.

Chapter 7

Experimental Section

Experimental Section

7.1 Measurements

In this study, several techniques were user to characterize and analyse the synthesized compounds. These include; mass spectrometry, ^{1}H, ^{13}C and ^{19}F nuclear magnetic resonance NMR, CHN elemental analysis, thermal gravimetric analysis (TGA), ultraviolet visible UV-visible, cyclic voltammetry (CV), gel permeation chromatography GPC and powder x-ray diffraction (XRD).

Mass spectrometry device Perkin Elmer Turbomass was used to record the mass spectra of the compounds, the device was equipped with XL GC auto system which operates in two different modes including electron ionization (EI) and chemical ionization (CI). ^{1}H and ^{13}C NMR of the compounds were recorded on Bruker Avance 400 MHz spectrometers at 25 °C temperature using deuterated chloroform ($CDCl_3$) as a solvent. Chemical shifts are calculated in part per million (ppm) and the coupling constant (*J*) is measured in Hertz (Hz). Elemental analyses of the prepared compounds were recorded on Perkin Elmer 2400 CHN elemental analyser. Moreover, sulphur and halides analysis were measured by the flask combustion method. UV-visible absorption spectra were recorded using double beam Analytik Jena Specord S600 spectrophotometer. Solutions of the synthesized polymers dissolved in chloroform were measured by using quartz cuvettes (width = 1cm), in addition to thin films casting from chloroform solutions which were also prepared for UV-visible absorption spectra measurements on quartz slides dipped in chloroform solution of the ($1mg/cm^3$) polymer. These slides were dried at room temperature and then measured under normal laboratory conditions. Gel permeation chromatography GPC were recorded on solutions of polymers using toluene as a reference and chloroform and chlorobenzene as eluents at 40 °C and 120 °C respectively, these measurements were performed at a flow rate of $1cm^3.min^{-1}$. Using a 1037 differential refractive index detector, the GPC system was calibrated against narrow polystyrene standards.

Cyclic voltammetry measurements were recorded using a Princeton Applied research apparatus Model 263 Potential/Galvanostat. Inert atmosphere was used to conduct the electrochemical data in a three-electrode cell system using a concentration of (0.1M) tetrabutylammonium perchlorate dissolved in dry acetonitrile as a medium. Pt wire as counter electrode, platinum disk was used as the working electrode. In addition, Ag/Ag^{+} (0.01M of $AgNO_3$ in dry acetonitrile) as reference electrode which contains an internal silver wire.

Polymer films were prepared by drop casting from a solution of (1mg/cm^3) (polymer/ HPLC graded chloroform) on the platinum disk and dried at room temperature. The three electrodes were inserted to the cell which contains the electrolyte solution, calibrated with ferrocene as a standard reference redox system according to the literature[1]. Profiles taken by powder X-ray diffraction for the polymers were recorded using Bruker D8 diffractometer with CuK-α radiation source (1.5418Å, rated as 16kW) with scanning range of (2-60°). Thermal gravimetric analyses (TGAs) were performed using a Perkin Elmer TGA-1 Thermogravimetric Analyzer at a scan rate of (10 °C/min) under an inert atmosphere.

7.2 Materials

All the chemicals used in this study were purchased from Alfa Aesar, Sigma-Aldrich and Fisher Scientific Ltd. These chemical were used as received with no further purification unless otherwise stated. Reagent grade common solvents were purchased from the internal chemicals store. Other dry solvents such as dichloromethane (DCM), chloroform and toluene were used in reactions as they are unless otherwise noted. 1,2-diamine-4,5-difluorobenzene- **(SM1)**, 2-octyldodecan-1-ol **(SM2)**, 3-bromothiophene **(SM3)**, 2,6-dibromonaphthalene **(SM4)**, 2-6-dibromoanthracene-9,10-dione **(SM5)**, pyrene **(SM6)**, 2-(tributylstannane)thiophene **(SM7)**, 1,4-dibromo-2-nitrobenzene **(SM8)**, 2,7-dibromo-9*H*-fluorene **(SM9)** shown in figure (7-1) below were purchased from commercial suppliers and used as they are without purification.

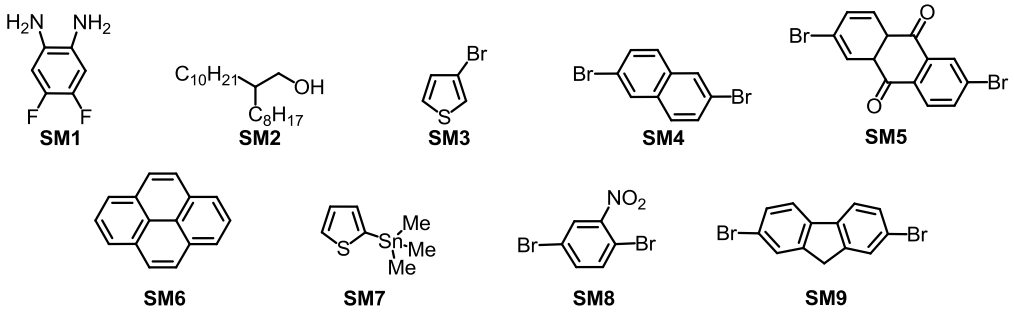

Figure 0-1: Structures of purchased materials.

4,7-Dibromobenzo[c][1,2,5]thiadiazole **(SM11)**, 4,7-bis(5-bromothiophen-2-yl)benzo[*c*][1,2,5]thiadiazole **(SM12),** 4,7-bis(5-bromothiophen-2-yl)5,6-difluorobenzo [*c*][1,2,5]thiadiazole **(SM13)**, 2,7-dibromo-3,6-difluoro-9,9-dioctyl-9H-fluorene **(SM14)**, 2,2'-bithiophene **(SM15)** shown in figure (7-2) below were synthesized by Iraqi group according to modified procedures in the literature.[2-6]

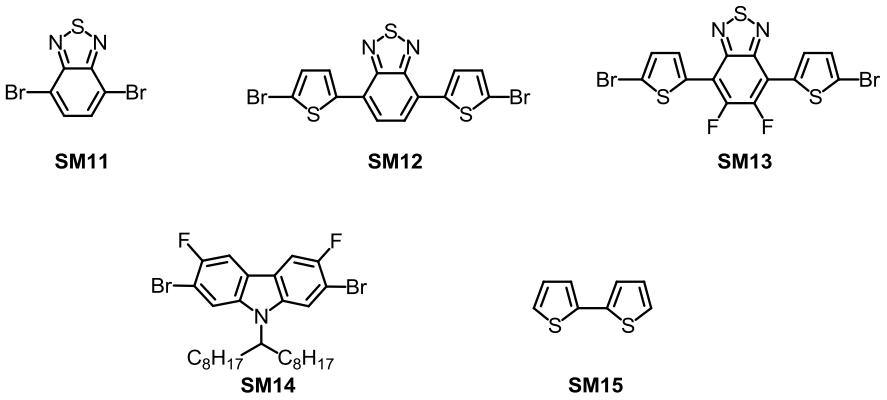

Figure 0-2: Materials synthesized by Iraqi group.

7.3 Synthesis of monomers and polymers (series 1) (Chapter 2)

7.3.1 5,6-Difluorobenzo[c][1,2,5]thiadiazole (1).[7]

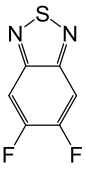

Under a protective atmosphere of argon, a reaction vessel was charged with 1,2-diamine-4,5-difluorobenzene- **(SM1)** (5.0 g, 34.7 mmol), $CHCl_3$ (500 cm^3) and triethylamine (14.25 cm^3) . The mixture was stirred until the complete dissolution of diamine. Thionyl chloride (9 g, 75.7 mmol) was added drop-wise to the reaction mixture, then the mixture was heated to reflux and continued to stir overnight. Upon completion, the mixture was cooled to room temperature and quenched with water, extracted with (3 x 300 cm^3) of DCM. The organic layer was dried over $MgSO_4$ and the solvent was removed *in vacuo* The crude product 5,6-difluorobenzo[*c*][1,2,5]thiadiazole **(1)** was purified using column chromatography eluting with PE:DCM (5:1). Ivory crystals were collected after removing the solvent (4.02 g, 23.35 mmol, 68%, m.p. = 74 °C).

^{1}H NMR (400 MHz, $CDCl_3$) δ (ppm): 7.78 (*t*, *J* = 8.5 Hz, 2H). ^{13}C NMR (100 MHz, $CDCl_3$) δ (ppm): 155.1, 154.9, 152.2, 152.3, 150.8, 150.7, 150.7, 106.2, 106.1, 106.1, 106.0, 105.9 and 105.8. ^{19}F NMR (100 MHz, $CDCl_3$) δ (ppm): -127.90, -127.92, -127.95. EI-MS (*m/z*): $[M]^+$ calculated for $C_6H_2F_2N_2S$, 172; found: 172. Elemental analysis calculated for $C_6H_2F_2N_2S$; C, 41.86, H, 1.17, S, 18.62%, found: C, 41.77; H, 1.68; S, 17.46%.

7.3.2 5,6-Difluoro-4,7-diiodobenzo[c][1,2,5]thiadiazole (2).[7]

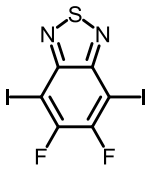

A reaction vessel was charged with 5,6-difluorobenzo[c][1,2,5]thiadiazole **(1)** (2.67 g, 15 mmol), I_2 (15.0 g, 60 mmol) and fuming H_2SO_4. The reaction mixture was stirred at 60 °C for 24 hours. Upon completion, the reaction mixture was cooled to room temperature and poured into a large beaker with crushed ice. $CHCl_3$ was added and the mixture was moved into a separating funnel, and then extracted with deionized water (3 x 250 cm^3). This step was followed by treating the mixture with (1.0 M) NaOH solution and saturated solution of $NaHCO_3$ to remove the excess of iodine. The organic layer was separated and dried over $MgSO_4$ and the solvent was evaporated *in vacuo* The final product 5,6-difluoro-4,7-diiodobenzo[*c*][1,2,5]thiadiazole **(2)** was cream yellow coloured crystals (4.46 g, 100.5 mmol, 70%).

^{19}F NMR (400 MHz, $CDCl_3$) δ (ppm): -105.00. ^{13}C NMR (100 MHz, $CDCl_3$) δ (ppm): 155.8, 152.9, 150.1, 141.1, 127.8, and 116.0. EI-MS (*m/z*): $[M]^+$ calculated for $C_6H_2F_2I_2N_2S$, 423; found; 423, 424 and 425. Elemental analysis calculated for $C_6F_2I_2N_2S$; C, 17.00, H, 6.61, I, 59.87, S, 7.56%, found: C, 17.00; H, 6.63, I, 59.77, S, 7.72%.

7.3.3 1-Bromo-2-octyldodecane (3).[8]

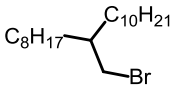

In a reaction vessel, was added 2-octyldodecan-1-ol **(SM2)** (5.0 g, 16.7 mmol) and triphenylphosphine (4.4 g, 16.7 mmol) and (50 cm^3) of DCM. The mixture was stirred until the triphenylphosphine was completely dissolved. N-bromosuccinimide (2.89g, 16.7mmol) was added portion-wise to the mixture with stirring for 15 minutes. Upon completion, the reaction mixture was washed with a saturated solution of $NaHCO_3$ (4 x 500 cm^3) and water (2 x 500 cm^3). The organic layer was collected, reduced *in vacuo*., dried over $MgSO_4$, filtered and the solvent was evaporated to dryness. The black product was soaked with petroleum ether with stirring for 4 hours, filtered and the solvent was evaporated to dryness to afford a yellow oily product. The product 1-bromo-2-octyldodecane **(3)** was purified using column chromatography eluting with PE (40-60) to give 1-bromo-2-octyldodecane as colourless oil (4.93 g, 13.63 mmol, 81%).

^{1}H NMR (400 MHz, $CDCl_3$) δ (ppm) 3.55 (*d*, *J* = 5.0 Hz, 2H), 1.61 (*bs*, 1H), 1.39-1.18 (*m*, 22H), 0.91 (*t*, *J* = 6.0 Hz, 6H).^{13}C NMR (100 MHz, $CDCl_3$): δ (ppm) 39.7, 39.4, 32.5, 31.9, 31.9, 29.8, 29.6, 29.6, 29.5, 29.3, 29.3, 29.0, 26.5, 22.7, and 14.1. EI-MS (m/z): $[M]^+$ calculated for $C_{20}H_{41}Br$, 360; found 358 and 360. Elemental analysis calculated for $C_{20}H_{41}Br$ C, 66.46, H, 11.43, Br, 22.11%, found; C, 66.18; H, 11.31; Br, 22.20%.

7.3.4 (2-Octyldodecyl)magnesium bromide (4).[9]

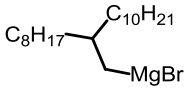

To a reaction vessel under a protective atmosphere of argon, was added magnesium turnings (0.47 g, 19.3 mmol) and (25 cm^3) of anhydrous THF, 1-bromo-2-octyldodecane (7.0 g, 19.3 mmol) was added drop wise to the magnesium turnings suspension to maintain the reaction reflux. Upon addition completion, the reaction mixture was heated to 75 °C for 3 hours until the solution colour was changed into dark grey which indicated the end of the reaction. This product (2-octyldodecyl)magnesium bromide **(4)** was used in the next reaction without further steps.

7.3.5 3-(2-Octyldodecyl)thiophene (5).[10]

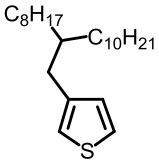

To a reaction vessel under a protective atmosphere of argon, compound **(4)** was added to a solution of anhydrous THF (25 cm^3) containing 3-bromothiophene **(SM3)** (6.3 g, 38.6 mmol) and Ni(dppp)Cl_2 (261 mg, 0.48 mmol) at room temperature. After addition, the reaction mixture was stirred overnight at the same temperature. Upon completion, the reaction mixture was quenched with NH_4Cl solution (100 cm^3). The organic layer was extracted with anhydrous ether (3 x 75 cm^3). All the organic layers were combined, washed with deionized water, dried over $MgSO_4$ and the solvent was removed *in vacuo* The crude product was purified using silica gel column chromatography eluting with PE to afford the product 3-(2-octyldodecyl)thiophene **(5)** as a colourless oil (5.42 g, 14.8 mmol, 77%).

^{1}H NMR (400 MHz, $CDCl_3$) δ (ppm) 7.25 (*dd*, J_1 = 5.0 Hz, J_2 = 3.0 Hz, 1H), 6.92 (*m*, 2H), 2.58 (*d*, *J* = 3.5 Hz, 1H), 1.66-1.55 (*m*, 1H), 1.47-1.10 (*m*, 22H), 0.91 (*t*, *J* = 7.0 Hz, 6H). ^{13}C NMR (100 MHz, $CDCl_3$): δ (ppm) 141.9, 128.8, 124.7, 120.6, 39.7, 39.5, 38.9, 34.7, 33.3, 32.5, 31.9, 30.0, 29.8, 29.6, 29.6, 29.5, 29.3, 26.6, 26.5, 22.7 and 14.1. EI-

MS (*m/z*): $[M]^+$ calculated for $C_{24}H_{44}S$, 364; found 364. Elemental analysis calculated for $C_{24}H_{44}S$; C, 79.05; H, 12.16; S, 8.79% found C, 77.01; H, 11.52; S, 7.77%

7.3.6 2-Bromo-3-(2-octyldodecyl)thiophene (6).[11]

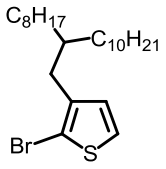

To a reaction vessel under a protective atmosphere of argon was added 3-(2-octyldodecyl)thiophene **(5)** (0.5 g, 1.371 mmol), $CHCl_3$ (10 cm^3) and acetic acid (10 cm^3). N-bromosuccinimde (0.244 g, 1.371 mmol) was added to the mixture and stirred for 24 hours. Upon completion, the mixture was poured into water (150 cm^3) and extracted with DCM (100 cm^3), the organic layer was extracted again with an aqueous solution of $NaHCO_3$ (1 x 100 cm^3), dried over $MgSO_4$ and the solvent was evaporated *in vacuo* The crude product was purified using column chromatography eluting with PE (40-60) to afford the product 2-bromo-3-(2-octyldodecyl)thiophene **(6)** as colourless oil (0.5 g, 1.12 mmol, 81%).

^{1}H NMR (400 MHz, $CDCl_3$): δ (ppm) 7.19 (*d*, *J* = 5. 5 Hz, 1H), 6.77 (*d*, *J* = 5.5 Hz, 1H) , 2.51 (*d*, *J* = 7.0 Hz, 2H), 1.57 (*bs*, 1H), 1.37-1.19 (*m*, 22H), 0.91 (*t*, *J* = 6.5 Hz, 6H). ^{13}C NMR (100 MHz, $CDCl_3$): δ (ppm) 141.9, 128.8, 124.7, 120.6, 38.5, 37.7, 37.1, 34.0, 33.7, 33.3, 31.9, 30.2, 30.1, 30.0, 29.9, 29.7, 29.7, 29.7, 29.6, 29.6, 29.3, 29.3, 27.1, 26.7, 26.5, 22.7 and 14.1. EI-MS (*m/z*): $[M]^+$ calculated for $C_{24}H_{43}BrS$, 422; found 442 and 444. Elemental analysis calculated for $C_{24}H_{43}BrS$; C, 64.99; H, 9.77; Br, 18.01; S, 7.23% found C, 65.05; H, 9.71; Br, 17.99; S, 7.21%.

7.3.7 2,6-Bis(4,4,5,5-tetramethyl-1,3,2-dioxaborolan-2-yl)naphthalene (7).[12]

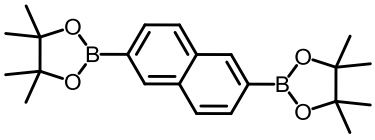

To a reaction vessel under a protective atmosphere of argon was added 2,6-dibromonaphthalene **(SM4)** (0.5 g, 1.75 mmol), bis(pinacolato)diboron (1.99 g, 7.8 mmol), and a mixture of $Pd(dppf)Cl_2$ (0.074 g, 0.1 mmol), KOAc aqueous solution and DMF (50 cm^3). The whole mixture was stirred at 100 °C for 24 hours. Upon reaction completion, the resulted black solution was dissolved in $CHCl_3$ (150 cm^3) and extracted with distilled water (2 x 500 cm^3) the organic layer was separated, dried over $MgSO_4$ and filtered and the solvent was reduced *in vacuo* The remaining black solution was precipitated in MeOH (150 cm^3) (which had been passed through basic alumina) to

form a suspension of grey solid and liquid, this product was filtered and washed with methanol and then dried in the oven overnight to give the pure product 2,6-bis(4,4,5,5-tetramethyl-1,3,2-dioxaborolan-2-yl)naphthalene **(7)** as a grey powder (0.285 g, 0.75 mmol, 43%).

^{1}H NMR (400 MHz, $CDCl_3$): δ (ppm) 8.37 (*s*, 2H), 7.88 (*d*, *J* = 8.0 Hz, 2H), 7.84 *(d, J* = 8.0 Hz*,* 2H), 1.69-120 (*m*, 24H). ^{13}C NMR (100 MHz, $CDCl_3$): δ (ppm) 135.9, 134.3, 130.3, 127.6, 30.9 and 24.9. EI-MS (*m/z*): $[M]^+$ calculated for $C_{22}H_{30}BO_4$, 380; found 378, 379, 380, 381 and 382. Elemental analysis calculated for $C_{22}H_{30}BO_4$; C, 69.52; H, 7.96% found C, 69.09; H, 7.68%.

7.3.8 2,6-Bis(4-(2-octyldodecyl)thiophen-2-yl)naphthalene (M1).[13]

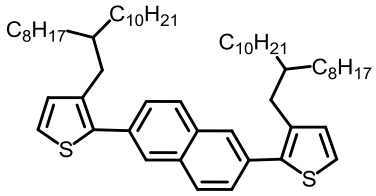

To a reaction vessel under a protective atmosphere of argon, was added 2,6-bis(4,4,5,5-tetramethyl-1,3,2-dioxaborolan-2-yl)naphthalene **(7)** (0.23 g, 0.605 mmol) to 2-bromo-3-(2-octyldodecyl)thiophene **(6)** along with $Pd(OAc)_2$ (0.017 g, 0.076 mmol) and tri(*o*-tolyl)phosphine (0.0306 g, 0.1 mmol). The whole mixture was dissolved in dry THF (5 cm^3) before adding saturated $NaHCO_3$ (4 cm^3). The reaction mixture was stirred at 90 °C and left to stir overnight. Upon completion, the solvent was removed *in vacuo* and the water was removed by washing with MeOH and decanting. The crude product was collected as a dark black solid and was purified using silica gel column chromatography eluting with PE (40-60) to afford the product 2,6-bis(4-(2-octyldodecyl)thiophen-2-yl)naphthalene **(M1)** as a green oil (0.31 g, 0.346 mmol, 60%).

^{1}H NMR (400 MHz, $CDCl_3$): δ (ppm) 7.91 (*s*, 2H), 7.87 (*d, J* = 8.5 Hz, 2H), 7.60 (*d*, *J* = 8.5 Hz, 2H), , 7.29 (*d*, *J* = 5.0 Hz, 2H) 7.0 (*d, J* = 5.0 Hz, 2H), 2.70 (*d, J* = 7.0 Hz, 4H), 1.65 (*bs*, 2H), 1.35-1.09 (*m*, 64H), 0.90-0.83 (*m*, 12H). ^{13}C NMR (100 MHz, $CDCl_3$): δ (ppm) 130.0, 128.2, 128.0, 123.7, 39.1, 33.4, 33.1, 31.9, 29.9, 29.6, 29.3, 29.3, 26.4, 22.7 and 14.1. EI-MS (*m/z*): $[M]^+$ calculated for $C_{58}H_{92}S_2$, 852; found 852. Elemental analysis calculated for $C_{58}H_{92}S_2$; C, 81.62; H, 10.86; S, 7.51% found C, 81.71; H, 10.79; S, 7.53%.

7.3.9 Poly 2,6-bis(4-(2-octyldodecyl)thiophen-2-yl)naphthalene-alt-4,7-benzo[c] [1,2,5]thiadiazole (P1).[14]

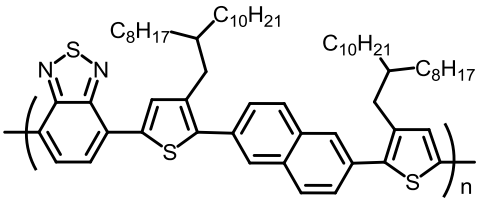

A top sealing tube under a protective atmosphere of argon was charged with 2,6-bis(4-(2-octyldodecyl)thiophen-2-yl)naphthalene **(M1)** (0.1 g, 0.117 mmol), 4,7-dibromobenzo[*c*][1,2,5]thiadiazole **(SM11)** (0.034 g, 0.117 mmol), $Pd_2(dba)_3$ (7.5 mg, 0.025 mmol), P(*o*-MeOPh)$_3$ (7.9 mg, 0.01 mmol), cesium carbonate (0.1g, 0.307mmol) and pivalic acid (9.6 mg, 0.094 mmol). All the chemicals were dissolved in dry THF (1 cm^3) and the reaction mixture was stirred at 120 °C for 24 hours. Upon completion, a dark red precipitate was formed around the bottom of the tube which was collected and dissolved in $CHCl_3$ and stirred with NH_4OH solution (50 cm^3) for 3 hours. The latter was transferred to an extraction funnel and washed with distilled water (3 x 100 cm^3). The organic layer was collected and the solvent was reduced *in vacuo*. The polymer solution was precipitated in MeOH (150 cm^3), filtered and the collected polymer was extracted with Soxhlet using a series of solvents; MeOH, acetone, hexane and toluene respectively. The toluene fraction was then collected and the solvent was reduced *in vacuo* and the polymer solution was precipitated again in MeOH (150 cm^3) to afford the polymer as a red powder (0.079 g, 0.0799 mmol).

Toluene fraction (43 % yield) GPC in toluene at 100 °C (*Mn* = 8,500), (*Mw* = 15,100) (PDI = 1.77). ^{1}H NMR (400 MHz, $C_2D_2Cl_4$): δ (ppm) 8.25 (*s*, 2H), 8.07-7.94 (*m*, 4H), 7.97 (*d, J* = 9.0 Hz, 2H), 7.75 (*d, J* = 9.0 Hz, H) 2.86 (*d, J* = 6.0 Hz, 4H), 1.81-1.77 (*m*, 2H) , 1.42-1.13 (*m*, 64H), 0.88 (*t, J* = 7.0 Hz, 12H). Elemental analysis calculated for $C_{64}H_{92}N_2S_3$; C, 77.99; H, 9.41; N, 2.84; S, 9.76 % found C, 74.30; H, 8.98; N, 2.98; S, 8.91 %.

7.3.10 Poly 2,6-bis(4-(2-octyldodecyl)thiophen-2-yl)naphthalene-alt-5,6-difluoro-4,7-benzo[c][1,2,5]thiadiazole (P2).[14]

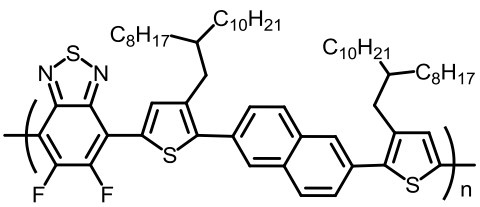

A top sealing tube under a protective atmosphere of argon was charged with 2,6-bis(4-(2-octyldodecyl)thiophen-2-yl)naphthalene **(M1)** (0.1 g, 0.117 mmol), 5,6-difluoro-4,7-dibromobenzo[c][1,2,5]thiadiazole **(2)** (0.049 g, 0.117 mmol), $Pd_2(dba)_3$ (7.5 mg, 0.025 mmol), P(*o*-MeOPh)$_3$ (7.9 mg, 0.01 mmol), cesium carbonate (0.1 g, 0.307 mmol) and pivalic acid (9.6 mg, 0.094 mmol). All the chemicals were dissolved in dry THF (1 cm^3) and the reaction mixture was stirred at 120 °C for 24 hours. Upon completion, a deep red precipitate was formed around the bottom of the tube which was collected and dissolved in $CHCl_3$ and stirred with NH_4OH solution (50 cm^3) for 3 hours. The latter was transferred to an extraction funnel and washed with distilled water (3 x 100 cm^3). The organic layer was collected and the solvent was reduced *in vacuo*, the polymer solution was precipitated in MeOH (150 cm^3), filtered and the collected polymer was extracted with Soxhlet using a series of solvents; MeOH, acetone, hexane and toluene respectively. The toluene fraction was then collected and the solvent was reduced *in vacuo* and the polymer solution was precipitated again in MeOH (150 cm^3) to afford the polymer as a red powder (0.036 g, 0.035 mmol).

Toluene fraction (36 % yield) GPC in $CHCl_3$ at 40 °C (*Mn* = 26,000), (*Mw* = 44,500) (PDI = 1.71). ^{1}H NMR (400 MHz, $C_2D_2Cl_4$): δ (ppm) 8.10-8.05 (*m*, 2H), 7.96-7.83 (*m*, 4H), 7.75 (*d, J* = 8.0 Hz, 2H), 2.85 (*bs*, 4H), 1.82 (*bs*, 2H), 1.52-1.16 (*m*, 64H), 0.90 (*t*, *J* = 7.0 Hz, 12H). Elemental analysis calculated for $C_{64}H_{90}F_2N_2S_3$; C, 75.24; H, 8.88; N, 2.74; S, 9.42 % found C, 74.88; H, 8.75; N, 2.79; S, 9.15 %.

7.3.11 Poly 2,6-bis(4-(2-octyldodecyl)thiophen-2-yl)naphthalene-alt-4,7-di(thiophene-2-yl)benzo[c][1,2,5]thiadiazole (P3).[14]

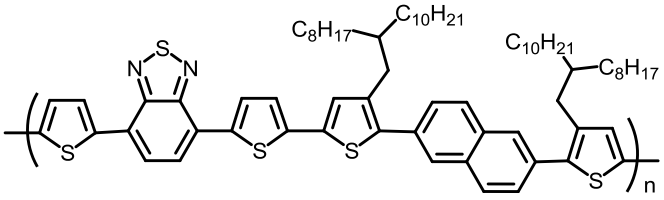

A top sealing tube under a protective atmosphere of argon was charged with 2,6-bis(4-(2-octyldodecyl)thiophen-2-yl)naphthalene **(M1)** (0.1 g, 0.117 mmol), 4,7-bis(5-bromothiophen-2-yl)benzo[*c*][1,2,5]thiadiazole **(SM12)** (0.053 g, 0.117 mmol), $Pd_2(dba)_3$ (6.8 mg, 0.025 mmol), P(*o*-MeOPh)$_3$ (7.9 mg, 0.01 mmol), cesium carbonate (0.1g, 0.307mmol) and pivalic acid (9.6mg, 0.094mmol). All the chemicals were dissolved in dry THF (1 cm^3) and the reaction mixture was stirred at 120 °C for 24 hours. Upon completion, a dark purple precipitate was formed around the bottom of the tube which was collected and dissolved in $CHCl_3$ and stirred with NH_4OH solution (50 cm^3) for 3 hours. The latter was transferred to an extraction funnel and washed with

distilled water (3 x 100 cm^3). The organic layer was collected and the solvent was reduced *in vacuo*, the polymer solution was precipitated in MeOH (150 cm^3), filtered and the collected polymer was extracted with Soxhlet using a series of solvents; MeOH, acetone, hexane and toluene respectively. The toluene fraction was then collected and the solvent was reduced *in vacuo* and the polymer solution was precipitated again in MeOH (150 cm^3) to afford the polymer as a dark purple powder (0.045g, 0.038mmol).

Toluene fraction (43 % yield) GPC in toluene at 100 °C (*Mn* = 33,400), (*Mw* = 38,600) (PDI = 1.15). ^{1}H NMR (400 MHz, $C_2D_2Cl_4$): δ (ppm) 8.12 (*s*, 2H), 8.01 (*d, J* = 7.0 Hz, 4H), 7.94-7.85 (*m*, 4H), 7.71-7.66 (*m*, 2H), 7.35-7.29 (*m*, 2H), 7.26-7.21 (*m*, 2H), 2.77-2.70 (*m*, 4H), 1.76 (*bs*, 2H), 1.52-1.13 (*m*, 64H), 0.92-0.87 (*m*, 12H). Elemental analysis calculated for $C_{72}H_{96}F_2N_2S_5$; C, 75.21; H, 8.42; N, 2.44; S, 13.94%, found; C, 74.98; H, 8.13; N, 2.47; S, 13.78 %.

7.4 Synthesis of monomers and polymers (series 2) (Chapter 3)

7.4.1 2,6-Dibromoanthracene (8).[15]

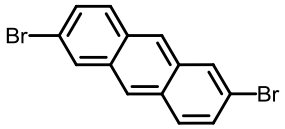

To a reaction vessel under protective atmosphere was added 2-6-dibromoanthracene-9,10-dione **(SM5)** (2.80 g, 7.60 mmol), acetic acid (65 cm^3), hydroiodic acid (13 cm^3, 57%) and hypophosphorous acid (5.5 cm^3, 50%). The reaction mixture was heated to reflux for 72 hours. Upon completion, the reaction mixture was cooled to room temperature and poured onto crushed ice (400 cm^3). The yellow precipitate formed was filtered then washed with water and methanol. The product 2,6-dibromoanthracene **(8)** was collected as yellow solid (1.33 g, 3.96 mmol, 52%).

^{1}H NMR (400 MHz, $CDCl_3$): δ (ppm) 8.32 (*s*, 2H), 8.18 (*dd, J_1* = 9.0 Hz, *J_2* = 2.0 Hz, 2H), 7.55 (*dd*, *J_1* = 9.0 Hz, *J_2* = 2.0 Hz, 2H). ^{13}C NMR (100 MHz, $CDCl_3$): δ (ppm) 137.3, 132.5, 131.8, 129.1, 127.5, 127.1 and 84.0. Elemental analysis calculated for $C_{14}H_8Br_2$; C, 50.04; H, 2.40; Br, 47.56%, found; C, 47.30; H, 2.34; Br, 43.58%. EI-MS (*m/z*): $[M]^+$ calculated for $C_{14}H_8Br_2$, 333; found 333, 335 and 337. m. p. = decomposes at 247 °C.

7.4.2 2,2'-(2,6-Anthracenediyl)bis[4,4,5,5-tetramethyl]-1,3,2-dioxaborolane (9).[12]

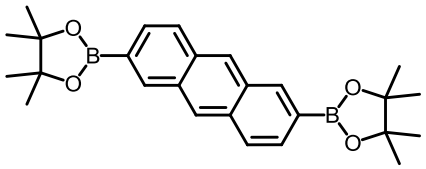

To a reaction vessel under a protective atmosphere of argon was added 2,6-dibromoanthracene **(8)** (0.40 g, 1.49 mmol), $Pd(dppf)Cl_2$ (0.0549 g, 0.075 mmol), KOAc (0.874g, 8.94mmol) and anhydrous DMF (40 cm^3). The mixture was stirred for 48 hours at 100 °C. Upon completion, the reaction mixture was cooled to room temperature, extracted into $CHCl_3$, washed with distilled water (3 x 200 cm^3) and the solvent was reduced *in vacuo.* The remaining solution was then added to stirred methanol which had been passed on basic alumina. The formed solid was filtered and washed with methanol to afford 2,2'-(2,6-anthracenediyl)bis[4,4,5,5-tetramethyl]-1,3,2-dioxaborolane **(9)** as black solid (0.25g, 0.603mmol, 40%).

^{1}H NMR (400 MHz, $CDCl_3$): δ (ppm) 8.57 (*s*, 2H), 8.46 (*s*, 2H), 8.02 (*d, J* = 8.5 Hz, 2H), 7.80 (*dd, J_1* = 8.5 Hz, *J_2* = 1.0 Hz, 2H), 1.42 (*s*, 24H). ^{13}C NMR (100 MHz, $CDCl_3$): δ (ppm) 137.2, 132.7, 131.8, 129.0, 127.3, 127.1, 83.9 and 24.9. Elemental Analysis calculated for $C_{26}H_{32}B_2O_4$; C, 72.60; H, 7.50%, found; C, 70.30; H, 7.18%. EI-MS (*m/z*): $[M]^+$ calculated for $C_{26}H_{32}B_2O_4$, 430.16; found 428, 429, 430, 431 and 432.

7.4.3 2,6-Bis(3-(2-octyldodecyl)thiophene-2-yl)anthracene (M2).[13]

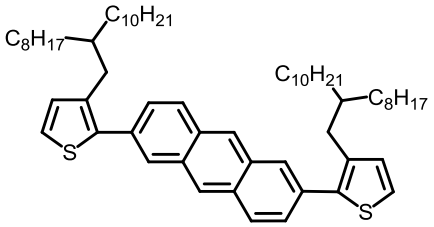

To a reaction vessel under a protective atmosphere of argon was added 2-bromo-(3-octyldodecyl)thiophene **(6)** (0.81 g, 2.2 mmol), 2,2'-(2,6-anthracenediyl)bis[4,4,5,5-tetramethyl]-1,3,2-dioxaborolane **(9)** (0.358 g, 0.83 mmol), $Pd(OAc)_2$ (0.013 g, 0.085 mmol, 7%), tri(*o*-tolyl)phosphine (0.035 g, 0.116 mmol), dry THF (14 cm^3) and a saturated aqueous solution of $NaHCO_3$ (4.0 cm^3). The reaction mixture was stirred at 90 °C for 24 hours. Upon completion, the reaction mixture was cooled to room temperature, extracted with $CHCl_3$ (50 cm^3). The organic layer was then washed with distilled water (3 x 50 cm^3), dried over $MgSO_4$, filtered and the solvent was *in vacuo* The crude product was purified using silica gel column chromatography eluting

petroleum ether (40-60): DCM (10:0.2, v/v) to afford 2,6-bis(3-(2-octyldodecyl)thiophene-2-yl)anthracene **(M2)** as yellow oil (0.45 g, 0.498 mmol, yield 60%).

^{1}H NMR (400 MHz, $CDCl_3$): δ (ppm) 8.44 (*s*, 2H), 8.05 (*s*, 2H), 7.99 (*d*, *J* = 8.5 Hz, 2H), 7.59 (*d*, *J* = 8.5 Hz, 2H), 7.30 (*d*, *J* = 5. 0 Hz, 2H), 7.01 (*d*, *J* = 5. 0 Hz,2H), 2.74 (*d*, *J* = 7.0 Hz, 4H), 2.18 (*s*, 1H), 1.66-1.14 (*m*, 64H), 0.91-0.85 (*m*, 12H). ^{13}C NMR (100 MHz, $CDCl_3$): δ (ppm) 138.4, 138.3, 132.0, 131.6, 131.0, 130.2, 128.2, 128.2, 127.8, 126.2, 123.7, 39.2, 37.7, 33.4, 33.2, 31.9, 31.9, 30.2, 30.2, 30.0, 29.7, 29.6, 29.4, 29.3, 29.3, 26.7, 26.4, 22.7, 22.6 and 14.1. EI-MS (*m/z*): $[M]^+$ calculated for $C_{62}H_{94}S_2$, 902; found 902. Elemental analysis calculated for $C_{62}H_{94}S_2$; C, 82.42; H, 10.49; S, 7.09% found C, 82.46; H, 10.34; S, 6.96%.

7.4.4 Poly(2,6-bis(3-(2-octyldodecyl)thiophene-2-yl)anthracene-alt-benzo[c][1,2,5] thiadiazole (P4).[14]

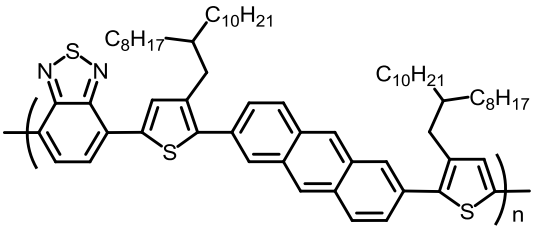

A top sealing tube under a protective atmosphere of argon was charged with 2,6-bis(3-(2-octyldodecyl)thiophene-2-yl)anthracene **(M2)** (0.1 g, 0.11 mmol), 4,7-dibromobenzo[*c*][1,2,5]thiadiazole **(SM11)** (0.032 g, 0.110 mmol), $Pd_2(dba)_3$ (6.8mg, 0.025mmol), P(*o*-MeOPh)$_3$ (7.9 mg, 0.01 mmol), cesium carbonate (0.1 g, 0.307 mmol) and pivalic acid (9.6 mg, 0.094 mmol). All the chemicals were dissolved in dry THF (1 cm^3) and the reaction mixture was stirred at 120 °C for 24 hours. Upon completion, a deep red precipitate was formed around the bottom of the tube which was dissolved in $CHCl_3$ and stirred with NH_4OH solution (50 cm^3) for 3 hours. The latter was transferred to an extraction funnel and washed with distilled water (3 x 100 cm^3). The organic layer was collected and the solvent was reduced *in vacuo*, the polymer solution was precipitated in MeOH (150 cm^3), filtered and the collected polymer was extracted with Soxhlet using a series of solvents; MeOH, acetone, hexane and toluene respectively. The toluene fraction was then collected and the solvent was reduced *in vacuo* and the polymer solution was precipitated again in MeOH (150 cm^3) to afford the polymer as a deep red powder (0.106 g, 0.102 mmol, 93%).

Toluene fraction (74 % yield) GPC in toluene at 100 °C (*Mn* = 16,000), (*Mw* = 38,900) (PDI = 2.43). ^{1}H NMR (400 MHz, $C_2D_2Cl_4$): δ (ppm) 8.37 (*s*, 2H), 8.06 (*s,* 2H), 7.94-7.88

(*m*, 4H), 7.80 (*s*, 2H), 7.57-7.51 (*m*, 2H), 2.71 (*s*, 4H), 1.64 (*s*, 2H), 1.05-0.91 (*m*, 64H), 0.73-0.69 (*m*, 12H). Elemental analysis calculated for $C_{68}H_{94}N_2S_3$; C, 78.86; H, 9.15; N, 2.70; S, 9.29 % found C, 81.51; H, 11.14; N, 1.41; S, 4.82 %.

7.4.5 Poly(2,6-bis(3-(2-octyldodecyl)thiophene-2-yl)anthracene-alt-5,6-difluorobenzo[c][1,2,5]thiadiazole (P5).[14]

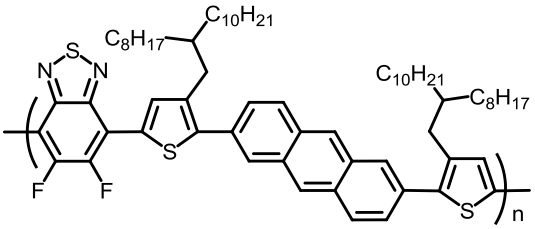

A top sealing tube under a protective atmosphere of argon was charged with 2,6-bis(3-(2-octyldodecyl)thiophene-2-yl)anthracene **(M2)** (0.1 g, 0.11 mmol), 5,6-difluoro-4,7-diiodo-benzo[*c*][1,2,5]thiadiazole **(2)** (0.046 g, 0.11 mmol), $Pd_2(dba)_3$ (6.8mg, 0.025mmol), P(*o*-MeOPh)$_3$ (7.9 mg, 0.01 mmol), cesium carbonate (0.1g, 0.307mmol) and pivalic acid (9.6mg, 0.094mmol). All the chemicals were dissolved in dry THF (1 cm^3) and the reaction mixture was stirred at 120 °C for 24 hours. Upon completion, a red precipitate was formed around the bottom of the tube which was dissolved in $CHCl_3$ and stirred with NH_4OH solution (50 cm^3) for 3 hours. The latter was transferred to an extraction funnel and washed with distilled water (3 x 100 cm^3). The organic layer was collected and the solvent was reduced *in vacuo*, the polymer solution was precipitated in MeOH (150 cm^3), filtered and the collected polymer was extracted with Soxhlet using a series of solvents; MeOH, acetone, hexane and toluene respectively. The toluene fraction was then collected and the solvent was reduced *in vacuo* and the polymer solution was precipitated again in MeOH (150 cm^3) to afford the polymer as a red powder (0.101 g, 0.094 mmol, 91%).

Toluene fraction (83 % yield) GPC in toluene at 100 °C (*Mn* = 15,900), (*Mw* = 28,000) (PDI = 1.76). ^{1}H NMR (400 MHz, $C_2D_2Cl_4$): δ (ppm) 8.41 (*s*, 2H), 8.16 (*s,* 2H), 8.12 (*s*, 2H), 8.01 (*d*, *J* = 9.0 Hz, 2H), 7.64 (*d*, *J* = 9.0 Hz, 2H), 2.80 (*s*, 4H), 1.72 (*s*, 2H), 1.39-0.95-0.84 (*m*, 64H), 0.80-0.75 (*m*, 12H). Elemental analysis calculated for $C_{68}H_{92}F_2N_2S_3$; C, 76.21; H, 8.65; N, 2.61; S, 8.98 % found C, 75.81; H, 8.37; N, 2.53; S, 8.63 %.

7.5 Synthesis of monomers and polymers (series 3) (Chapter 4)

7.5.1 2,7-Bis(4,4,5,5,-tetramethyl-1,3,2,-dioxaborolan-2-yl)pyrene (10).[16]

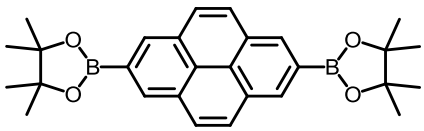

To a reaction vessel under a protective atmosphere of argon was added pyrene **(SM6)** (2.0g, 9.79mmol), bis(pinacolato)diboron (5.524 g, 21.75 mmol), $[Ir(OMe)COD]_2$ (0.327 g, 5 mol%), 4,4'-di-*tert*-butyl-2,2'bipyridine (0.265 g, 10 mol%) and dry THF (25 cm^3). The reaction mixture was stirred for 16 hours at 80 °C. Upon completion, the mixture was cooled to room temperature, washed with distilled water (150 cm^3) and extracted with chloroform (2 x 150 cm^3). The organic phases were collected, solvent reduced *in vacuo.* The remaining solution was then added to a stirred methanol which had been passed on basic alumina. The formed solid was filtered and washed with methanol to afford 2,7-bis(4,4,5,5,-tetramethyl-1,3,2,-dioxaborolan-2-yl)pyrene **(10)** as a grey solid (2.21 g, 2.80 mmol, yield 49%).

^{1}H NMR (400 MHz, $C_2D_2Cl_4$): δ (ppm) 8.45 (*s*, 4H), 8.10 (*s*, 4H), 1.47 (*s*, 24H). ^{13}C NMR (100 MHz, $CDCl_3$): δ (ppm) 131.2, 130.8, 127.6, 126.3, 84.2 and 25.0. Elemental analysis calculated for $C_{28}H_{34}B_2O_4$; C 73.72; H, 7.51 % found C, 73.43; H, 6.98 %. EI-MS (*m/z*): $[M]^+$ calculated for $C_{28}H_{34}B_2O_4$, 454.25; found 452, 453, 454.30, 455 and 456.

7.5.2 2,7-Bis(3-(2-octyldodecyl)thiophen-2-yl)pyrene (M3).[13]

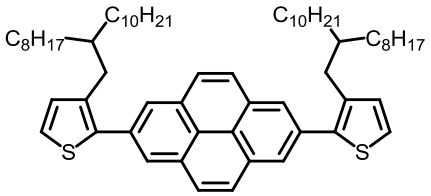

To a reaction vessel under a protective atmosphere of argon was added 2-bromo-(3-octyldodecyl)thiophene **(6)** (1.0 g, 2.25 mmol), 2,7-bis(4,4,5,5,-tetramethyl-1,3,2,-dioxaborolan-2-yl)pyrene **(10)** (0.465 g, 1.024 mmol), $Pd(OAc)_2$ (0.010 g, 7 mol%), tri(*o*-tolyl)phosphine (0.020 g, 0.14 mol%), dry THF (10 cm^3) and a saturated aqueous solution of $NaHCO_3$ (4.0 cm^3). The reaction mixture was stirred at 90 °C for 24 hours. Upon completion, the reaction mixture was cooled to room temperature, extracted with $CHCl_3$ (50 cm^3). The organic layer was then washed with distilled water (3 x 50 cm^3), dried over $MgSO_4$, filtered and the solvent was *in vacuo* The crude product was purified using silica gel column chromatography eluting petroleum ether (40-60): DCM (10:0.2)

to afford 2,7-bis(3-(2-octyldodecyl)thiophen-2-yl)pyrene **(M3)** as green oil (0.83 g, 0.89 mmol, yield 87%).

^{1}H NMR (400 MHz, $CDCl_3$): δ (ppm) 8.25 (*s*, 4H), 8.11 (*s*, 4H), 7.36 (*d*, *J* = 5.0 Hz, 2H), 7.07 (*d*, *J* = 5.0 Hz, 2H), 2.79 (*d*, *J* = 7.0 Hz, 4H), 1.28-1.14 (*m*, 64H), 0.90-0.84 (m, 12H). ^{13}C NMR (100 MHz, $CDCl_3$): δ (ppm) 131.2, 130.3, 127.9, 126.4, 95.1, 33.4, 31.9, 30.0, 29.6, 29.3, 26.4, 22.7 and 14.1. EI-MS (*m/z*): $[M]^+$ calculated for $C_{64}H_{94}S_2$, 927; found 927. Elemental analysis calculated for $C_{62}H_{94}S_2$; C, 82.87; H, 10.21; S, 6.91% found C, 81.75; H, 9.94; S, 6.81%.

7.5.3 Poly 2,7-bis(3-(2-octyldodecyl)thiophen-2-yl)pyrene-alt-4,7-benzo[c][1,2,5] thiadiazole (P6).[14]

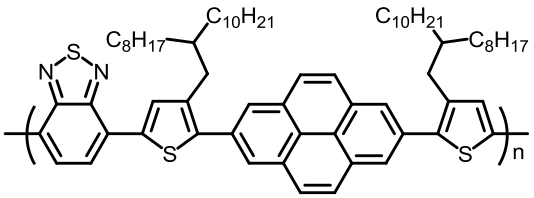

A top sealing tube under a protective atmosphere of argon was charged with 2,7-bis(3-(2-octyldodecyl)thiophen-2-yl)pyrene **(M3)** (0.1 g, 0.107 mmol), 4,7-dibromobenzo[c][1,2,5] thiadiazole **(SM11)** (0.0314 g, 0.107 mmol), $Pd_2(dba)_3$ (6.8 mg, 0.025 mmol), P(*o*-MeOPh)$_3$ (7.9 mg, 0.01 mmol), cesium carbonate (0.1 g, 0.307 mmol) and pivalic acid (9.6 mg, 0.094 mmol). All the chemicals were dissolved in dry THF (1 cm^3) and the reaction mixture was stirred at 120 °C for 72 hours. Upon completion, a dark red precipitate was formed around the bottom of the tube which was collected and dissolved in $CHCl_3$ and stirred with NH_4OH solution (50 cm^3) for 3 hours. The latter was transferred to an extraction funnel and washed with distilled water (3 x 100 cm^3). The organic layer was collected and the solvent was reduced *in vacuo*, the polymer solution was precipitated in MeOH (150 cm^3), filtered and the collected polymer was extracted with Soxhlet using a series of solvents; MeOH, acetone, hexane and toluene respectively. The toluene fraction was then collected and the solvent was reduced *in vacuo* and the polymer solution was precipitated again in MeOH (150 cm^3) to afford the polymer as a dark red powder (0.0772 g, 0.072 mmol, 68%).

Toluene fraction (68 % yield) GPC in toluene at 100 °C (*Mn* = 17,200), (*Mw* = 27,000) (PDI = 1.57). ^{1}H NMR (400 MHz, $C_2D_2Cl_4$): δ (ppm) 8.39 (*s*, 2H), 8.16 (*d, J* = 4.0 Hz*,* 4H), 7.98 (b*s*, 2H), 7.26 (*s*, 2H), 2.92 (*s*, 4H), 1.83-1.78 (*m*, 2H), 1.44-1.28 (*m*, 64H), 0.90-0.86 (*m*, 12H). Elemental analysis calculated for $C_{70}H_{94}N_2S_3$; C, 79.34; H, 8.94; N, 2.64; S, 9.08 % found C, 73.43; H, 8.45; N, 2.29; S, 8.99 %.

7.5.4 Poly 2,7-bis(3-(2-octyldodecyl)thiophen-2-yl)pyrene-alt-4,7-diyl-5,6-difluorobenzo[c][1,2,5]thiadiazole (P7).[14]

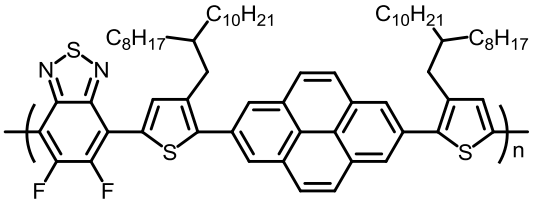

A top sealing tube under a protective atmosphere of argon was charged with 2,7-bis(3-(2-octyldodecyl)thiophen-2-yl)pyrene **(M3)** (0.1 g, 0.107 mmol), 4,7-diiodo-5,6-difluorobenzo[*c*][1,2,5]thiadiazole **(2)** (0.046 g, 0.110 mmol), $Pd_2(dba)_3$ (6.8 mg, 0.025 mmol), P(*o*-MeOPh)$_3$ (7.9 mg, 0.01 mmol), cesium carbonate (0.1 g, 0.307 mmol) and pivalic acid (9.6 mg, 0.094 mmol). All the chemicals were dissolved in dry THF (1 cm^3) and the reaction mixture was stirred at 120 °C for 24 hours. Upon completion, a deep red precipitate was formed around the bottom of the tube which was collected and dissolved in $CHCl_3$ and stirred with NH_4OH solution (50 cm^3) for 3 hours. The latter was transferred to an extraction funnel and washed with distilled water (3 x 100 cm^3). The organic layer was collected and the solvent was reduced *in vacuo*, the polymer solution was precipitated in MeOH (150 cm^3), filtered and the collected polymer was extracted with Soxhlet using a series of solvents; MeOH, acetone, hexane and toluene respectively. The toluene fraction was then collected and the solvent was reduced *in vacuo* and the polymer solution was precipitated again in MeOH (150 cm^3) to afford the polymer as a deep red powder (0.083 g, 0.075 mmol, 70%).

Toluene fraction (70 % yield) GPC in toluene at 100 °C (*Mn* = 10,300), (*Mw* = 25,700) (PDI = 2.49). ^{1}H NMR (400 MHz, $C_2D_2Cl_4$): δ (ppm) 8.40-8.38 (*m*, 2H), 8.31-8.26 (*m,* 2H), 8.17-8.09 (*m*, 2H), 2.58 (*bs*, 4H), 1.81-1.76 (*m*, 2H), 1.45-1.14 (*m*, 64H), 0.90-0.86 (*m*, 12H). Elemental analysis calculated for $C_{70}H_{92}F_2N_2S_3$; C, 76.73; H, 8.46; N, 2.56; S, 8.78 % found C, 77.06; H, 8.56; N, 2.10; S, 8.27 %.

7.5.5 Poly 2,7-bis(3-(2-octyldodecyl)thiophen-2-yl)pyrene-alt-4,7-bis(thiophen-2-yl)benzo[c][1,2,5]thiadiazole (P8).[14]

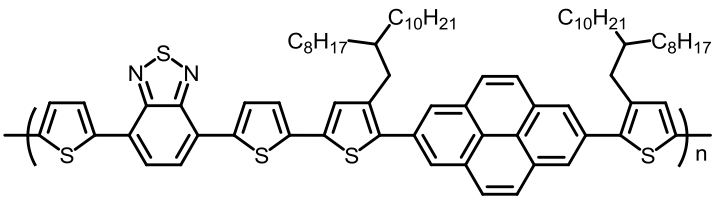

A top sealing tube under protective atmosphere was charged with 2,7-bis(3-(2-octyldodecyl)thiophen-2-yl)pyrene **(M3)** (0.1 g, 0.107 mmol), 4,7-bis(5-bromothiophen-2-yl)benzo[*c*][1,2,5]thiadiazole **(SM12)** (0.049 g, 0.107 mmol), $Pd_2(dba)_3$ (6.8 mg, 0.025

mmol), P(*o*-MeOPh)$_3$ (7.9 mg, 0.01 mmol), cesium carbonate (0.1 g, 0.307 mmol) and pivalic acid (9.6 mg, 0.094 mmol). All the chemicals were dissolved in dry THF (1 cm^3) and the reaction mixture was stirred at 120 °C for 24 hours. Upon completion, a dark purple precipitate was formed around the bottom of the tube which was collected and dissolved in $CHCl_3$ and stirred with NH_4OH solution (50 cm^3) for 3 hours. The latter was transferred to an extraction funnel and washed with distilled water (3 x 100 cm^3). The organic layer was collected and the solvent was reduced *in vacuo* and the polymer solution was precipitated in MeOH (150 cm^3), filtered and the collected polymer was extracted with Soxhlet using a series of solvents; MeOH, acetone, hexane and toluene respectively. The toluene fraction was then collected and the solvent was reduced *in vacuo* and the polymer solution was precipitated again in MeOH (150 cm^3) to afford the polymer as a dark purple powder (0.046 g, 0.072 mmol, 35%).

Toluene fraction (35 % yield) GPC in toluene at 100 °C (*Mn* = 5,300), (*Mw* = 8,700) (PDI = 1.64). ^{1}H NMR (400 MHz, $C_2D_2Cl_4$): δ (ppm) 8.31-8.28 (*m*, 2H), 8.13-8.08 (*m,* 4H), 7.89 (*bs*, 2H), 7.34-7.28 (*m*, 4H), 7.06-7.01 (*m*, 2H), 2.81 (*s*, 4H), 1.72-1.69 (*m*, 2H), 1.47-1.14 (*m*, 64H), 0.90-0.85 (*m*, 12H). Elemental analysis calculated for $C_{78}H_{98}N_2S_5$; C, 76.54; H, 8.07; N, 2.29; S, 13.10 % found C, 75.89; H, 8.92; N, 2.88; S, 7.34 %.

7.5.6 Poly 2,7-bis(3-(2-octyldodecyl)thiophen-2-yl)pyrene-alt-4,7-bis(thiophen-2-yl)-5,6-difluoro benzo[c][1,2,5]thiadiazole (P9).[14]

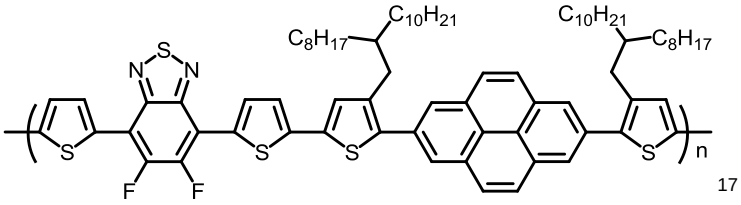

A top sealing tube under protective atmosphere was charged with 2,7-bis(3-(2-octyldodecyl)thiophen-2-yl)pyrene **(M3)** (0.1 g, 0.107 mmol), 4,7-bis(5-bromothiophen-2-yl)5,6-difluorobenzo[*c*][1,2,5]thiadiazole **(SM13)** (0.053 g, 0.107 mmol), $Pd_2(dba)_3$ (6.8 mg, 0.025 mmol), P(*o*-MeOPh)$_3$ (7.9 mg, 0.01 mmol), cesium carbonate (0.1 g, 0.307 mmol) and pivalic acid (9.6 mg, 0.094 mmol). All the chemicals were dissolved in dry THF (2 cm^3) and the reaction mixture was stirred at 120 °C for 24 hours. Upon completion, a dark purple precipitate was formed around the bottom of the tube which was collected and dissolved in $CHCl_3$ and stirred with NH_4OH solution (50 cm^3) for 3 hours. The latter was transferred to an extraction funnel and washed with distilled water (3 x 100 cm^3). The organic layer was collected and the solvent was reduced *in vacuo* and the polymer solution was precipitated in MeOH (150 cm^3), filtered and the collected

polymer was extracted with Soxhlet using a series of solvents; MeOH, acetone, hexane and toluene respectively. The toluene fraction was then collected and the solvent was reduced *in vacuo* and the polymer solution was precipitated again in MeOH (150 cm^3) to afford the polymer as a dark purple powder (0.046 g, 0.036 mmol, 43%).

Toluene fraction (83 % yield) GPC in toluene at 100 °C (*Mn* = 8,600), (*Mw* = 17,100) (PDI = 1.98). ^{1}H NMR (400 MHz, $C_2D_2Cl_4$): δ (ppm) 8.29-8.21 (*m*, 6H), 8.15 (*s,* 2H), 8.14-8.10 (*m*, 4H), 7.39-7.34 (*m*, 4H), 2.81 (*s*, 4H), 1.75 (*s*, 2H), 1.61-1.14 (*m*, 64H), 0.90-0.86 (*m*, 12H). Elemental analysis calculated for $C_{78}H_{96}F_2N_2S_5$; C, 74.36; H, 7.68; N, 2.22; S, 12.72 % found C, 73.52; H, 7.64; N, 2.02; S, 12.18 %.

7.6 Synthesis of monomers and polymers (series 4) (Chapter 5)

7.6.1 (4-(2-Octyldodecyl)thiophene-2-yl)trimethylstannane (11).[17]

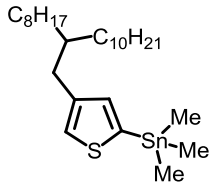

To a reaction vessel under protective atmosphere was added 3-(2-octyldodecyl)thiophene **(5)** (2.5 g, 6.85 mmol), N,N,N',N'-tetramethylethylne diamine (0.872 g, 7.52 mmol) and dry THF (25 cm^3). The reaction mixture was cooled to 0 °C and n-BuLi (3.0 cm^3, 7.52 mmol, 2.5 M in hexane) was added drop-wise. The reaction mixture was stirred for 15 minutes and followed by the next step without further purification. The product was cooled to 0 °C again, and trimethyltin chloride (1.5g, 7.52mmol, 1M in hexane) was added drop-wise to the mixture. The reaction mixture was stirred for 30 minutes at 0 °C then for 2 hours at room temperature. Upon completion, the resulting solution was poured into distilled water and was extracted with diethyl ether. The organic phase was collected and washed with brine, dried over $MgSO_4$ then filtered. The solvent was then removed *in vacuo* to obtain (4-(2-octyldodecyl)thiophene-2-yl)trimethylstannane **(11)** as yellow oil (2.6 g, 4.93 mmol, yield 65%).

^{1}H NMR (400 MHz, $CDCl_3$): δ (ppm) 7.16 (*s*, 1H), 6.96 (*s*, 1H), 2.60 (*d*, *J* = 7.0 Hz, 2H), 1.61 (*bs*, 1H), 1.42-1.14 (*m*, 32H), 0.91-0.86 (*m*, 6H), 0.36 (s, 9H). ^{13}C NMR (100 MHz, $CDCl_3$): δ (ppm) 143.1, 137.2, 126.4, 108.3, 65.8, 45.8, 38.9, 36.1, 34.3, 33.5, 33.4, 31.9, 30.0, 29.6, 29.6, 29.4, 29.3, 27.8, 26.6, 22.6, 15.2 and 14.09. EI-MS (*m/z*): $[M]^+$ calculated for $C_{27}H_{52}SSn$, 528; found 524, 525, 526, 527, 528, 529, 530 and 532.

Elemental analysis calculated for $C_{27}H_{52}SSn$; C, 61.48; H, 9.94; S, 6.08% found C, 64.63; H, 9.78S, 4.96%.

7.6.2 5,6-Difluoro-4,7-bis(4-(2-octyldodecyl)thiophen-2-yl)benzo[c][1,2,5] thiadiazole (12).[18]

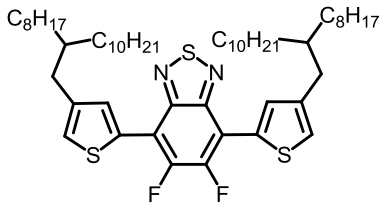

To a reaction vessel under protective atmosphere was added (4-(2-octyldodecyl)thiophene-2-yl)trimethylstannane **(12)** (1 g, 1.89 mmol), 4,7-diiodo-5,6-difluorobenzo[*c*][1,2,5]thiadiazole **(2)** (0.036 g, 0.853 mmol) and $Pd(PPh_3)Cl_2$ (0.029 g, 5 mol%). The mixture was dissolved in toluene (10 cm^3) and stirred at 90 °C for 48 hours. Upon completion, the reaction mixture was poured into distilled water (100 cm^3) and extracted with DCM (3 x 100 cm^3), the organic phases were collected and the solvent removed in The crude product was purified using silica gel column chromatography eluting with PE: ethyl acetate (9:1, v/v) to afford 5,6-difluoro-4,7-bis(4-(2-octyldodecyl)thiophen-2-yl)benzo[*c*][1,2,5]thiadiazole **(12)** as orange oil (1.36 g, 1.51 mmol, yield 80%, m. p.= 73 °C).

^{1}H NMR (400 MHz, $CDCl_3$): δ (ppm) 8.10 (*d*, *J* = 1.0 Hz, 2H), 7.19 (*d*, *J* = 1.0 Hz, 2H), 2.67 (*d*, *J* = 7.0 Hz, 4H), 1.72-1.67 (*m*, 2H), 1.56-1.15 (*m*, 64H), 0.89-0.83 (*t*, *J* = 7.0 Hz, 12H). ^{13}C NMR (100 MHz, $CDCl_3$): δ (ppm) 164.9, 149.0, 148.3, 142.4, 132.8, 130.9, 124.1, 39.0, 35.6, 34.8, 32.0, 30.0, 29.7, 29.4, 26.7, 22.7 and 14.2 EI-MS (*m/z*): $[M]^+$ calculated for $C_{54}H_{86}F_2N_2S_3$, 896; found 896. Elemental analysis calculated for $C_{54}H_{86}F_2N_2S_3$; C, 72.27; H, 9.66; N, 3.12; S, 10.72% found C, 72.17; H, 9.38, N, 2.98; S, 10.53%.

7.6.3 5,6-Difluoro-4,7-bis(3-(2-octyldodecyl)-[2,2'-bithiophen]-5-yl)benzo[c][1,2,5] thiadiazole (13).[19]

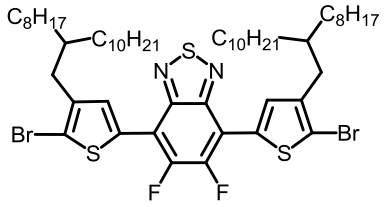

To a reaction vessel under a protective atmosphere of argon was added 5,6-difluoro-4,7-bis(4-(2-octyldodecyl)thiophen-2-yl)benzo[*c*][1,2,5]thiadiazole **(12)** (0.25 g, 0.278 mmol), N-bromosuccinimide (0.099 g, 0.557 mmol) and a mixture of

($CHCl_3$:AcOH)(10/10, v/v). The reaction mixture was stirred at 60 °C for 14 hours. Upon completion, the reaction mixture was poured into distilled water (75 cm^3) and extracted with $CHCl_3$ (2 x 75 cm^3). the organic phases were combined, dried over $MgSO_4$ and filtered and the solvent was removed *in vacuo* The crude product was purified using a silica gel column chromatography eluting with PE only to afford 5,6-difluoro-4,7-bis(3-(2-octyldodecyl)-[2,2'-bithiophen]-5-yl)benzo[*c*][1,2,5] thiadiazole **(13)** as an dark orange powder (0.183 g, 0.173 mmol, yield 62%, m. p.= 67 °C).

^{1}H NMR (400 MHz, $CDCl_3$): δ (ppm) 7.94 (*s*, 2H), 2.61 (*d*, *J* = 7.0 Hz, 4H), 1.76-1.73 (*m*, 2H), 1.55-1.15 (*m*, 64H), 0.89-0.84 (*m*, 12H). ^{13}C NMR (100 MHz, $CDCl_3$): δ (ppm) 151.1, 148.4, 141.8, 132.4, 131.0, 115.0, 38.5, 34.1, 33.3, 31.9, 30.0, 29.7, 29.6, 29.6, 29.3, 26.5, 22.6 and 14.1. EI-MS (*m/z*): $[M]^+$ calculated for $C_{54}H_{84}Br_2F_2N_2S_3$, 1052; found 1052, 1054 and 1056. Elemental analysis calculated for $C_{54}H_{84}Br_2F_2N_2S_3$; C, 61.46; H, 8.02; N, 2.65; Br, 15.14, S, 9.11% found C, 62.55; H, 8.15; N, 2.48; Br, 13.85, S, 8.75%.

7.6.4 5,6-Difluoro-4,7-bis(3-(2-octyldodecyl)-[2,2'-bithiophen]-5-yl)benzo[c][1,2,5] thiadiazole (M4).[18]

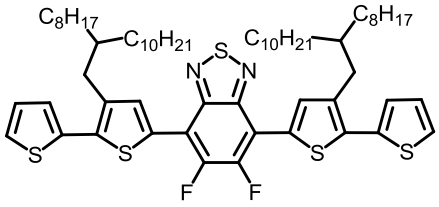

A reaction vessel under a protective atmosphere of argon was charged with 4,7-bis(5-bromo-4-(2-octyldodecyl)thiophen-2-yl)-5,6-difluorobenzo [c][1,2,5]thiadiazole **(13)** 0.122g, 0.116mmol), 2-(tributylstannane)thiophene **(SM7)** (0.13 g, 0.35 mmol), $Pd(PPh_3)Cl_2$ (3.3 mg, 5 mol%) and dry toluene (5 cm^3). the reaction mixture was stirred at 120 °C for 24 hours. Upon completion, the reaction mixture was poured into distilled water (50 cm^3) and extracted with $CHCl_3$ (2 x 50 cm^{33}), dried over MgSO4 and filtered. The solvent was evaporated *in vacuo* and the crude product was purified using silica gel column chromatography eluting with PE: DCM (10:1, v/v) to obtain the product 5,6-difluoro-4,7-bis(3-(2-octyldodecyl)-[2,2'-bithiophen]-5-yl)benzo[*c*][1,2,5] thiadiazole **(M4)** as a dark red powder (0.098 g, 0.092 mmol, yield 79%, m. p.= 81 °C).

^{1}H NMR (400 MHz, $CDCl_3$): δ (ppm) 8.11 (*s*, 2H), 7.39 (*d, J* = 5. 0 Hz, 2H), 7.28-7.24 (*m*, 2H), 7.13 (*dd*, J_1 = 5.0 Hz, J_2= 3.0 Hz, 2H), 2.82 (*d*, *J* = 7.0 Hz, 4H), 1.78-1.75 (*m*, 2H), 1.57-1.15 (*m*, 64H), 0.89-0.84 (*m*, 12H). ^{13}C NMR (100 MHz, $CDCl_3$): δ (ppm) 151.2, 148.8, 139.1, 135.5, 135.1, 134.5, 129.3, 127.4, 126.7, 126.0, 38.8, 33.7, 33.4,

31.9, 30.0, 29.6, 29.6, 29.3, 26.4, 22.7 and 14.1. EI-MS (*m/z*): $[M]^+$ calculated for $C_{62}H_{90}F_2N_2S_5$, 1060.57; found 1060.80. Elemental analysis calculated for $C_{62}H_{90}F_2N_2S_5$; C, 70.14; H, 8.54; N, 2.64; S, 15.10% found C, 69.86; H, 8.63; N, 2.43; S, 14.54 %.

7.6.5 4,4'-Dibromo-2,2'-dinitro-1,1'-biphenyl (14).[20]

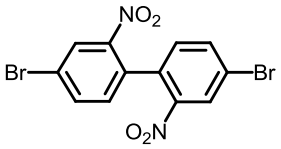

To a reaction vessel under a protective atmosphere of argon was added 1,4-dibromo-2-nitrobenzene **(SM8)** (25 g, 89.0 mmol), Cu powder (12.5 g, 196.7 mmol) and dry DMF (110 cm^3). The reaction mixture heated to reflux at 125 °C for 4 hours. Upon completion, the mixture was cooled to room temperature, dissolved in toluene (250 cm^3) and filtered. A solution of 10% $NaHCO_3$ added and the mixture was extracted with toluene (3 x 150 cm^3), then the organic phase was washed with distilled water (250 cm^3) with monitoring the pH to be approximately 6, dried over MgSO4 and filtered and the solvent was removed *in vacuo* to give the crude product as yellow crystals. The crude product was recrystallized using isopropanol at 90 °C and then filtered to afford the pure 4,4'-dibromo-2,2'-dinitro-1,1'-biphenyl **(14)** as pale yellow crystals (16.30 g, 81.11 mmol, yield 91%, m. p.=117 °C).

^{1}H NMR (400 MHz, $CDCl_3$): δ (ppm) 8.39 (*d*, *J* = 2.0 Hz, 2H), 7.85 (*dd, J_1* = 8.0 Hz, J_2 = 2.0 Hz, 2H), 7.18 (*d*, *J* = 8.0 Hz, 2H). ^{13}C NMR (100 MHz, $CDCl_3$): δ (ppm) 147.3, 163.6, 132.0, 131.9, 128.1 and 122.9. EI-MS (*m/z*): $[M]^+$ calculated for $C_{12}H_6Br_2N_2O_4$, 399; found 399, 401 and 403. Elemental analysis calculated for $C_{12}H_6Br_2N_2O_4$; C, 35.85; H, 1.50; Br, 39.75; N, 6.97%; found: C, 35.95; H, 1.26; Br, 39.93; N, 6.89%.

7.6.6 2,2'-Diamine-4,4'-dibromo-1,1'-biphenyl (15).[20]

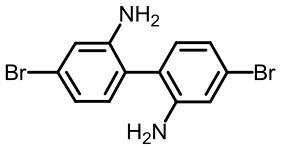

A reaction vessel under a protective atmosphere of argon was charged with 4,4'-dibromo-2,2'-dinitro-1,1'-biphenyl **(14)** (12.0 g, 29.88 mmol), absolute ethanol (150 cm^3) and 32% HCl (90 cm^3). The reaction mixture was stirred at room temperature. This was followed by the addition of Sn powder (14.0g, 119.32mmol) and the mixture was heated to reflux at 100 °C for 2 hours. Upon completion, the reaction mixture was filtered, washed with distilled water (2 x 300 cm^3) and treated with NaOH (20%) with maintaining the pH at 9 approximately. The crude product was extracted with diethyl

ether (3 x 300 cm^3) and the organic layer washed with brine (3 x 500 cm^3), dried over $MgSO_4$ and filtered and the solvent was removed *in vacuo* to afford 2,2'-diamine-4,4'-dibromo-1,1'-biphenyl **(15)** as brown crystals (8.05 g, 23.53 mmol, yield 78%).

^{1}H NMR (400 MHz, $CDCl_3$): δ (ppm) 6.95 (*s*, 6H), 3.75 (*bs,* 4H). ^{13}C NMR (100 MHz, $CDCl_3$): δ (ppm) 145.3, 132.3, 122.7, 122.1, 121.7 and 118.2. EI-MS (*m/z*): $[M]^+$ calculated for $C_{12}H_{10}Br_2N_2$, 339; found 339, 341 and 343. Elemental analysis calculated for $C_{12}H_{10}Br_2N_2$; C, 42.14; H, 2.95; Br, 46.72; N, 8.19%; found: C, 43.12; H, 2.66; Br, 45.83; N, 7.96%. m. p.= 109 °C.

7.6.7 2,7-Dibromo-9H-carbazole (16).[20]

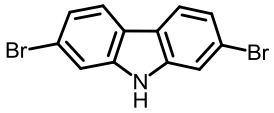

A reaction vessel under a protective atmosphere of argon was charged with 2,2'-diamine-4,4'-dibromo-1,1'-biphenyl **(15)** (4.0g, 12.30mmol) and concentrated phosphoric acid (100 cm^3). The reaction mixture was stirred at 185 °C for 24 hours. Upon completion, the reaction mixture was then poured onto distilled water (300 cm^3) and then filtered, washed with distilled water (250 cm^3). The crude product was purified by recrystallizing from toluene/hexane (10:1, v/v) to give 2,7-dibromo-*9H*-carbazole **(16)** as an off-white powder (3.10 g, 9.53 mmol, yield 77%).

^{1}H NMR (400 MHz, CDCl3): δ (ppm) 8.10 (*s*, 1H), 7.89 (*d*, *J* = 8.5 Hz, 2H), 7.58 (*d*, *J* = 2.0 Hz, 2H), 7.38 (*dd*, J_1 = 8.5 Hz, J_2 = 2.0 Hz, 2H). ^{13}C NMR (100 MHz, $CDCl_3$): δ (ppm) 205.3, 141.0, 122.4, 121.7, 121.6, 119.3, 114.0 and 113.9. EI-MS (*m/z*): $[M]^+$ calculated for $C_{12}H_7Br_2N$, 322; found 322, 324 and 326. Elemental analysis calculated for $C_{12}H_7Br_2N$; C, 44.35; H, 2.17; Br, 49.17, N, 4.31 %; found: C, 44.41; H, 2.05; Br, 48.75; N, 4.18 %. m. p.= 223 °C.

7.6.8 2,7-Dibromo-9-(heptadecan-9-yl)-9H-carbazole (M5).[21]

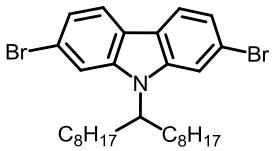

To a reaction vessel under a protective atmosphere of argon was added 2,7-dibromo-*9H*-carbazole **(16)** (2.50 g, 7.70 mmol), KOH powder (2.15 g, 38.45 mmol), pentacosan-13-yl-4-methylbenzene (6.0 g, 11.0 mmol) and dry THF (10 cm^3). The reaction mixture was stirred at 40 °C for 18 hours. Upon completion, the reaction

mixture was poured into distilled water (200 cm^3) and the product was extracted with diethyl ether (3 x 200 cm^3). The organic phase was collected, dried over $MgSO_4$ and the solvent was removed *in vacuo,* The crude product was purified using silica gel column chromatography eluting with PE to afford the pure 2,7-dibromo-9-(heptadecan-9-yl)-9H-carbazole **(M5)** as an ivory solid (2.42 g, 4.29 mmol, yield 55%)

^{1}H NMR (400 MHz, $CDCl_3$): δ (ppm) 7.93 (*dd*, J_1 = 13.0, J_2 = 8.0 Hz, 2H), 7.71 (*bs*, 1H), 7.55 (*bs*, 1H), 7.34 (*t*, *J* = 7.0 Hz, 2H), 4.43-4.37 (*m*, 1H), 2.23-2.19 (*m*, 2H), 1.94-1.90 (*m*, 2H), 1.33-1.05 (*m*, 24H), 0.99-0.95 (*m*, 2H), 0.86-0.80 (*t*, *J* = 7.0 Hz, 6H). ^{13}C NMR (100 MHz, $CDCl_3$): δ (ppm) 122.3, 121.4, 121.2, 114.5, 112.1, 56.9, 33.5, 31.9, 29.6, 29.5, 29.5, 29.3, 29.3, 26.7, 22.7 and 14.1. EI-MS (*m/z*): $[M]^+$ calculated for $C_{29}H_{41}Br_2N$, 561; found 561, 563 and 565. Elemental analysis calculated for $C_{29}H_{41}Br_2N$; C, 61.82; H, 7.33; Br, 28.36, N, 2.49 %; found: C, 62.02; H, 7.20; Br, 28.19; N, 2.31%. m. p.= 79 °C.

7.6.9 9-(Heptadecan-9-yl)-2,7-bis(thiophen-2-yl)-9H-carbazole (17).[18]

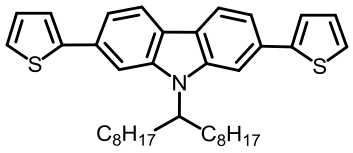

A reaction vessel under a protective atmosphere of argon was charged with 2,7-dibromo-9-(heptadecan-9-yl)-9H-carbazole **(M5)** (0.40 g, 0.71 mmol), 2-(tributylstannyl)thiophene (0.53 g, 1.42 mmol), $PdCl_2(PPh_3)_2$ (18 mg, 5 mol%) and dry chlorobenzene (10 cm^3). The reaction mixture was stirred at 125 °C for 24 hours. Upon completion, the reaction mixture was washed with brine (200 cm^3) and extracted with $CHCl_3$ (3 x 200 cm^3). The combined organic phases were collected, dried over $MgSO_4$, filtered and the solvent was removed *in vacuo* the crude product was purified using silica gel plug eluting with $CHCl_3$ to afford 9-(heptadecan-9-yl)-2,7-di(thiophen-2-yl)-9H-carbazole **(17)** as pale yellow solid (0.48 g, 0.66 mmol, yield 93%).

^{1}H NMR (400 MHz, $CDCl_3$): δ (ppm) 8.06 (*t*, *J* = 8.0 Hz, 2H), 7.79 (*bs*, 1H), 7.60 (*bs*, 1H), 7.51 (*d*, *J* = 8.0 Hz, 2H), 7.41 (*bs*, 2H), 7.32 (*d*, *J* = 5.5 Hz, 2H), 7.15 (*t*, *J* = 5.5 Hz, 2H), 4.65-4.58 (*m*, 1H), 2.41-2.38 (*m*, 2H), 2.03-1.98 (*m*, 2H), 1.32-1.05 (*m*, 24H), 0.82 (*t*, *J* = 7.0 Hz, 6H). ^{13}C NMR (100 MHz, $CDCl_3$): δ (ppm) 145.8, 137.6, 128.0, 124.5, 123.0, 120.6, 117.7, 109.0, 106.3, 56.4, 33.7, 31.7, 29.4, 29.3, 29.1, 26.7, 22.5 and 14.0. EI-MS (*m/z*): $[M]^+$ calculated for $C_{37}H_{47}NS_2$, 569; found 569. Elemental analysis calculated for $C_{37}H_{47}NS_2$; C, 77.98; H, 8.31; N, 2.46; S, 11.25 %; found: C, 78.65; H, 8.05; N, 2.12; S, 10.23 %.

7.6.10 2,7-Bis(5-bromothiophen-2-yl)-9-(heptadecan-9-yl)-9H-carbazole (M6).[19]

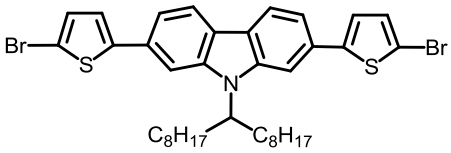

9-(Heptadecan-9-yl)-2,7-di(thiophen-2-yl)-9H-carbazole **(17)** (0.28 g, 0.49 mmol) and N-bromosuccinimide (0.17 g, 0.95 mmol, 1.95 equivalent) were added to a reaction vessel and dissolved in a mixture of dry $CHCl_3$:acetic acid (1:1, v/v, 5 cm^3 each). The resulting mixture was stirred at 60 °C for 4 hours. Upon completion, the reaction mixture was poured into saturated aqueous solution of Na_2CO_3 (25 cm^3), extracted with $CHCl_3$ (3 x 30 cm^3). The combined organic phases were washed with distilled water (30 cm^3), dried over $MgSO_4$ and filtered and the solvent was reduced *in vacuo* The crude product was purified by precipitating in MeOH to afford 2,7-bis(5-bromothiophen-2-yl)-9-(heptadecan-9-yl)-9H-carbazole **(M6)** as a light green oil (0.31 g, 0.42 mmol, yield 87%).

^{1}H NMR (400 MHz, $CDCl_3$): δ (ppm) 8.08 (*dd*, J_1 = 12.0 Hz, J_2 = 8.0 Hz, 2H), 7.67 (*bs*, 1H), 7.49 (*bs*, 1H), 7.43-7.38 (*m*, 2H), 7.14 (*bs*, 2H), 7.09 (*d*, *J* = 4.0 Hz, 2H), 4.61-4.57 (*m*, 1H), 2.35-2.31 (*m*, 2H), 2.0-1.95 (*m*, 2H), 1.31-1.04 (*m*, 24H), 0.83 (*t*, *J* = 7.0 Hz, 6H). ^{13}C NMR (100 MHz, $CDCl_3$): δ (ppm) 147.1, 130.9, 128.0, 125.8, 123.1, 120.8, 117.3, 111.0, 108.6, 56.5, 33.6, 31.8, 29.3, 26.8, 22.6 and 14.1. EI-MS (*m/z*): $[M]^+$ calculated for $C_{37}H_{45}Br_2NS_2$, 725; found 725, 727 and 729. Elemental analysis calculated for $C_{37}H_{45}Br_2NS_2$; C, 61.07; H, 6.23; Br, 21.96; N, 1.92; S, 8.81%; found: C, 60.94; H, 6.39; Br, 22.01; N, 1.80; S, 7.98%.

7.6.11 2,7-Dibromo-9,9-dioctyl-9H-fluorene (M7).[22]

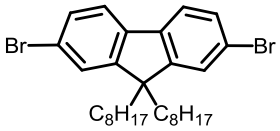

A reaction vessel under a protective atmosphere of argon was charged with 2,7-dibromo-9*H*-fluorene **(SM9)** (0.5 g, 1.54 mmol), KOH (0.34 g, 6.172 mmol) and KI (12.8 mg, 0.077 mmol). The mixture was dissolved in (5 cm^3) of dry DMSO and stirred for 15 minutes. 1-bromooctane (1.6 g, 3.08 mmol) was added slowly for 45 minutes. The reaction mixture was stirred at room temperature for 20 hours. Upon completion, the reaction mixture was poured into (250 cm^3) of distilled water and extracted with $CHCl_3$ (3 x 50 cm^3). The organic phase was dried over $MgSO_4$, filtered and the solvent was

removed *in vacuo* The crude product was purified using silica gel column chromatography eluting with DCM to afford 2,7-dibromo-9,9-dioctyl-9*H*-fluorene **(M7)** as yellow powder (0.71 g, 1.29 mmol, yield 84%).

^{1}H NMR (400 MHz, $CDCl_3$): δ (ppm) 7.54 (*d*, *J* = 2.0 Hz, 2H), 7.47 (*d*, *J* = 2.0 Hz, 2H), 7.45 (*s*, 2H) 1.94-1.90 (*m*, 2H), 1.25-1.02 (*m*, 20H), 0.85 (*t*, *J* = 7.0 Hz, 6H), 0.61-0.56 (*m*, 4H). ^{13}C NMR (100 MHz, $CDCl_3$): δ (ppm) 152.5, 139.0, 130.1, 126.1, 121.4, 121.1, 55.6, 40.1, 31.7, 29.8, 29.1, 29.1, 23.6, 22.6 and 14.1. EI-MS (*m/z*): $[M]^+$ calculated for $C_{29}H_{40}Br_2$, 546; found 546, 548 and 550. Elemental analysis calculated for $C_{29}H_{40}Br_2$; C, 63.51; H, 7.35; Br, 29.14%; found: C, 64.78; H, 7.40; Br, 28.15%. m. p.= 68 °C.

7.6.12 2,2'-Bithiophene-9,9-dioctyl-9H-fluorene-2,7-diyl (18).[18]

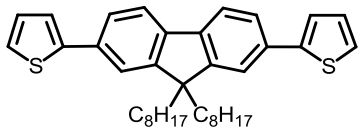

To a reaction vessel under a protective atmosphere of argon was added 2,7-dibromo-9,9-dioctyl-9*H*-fluorene **(M7)** (1.0 g, 1.823 mmol), 2-(tributylstannyl)thiophene (1.36 g, 3.64 mmol), $Pd(OAc)_2$ (20 mg, 5 mol%), tri(o-tolyl)phosphine (54 mg, 10 mol%) and chlorobenzene (10 cm^3). the reaction mixture was stirred at 125 C for 18 hours. Upon completion, the reaction mixture was poured onto brine solution (200 cm^3) and extracted with diethyl ether (3 x 200 cm^3). The organic phases were collected, dried over $MgSO_4$ and the solvent was removed *in vacuo* The crude product was purified using silica gel column chromatography eluting with PE:DCM (10/1, v/v) to obtain 2,2'-bithiophene-9,9-dioctyl-9*H*-fluorene-2,7-diyl **(18)** as a light green oil (0.98 g, 1.76 mmol, yield 97%).

^{1}H NMR (400 MHz, $CDCl_3$): δ (ppm) 7.71 (*s*, 1H), 7.68 (s, 1H), 7.63 (*d*, J_1 = 8.0 Hz, J_2 = 1.5 Hz, 2H), 7.58 (*d*, *J* = 1.5 Hz, 2H), 7.41 (*dd*, J_1 = 3.5 Hz, J_2 = 1. 5 Hz, 2H), 7.32 (*dd*, J_1 = 5.0 Hz, J_2 = 1. 5 Hz, 2H), 7.14 (*dd*, J_1 = 5.0 Hz, J_2 = 3.5 Hz, 2H), 2.04-1.99 (*m*, 4H); 1.37–0.95 (*m*, 24H); 0.81 (*t*, *J* = 7.0 Hz, 6H). ^{13}C NMR (100 MHz, $CDCl_3$): δ (ppm) 151.7, 145.1, 140.1, 133.2, 128.0, 124.9, 124.5, 122.8, 120.1, 120.0, 55.2, 40.4, 31.7, 29.9, 29.2, 29.1, 23.7, 22.5 and 14.0. EI-MS (*m/z*): $[M]^+$ calculated for $C_{37}H_{46}S_2$, 554; found 554. Elemental analysis calculated for $C_{37}H_{46}S_2$; C, 80.09; H, 8.36; S, 11.55%; found: C, 79.88; H, 8.24; S, 11.33%.

7.6.13 5,5'-Bis(2-bromothiophene)-9,9-dioctyl-9H-fluorene-2,7-diyl (M8)[19]

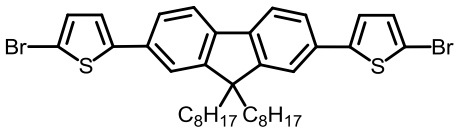

2,2'-Bithiophene-9,9-dioctyl-9*H*-fluorene-2,7-diyl **(18)** (0.14 g, 0.245 mmol), N-bromosuccinimide (0.093 g, 0.52 mmol) were added to a reaction vessel and dissolved in a mixture of dry $CHCl_3$:acetic acid (1:1, v/v, 5 cm^3 each). The resulting mixture was stirred at 65 °C for 4 hours. Upon completion, the reaction mixture was poured into saturated aqueous solution of Na_2CO_3 (25 cm^3), extracted with $CHCl_3$ (3 x 30 cm^3). The combined organic phases were washed with distilled water (30 cm^3), dried over $MgSO_4$ and filtered and the solvent was reduced *in vacuo* The crude product was purified by precipitating in MeOH to afford 5,5'-bis(2-bromothiophene)-9,9-dioctyl-9*H*-fluorene-2,7-diyl **(M8)** as a dark green oil (0.16 g, 0.23 mmol, yield 85%).

^{1}H NMR (400 MHz, $CDCl_3$) δ (ppm) 7.69 (*s*, 1H), 7.67 (s, 1H) 7.52 (*dd*, J_1 = 8.0 Hz, J_2 = 1.5 Hz, 2H); 7.46 (*d*, *J* = 1.5 Hz, 2H), 7.13 (*d*, *J* = 4.0 Hz, 2H), 7.07 (*d*, *J* = 4.0 Hz, 2H), 1.99-1.95 (*m*, 4H); 1.37–0.98 (*m*, 24H); 0.79 (*t*, *J* = 7.1 Hz, 6H). ^{13}C NMR (100 MHz, $CDCl_3$): δ (ppm) 151.8, 146.5, 140.4, 132.6, 130.8, 124.6, 123.0, 120.2, 119.8, 111.1, 55.3, 40.3, 31.7, 29.9, 29.1, 29.1, 23.7, 22.6 and 14.0. EI-MS (*m/z*): $[M]^+$ calculated for $C_{37}H_{44}Br_2S_2$, 710; found 710, 712 and 714. Elemental analysis calculated for $C_{37}H_{44}Br_2S_2$; C, 62.36; H, 6.22; Br, 22.42; S, 9.00% found C, 62.57; H, 6.23; Br, 22.98; S, 8.95%.

7.6.14 5,5'-Dibromo-2,2'-bithiophene (M9).[23]

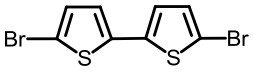

To a reaction vessel under a protective atmosphere of argon was added 2,2'-bithiophene **(SM15)** (1.0 g, 6.0 mmol), N-bromosuccinimide (2.08 g, 11.7 mmol, 1.95 equivalent). The solid starting materials were dissolved in a mixture of dry $CHCl_3$:acetic acid (1:1, v/v, 30 cm^3 each). The reaction mixture was stirred at 70 °C for 4 hours. Upon completion, the reaction mixture was poured onto saturated solution of Na_2CO_3 (75 cm^3) and extracted with $CHCl_3$. The organic phases were collected, dried over $MgSO_4$, filtered and the solvent was removed *in vacuo.* The crude product was purified by silica gel column chromatography eluting with PE:DCM (10:2) to give 5,5'-dibromo-2,2'-bithiophene **(M9)** as a silver powder (1.48 g, 4.56 mmol, yield 76%).

^{1}H NMR (400 MHz, $CDCl_3$) δ (ppm) 6.88 (*d*, *J* = 4.0 Hz, 2H); 6.86 (*d*, *J* = 4.0 Hz, 2H). ^{13}C NMR (100 MHz, $CDCl_3$): δ (ppm) 137.7, 130.6, 124.1 and 111.5. EI-MS (*m/z*): $[M]^+$ calculated for $C_8H_4Br_2S_2$, 321; found 321, 323 and 325. Elemental analysis calculated for $C_8H_4Br_2S_2$; C, 29.65; H, 1.24; Br, 49.32; S, 19.79%, found C, 29.37; H, 1.21; Br, 50.01; S, 18.74%. m. p.= 148 °C.

7.6.15 Poly(2,7-di-yl)-9-(heptadecan-9-yl)-9H-carbazole-alt-5,6-difluoro-4,7-bis(3-(2-octyldodecyl)thiophene-[2,2'-bithiophen]-5-yl)benzo[c][1,2,5] thiadiazole) (P10).[14]

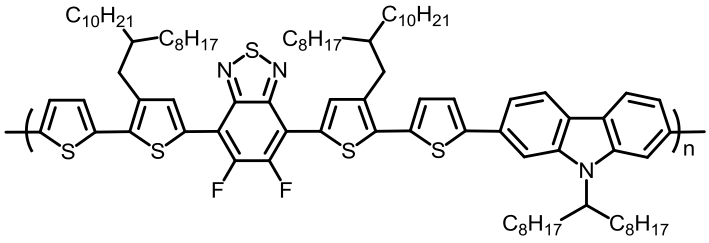

A top sealing tube under a protective atmosphere of argon was charged with 5,6-difluoro-4,7-bis(3-(2-octyldodecyl)-[2,2'-bithiophen]-5-yl)benzo[*c*][1,2,5] thiadiazole **(M4)** (0.089 g, 0.084 mmol), 2,7-dibromo-9-(heptadecan-9-yl)-9H-carbazole **(M5)** (0.047 g, 0.084 mmol), $Pd_2(dba)_3$ (2.6 mg), P(*o*-MeOPh)$_3$ (2.5 mg), cesium carbonate (90 mg) and pivalic acid (8.5 mg). All the chemicals were dissolved in dry THF (1 cm^3) and the reaction mixture was stirred at 120 °C for 18 hours. Upon completion, a dark red precipitate was formed around the bottom of the tube which was collected and dissolved in $CHCl_3$ and stirred with NH_4OH solution (50 cm^3) for 10 hours. The latter was transferred to an extraction funnel and washed with distilled water (3 x 100 cm^3). The organic layer was collected and the solvent was reduced *in vacuo* and the polymer solution was precipitated in MeOH (150 cm^3), filtered and the collected polymer was extracted with Soxhlet using a series of solvents; MeOH, acetone, hexane and toluene respectively. The toluene fraction was then collected and the solvent was reduced *in vacuo* and the polymer solution was precipitated again in MeOH (150 cm^3) to afford the polymer as a dark red powder (0.099 g, 0.068 mmol, yield 81%).

Toluene fraction (81 % yield) GPC in toluene at 100 °C (*Mn* = 20,700), (*Mw* = 51,500) (PDI = 2.46). ^{1}H NMR (400 MHz, $C_2D_2Cl_4$): δ (ppm) 8.29-8.26 (*m*, 2H), 8.18 (*s,* 2H), 8.07 (*d, J* = 8.0 Hz, 2H), 7.74 (*bs*, 2H), 7.54 (*d, J* = 8.0 Hz, 2H), 7.41 (*d, J* = 3.5 Hz, 2H), 7.30 (*d, J* = 3.5 Hz, 2H), 4.65-4.62 (m, 1H), 2.93-2.90 (*m*, 4H), 2.40-2.37 (m, 2H), 2.11-2.06 (m, 2H), 1.91-1.87 (*m*, 2H), 1.60-1.09 (*m*, 80H), 0.89-0.85 (*m*, 18H). Elemental analysis calculated for $C_{91}H_{129}F_2N_3S_5$; C, 74.69; H, 8.89; N, 2.87; S, 10.96% found C, 75.16; H, 9.15; N, 2.53; S, 9.62%.

7.6.16 Poly(2,7-bis(thiophen-2-yl)-9-(heptadecan-9-yl)-9H-carbazole-alt-5,6-difluoro-4,7-bis(3-(2-octyldodecyl)thiophene-[2,2'-bithiophen]-5-yl)benzo[c] [1,2,5] thiadiazole) (P11).[14]

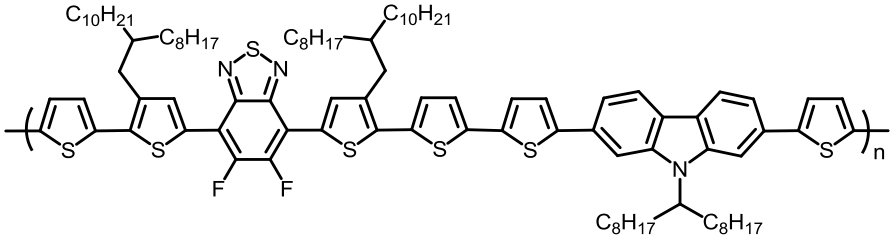

A top sealing tube under a protective atmosphere of argon was charged with 5,6-difluoro-4,7-bis(3-(2-octyldodecyl)-[2,2'-bithiophen]-5-yl)benzo[*c*][1,2,5] thiadiazole **(M4)** (0.1 g, 0.094 mmol), 2,7-bis(5-bromothiophen-2-yl)-9-(heptadecan-9-yl)-9H-carbazole **(M6)** (0.068g, 0.094mmol), $Pd_2(dba)_3$ (6.8 mg, 0.025 mmol), P(*o*-MeOPh)$_3$ (7.9mg, 0.01mmol), cesium carbonate (0.1g, 0.307mmol) and pivalic acid (9.6mg, 0.094mmol). All the chemicals were dissolved in dry THF (1 cm^3) and the reaction mixture was stirred at 120 °C for 72 hours. Upon completion, a black precipitate was formed around the bottom of the tube which was collected and dissolved in $CHCl_3$ and stirred with NH_4OH solution (50 cm^3) for 10 hours. The latter was transferred to an extraction funnel and washed with distilled water (3 x 100 cm^3). The organic layer was collected and the solvent was reduced *in vacuo* and the polymer solution was precipitated in MeOH (150 cm^3), filtered and the collected polymer was extracted with Soxhlet using a series of solvents; MeOH, acetone, hexane and toluene respectively. The toluene fraction was then collected and the solvent was reduced *in vacuo* and the polymer solution was precipitated again in MeOH (150 cm^3) to afford the polymer as a black powder (0.107 g, 0.065 mmol, yield 65%).

Toluene fraction (65 % yield) GPC in toluene at 100 °C (*Mn* = 15,800), (*Mw* = 39,300) (PDI = 2.48). ^{1}H NMR (400 MHz, $C_2D_2Cl_4$): δ (ppm) 8.15-7.94 (*m*, 2H), 8.06 (*d*, *J* = 8.0, 2H), 7.70 (*bs*, 2H), 7.50-7.42 (*m,* 2H), 7.37-7.34 (*m,* 2H), 7.26-7.23 (*m,* 4H), 7.11-7.08 (*m,* 2H), 4.65-4.61 (m, 1H), 2.88-2.80 (*m*, 4H), 2.38-2.32 (m, 2H), 2.08-2.03 (m, 2H), 1.89-1.85 (*m*, 2H), 1.61-1.06 (*m*, 80H), 0.90-0.86 (*m*, 18H). Elemental analysis calculated for $C_{99}H_{133}F_2N_3S_7$; C, 73.06; H, 8.24; N, 2.58; S, 13.79% found C, 78.14; H, 10.38; N, 1.46; S, 7.98%.

7.6.17 Poly(2,7-di-yl)-3,6-difluoro-9-(heptadecan-9-yl)-9H-carbazole-alt-5,6-difluoro-4,7-bis(3-(2-octyldodecyl)-[2,2'-bithiophen]-5-yl)benzo[c][1,2,5] thiadiazole) (P12).[14]

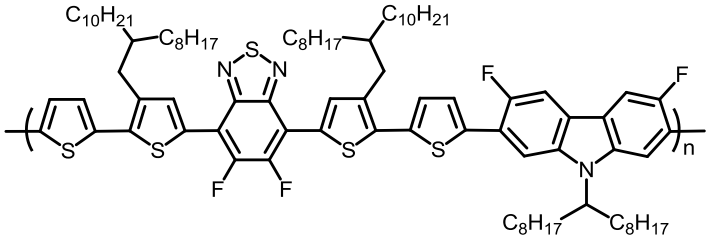

A top sealing tube under a protective atmosphere of argon was charged with 5,6-difluoro-4,7-bis(3-(2-octyldodecyl)-[2,2'-bithiophen]-5-yl)benzo[*c*][1,2,5] thiadiazole **(M4)** (0.1 g, 0.094 mmol), 2,7-dibromo-3,6-difluoro-9,9-dioctyl-9*H*-fluorene **(SM14)** (0.056g, 0.094mmol), $Pd_2(dba)_3$ (6.8 mg, 0.025 mmol), P(*o*-MeOPh)$_3$ (7.9 mg, 0.01 mmol), cesium carbonate (0.1 g, 0.307 mmol) and pivalic acid (9.6 mg, 0.094 mmol). All the chemicals were dissolved in dry THF (2 cm^3) and the reaction mixture was stirred at 120 °C for 72 hours. Upon completion, a black precipitate was formed around the bottom of the tube which was collected and dissolved in $CHCl_3$ and stirred with NH_4OH solution (50 cm^3) for 10 hours. The latter was transferred to an extraction funnel and washed with distilled water (3 x 100 cm^3). The organic layer was collected and the solvent was reduced *in vacuo* and the polymer solution was precipitated in MeOH (150 cm^3), filtered and the collected polymer was extracted with Soxhlet using a series of solvents; MeOH, acetone, hexane and toluene respectively. The toluene fraction was then collected and the solvent was reduced *in vacuo* and the polymer solution was precipitated again in MeOH (150 cm^3) to afford the polymer as a black powder (0.083 g, 0.088 mmol, yield 93%).

Hexane fraction (58 % yield) GPC in THF at 40 °C (*Mn* = 16,900), (*Mw* = 66,500) (PDI = 3.93). ^{1}H NMR (400 MHz, $C_2D_2Cl_4$): δ (ppm) 8.18 (*bs*, 2H), 7.77-7.74 (*m*, 2H), 7.70 (*bs*, 2H), 7.56 (*bs,* 2H), 7.51-7.48 (*m*, 2H), 7.33 (*d*, *J* = 3.0 Hz, 2H), 4.57 (*bs*, 1H), 2.92-2.88 (*m*, 4H), 2.34-2.30 (m, 2H), 2.03-2.0 (m, 2H), 1.88-1.85 (*m*, 2H), 1.43-1.13 (*m*, 80H), 0.88-0.82 (*m*, 18H). Elemental analysis calculated for $C_{91}H_{127}F_4N_3S_5$; C, 72.90; H, 8.54; N, 2.80; S, 10.69% found C, 72.90; H, 8.44; N, 2.63; S, 10.37%.

7.6.18 Poly(2,7-di-yl)-9,9-dioctyl-9H-fluorene-alt-5,6-difluoro-4,7-bis(3-(2-octyldodecyl) thiophene-[2,2'-bithiophen]-5-yl)benzo[c][1,2,5] thiadiazole) (P13).[14]

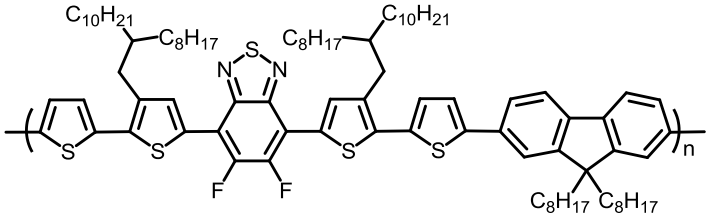

A top sealing tube under a protective atmosphere of argon was charged with 5,6-difluoro-4,7-bis(3-(2-octyldodecyl)-[2,2'-bithiophen]-5-yl)benzo[c][1,2,5] thiadiazole **(M4)** (0.1 g, 0.094 mmol), 2,7-dibromo-9,9-dioctyl-9*H*-fluorene **(M7)** (0.051 g, 0.094 mmol), $Pd_2(dba)_3$ (6.8 mg, 0.025 mmol), P(*o*-MeOPh)$_3$ (7.9 mg, 0.01 mmol), cesium carbonate (0.1 g, 0.307 mmol) and pivalic acid (9.6 mg, 0.094 mmol). All the chemicals were dissolved in dry THF (2 cm^3) and the reaction mixture was stirred at 120 °C for 10 hours. Upon completion, a black precipitate was formed around the bottom of the tube which was collected and dissolved in $CHCl_3$ and stirred with NH_4OH solution (50 cm^3) for 10 hours. The latter was transferred to an extraction funnel and washed with distilled water (3 x 100 cm^3). The organic layer was collected and the solvent was reduced *in vacuo* and the polymer solution was precipitated in MeOH (150 cm^3), filtered and the collected polymer was extracted with Soxhlet using a series of solvents; MeOH, acetone, hexane and toluene respectively. The toluene fraction was then collected and the solvent was reduced *in vacuo* and the polymer solution was precipitated again in MeOH (150 cm^3) to afford the polymer as a black powder (0.075 g, 0.051 mmol, yield 55%).

Hexane fraction (55 % yield) GPC in toluene at 100 °C (*Mn* = 13,200), (*Mw* = 36,000) (PDI = 2.72). ^{1}H NMR (400 MHz, $C_2D_2Cl_4$): δ (ppm) 8.17 (*bs*, 2H), 7.72 (*d*, *J* = 8.5 Hz, 2H), 7.64 (*d*, *J* = 8.5 Hz, 4H), 7.38 (*d*, *J* = 3.50 Hz, 2H), 7.28 (*d*, *J* = 3.50 Hz, 2H), 2.91 (*d*, *J* = 6.5 Hz, 4H), 2.11-2.07 (m, 4H), 1.90-1.87 (*m*, 2H), 1.41-1.10 (*m*, 80H), 0.89-0.86 (*m*, 18H). Elemental analysis calculated for $C_{91}H_{128}F_2N_2S_5$; C, 75.46; H, 8.91; N, 1.93; S, 11.07% found C, 75.97; H, 8.81; N, 1.76; S, 10.17%.

7.6.19 Poly(2,7-bis(thiophen-2-yl)-)-9,9-dioctyl-9H-fluorene-alt-5,6-difluoro-4,7-bis(3-(2-octyldodecyl)-[2,2'-bithiophen]-5-yl)benzo[c][1,2,5] thiadiazole) (P14).[14]

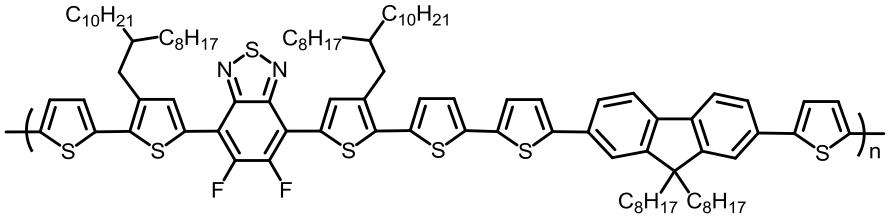

A top sealing tube under a protective atmosphere of argon was charged with 5,6-difluoro-4,7-bis(3-(2-octyldodecyl)-[2,2'-bithiophen]-5-yl)benzo[c][1,2,5] thiadiazole **(M4)** (0.1 g, 0.094 mmol), 5,5'-bis(2-bromothiophene)-9,9-dioctyl-9*H*-fluorene-2,7-diyl **(M8)** (0.067 g, 0.094 mmol), $Pd_2(dba)_3$ (6.8 mg, 0.025 mmol), P(*o*-MeOPh)$_3$ (7.9 mg, 0.01 mmol), cesium carbonate (0.1 g, 0.307 mmol) and pivalic acid (9.6 mg, 0.094 mmol). All the chemicals were dissolved in dry THF (2 cm^3) and the reaction mixture was stirred at 120 °C for 10 hours. Upon completion, a black precipitate was formed around the bottom of the tube which was collected and dissolved in $CHCl_3$ and stirred with NH_4OH solution (50 cm^3) for 16 hours. The latter was transferred to an extraction funnel and washed with distilled water (3 x 100 cm^3). The organic layer was collected and the solvent was reduced *in vacuo* and the polymer solution was precipitated in MeOH (150 cm^3), filtered and the collected polymer was extracted with Soxhlet using a series of solvents; MeOH, acetone, hexane and toluene respectively. The toluene fraction was then collected and the solvent was reduced *in vacuo* and the polymer solution was precipitated again in MeOH (150 cm^3) to afford the polymer as a black powder (0.076 g, 0.051 mmol, yield 50%).

Toluene fraction (50 % yield) GPC in $CHCl_3$ at 40 °C (*Mn* = 7,900), (*Mw* = 17,400) (PDI = 2.20). ^{1}H NMR (400 MHz, $C_2D_2Cl_4$): δ (ppm) 8.14-8.11 (*m*, 2H), 7.70-7.67 (*m*, 2H), 7.61-7.57 (*m*, 4H), 7.37-7.34 (*m*, 4H), 7.20-7.17 (*m*, 4H), 2.86-2.83 (*m*, 4H), 2.11-2.08 (m, 4H), 1.85-1.82 (*m*, 2H), 1.48-1.09 (*m*, 80H), 0.86-0.79 (*m*, 18H). Elemental analysis calculated for $C_{99}H_{132}F_2N_2S_7$; C, 73.74; H, 8.25; N, 1.74; S, 13.92% found C, 73.92; H, 8.14; N, 1.48; S, 13.28%.

7.6.20 Poly(2,2'-bithiophene-alt-5,6-difluoro-4,7-bis(3-(2-octyldodecyl)-[2,2'-bithiophen]-5-yl)benzo[c][1,2,5] thiadiazole) (P15).[14]

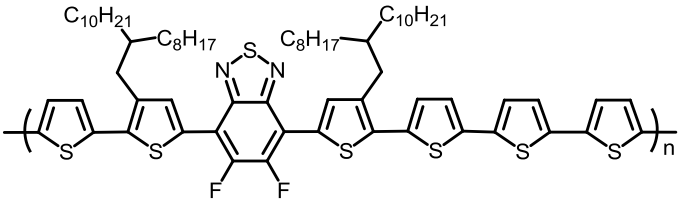

A top sealing tube under a protective atmosphere of argon was charged with 5,6-difluoro-4,7-bis(3-(2-octyldodecyl)-[2,2'-bithiophen]-5-yl)benzo[c][1,2,5] thiadiazole **(M4)** (0.1 g, 0.094 mmol), 5,5'-dibromo-2,2'-bithiophene **(M9)** (0.0304 g, 0.094 mmol), $Pd_2(dba)_3$ (6.8 mg, 0.025 mmol), P(*o*-MeOPh)$_3$ (7.9 mg, 0.01 mmol), cesium carbonate (0.1 g, 0.307 mmol) and pivalic acid (9.6 mg, 0.094 mmol). All the chemicals were dissolved in dry THF (1.5 cm^3) and the reaction mixture was stirred at 120 °C for 10 hours. Upon completion, a dark purple precipitate was formed around the bottom of the tube, which was collected and dissolved in $CHCl_3$ and stirred with NH_4OH solution (50 cm^3) for 16 hours. The latter was transferred to an extraction funnel and washed with distilled water (3 x 100 cm^3). The organic layer was collected and the solvent was reduced *in vacuo* and the polymer solution was precipitated in MeOH (150 cm^3), filtered and the collected polymer was extracted with Soxhlet using a series of solvents; MeOH, acetone, hexane and toluene respectively. The toluene fraction was then collected and the solvent was reduced *in vacuo* and the polymer solution was precipitated again in MeOH (150 cm^3) to afford the polymer as a dark purple powder (0.069 g, 0.056 mmol, yield 60%).

Toluene fraction (60 % yield) GPC in toluene at 100 °C (*Mn* = 13,200), (*Mw* = 19,200) (PDI = 1.45). ^{1}H NMR (400 MHz, $C_2D_2Cl_4$): δ (ppm) 8.12-8.08 (*m*, 2H), 7.37-7.10 (*m*, 8H), 2.84-2.78 (*m*, 4H), 1.83-1.77 (*m*, 2H), 1.37-1.25 (*m*, 64H), 0.88-0.78 (*m*, 12H). Elemental analysis calculated for $C_{70}H_{92}F_2N_2S_7$; C, 68.69; H, 7.58; N, 2.29; S, 18.34% found C, 70.02; H, 8.11; N, 1.93; S, 16.74%.

Chapter 7 References

1. G. Gritzner, *Pure and Applied Chemistry*, 1990, **62**, 1839-1858.
2. A. Liang, H. Wang, Y. Chen, X. Zheng, T. Cao, X. Yang, P. Cai, Z. Wang, X. Zhang and F. Huang, *Dyes and Pigments*, 2018, **149**, 399-406.
3. N. S. Gobalasingham, S. Ekiz, R. M. Pankow, F. Livi, E. Bundgaard and B. C. Thompson, *Polymer Chemistry*, 2017, **8**, 4393-4402.
4. P. Deng, J. Yu, X. Yin, Y. Geng, B. Zhou, F. Zhang and W. Tang, *Dyes and Pigments*, 2017, **138**, 47-55.
5. A. M. Alsalme, A. A. B. Alghamdi, A. Alhamdani and A. Iraqi, *Int. J. Electrochem. Sci*, 2014, **9**, 1920-1941.
6. D. Chen, C. Zhong, Y. Zhao, L. Nan, Y. Liu and J. Qin, *Journal of Materials Chemistry C*, 2017, **5**, 5199-5206.
7. N. Wang, Z. Chen, W. Wei and Z. Jiang, *Journal of the American Chemical Society*, 2013, **135**, 17060-17068.
8. M. Scheuble, Y. Gross, D. Trefz, M. Brinkmann, J. López Navarrete, M. Ruiz Delgado and S. Ludwigs, *Macromolecules*, 2015, **48**, 7049-7059.
9. Y. Takamura, K. Takenaka, T. Toda, H. Takeshita, M. Miya and T. Shiomi, *Macromolecular Chemistry and Physics*, 2018, **219**.
10. L. Du, W. Xiong, S.-C. Cheng, H. Shi, W. K. Chan and D. L. Phillips, *The Journal of Physical Chemistry Letters*, 2017, **8**, 2475-2479.
11. L. Verheyen, B. Timmermans and G. Koeckelberghs, *Polymer Chemistry*, 2017, **8**, 2327-2333.
12. P. Sonar, S. P. Singh, Y. Li, Z.-E. Ooi, T.-j. Ha, I. Wong, M. S. Soh and A. Dodabalapur, *Energy & Environmental Science*, 2011, **4**, 2288-2296.
13. H. Zhao, C. Xu, B. Wang, J. Zhao, C. Cui and X. Zhang, *Int. J. Electrochem. Sci*, 2012, **7**, 10685-10697.
14. P.-O. Morin, T. Bura, B. Sun, S. I. Gorelsky, Y. Li and M. Leclerc, *ACS Macro Letters*, 2014, **4**, 21-24.
15. Đ. Škalamera, J. Veljković, L. Ptiček, M. Sambol, K. Mlinarić-Majerski and N. Basarić, *Tetrahedron*, 2017, **73**, 5892-5899.
16. L. Ji, K. Fucke, S. K. Bose and T. B. Marder, *The Journal of organic chemistry*, 2014, **80**, 661-665.
17. H. Goto and K. Akagi, *Angewandte Chemie International Edition*, 2005, **44**, 4322-4328.
18. E. Bundgaard and F. C. Krebs, *Polymer Bulletin*, 2005, **55**, 157-164.
19. M. Takahashi, K. Masui, H. Sekiguchi, N. Kobayashi, A. Mori, M. Funahashi and N. Tamaoki, *Journal of the American Chemical Society*, 2006, **128**, 10930-10933.
20. V. H. Fell, A. Mikosch, A.-K. Steppert, W. Ogieglo, E. Senol, D. Canneson, M. Bayer, F. Schoenebeck, A. Greilich and A. J. Kuehne, *Macromolecules*, 2017, **50**, 2338-2343.
21. G. Garbay, L. Muccioli, E. Pavlopoulou, A. Hanifa, G. Hadziioannou, C. Brochon and E. Cloutet, *Polymer*, 2017, **119**, 274-284.
22. H. Saito, J. Kuwabara and T. Kanbara, *Journal of Polymer Science Part A: Polymer Chemistry*, 2015, **53**, 2198-2201.
23. P. Arsenyan, E. Paegle and S. Belyakov, *Tetrahedron Letters*, 2010, **51**, 205-208.

Chapter 8

Supplementary Information

8.1 Supplementary Information

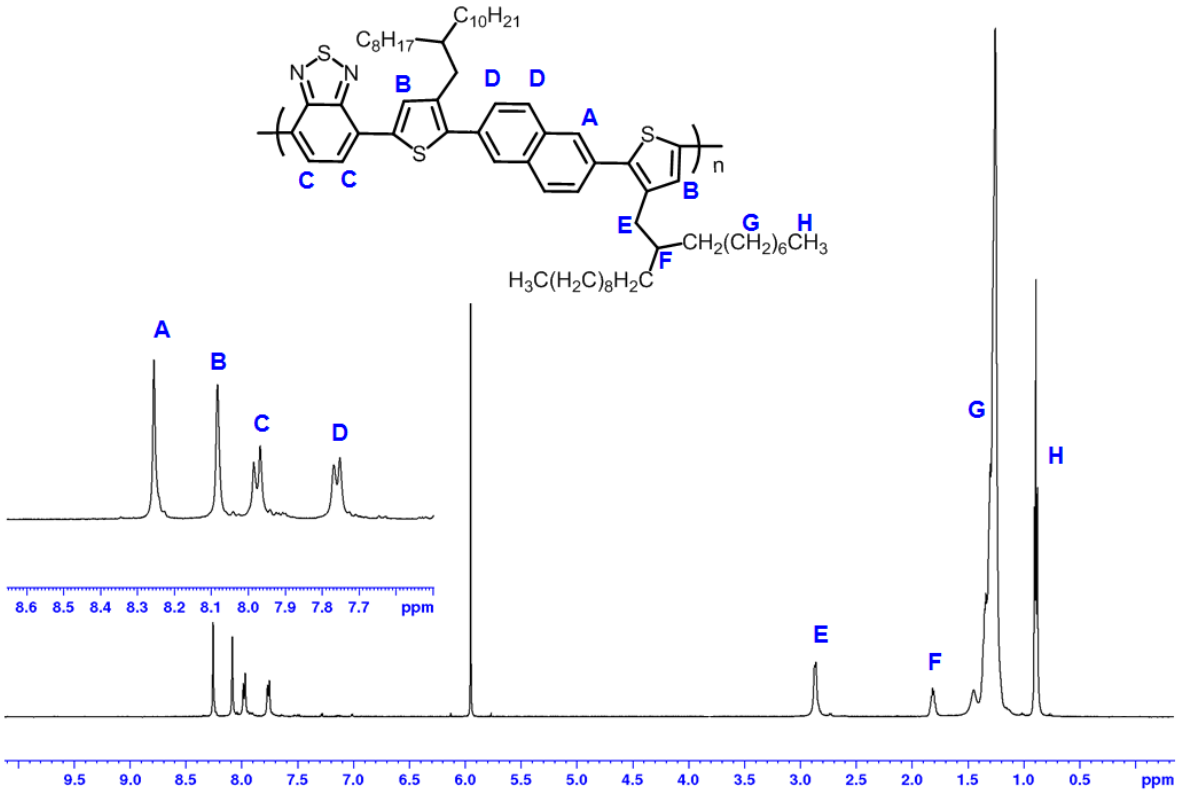

Figure 0-1: ^{1}H NMR spectrum of **P1** in $C_2D_2Cl_4$ at 100 °C.

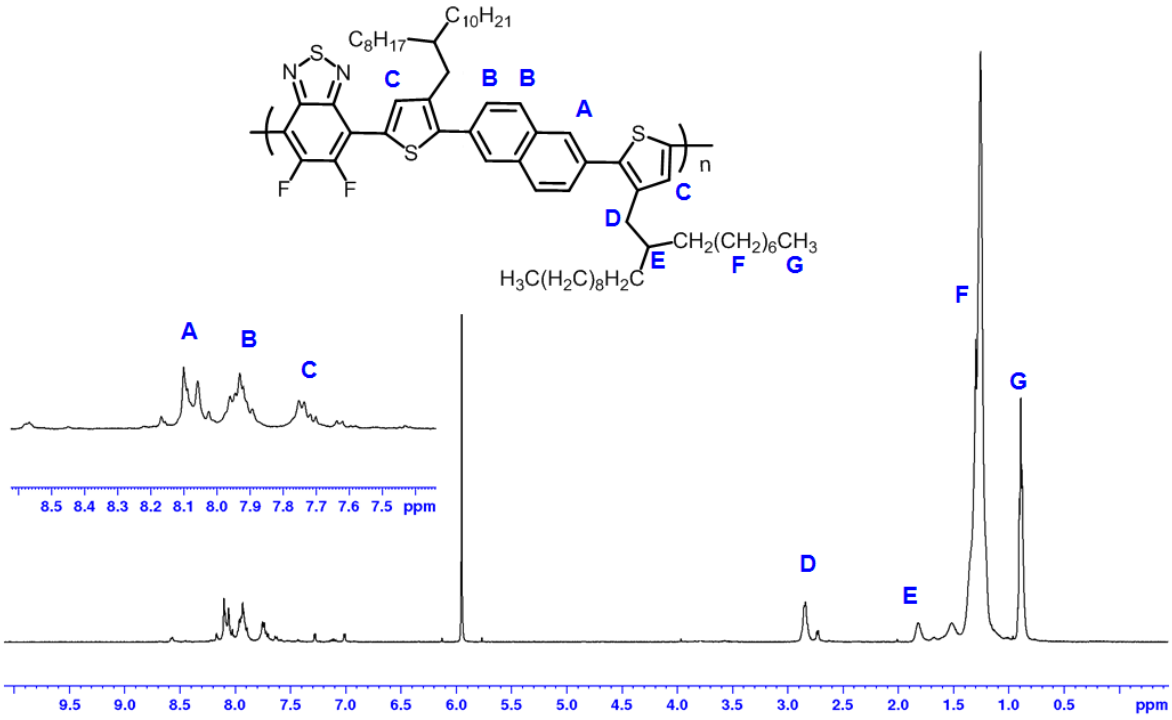

Figure 0-2: ^{1}H NMR spectrum of **P2** in $C_2D_2Cl_4$ at 100 °C.

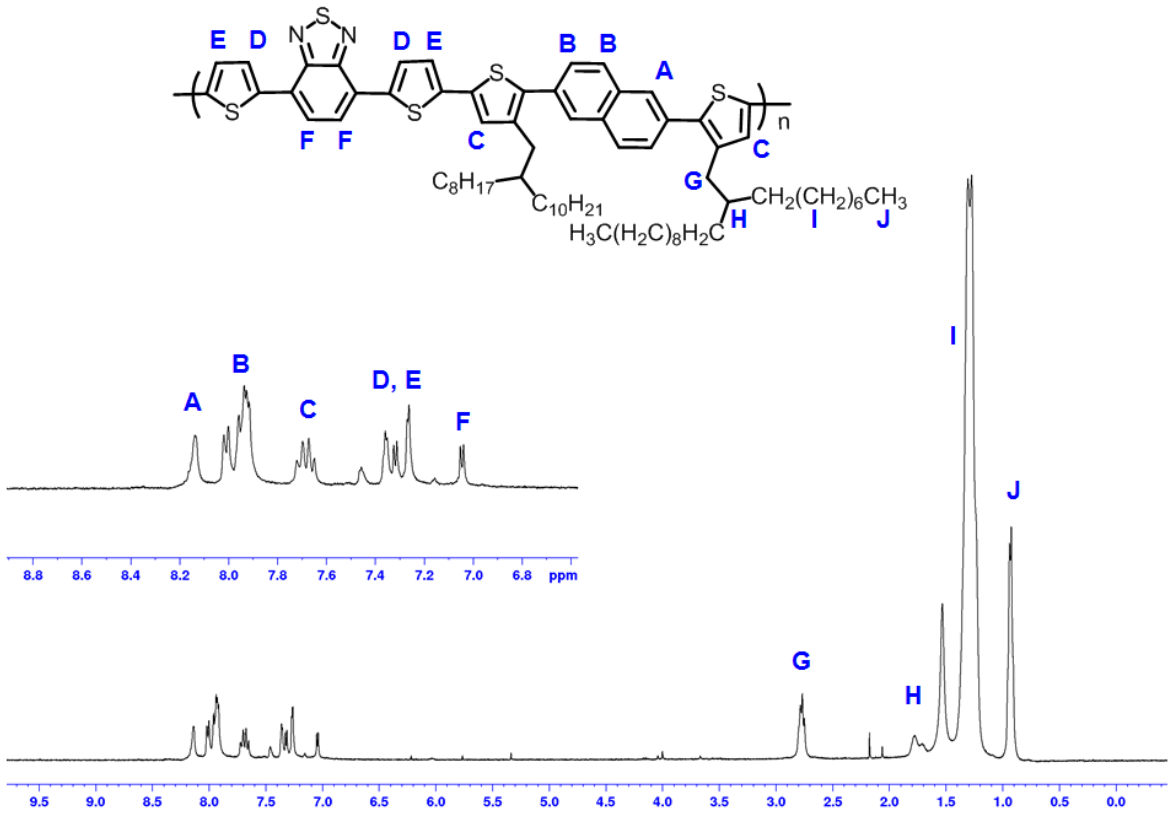

Figure 0-3: ^{1}H NMR spectrum of **P3** in $C_2D_2Cl_4$ at 100 °C.

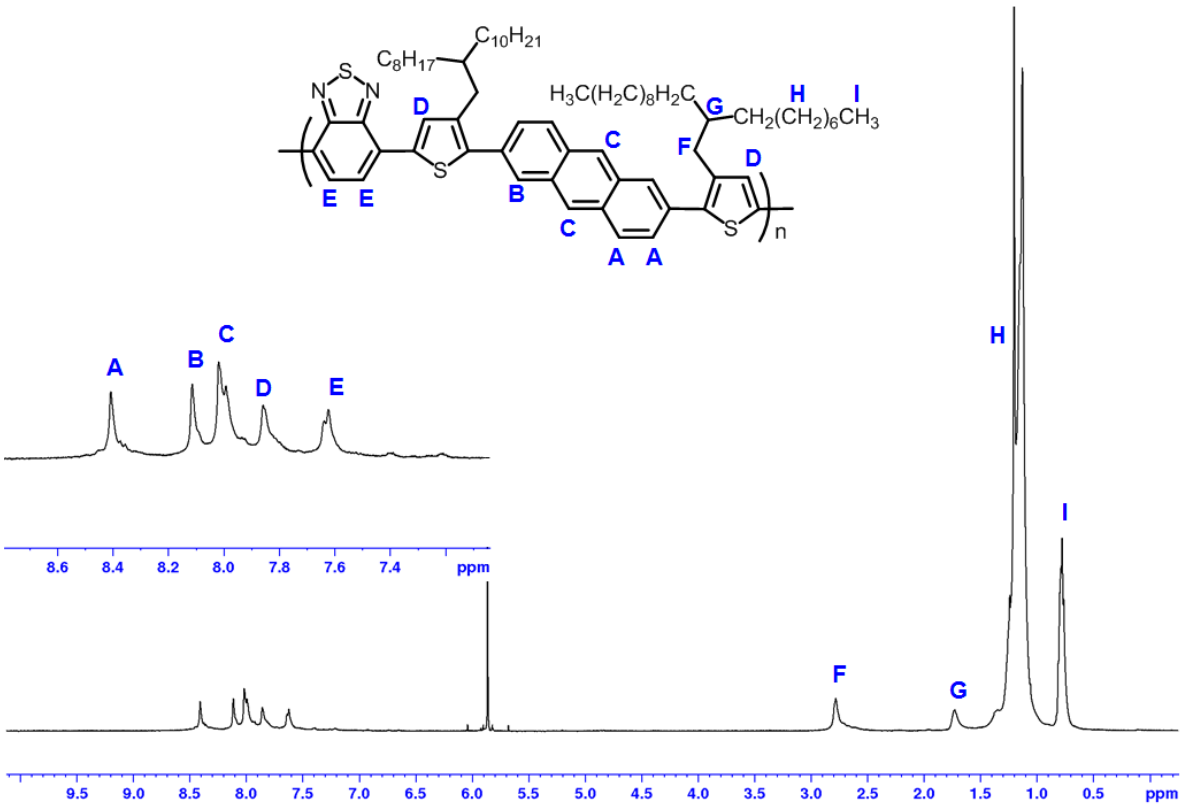

Figure 0-4: ^{1}H NMR spectrum of **P4** in $C_2D_2Cl_4$ at 100 °C.

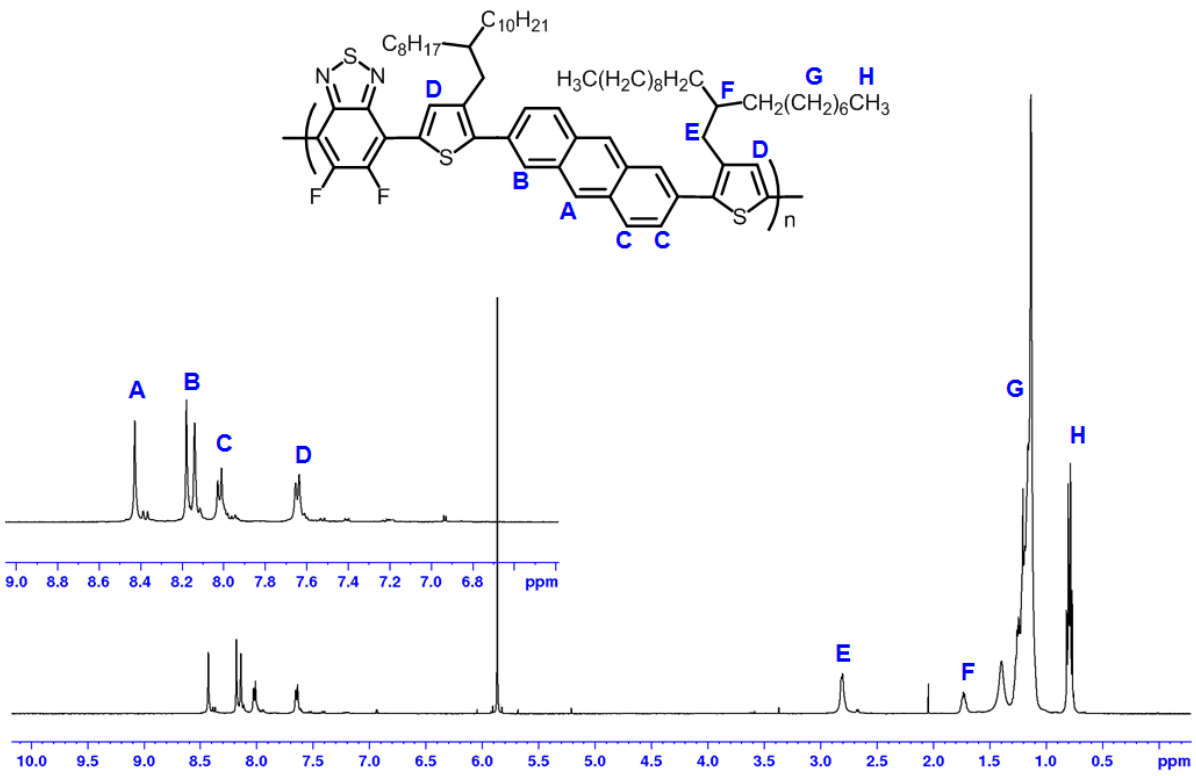

Figure 0-5: ^{1}H NMR spectrum of **P5** in $C_2D_2Cl_4$ at 100 °C.

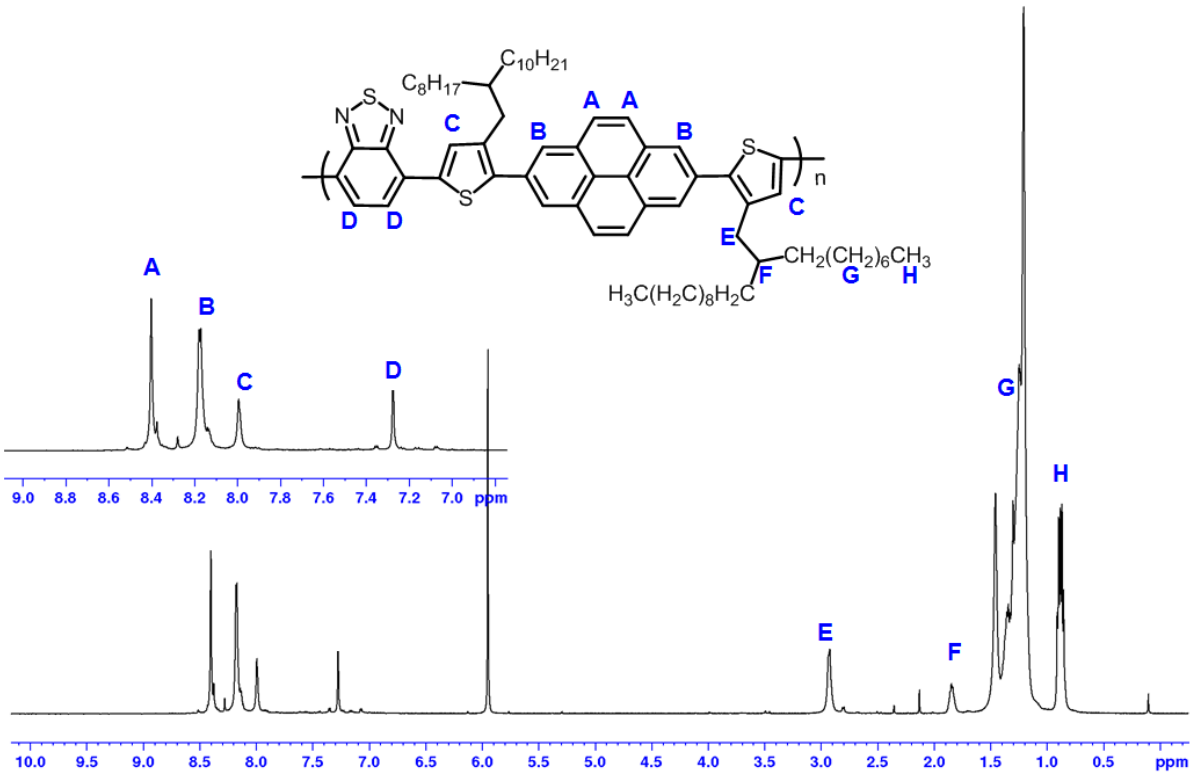

Figure 0-6: ^{1}H NMR spectrum of **P6** in $C_2D_2Cl_4$ at 100 °C.

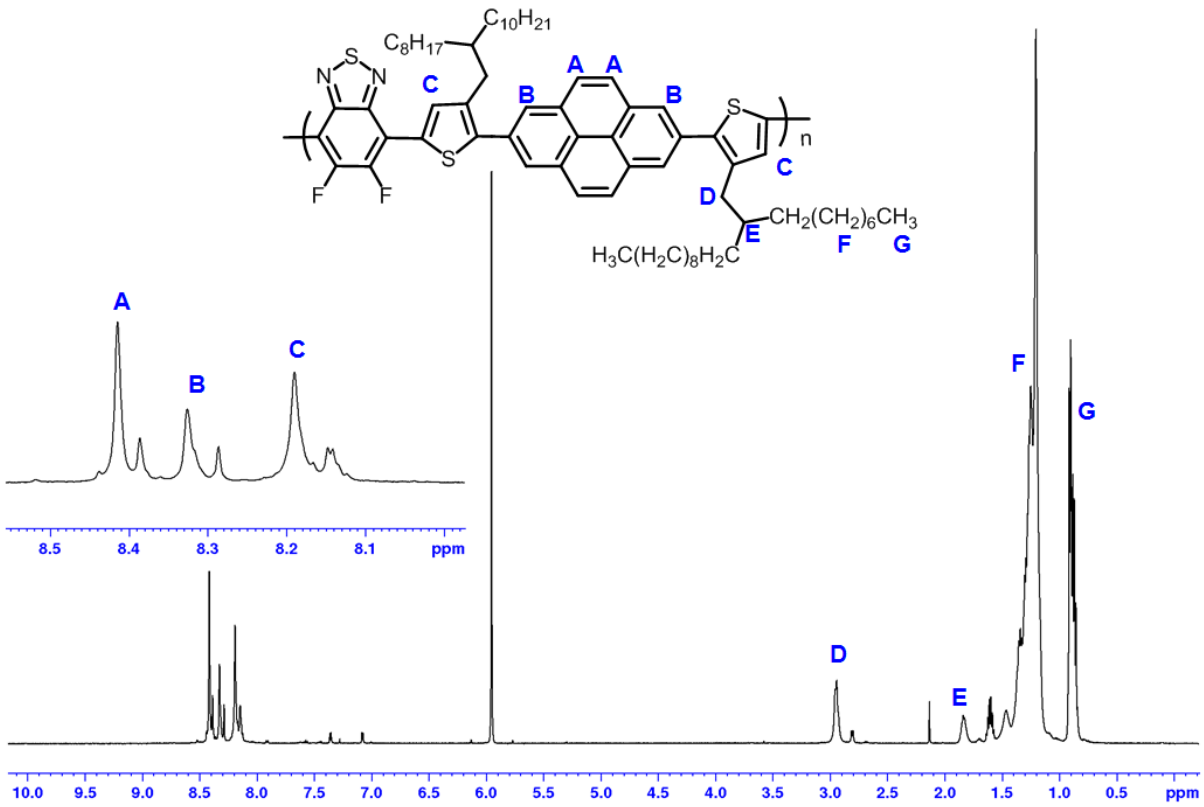

Figure 0-7: ^{1}H NMR spectrum of **P7** in $C_2D_2Cl_4$ at 100 °C.

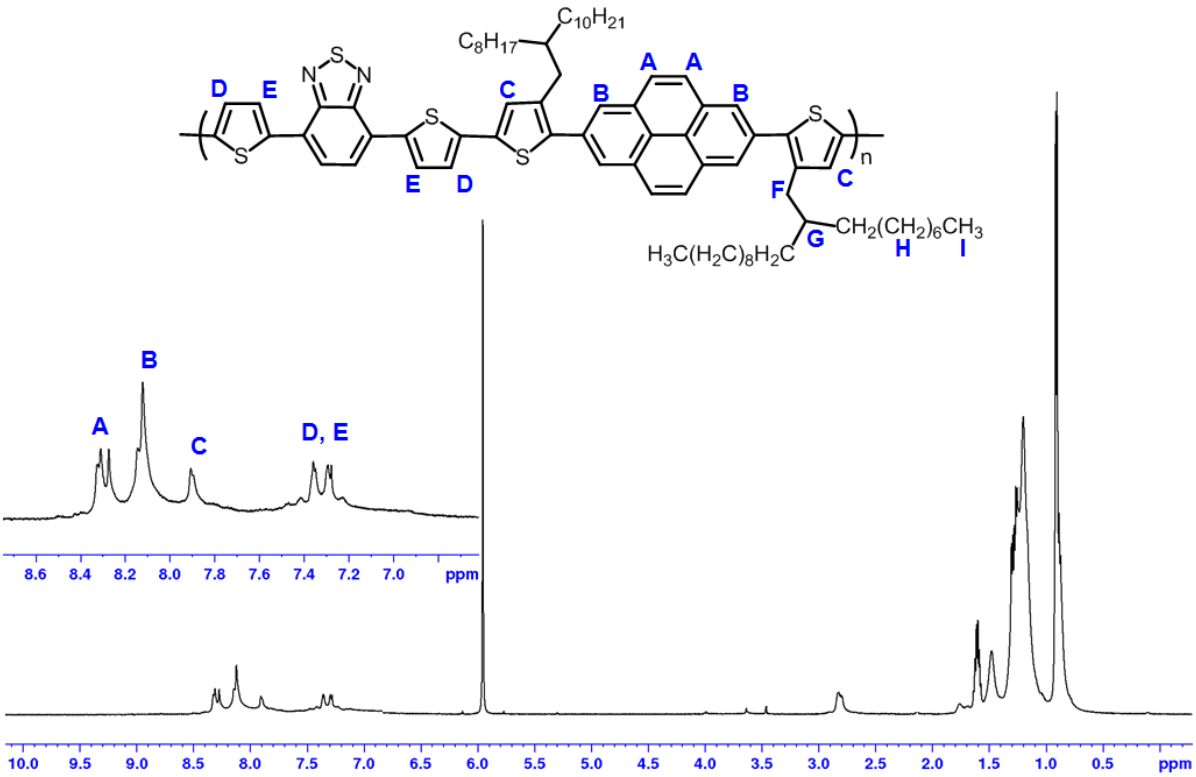

Figure 0-8: ^{1}H NMR spectrum of **P8** in $C_2D_2Cl_4$ at 100 °C.

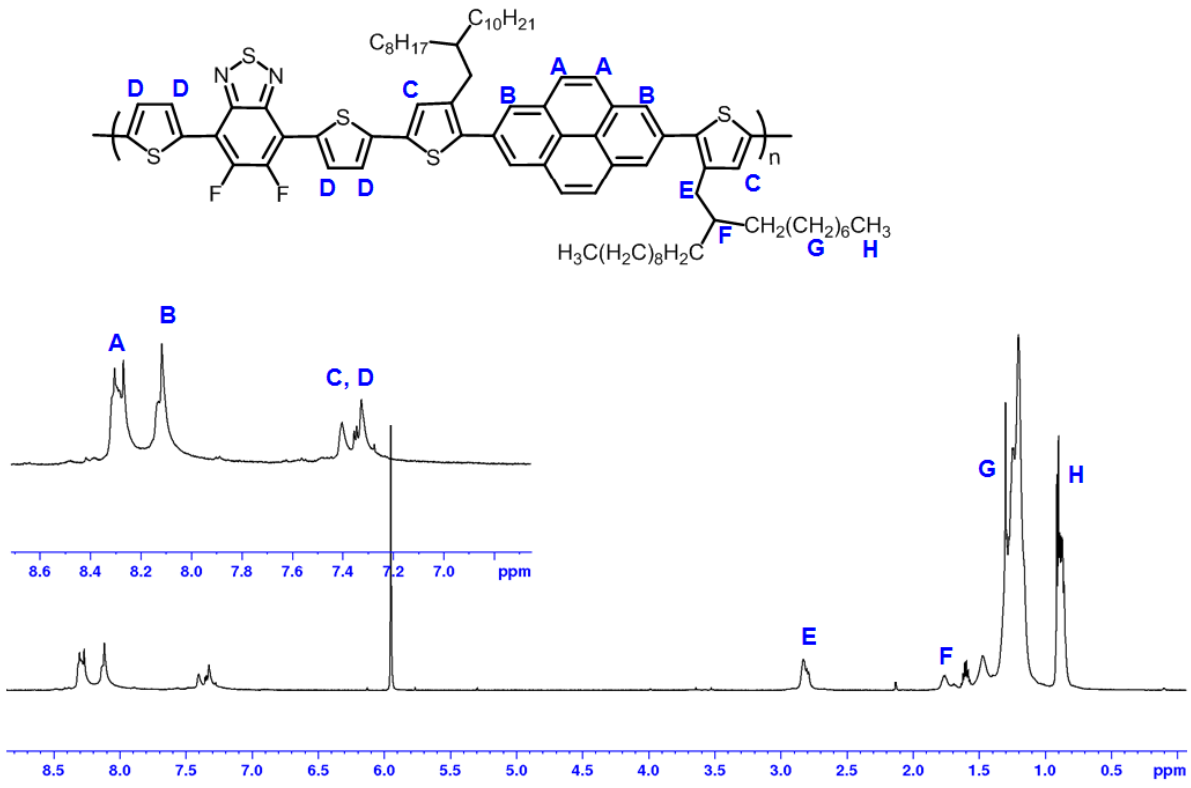

Figure 0-9: ^{1}H NMR spectrum of **P9** in $C_2D_2Cl_4$ at 100 °C.

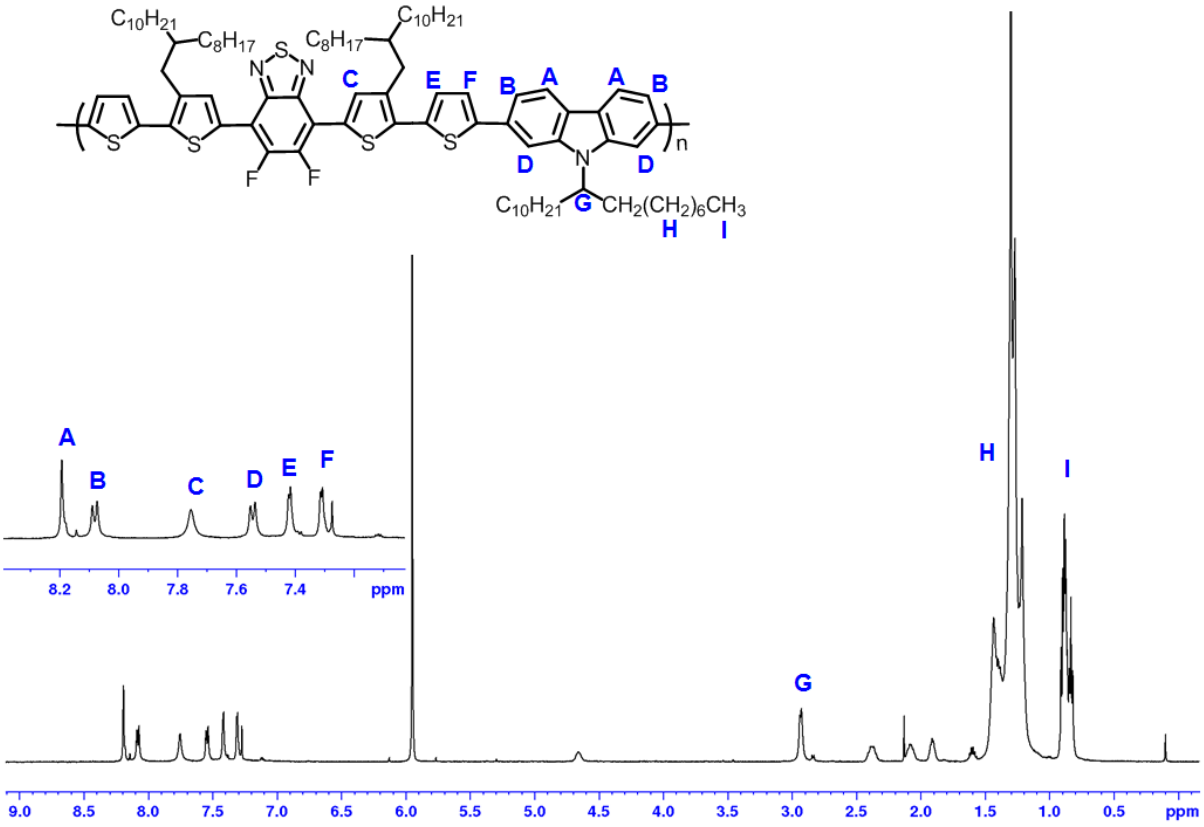

Figure 0-10: ^{1}H NMR spectrum of **P10** in $C_2D_2Cl_4$ at 100 °C.

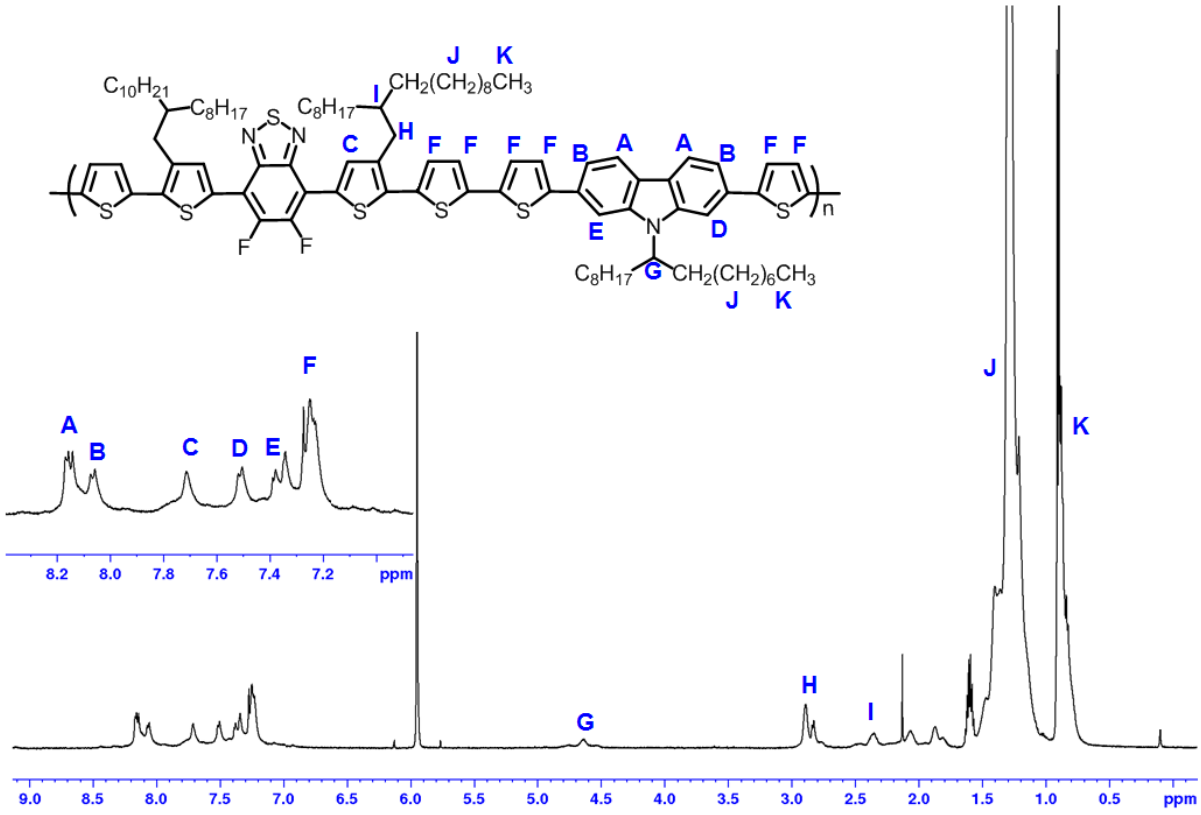

Figure 0-11: ^{1}H NMR spectrum of **P11** in $C_2D_2Cl_4$ at 100 °C.

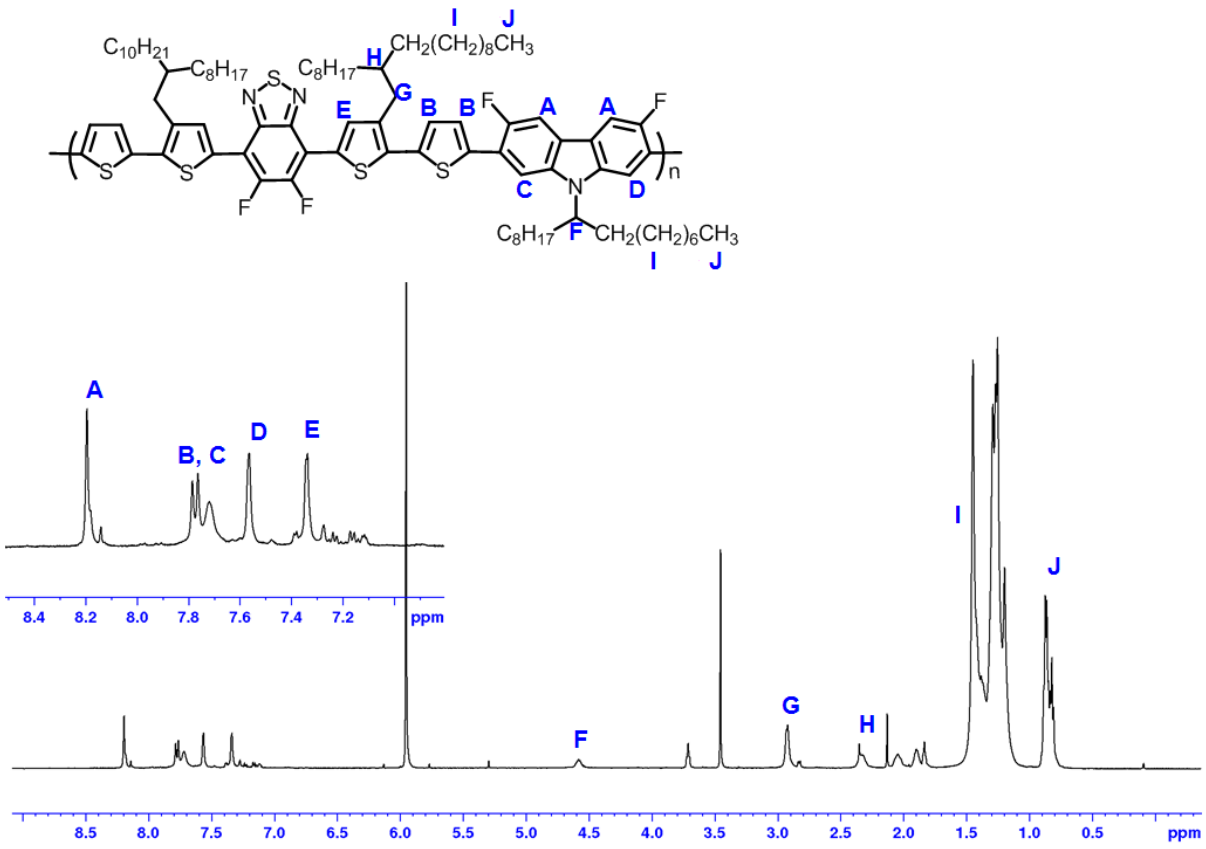

Figure 0-12: ^{1}H NMR spectrum of **P12** in $C_2D_2Cl_4$ at 100 °C.

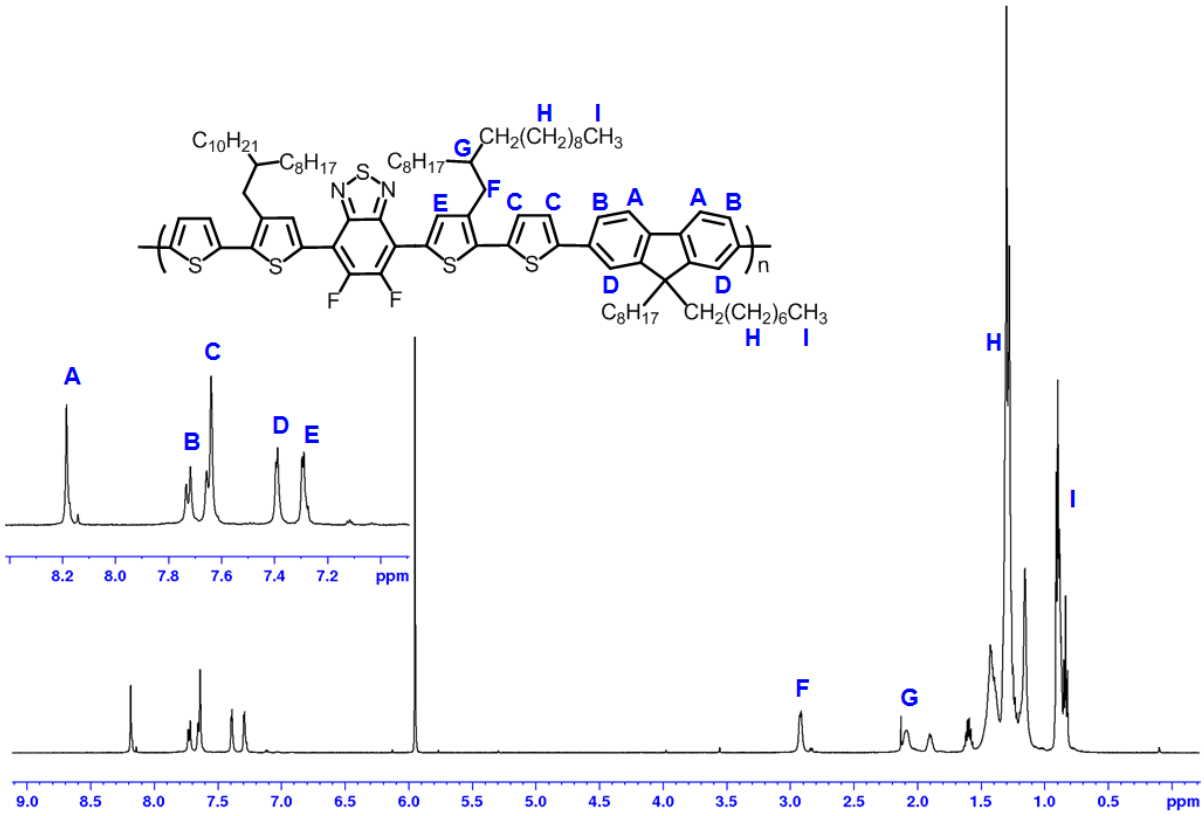

Figure 0-13: ^{1}H NMR spectrum of **P13** in $C_2D_2Cl_4$ at 100 °C.

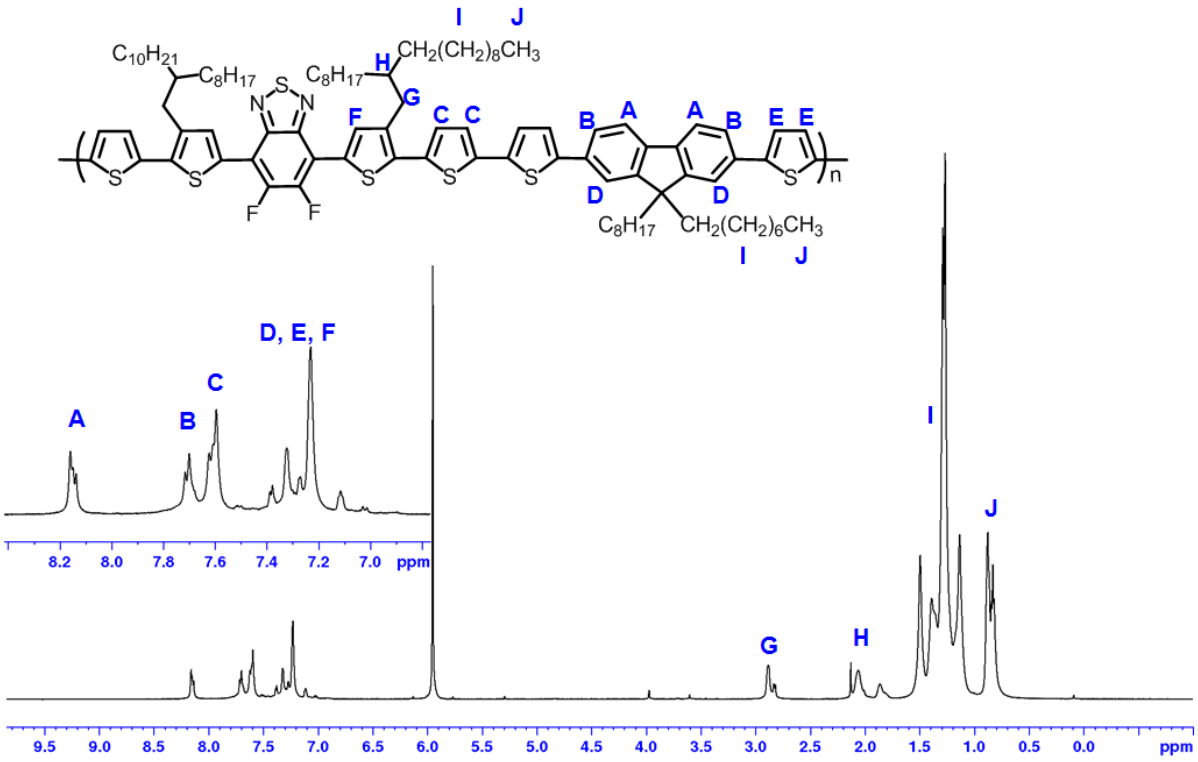

Figure 0-14: ^{1}H NMR spectrum of **P14** in $C_2D_2Cl_4$ at 100 °C.

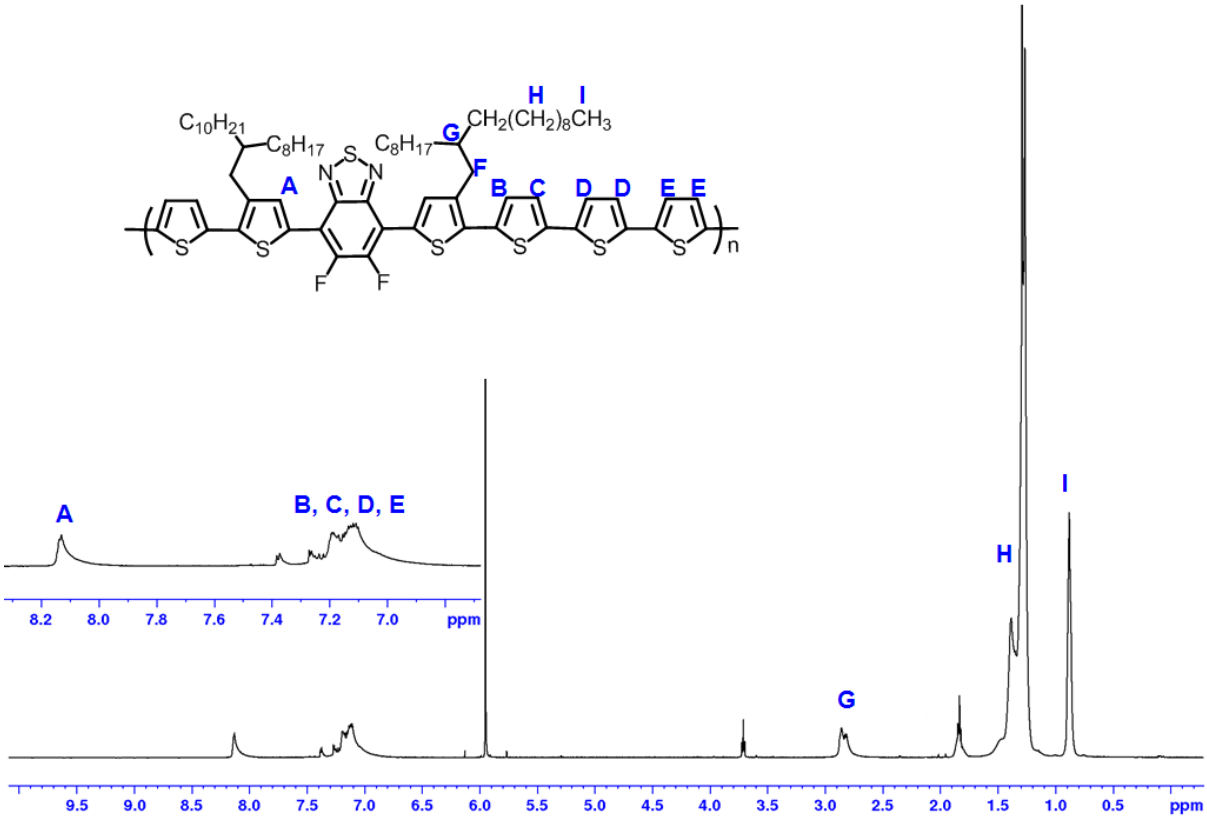

Figure 0-15: ^{1}H NMR spectrum of **P15** in $C_2D_2Cl_4$ at 100 °C.